LEU KIM FEY

A MULTIPLEXED GENE EXPRESSION STUDY ON NASOPHARYNGEAL CARCINOMA TREATED WITH XIAO XIAN XIONG DECOCTION

February 2022

A MULTIPLEXED GENE EXPRESSION STUDY ON NASOPHARYNGEAL CARCINOMA TREATED WITH XIAO XIAN XIONG DECOCTION

LEU KIM FEY

DOCTOR OF PHILOSOPHY (CHINESE MEDICINE)

FACULTY OF MEDICINE AND HEALTH SCIENCES
UNIVERSITI TUNKU ABDUL RAHMAN

FEBRUARY 2022

A MULTIPLEXED GENE EXPRESSION STUDY ON NASOPHARYNGEAL CARCINOMA TREATED WITH XIAO XIAN XIONG DECOCTION

By

LEU KIM FEY

A thesis submitted to the Department of Chinese Medicine,
Faculty of Medicine and Health Sciences,
Universiti Tunku Abdul Rahman,
in partial fulfillment of the requirements for the degree of
Doctor of Philosophy (Chinese Medicine)

FEBRUARY 2022

ABSTRACT

A MULTIPLEXED GENE EXPRESSION STUDY ON NASOPHARYNGEAL CARCINOMA TREATED WITH XIAO XIAN XIONG DECOCTION

Leu Kim Fey

Nasopharyngeal carcinoma (NPC) is a rare head and neck malignancy in the Western countries, but relatively common in Southern Asia. So far, the most common clinical means of treatment are generally radiotherapy (RT), with or without concurrent chemotherapy (CT). The use of traditional Chinese medicine (TCM) as a complementary and adjuvant medicine for the treatment of NPC is getting more attention as to reduce the side effects caused by radiotherapy and chemotherapy. Traditional Chinese herbal prescription Xiao Xian Xiong Decoction (XXXD), is made up of 3 Chinese herbal medicines, namely Huanglian (*Coptis chinensis* Franch. *C. deltoidea, or C. teeta* Wall), Banxia (*Pinellia ternate (*Thunb.)Breit.), Gualuo (*Trichosanthes kirilowaii* Maxim. *or Trichosanthes rosthornii* Harms). This project was designed to study the cytotoxic effect and global gene expression induced by XXXD on a selected NPC cell lines as well as to reveal the phytochemicals found in these Chinese herbal medicines. A Nanostring platform named nCounter XT Gene Expression Assay was carried out on extracted RNA and to further study on the gene expression in 13 canonical pathways, the cytotoxic effects of the individual herb and in combination of two and three herbs were studied

on 8 nasopharyngeal cancer cell lines, namely TWO-1, TWO-4, HONE-1, SUNE-1, CNE-2, HK-1, CNE-1 and C666-1. Out of the 7 groups of herbal extract samples, Huanglian showed the highest cytotoxicity against 8 NPC cell lines with the lowest IC_{50} of 4.48 µg/mL recorded for HONE-1. The IC_{50} values obtained for XXXD treated HONE-1 and CNE-2 cell lines were 88.55 and 92.95 µg/mL respectively. The Nanostring gene expression result showed that of HONE-1 upon treatment with L1(Huanglian) at 4 hours, 8 hours and 12 hours vs. 0 hour, initiated downregulation of *THBS1, IL7R, CCND1, FN1, BCL2L and VEGEFC* genes in PI3K, MAPK and RAS pathways which conventionally associated with functions of promoting cell proliferation and growth. The cytotoxicity of Huanglian towards HONE-1 could further be ascertained. Besides, gene expression of HONE-1 upon treatment with L7 (XXXD) at 4 hours, 8 hours and 12 hours vs. 0 hour showed that HONE-1 was imposed to apoptosis. The amplified expression of *CDKNIA*, *CDKNIC* and *TNFSF10* initiated in Cell Cycle pathway apparently inhibited cell cycle progression in HONE-1. Moreover, enhanced expression in *SOCS3* and *ID2* together with down-regulation of anti-apoptotic genes *BCL-2* and *BCL-XL* initiated in JAK-STAT pathway further exacerbated cell fate of HONE-1.This study suggests that XXXD could be envisaged as a potent anticancer traditional Chinese herb targeting HONE-1 cancer cell line.

Keywords: Nasopharyngeal carcinoma, Huanglian, Xiao Xian Xiong Decoction, Nanostring

ACKNOWLEDGEMENT

I would like to thank several people for their useful comments, guidance and advice given to me in preparing this thesis. In particular, I would like to give my deepest appreciation to main supervisor, Prof. Wang Xing Hua and co-supervisor Associate Prof. Dr. Yang Zao for providing me the valuable advice in thesis writing and the knowledge on the nasopharyngeal carcinoma from the Chinese Medicine philosophical understanding.

I would also like to express my most sincere gratitude to co-supervisor, Prof. Dr. Lim Yang Mooi for having the confidence in me for carrying out the project experiment and her dedication in guiding me to complete the whole experiment as well as her valuable advice in the thesis writing.

Next, I would like to record my utmost appreciation to Professor Dr. Lo Kwok Wai, and Professor S.W. Tsao for providing NPC cell lines C666-1 as well as Associate Professor Dr. Yap Lee Fah for providing NPC cell lines (TWO-4, HONE-1 TWO-1, SUNE-1, CNE-1 and CNE-2) and their technical support and advice for the study pertaining to cell lines handling.

Besides, I would like to express my appreciation to Dr. Wong Teck Yew and Dr. Menaga Subramaniam for imparting their knowledge and sharing their experience with me to help make the project experiment run smoothly. I am deeply felt thankful to all laboratory officers for their kind assistance and guidance. Furthermore, I would like to express my gratitude to all seniors and fellow PG members who have contributed their valuable assistance

and advice during my project experiment.

Last but not least, I would like to express my special thanks to my family members for giving me their full support upon my study.

APPROVAL SHEET

This thesis entitled "**A MULTIPLEXED GENE EXPRESSION STUDY ON NASOPHARYNGEAL CARCINOMA TREATED WITH XIAO XIAN XIONG DECOCTION**" was prepared by Leu Kim Fey and submitted as partial fulfillment of the requirements for the degree of Doctor of Philosophy（Chinese Medicine） at Universiti Tunku Abdul Rahman.

Approved by:

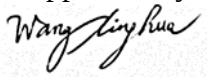

5/2/2022

(Prof. Wang Xing Hua) Date: ……..
Main Supervisor
Department of Chinese Medicine, Faculty of Medicine and Health Sciences, Universiti Tunku Abdul Rahman

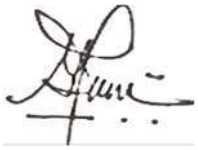

6/2/2022

(Prof. Dr. Lim Yang Mooi Date: ……..
Co-Supervisor
Department of Pre-clinical Sciences Faculty of Medicine and Health Sciences, Universiti Tunku Abdul Rahman

6/2/2022

(Assoc. Prof. Yang Zho Date: ……..
Co-Supervisor
Department of Chinese Medicine, Faculty of Medicine and Health Sciences, Universiti Tunku Abdul Rahman

FACULTY OF MEDICINE AND HEALTH SCIENCES UNIVERSITI TUNKU ABDUL RAHMAN

Date: 6/2/2022

SUBMISSION OF THESIS

It is hereby certified that **Leu Kim Fey** (ID No:**18UMD00842**) has completed this thesis entitled: "A MULTIPLEXED GENE EXPRESSION STUDY ON NASOPHARYNGEAL CARCINOMA TREATED WITH XIAO XIAN XIONG DECOCTION" under the supervision of Prof. Wang Xing Hua (Supervisor), from the Department of Chinese Medicine, Prof. Dr. Lim Yang Mooi (Co-supervisor) from the Department of Pre-clinical Sciences and Associate Professor Yang Zhao (Co-Supervisor) from the Department of Chinese Medicine, Faculty of Medicine and Health Sciences.

I understand that the University will upload softcopy of my thesis in pdf format into UTAR Institutional Repository, which may be made accessible to UTAR community and public.

Yours truly,

(LEU KIM FEY)

DECLARATION

I hereby declare that the dissertation is based on my original work except for quotations and citations which have been duly acknowledged. I also declare that it has not been previously or concurrently submitted for any other degree at UTAR or other institutions.

(LEU KIM FEY)

Date 6/2/2022

TABLE OF CONTENTS

LIST OF TABLES

LIST OF FIGURES

LIST OF ABBREVIATIONS

%	Percentage
℃	Degree celsius
µg	Microgram
µL	Microlitre
µm	Micrometre
µM	Micromolar
aPKC	Atypical Protein Kinase C
ADP	Adenosine 5'-diphosphate
ATCC	American type culture collection
ATF	Activating transcription factor
ATM	Ataxia telangiectasia mutated
ATP	Adenosine 5'-triphosphate
ATRX	ATRX Chromatin Remodeler
Bad	Bcl-X_L/Bcl-2-associated Death Promoter
BAX	BCL2-associated X
BCL	B-cell lymphoma
Bcl-2	B-cell Lympoma 2
BCL2L	BCL2 Like 1
Bcl-X_L	B-cell Lymphoma-extra Large
Bid	Bcl-2 Interacting Domain
BMP6	Bone Morphogenetic Protein 6
BNIP3	BCL2 Interacting Protein 3
BSA	Bovine serum albumin
C19orf40	FA Core Complex Associated Protein 24
CACNG6	Calcium Voltage-Gated Channel
CASP7	Cysteine-aspartic acid protease7
CASP8	Cysteine-aspartic acid protease8
CCND1	Cyclin D1
CDC	Cell division cycle
CDH1	Cadherin 1
CDK4	Cyclin-dependent Kinase
CDKN1C	Cyclin Dependent Kinase Inhibitor 1C
CO_2	Carbon dioxide
COL4A6	Collagen Type IV Alpha 6 Chain
CREB3L1	CAMP Responsive Element Binding Protein 3 Like

Cm	Centimetre
DDB2	Damage Specific DNA Binding Protein 2
DDIT3	DNA Damage Inducible Transcript 3
DKK1	Dickkopf WNT signaling pathway inhibitor 1
DLL1	Delta Like Canonical Notch Ligand 1
DMSO	Dimethyl sulfoxide
DNA	Deoxyribonucleic acid
DUSP4	Dual specificity protein phosphatase 4
DUSP6	Dual Specificity Phosphatase 6
EBV	Epstein-Barr virus
EBV-EA	Epstein-Barr virus early antigen
ERK	Extracellular signal-regulated kinases
ERCC6	ERCC Excision Repair 6, Chromatin Remodeling Factor
EtOH	Ethanol
ETS2	ETS Proto-Oncogene 2, Transcription Factor
ETV1	ETS Variant Transcription Factor 1
FANC	FA Complementation Group A
FANCG	FA Complementation Group G
FN1	Fibronectin 1
IC50	50 % inhibition concentration
ID1	Inhibitor of DNA Binding 1, HLH Protein
ID2	Inhibitor Of DNA Binding 2
IGFBP3	Insulin-like growth factor binding protein 3
IRS1	Insulin Receptor Substrate 1
ITGA2	Integrin Subunit Beta 2
ITGB8	Integrin Subunit Beta 8
ITGB6	Integrin Subunit Beta 6
GSK3B	Glycogen Synthase Kinase 3 Beta
JAG1	Jagged Canonical Notch Ligand 1
JUN	Jun Proto-Oncogene, AP-1 Transcription
KLF4	Kruppel Like Factor 4

LCMS	Liquid chromatography-mass spectrometry
m/z	Mass to charge ratio
MAPK	Mitogen-activated protein kinase
MAPK9	Mitogen-Activated Protein Kinase 9
MAPKK	Mitogen-activated protein kinase kinase
MEK	Mitogen-activated protein kinase
min	Minute
ml	Millilitre
mM	Milimolar
MMP	Matrix Metalloproteinases
mRNA	Messenger Ribonucleic Acid
MS	Mass spectroscopy
MSH2	MutS Homolog 2
MTT	3-(4,5-demethylthiazol-2-yl)-2,5-diphenyl tetrazolium bromide
MYB	MYB Proto-Oncogene
MYD88	MYD88 Innate Immune Signal Transduction Adaptor
NF-κB	Nuclear transcription factor-kappa B
NGF	Nerve growth factor
Nm	Nanometre
NF2	Neurofibromatosis type 2
NOG	Noggin
NOTCH	Notch gene homolog
NPC	Nasopharyngeal carcinoma
NR4A1	Nuclear receptor subfamily 4, group A, member1
NTHL1	Nth Like DNA Glycosylase 1
Nur77	Nuclear receptor subfamily 4, group A, member1
PIK3CA	Phosphoinositide 3-Kinase Alpha
PBS	Phosphate buffered saline
PLAT	Plasminogen Activator, Tissue Type

PLD1	Phospholipase D1
pH	Potential of Hydrogen
PI3K	Phosphoinositide 3-kinases
PLA2G2A	Phospholipase A2 Group IIA
POLR2D	RNA Polymerase II Subunit D
PRKCA	Protein Kinase C Alpha
PTEN	Phosphatase And Tensin Homolog
RAC2	Rac Family Small GTPase 2
RELA	RELA proto-oncogene, NF-kB subunit
RRAS2	RAS Related 2
ROS	Reactive Oxygen Species
RPMI-1640	Roswell Park Memorial Institute medium
Rpm	Rotation per minute
SOCS3	Suppressor of cytokine signaling 3
SOX9	SRY-Box Transcription Factor 9
SPRY2	Sprouty RTK Signaling Antagonist 2
SRSF2	Serine And Arginine Rich Splicing Factor 2 Structural
SMC3	Maintenance of Chromosomes 3
TCM	Traditional Chinese medicine
TGF	Transforming growth factor
TGFB1	TGF-beta 1
TGFBR2	Transforming Growth Factor Beta Receptor 2
TGF-β	Tumour Growth Factor β
THBS1	Thrombospondin 1
TNFSF10	Tumor Necrosis Factor Ligand
TNFAIP3	TNF alpha induced protein 3
VEGFC	Vascular Endothelial Growth Factor C
WNT10A	Wnt Family Member 10A
XXXD	Xiao Xian Xiong Decoction

CHAPTER 1

INTRODUCTION

Malignant tumour is a concerning illness principally occurred as a consequence of uncontrollable proliferation of mutated cells and their metastasis to other parts of the body. According to GLOBOCAN 2020 estimates of cancer incidence and mortality, there will be an increase of 47% of the global cancer burden from year 2020 to 2040 and 28.4 million cases is anticipated. In 2019, World Health Organization (WHO) reported that out of 183 nations, population in 112 nations whom the age is more than 70 die because of malignant tumour. The management of cancer encompasses clinical diagnose, treatment and follow-up works which demands considerable cost as well as attention for medicinal solution.

Nasopharyngeal carcinoma (NPC) arises from the nasopharyngeal epithelial squamous layer. Malaysian National Cancer Registry Reported that for the years of 2012 to 2016, new cancer cases increased by 11.3% from the past 10 years . There were 115,238 new occurrences from 2012 to 2016. compared to 103,507 for the years 2007 to 2011. In Malaysia, NPC is the 5th (4.0 %) most occurring malignant tumour and in terms of gender, it is the number three highest in male for cancer occurrence rate (8.4%). The present common clinical treatments for NPC are liquid biopsy, surgery, intensity-modulated radiotherapy and chemotherapy. Due to the side effects and complications resulted from conventional cancer therapies, there is a growing attention being focused on

secondary metabolites in natural plants for cancer treatment purposes. Chinese medicine has been practised since ancient China. Chinese medicinal herbs are mostly derived from natural plants. Today, Chinese medicine is often being utilised as an adjuvant medication for varios types of cancer treatments.

Xiao Xian Xiong Decoction (XXXD) is prescription originally found in "Shang Han Lun" about two thousand years ago in ancient China. It is a common and popular Chinese Medicine prescription. The constituents of this prescription are Huanglian (*Coptis chinensis* Franch. *C. deltoidea*, or *C. teeta* Wall), Banxia (*Pinellia ternate* (Thunb.)Breit.), and Gualou (*Trichosanthes kirilowaii* Maxim. *or Trichosanthes rosthornii* Harms). Sun et al. (1993) reported that its medical functions include removing body heatiness, eliminating phlegm, soothing abdominal stuffiness. Conventionally, it is being used to cure diseases involving vascular, digestive and respiratory disorder. Xu (2011) reported that recently, XXXD has been used to enrich body resistance to tumour occurrence. Huang (2011) reported remarkable effect of XXXD in inhibiting tumour growth in Ehrlich ascites carcinoma (EAC). Moreover, Ni et al. (2014) reported the anti-tumour effect for non-small cells lung cancer (NSCLC). Previous studies on individual Huanglian and Gualou have noted a remarkable inhibitory effect on tumour growth of nasopharyngeal carcinoma (NPC) (Chi et al., 2009; Chen, 1997). However, no report has been found regarding the cytotoxicity effect of XXXD on NPC cell lines. The effect of XXXD in this aspect may be overlooked.

This project is designed to compile the literature aspect of XXXD and to perform cytotoxicity effect of XXXD on 8 nasopharyngeal carcinoma cell lines such as TWO-4, CNE-1, C666-1, TWO-1, HONE-1, SUNE-1, CNE-2, HK-1 and CNE-2. The most susceptible cell line towards XXXD and individual herb treatement was selected for further study on global gene expression. A Nanostring platform named nCounter XT Gene Expression Assay was used to study the gene expression in 13 canonical pathways, such as MAPK, Wnt, RAS, apoptosis, PI3K, STAT, Notch, Hedgehog, TGF-β, chromatin modification, transcriptional regulation cell cycle, and DNA damage control pathways. The metabolic profiling of XXXD and all the individual Chinese herbs were analysed by LC-MS.

A total of 7 herbal extract samples were prepared and used to test for its cytotoxity effect on 8 NPC cell lines. The samples were named as follows: L1 (Huanglian), L2 (Banxia), L3 (Gualou), L4 (Banxia and Huanglian), L5 (Gualou and Huanglian), L6 (Gualou and Banxia) and L7 (XXXD).

The result of metabolite profiling obtained by Liquid Chromatography Mass Spectrometry (LC-MS) in this study showed that all samples consisted of both primary and secondary metabolites. Huanglian (*Coptis chinensis* Franch. *C. deltoidea*, or *C. teeta* Wall) consisted of amino acid (7 %), carbohydrate (3 %), fatty acid (10 %), protein (3 %), vitamin (3 %), alkaloid (34 %), glucoside (7 %), phenolic (27 %), phthalide (3 %) and terpene (3 %). Secondary metabolite such as alkaloid and phenolic composed the largest percentage. L3 (Gualou)

consisted of primary metabolites which were made up of amino acid (15 %), carbohydrate (3 %), fatty acid (27 %), glucose (3 %) and protein (5 %). Its secondary metabolites comprised alkaloid (18 %), benzamide (3 %), phenolic (17 %), phthalide (3 %), phthalate (3 %) and terpene (3 %). In L4 (Huanglian+ Banxia) consisted primary metabolites which were made up of amino acid (11 %), carbohydrate (4 %), fatty acid (7 %) and glucose (4 %). Secondary metabolites comprised alkaloid (41 %), phenolic (19 %), saponin (4%) and terpene (3 %). Primary metabolites L5 (Huanglian+ Gualou) consisted of of amino acid (16 %), carbohydrate (3 %), fatty acid (16 %), glucose (3 %), protein (9 %) and vitamin (3 %). Secondary metabolites comprised alkaloid (28 %), phenolic (13 %), terpene (3 %), coblamin (3 %) and benzamide (3%). In L6 (Banxia + Gualou), the comparative ratio of primary metabolites to secondary metabolites was 55 % to 45 %. The primary metabolites were made up of amino acid (22 %), protein (14 %), fatty acid (14 %) and glucose (5 %). Secondary metabolites comprised alkaloid (22 %), phenolic (18 %), and flavanoid (5 %). As for L7 (XXXD), the metabolites composition is as follows: amino acid (11 %), carbohydrate (4 %), fatty acid (26 %), protein (7 %), glucose (4 %), alkaloid (37 %) and phenolic (11 %). Similarly, secondary metabolite such as alkaloid composed the largest percentage. Alkaloid in L7 (XXXD) composed of indoles (20 %), deoxycytidine analog (10 %), purine (30 %), pyrimidines (10 %), carbohydrazide (10 %), terpenoid (10 %) and methylhydrazine (10%).

Cell viability of 8 NPC cell lines were tested by MTT upon treatment of each herbal sample namely L1~L7 separately. Result showed that Huanglian was most effective in inhibiting cell growth than seven other samples. IC_{50} of

4.48 to 27.30 μg/mL was witnessed in Huanglian upon eight NPC cell lines in which 4.48 was the lowest when applied to HONE-1. Banxia and Gualou alone as well as combined herbs of Banxia and Gualou did not exhibit killing effect on all NPC cell lines involved. When applied to CNE-2, combined herbs of Huanglian and Banxia achieved IC_{50} of 19.00 μg/mL. Combination of Huanglian and Gualou could only achieved IC_{50} value of 40.70 μg/mL when treated to HONE-1. XXXD could gain IC_{50} values of 92.95 and 88.55 μg/mL when treated to CNE2 and HONE-1 respectively. The finding concluded that HONE-1 cell line was most susceptible to herbal extracts L1 (Huanglian), and thus, HONE-1 was chosen for the subsequent experiments.

RNA extraction were prepared for HONE-1 treated with L1(Huanglian) as well as L7 (XXXD) as at 0hr, 4hrs, 8hrs and 12hrs. Subsequently, NanoString PanCancer Pathways Panel gene expression analysis was utilised to quantify measure level of genes expression in HONE-1when treated with XXXD and Huanglian. The gene expression was analysed at three time points such as 4hours, 8hours and 12hours to 0 hour. The result of gene expression of HONE-1 for Huanglian are as follows: (1) at 4 hours vs. 0 hour treatment time, among the top 10 most significant differentially expressed genes, the deregulated were *FOS, TNFSF10, PLD1, MYB, HES1, CDC25C, KLF4* and upregulated genes were *NGF, FST* and *DUSP4*. (2) At 8 hours vs. 0 hour treatment time, among the top 10 most significant differentially expressed genes, the deregulated were *HES1, CDC25C, HDAC6, FZD7, BMP6, MAPK9* and the upregulated gene was *SOCS3*. At 12 hours vs. 0 hour treatment time, among the top 10 most significant differentially expressed genes, the downregulated genes

were *THBS1, IL7R, VEGFC, HMGA2 JAG1* and the downregulated genes were *ETS2, VEGFC, NR4A1, DDIT, SOCS3*. Moreover, the result of gene expression of HONE-1 upon treatment of L7 (XXXD) are as follows: (1) at 4 hours vs. 0 hour treatment time, among the top 10 most significant differentially expressed genes , the deregulated were *FANC* and upregulated genes were *WNT10A, MYD88, ETS2, ITGB8, SOCS3, IGFBP3, CASP7, CDH1*and *RRAS2*. (2)At 8 hours vs. 0 hour treatment time, among the top 10 most significant differentially expressed genes, all were downregulated genes such as *DUSP6, ETV1, SOX9, SPRY2, ITGB6, TGFBR2, DKK1, DUSP4, ITGA2* and *IRS1*. (3) At 12 hours vs. 0 hour treatment time, among the top 10 most significant differentially expressed genes, the downregulated genes were *DKK1, TGFB2* and the upregulated genes were *TGFBR2, CDH1, ETS2, WNT10A, ID1, CDKN1A, HES1, SOCS3*

Gene expression of Huanglian treated HONE-1 at 4hours, 8hours and 12 hours vs. 0 hour showed that HONE-1 experienced reduction in sustainable cell proliferation and survival. The result indicated level of the expression of genes being initiated in PI3K, MAPK and RAS pathways where genes with biological functions of promoting cell proliferation and growth were downregulated such as *THBS1, IL7R, CCND1, FN1, BCL2L and VEGEFC*. The cytotoxicity of Huanglian apparently implicated in the cell arrest and boost apoptosis at final time point. Besides, gene expression of HONE-1 upon treatment with L7 (XXXD) at 4hours, 8hours and 12 hours vs. 0 hour showed that HONE-1 encountered viability menace from growth suppression. The elevated expression of *CDKNIA*, *CDKNIC* and *TNFSF10* initiated in Cell Cycle pathway apparently inhibited cell cycle progression in HONE-1. Moreover, enhanced expression in

SOCS3 and *ID2* together with deregulation of *BCL-2* and *BCL-XL* initiated in JAK-STAT pathway further exacerbated cell fate of HONE-1. Nevertheless, in view of the MAPK signalling pathway, high level expression of genes like *FOS, AP-1, ERK* and *CACN* may postulate a vigorous rebounce of cell resistance of HONE-1 against the interaction of XXXD after 12 hours of treatment. Nevertheless, the result revealed that XXXD could exhibit the cytotoxity upon HONE-1throughout the 12 hours treatment time.

It was detected that expression of *ETV1* was attenuated at 3 different time points such as 4 hours, 8 hours and 12 hours to 0 hour when HONE-1 was treated with L1(Huanglian) and L7 (XXXD) separately. The attenuated expression of *ETV1* was consistent as when HONE-1 was treated with L1 (Huanglian) and L7 (XXXD) in two different tests. *ETV-1*gene is ETS Variant Transcription Factor. Its main function is to modulate biological processes like cell growth, angiogenesis. Down-regulation of *ETV-1* could inhibit tumour cell growth and development. Thereupon, these findings suggest that *ETV1* could be targeted as the core gene for therapeutic purpose in treating NPC particularly HONE-1.

The difficult factor contributed to this reseach was the complicacy of carcinogenesis which entails multiple signalling pathways. The experimental result can hardly provide sufficient information in molecular mechanism of interaction between proteins and drugs (XXXD or Huanglian) in HONE-1 cells. In this reseach, differential expression which upregulated or downregulated by

XXXD or Huanglian in the key genes associated with 13 canoniacl signalling pathways namely MAPK, PI3K, RAS, WNT, TGFβ, JAK-STAT and NF-κB have been studied. However, the detail on cellular mechanism of action caused by the interaction between relevant proteins expressed and the said herbs were not elaborated.

This research is aimed to justify the potential effect of XXXD and its constituents in anti tumour aspect. The results obtained has validated the anti-cancer effect of Huanglian and XXXD in HONE-1 cells. Consequently, it may further lead to more exploration in the usage of natural plants to cure cancer. New knowledge generated from this study could be referred by fellow traditional Chinese medicine practitioners as well as oncologists for further research and treating the relevant cancer diseases in Malaysia and worldwide.

The main objectives of the research are as follows:

1. To prepare the aqueous-extracted of individual and combination extracts of Huanglian (*Coptis chinensis* Franch. *C. deltoidea*, or *C. teeta* Wall), Banxia (*Pinellia ternate* (Thunb.)Breit.), and Gualou (*Trichosanthes kirilowaii* Maxim. or *Trichosanthes rosthornii* Harms). To conduct metabolite profiling on these herbal extracts by Liquid Chromatography Mass Spectrometry (LC-MS)

2. To conduct LC-MS for metabolite profiling on these herbal extracts.

3. To screen cell viability of C666-1, TWO-1, CNE- 1, TWO-4, HONE- 1, SUNE- 1, HK- 1 and CNE- 2 upon treatment of the herbal extracts.

4. To evaluate the efficacy of the single herb and combined herbs in Huanglian (*Coptis chinensis* Franch. *C. deltoidea*, or *C. teeta* Wall), Banxia (*Pinellia ternate* (Thunb.)Breit.), and Gualou (*Trichosanthes kirilowaii* Maxim. or *Trichosanthes rosthornii* Harms) on the gene expression on a selected NPC cell line.

CHAPTER 2

LITERATURE REVIEW

2.1 Nasopharyngeal carcinoma

Nasopharyngeal carcinoma (NPC) is a kind of malignant cancer growing at lateral wall of the nasopharynx which most frequently emerges from the recess behind the orifice of eustachian tube namely fossa of Rosenmüller.

2.1.1 WHO histological classification of NPC

World Health Organization (WHO) presently determined histological classification of NPC for three categories such as keratinizing squamous cell carcinoma (KSCC), non-keratinizing differentiated carcinoma (NKDC) and non-keratinizing undifferentiated carcinoma (NKUC) (Wang HY et al., 2016).

2.1.2 Epidemiology of NPC

According to Nasopharyngeal Cancer Statistics 2018 announced by America Institute of Cancer Research, NPC is the 23rd most prevalent cancer in the world. 129,000 new NPC cases was recorded in 2018. Nations recorded for

having most prevalent occurrence rate of this disease during 2018 were the top 5 countries with the highest rates of nasopharyngeal cancer in 2018 were Indonesia Brunei, Singapore, Maldives, and Malaysia. Moreover, among the top 10 in the list, 8 were from Southeast Asia countries. According to the report of Malaysia National Cancer Registry 2012-2016, NPC is the 5th (4.0 %) most occurring malignant cancer and in terms of gender, it is the number three highest in male for cancer occurrence rate (8.4%).

2.1.3 Risk Factor

Risk factors associated with pathogenesis of NPC include viral infection, environmental influences, and heredity (Zhang and Zhang, 1999). Epstein-Barr (EBV) virus is most often reported as viral influence to cause NPC (Lo et al., 2012). Environmental factors include exposure to air contamination, radiation and cigarretes smoking (Her, 2001). The habitual consumption of seasoned and salted foodstuff can be a reason for high occurrence rate in NPC in South East Asia countries

2.1.4 EBvirus Infection

Most of the NPC cells can be discovered for EBV episomes (Tsang CM and Tsao SW, 2015). The role of EBV in NPC pathogenesis has long been suggested but remains rather inexplicable. Once the normal pharyngeal epithelial

being infected by EBV, the virus will not directly convert the epithelial cells into proliferative and malignant clones. Instead, a latent EBV infection is formed and the infected cells are mostly lytic in nature. Expression of latent viral genes such as BART transcripts and BART-encoded microRNAs will be induced and subsequently transform the nasopharyngeal epithelial cells into malignancy (Tsang CM and Tsao SW, 2015).

2.1.5 NPC Cell Lines

The most prevalent NPC cell lines are HONE-1, HK1, C666-1, TWO-1, SUNE-1, CNE-1 and CNE-2. The background information and characteristic of these cell lines are summarized as follows:

C666-1 cell lines were derived from an EBV-associated and undifferentiated type of nasopharyngeal carcinoma (Cheung ST et al., 1999). Detection of EBNA1 protein, LMP1 and LMP2 was rather same with EBV latency II pattern. Latent membrane protein 1 gene by infection of EBV was easily found in NPC patients in Southern region of China (Cheung ST et al., 1999).

CNE-1 cell lines was procured in well-differentiated squamous species of a Chinese patients. CNE-1 was reported to be EBV- negative. Tumorgenesis

of CNE-1 is greater than CNE-2. The mutated gene p53 Thr280 in this cell line did not induced expression CD19, a B cell marker. CNE-1 are not somatic cell hybrid of HeLa and Burkitt's lymphoblastoid cells which are prevalently used to activities of EBV in epithelial cells (Yat et al., 2008).

CNE-2 cell lines were procured from the lightly differentiated tumour and reported as EBV-positive at the beginning. However, the virus infected genome disappeared in the following years. It was procured from a young Chinese patients two decades ago. A specific p53 Thr280 mutation in CNE-2 was reported. Kong FY and Gao J, 1991 reported mutated genes p53 Thr280 in CNE-2 and revealed that the tumour cells might invade into the cell layer of fibroblasts surrounding the heart tissue which subsequently caused degeneration, atrophy and necrosis of heart muscle.

HK-1 cell lines were procured through and well-differentiated squamous and EBV-negative tumour. HK1 xenograft was free from EBV infection.

TW0-1cell lines were established from an EBV-negative tumour. However, there was still a possibility to detect EBV genes in TWO-1 and so, the function of LMP1 could solely be suspected for tumour development. (Tan et. al., 2007).

HONE-1 cell line has been taken through lightly differentiated squamous tumour. It was found that EBV was massively implicated in HONE-1 (Glaser et al., 1989).

SUNE-1 cell lines had been procured through EBV-positive and lightly differentiated tumour in primary cultures but EBV was lost after long-term *in vitro* culture (Dong et al., 2012). SUNE1 has 3 biological behaviour sublines for instance 5-8F, 6-10B and 13-9B with highest to lowest carcinogenic and metastatic capacity respectively. (Song et al., 2002)

Ou et al., 2007 had reported undifferentiated carcinoma had better prognosis than the other two subtypes. Among the different histologic subtypes of NPC, the keratinizing type has the poorest prognosis and is the least radio-sensitive (Vazquez et al., 2014). Undifferentiated NPC, on the other hand, is radiosensitive, with a 60 to 70 % survival rate compared to 20 % for the keratinizing type of NPC of the same stage (RT et. al., 1978). Decker DA et al. (1983) reported that undifferentiated NPC was chemo-sensitive and that there was a potential curability when chemotherapy is used for recurrent or metastatic disease.

2.1.6 Symptoms of NPC

Generally, symptoms for NPC are commonly found as nasal bleeding, congestion, hearing loss, mass in neck, numb face muscle, head pain, vision disorder, dizziness and so on. Apart from mentioned symptoms, there will be risk for cranial nerve disorder affected by growing size of tumour (Baharudin Abdullah and Azila Alias, 2007). Early diagnoses of NPC is paramoutly important for efficient clinical treatment and good prognosis. Nasal tumour mass can be discovered by endoscope and MRI. However, many NPC mass are still quite difficult to detect at early stage.

2.1.7 Management of NPC

The current management of NPC includes liquid biopsy, minimally invasive surgery, intensity-modulated radiotherapy, chemotherapy and immunotherapy (Lam WKJ and Chan JYK, 2018). Biopsy is widely adopted for screening particularly for high risk NPC cluster (Ng RH et al., 2014). Nevertheless, current treatment methods for NPC do consist of clinical limitation. First of all, surgery can be invasive and inoperable because tumour often arises in deep-seated location which empasses risk to blood vessel and nerves in the surrounding area (Chan JYW and Wei WI, 2012). Radiotherapy and chemotherapy treatments can cause complications during treatment. For radiotherapy, short- and long-term side effects could be dizziness, dry mouth, facial muscle disorder, lossof appeptite and smelling senses and so on (B.

Galletti et al., 2016). Furthermore, most of the drugs used in chemotherapy can be toxic to normal healthy cell and cause side effects such as dizziness, loss of appetite and vomiting as well as adverse effects on liver functions (Ramadori and Cameron, 2010). The present drawback of immunotherapy includes its inability to predict treatment efficacy the need for additional biomarkers and high treatment cost involved (Ventola CL, 2017). As a consequences of numerous side effects and complications, it is imperative to embrace more adjuvant medications for faster and more efficient recovery.

2.2 Xiao Xian Xiong Decoction and its constituents

In view of the complications and shortcoming of existing clinical management of NPC, Chinese medicaines could be a promising option to cure and reduce side effects of patients. Nowadays, there is a trend for increasing efforts and attention being poured into research on potential beneficial natural materials (Greenwell M and Rahman PK, 2015)

2.2.1 Cancer in TCM Perspective

Traditional Chinese Medicine view tumour as the consequence of defective flow of qi and blood physically. In particular, cancer develops physically owing to certain latent advantages which contribute to its growth. These can be accounted for disorder of qi flow and blood circulationas well as the accumulation of phlegm which render detrimental tendency for tumour

growth. The shortcoming of functions in any part of human body may gives rise to the problem of stagnancy in qi and blood circulation as well as accumulation of phlegm which eventually facilitate development of cancer. This situation could be correlated to the mutation of genes in the body cells when modern sciences is concerned. As herbal medicines are gaining more attention worldwide, its intrinsic value will soon be embraced by large population. Herbal medicinces are derived from natural plants which contain rich metabolites particularly the second metabolites for its own protection, somehow, they can be utilised for medical purposes to cure diseases or to be used as an adjunct western medicines.The aim is to enhance the overall treatment efficiency and to reduce the side effect caused by surgery, chemotherapy, and radiation. Chinese medicine emphasizes restoration of normal circulation of blood and qi and a balance of five elements and yinyan in the course of treating a disease (Subhuti, 1997). Healthy human body will naturally possess normal circulation of blood and qi and a balance of five elements and yinyan to fend off cancer occurrence. Hence, if we physically can maintain a natural equilibrium within the body, there are strong resistance to overcome any internal and external factors for causing cancer.

2.2.2 Xiao Xian Xiong Decoction

Xiao Xian Xiong Decoction (XXXD) is prescription originally found in "Shang Han Lun" in ancient China for approximately two thousands years. It is a common and popular Chinese Medicine prescription. This decoction is made

up of three Chinese medical herbs, namely Huanglian , Banxia and Gualuo.The function of this Chinese medicine decocotion as recorded in“Shang Han Lun“is to eliminate phlegm and stuffiness in abdomen and chest by discharging internal body heat associated dampness. Literally, this TCM herbal formula is most suitable for treating entanglement of heat and phlegm **(痰热互结)** arisen in chest and abdominal part of body where in context of Chinese medicine, they belong to upper and middle jiao **(上焦与中焦).** Nevertheless, the prescription of Xiao Xian Xiong Decoction should apply to patients having symptoms such as abdominal and chest distention coupled with pain; coughing with yellow and thick sputum; constipation; linggering bitter sensation in mouth; yellowish and greasily coated tongue and accompanied by a slippery, floating and rapid pulse.

From ancient era till now, conventionally, Xiao Xian Xiong Decoction has been prescribed to cure illness such as lung, stomach disorder, blood circulation disorder and other diseases where the Chinese Medicinal syndrome suits. (Zhang, Z.J. and Wang, S.H., 2005). This is particularly important in Chinese Medicine practice in order to justify the right syndrome before initiating a treatment.

Xiao et al. (2017) reported the application of modified Xiao Xian Xiong decoction could effectively reduce the parameters of blood glucose at fasting (FBG), tolerance test for mouth feed glucose 2 h blood glucose (OGTT2hB)，total cholesterol (TC)，triglycerides (TG) and BMI of patients with impaired glucose tolerance (IGT) of obesity type. Wang (2018) used XXXD in treating

community acquired pneumonia of phlegm heat obstructing lung syndrome and reported that value of white blood cells WBC, Nitrogen %, C-reactive protein (CRP), Procalcitonin (PCT) in treatment group were lowered with the application of XXXD. Xiao et al. (2014) reported that combination of XXXD with Sini-san (四逆散), could effectively improve bile reflux gastritis patients' symptoms than Domperidone. Besides, Hou Bao-song et al. (2018) reported that XXXD can improve the curative effect on angina pectoris due to coronary heart disease with syndrome of phlegm-heat accumulation, and improved blood rheology indexes. Furthermore, Qiu Feng (2014) found out the clinical curative effect of hyperlipidemia treated by simvastatin combined with modified XXXD was significantly safe and reliable. He further postulated that the pathogenesis is phlegm dampness and blood stasis. Therefore, impoving blood flow and eliminating excessive water rentention was the curative method for hyperlipidaemia.

Several biological researches in XXXD had also shown positive results. Ni et al. (2014) reported that XXXD showed inhibitory effect against Ehrlich ascites carcinoma (EAC) and lung cancer (NSCLC). In this *in-vitro* research, the MTT assay witnessed that XXXD induced a time as well as dose-dependent decrease in cell viability in A549 and H1299 cells and thus, A549 and H1299 cells showed a significantly reduced rate of cell growth. Besides, the colony formation assay shown that a significant inhibition of growth by treatment of XXXD in a dose-dependent manner where A549 and H1299 cells formed significantly fewer colonies after XXXD treatment. On the other hand, result of

migration and cell cycle arrest assay (Flow cytometer and quantitative RT-PCR) shown that XXXD induced G2/M phase arrest in A549 and H1299 cells where 1mg/mL led to a significant increase in the number of cells. Meanwhile, XXXD up-regulated GADD45A expression but down-regulated CCNB1 and CCNB2 expressions in both A549 and H1299 cells. The *in vivo* study shown XXXD treatment inhibited the growth of tumors in nude mice compared with the control group. Ni et al. (2014) concluded that XXXD might be a potential natural product in treating or adjuvant radio (chemo-) therapy for non–small cell lung cancer (NSCLC) patients.

Huang Jin Ling (2007) had carried out reseach on XXXD by replicating Sarcoma 180 tumor cells and Ehrlich Ascites tumor cells in ICR mice. Mice were treated with XXXD and 5-Fu respectively by oral gavage. Carbon granule clearance method was used to detect the phagocytosis of mononuclear-macrophage cell line (MPS). The result shown that inhibitory rates on the tumor growth and life extension rate of S180 mice increased with increment of XXXD concentration and comparision of pathological changes in mice of each group shown that tumor reduced with the increment of XXXD concentration.

Li et al. (2017) had carried out an *in vivo* experimental study on 60 Sprague Dawley rats to find out the potential mechanism of XXXD on liver Caspase-12 expression in treating non-alcoholic fatty liver disease. The rats were fed with high fat diet for 12 weeks to build up NAFLD model except the control group. After 5-week of drug administration, liver tissue was collected and

stained by H&E staining, the expression of Caspase-12 protein was detected by immunohistochemistry and Western-blot. The result shown weight decreased with the increment of XXXD concentration. Histo-immunochemical analysis on liver tissue shown that hepatocytes in the model group exhibited obvious steatosis and inflammation compared with those in the blank group, while the degree of steatosis and inflammation in each XXXD group was significantly less than that in the model group and the Polyene phosphatidyl-choline PPC group. Meanwhile, Caspese-12 expression in the high dose XXXD group was significantly lower than that in PPC group and medium and low dose XXXD groups. During apoptosis induced by endoplasmic reticulum (ER) stress, caspase-12 was localized to the endoplasmic reticulum and was activated (Nakagawa T, 2000).

Lv et al. (2014) had carried out an *in vivo* study on 60 healthy male Wistar rats to investigate the effects of XXXD on the area of plaque formation and NF-κB expression in aorta of atherosclerotic rats. The control group fed with normal diet. The rest fed with high fat diet and injected VD 360 million IU/kg in the abdomen by once. Starting from third week till 12th week, XXXD were treated by gavage except control and model being given saline. Eventually, all rats were sacrificed and area of plaque formation were measured and NF-κB expression was evaluated. The result shown that plague area of aorta in rats was dose dependent in which it was reduced with higher dose of XXXD. Lv et al. (2014) concluded that XXXD could reduce NF-κB expression by inhibiting the plaque formation in aorta and further suggested the mechanism might due to the anti-atherosclerosis effect of Xiao Xian Xiong Decoction.

Hyperactive growth of epithelial cell and angiogenesis can be a concerning sign for onset of primary epithelial cancers. Excessive activation epithelial mesenchymal transition (EMT） may indicate the possibility of metastatasis of malignant phenotypes by epithelial cancer cells. Ding Rui et al. (2021) reported the investigation of the inhibitory effect of aqueous extract of modified Xiao Xian Xiong Decoction. upon the epithelial mesenchymal transition (EMT）and the metastatasis ability of human gastric cancer MGC-803 cells mediated by Transforming Growth Factor-β1 (TGF-β1) which regulated Wnt5a/ Ca^{2+}/ activated T-cell nuclear factor（NFAT）signaling pathway. In this research, Transwell chamber experiment, scratch healing experiment, Western blot and immunofluorescence assay were utilised to elucidate cell invasion and migration ability， expression of EMT marker protein and key protein expression of Wnt5a/ Ca^{2+}/ NFAT pathway and intracellular Ca^{2+} concentration. Modified Xiao Xian Xiong Decoction comprised mainly Huanglian, Banxia, Gualou and added with Da huang (Rheum palmatum L), red Ginseng (Panax ginseng C.A.Mey), Baihuasheshecao (Oldenlandia diffusa Roxb), Fuling (Poria cocos Wolf), Yiyiren (Coix lacryma-jobi L), Sanqi (Panax notoginseng Burk), Gecko. The result obtained showed 40mg/L of modified Xiao Xian Xiong Decoction could significantly inhibit the invasion and migration of MGC-803 cells mediated by TGF-β1，up-regulate the level of E-cadherin，and down-regulate expressions of N-cadherin，Snail, Vimentin, Wnt5a, CaN and NFAT1 proteins and reduce the intracellular accumulation of Ca^{2+}. Thus, Ding Rui et al. (2021) concluded that that modified modified Xiao Xian Xiong Decoction could deactivate the EMT mediated by

TGF-β1 via Wnt5a/ Ca^{2+}/NFAT pathway as well as decreasing the metastatic potential of MGC-803 cells.

Ding Rui et al. (2020) reported that the effective components of Xiao Xian Xiong Decoction for anti-tumour effect can be summarized as follows: Huanglian (Berberine, Corkone, Palmatine, Coptisine, Quercetin), Banxia (Baicalein, Baicalin, β-Sitosterol, Stigmasterol), Gualou (α-Spinasterol, Diosmetin, Genkwanin, Vitamin E). The anti-tumor mechanism of the effective components of Xiao Xian Xiong Decoction was reported as mainly by inhibiting the development of epithelial mesenchymal transition (EMT) which induced the invasion and migration of tumour cells. Berberine in Huanglian could decrease the expression of GRP78 which inhibited proliferation and migration of SW480 colorectal cancer cells by acting on the Ephrin-B2 target (Gong C, et al., 2020). Berberine could inhibit ZR-75-30 breast cancer cell proliferation and migration (Ma W, et al., 2017); and by inhibiting arachidonic acid metabolism pathway and FAK phosphorylation (Zhao Hao Y et al., 2017). Berberine could inhibit the reproliferation of SKOV3 ovarian cancer cells induced by chemotherapy. Corkone could exert cytotoxicity on LNCaP prostate cancer cells in dose dependent manner (Murthy KN et al., 2015). Coptisine could play a protective role in the liver and inhibit the growth of liver cancer cells by augmenting expression of miR-122 via decreasing the expression of MMP-2, MMP-9 (Chai FN et al., 2018). Palmatine could inhibit the expression of oncogene COL1A1 and apoptosis suppressor gene Survivin as well as increasing the sensitivity of pancreatic tumour cells towards chemotherapeutic drug Gemcitabine

(Chakravarthy D et al., 2018). Quercetin could significantly reduce MDA-MB-231 breast cancer cell migration ability (Sun Yi and Gu Jun, 2015).

In Banxia, Baicalein could inhibit T24 bladder cancer cells, A375 and SK-MEL-28 melanoma tumour cell by blocking communication between JNK and MEK/ERK (Yang X et al., 2019). Baicalin could exert anti-proliferative effects in HeLa and SiHa cervical cancer cells by downregulating MMP2 and MMP-9 via inhibiting PKC/STAT3 signaling pathway (Wang Q et al., 2018). B-sitosterol could promote anti-tumour properties in mouse serum by expressing IFN-γ protein to inhibit expression of IL-6 and VEGF which significantly inhibited H22 growth of xenograft tumour of liver cancer in mice (Lin Ming-Zhu et al., 2017).

In Gualou, Diosmetin could inhibit invasion, migration and adhesion of MHcc97H and SK-HEP-1 liver cancer cells by downregulating the expression of MMP-2 and MMP-9 (Liu J et al., 2016). Diosmetin is the lavonoid glycoside generally derived from olive leaves and oranges. Diosmetin could induce G1 phase arrest and increase sensitization of A549/IR lung cancer cells towards radiotherapy by inhibiting activation of Akt signaling pathway. Moreover, Diosmetin could inhibit cancer growth by restraining the development of angiogenesis (Xu Z et al., 2017). Vitamin E had the anti-tumour potential by converting tocopherols (TOCs) to tocotrienols (TTs). γ-TT and δ-TT were known to have ability in suppressing the development of invasion, angiogenesis and metastasis in tumour cells (Constantinou C, et al., 2020).

Ding Rui et al. (2020) summarized the anti-tumour active ingredients of Xiao Xian Xiong Decoction and its molecular mechanism as blow:

Related Mechanism in tumour cells	Target genes		Tumour types	Active components		
	Up-regulation	Down-regulation		Huanglian	Banxia	Gualou
Inhibiting proliferation, invasion and migration	*p53，miR-122，IFN γ，pH2 AX，E-cadherin，CytC，TNF α，IL6/12，p27*	*GRP78，p-FAK，MMP-2/9/14，IL-6，Twist1，Snail，VEGF，Vimentin，p-ERK，p-JNK，p-MEK，H3，p-Akt，p-GSK 3 β，Ezrin，CCAT1，I κ B，p-p38*	Colorectal cancer, breast cancer, ovarian cancer, prostate cancer, liver cancer, skin tumours, oral cancer, cervical cancer, lung cancer, pancreatic cancer	Berberine, Corkone, Coptisine, Quercetin	β -Sitosterol, Baicalin, Stigmasterol, Baicalein	Diosmetin, Genkwanin
Inducing apoptosis and autophagy	*miR-19a，SOD，CytC，Caspase-3/7/8/9，p53，p62，Bad，Bax，AMPK，JNK，I κ B，FOXO3 a，Beclin-1，Atg5/12，Apaf-1，LC3-II*	*Bcl-2，Bcl-xL，c-Myc，ROS，p-ERK，p-Akt，p-mTOR，p-I κ B，NF κ B*	Non-small cell lung cancer, bladder cancer, pancreatic cancer, ovarian cancer, multiple myeloma, prostate cancer, breast cancer, colon cancer, thyroid cancer	Berberine, Corkone, Coptisine, Quercetin	β -Sitosterol, Baicalin, Baicalein	Diosmetin,
Inhibiting cell cycle progression	*Bax，p21，p53，DEPP，Caspase-3/8/9，c-Myc，BRCA1/2*	*cyclin B1，cyclinD1，Cdc2，Cdc25C，CCNB1/2，CCND3，CDKN1A，Cdk2/4/6*	Bladder cancer, pancreatic cancer, lung cancer, cervical cancer, colon cancer, breast cancer, ovarian cancer, prostate cancer, oral cancer	Berberine, Coptisine, Quercetin	Baicalin	α -Spinasterol, Diosmetin, Genkwanin

Increasing sensitization	*E-cadherin ， LC3BII，Snail γ*	*COL1A1 ， Survivin ， GLI1/2 ， p-Akt ， RAGE，N-cadherin*	Pancreatic cancer, thyroid cancer, lung cancer	Palmatine, Quercetin		Diosmetin
Inhibiting angiogenesis	*γ H2AX ， GSH, SOD*	*TNF α ， VEGF ， p-VEGFR-2， p-p53， p-DNA-PK ， FGF ， pFAK ， RAD51 ， p-ATM，Cox-2， p-Src， p-PCL ， IL-6 ， CXCL-8 ， LPO ， Ang-1 ， p-Bad，TIMP-1/2*	Cholangiocarcinoma, skin tumors		Sitosterol	Diosmetin, vitamin E
Regulating body immunity	*IL-2/12*	*TNF α ，TGF β ，IL-1 β ， IL-10 ， Fas ， FasL，TERT，ARG 1*	Thymus tumors, pancreatic cancer, colon cancer	Palmatine, Quercetin		Diosmetin,

2.2.3 Huanglian

Huanglian is a prevalently used Chinese herbs. Nowadays, Huanglians are conventionally obtained from commercial cultivation. Production from Sichuan Province of China is renowned for its genuine and excellent quality. Huanglian plant belongs to perennial herbs. The medicinal part of the plant is the root which is yellow in colour and encompasses plentiful fibrils. Huanglian leaves are basal and the stalk that joins a leaf to a stem is about 5 to 16cm in length. Blade is fine and as thin as a paper, its shape is ovate-triangular and about 10 cm in size with 3-lobes. Flower stems are 1 to 2 in number, equal or longer to leaf in length.

Lin et al. (2007) had carried out an *in vitro* experiment to examine the effects of berberine on cell viability and progression in human oral squamous carcinoma HSC-3 cells and reported that this metabolite in Huanglian inhibit cell growth in human HSC-3 oral cancer HSC-3 cells showed a significantly reduced rate of cell growth treated with Berberine in which Berberine induced a time and dose-dependent decrease in cell viability in Human HSC-3 Oral Cancer Cells. The result showed shown that Berberine induced a dose-dependent increase of ROS and Ca^{2+} production in HSC-3 cells. Flow cytometric analysis of mitochondrial membrane potential shown that Berberine induced a dose-dependent declination of levels of mitochondrial membrane potential. The Western Blot result showed Berberine induced time-dependent increase in activation of Caspase 3 and the expression of p53. Besides, Berberine promoted

the FAS and FADD levels in HSC-3 cells and eventually, Lin et al. (2007) concluded that Berberine resulted a decrease in anti-apoptotic Bcl-2 expression and an increase in pro- apoptotic BAX expression in a time-dependent manner, promoting caspase-3 activation in HSC-3 cells.

Li et al. (2000) had carried out an *in vitro* experiment to determine whether Huanglian could inhibit tumor cell growth modulating molecular events directly associated with the cell cycle and reported that herbal extract of Huanglian could inhibit cell growth by suppressing the expression of cyclin B1 and inhibited CDC2 Kinase activity in human gastric cancer MKN-74, human breast cancer MDA-468, colon cancer HCT-116 as well as human breast cancer MCF-7. The MTT assays result showed that Huanglian induced a time- and dose-dependent increase in inhibition of cell growth in all cell lines. Western blot analysis showed Huanglian suppressed cyclin B1 protein expression MKN-74 cells 5- to 8- fold after 48 hrs and 72 hrs, respectively, with a–tubulin controls. Besides, Northern blot analysis showed for cyclin B1 with β– actin controls and the overall mRNA content of the cells decreased over time. Huanglian decreases the expression of cyclin B1. The suppression of cyclin B1 protein resulted in a decrease in cdc2 kinase activity.

2.2.4 Banxia

Banxia (*Pinellia ternate* (Thunb.)Breit.) grows abundantly in swampy land and hillside. This plant is named as Banxia because in China, it begins blossoming in fifth month of lunar calendar which is in the middle of summer

season. It belongs to perennial herb of Araceae family. The height of plant is about 15 to 35 cm. Tuber is the medicinal portion in which it is almost spherical in shape with a diameter of approximately 0.5 to 3.0 cm. Banxia has warm and toxic medicinal properties. Its main functions are eliminating dampness in the body, removing phlegm, regulating normal flow of Qi and relieving vomit and resolving hard mass. It is mainly used to treat stomach and lung disorder caused by water retention. Raw plant of Banxia is toxic and not suitable for oral consumption without pre-treatment. Conventionally, it will be pre-treated with ginger to eliminate its toxicity before being utilised for medical purposes. However, it can be used externally such as to cure wounds bitten by snake.

Li et al. (2010) had carried out an in vitro experiment to assess the inhibitory effect of Banxia on CaSki, HeLa and HBL-100 cells as well as HPV *E6* gene. *E6* is the main early gene of HPVs. The main activities of E6 protein include down-regulation of p53 to avoid apoptosis and modulating transcription factor for immunity purposes (Howie et al., 2009). The MTT assays result showed that Banxia can inhibit cell proliferation in CaSki and HeLa where it induced a dose- and time-dependent decrease in cell viabilities of CaSki and HeLa. It had no obvious inhibition on the growth of HBL-100 cells except at a relative high dose (500 g/mL). Eventually, Li et al. (2010) concluded that Banxia downregulated Bcl-2, upregulated Bax, caspase-8 and caspase-3. Besides, it could downregulate gene expression of E6. Subsequently, it activated p53.

Cui Y et al. (2016) had carried out an *in vitro* experiment to check for cell inhitory effect of the effects of ethanol extracts of ginger Pinellia on gastric cancer SGC7901 cells. The MTT assays result showed that inhibition ability of ginger Banxia on SGC7901 cells depended on concentration. The result showed that Banxia can suppress cell cycle progression. Hence, ethanol extracts of Banxia could retard cell viability of SGC-7901 cells and was presenting a marked time-dose-response relationship.

2.2.5 Gualuo

Gualuo (*Trichosanthes kirilowii*) is a flowering plant which belongs to the family of Cucurbitaceae. It is one of the 50 fundamental herbs used in traditional Chinese medicine. The fruit of the plant is known as Gualouin Mandarin. The medical function is to remove body heat and eliminate phlegm, relieve stuffiness in chest, reduce abscesses and dissipate nodules (Bensky et al., 2004).

Hui et al. (2011) had carried out an *in vitro* experiment to investigate the effects of Fructus trichosanthis (FT) in human erythroleukemic K562 cells for their gamma-globin mRNA and HbF-induction activities as well as pathway involved. MTT assays result revealed that the concentration of drug was the determining factor for cell inhibitory effect. Western blot showed that expression of p38 was induced during entire period; ERK deregulated upon FT treatment depending on drug concentration. These results indicated that activation of p38

is essential for FT induced fetal haemoglobin production. Hui et al. (2011) concluded that Gualuo could elevate γ-globin mRNA expression and HbF levels in K562 cells and induced activation of P38 MAPK pathways.

Wen Wang et al. (2018) had carried out an *in vitro* experiment to effects of Trichosanthin (TCS) in NPC cell line SUNE-1upon radiation treatment. Flow cytometric analysis showed radiation and TCS treatment suppress tumour cell development. Western blot result showed deregulation of SUNE-1 cells. Wen Wang et al. (2018) concluded that TCS with combined radiation treatment could enhance inhibitory effect to SUNE-1 cells.

Liu et al. (2012) had carried out an *in vitro* experiment to explore the medicinal potential of Trichosanthin on NPC cell line CNE2. Result of MTT assay revealed that TCS exhibit inhibitory effect on CNE-2 depended on concentration of drug. Moreover, Western blot showed expression of NICD and Hes-1increased with higher concentration of drug. Liu et al. (2012) concluded that TCS down-regulated Hes-1 and NICD of Notch signaling pathway and protein levels and further suggested that TCS might be an effective medicine to cure NPC.

CHAPTER 3

MATERIALS AND METHODS

3.1 Mediums and reagents

Dulbecco modified Eagle medium (DMEM) supplemented with 4.5 g glucose/L and 300 mg/L glutamine was purchased from Hyclone Laboratories Inc. (Logan, Utah, United States). Roswell Park Memorial Institute 1640 (RPMI-1640) powder was purchased from Mediatech, Inc. (Manassas, USA). The medium was prepared at 10.39g/L in ultrapure water and added with sodium bicarbonates 2 g/L. Fetal bovine serum (FBS) was purchased from Lonza Inc. (Allendale, NJ, USA). MTT reagents and phosphate buffer saline (PBS) were procured from Merck (Germany). All other chemicals were of analytical grade and commercially available.

3.2 Aqueous-extraction of the individual and combination herbs

The herbs were purchased from Tongrentang (M) Sdn. Bhd Petaling Jaya Selangor. Table 3.1 indicated the names of herbs and the weight in gramme used for preparation. Based on the traditional prescription preparation ratio specified from ancient China, the ratio proportion was 1:2:5. The materials were immersed

in water for half hour. The materials were boiled with water for 30 minutes. After that, cool the solution and collected with filtration by whatman paper. Later, lyophilized the filtrates and put in -20 ^{o}C refrigerator.

Group	**Name of herb**	**Weight (g)**
L1	Huanglian(*Coptis chinensis* Franch)	60g
L2	Banxia (*Pinellia ternate*)	120g
L3	Gualuo (*Trichosanthes kirilowaii*)	300g
L4	Huanglian + Banxia	60g + 120g
L5	Huanglian + Gualuo	60g + 300g
L6	Banxia + Gualuo	120g +300g
L7	Huanglian + Banxia + Gualuo	60g +120g + 300g

Table 3.1: Indication for names of material and weight for single and combination herbs

Figure 3.1: Photographs above show for preparation process of decoction and lyophilisation

3.3 NPC Cells cultivation method

Table 3.2 shows names of NPC cells types and mediums used for each cell cultivation. A humidified CO_2 incubator at 37 ℃ in 5.0 % CO_2 and 95.0 % air were set up to facilitate cultivation of cells.HK-1 was provided by Professor S.W. Tsao from the Department of Anatomy, University of Hong Kong, Hong Kong, China. C666-1 was provided by Professor K.W. Lo from Prince and Wales of Hospital, Hong Kong, China. CNE-2, HONE-1 CNE-1, SUNE-1, TWO-1and TWO-4 were obtained from Dr. Yap Lee Fah from the Department of Oral Biology and Biomedical Sciences, Faculty of Dentistry, University of Malaya, Malaysia. 10 % FBS was used to enrich medium.

Table 3.2: The types of human NPC cell lines

Cell line	Cell type	Medium
TWO-1	EBV-negative epithelial NPC	DMEM
TWO-4	Epithelial NPC	RPMI 1640
HONE-1	poorly differentiated squamous NPC	RPMI 1640
HK-1	differentiated squamous carcinoma	RPMI 1640
C666-1	Undifferentiated squamous	RPMI 1640
SUNE-1	undifferentiated epithelial carcinoma.	RPMI 1640
CNE-1	Lymphoblast differentiated squamous carcinoma (EBV- negative)	DMEM
CNE-2	poorly differentiated epithelial carcinoma.	RPMI 1640

3.4 Metabolite profiling of the individual and combination herbal extracts

LC-MS was adopted for finding metabolites profiling and it was conducted in Monash University, Malaysia The lyophilized extract for each sample was dissolved in pure water and was prepared for 100 ppm (part per million) which is equal to 0.1 mg/mL.

Figure 3.2: LCMS equipment in Monash University Laboratory

3.4.1 Instrumentation set up

The Liquid Chromatography-Mass Spectrometry system was equipped with Agilent 1290 Infinity LC system coupled to Agilent 6520 Accurate-Mass Q-TOF mass spectrometer with dual ESI source.

For Liquid Chromatography (LC) system, the employed column was Agilent Zorbax Eclipse XDB-C18, Narrow-Bore 2.1x150mm, 3.5 micron (P/N: 930990-902). The mobile phases were 0.1% formic acid in water (A) and 90 % acetonitrile in water 0.1 % formic acid (B) at a flow rate of 0.5mL min^{-1} where the injection volume was 1.0 µL. The temperature of column was at 25^0C and auto sampler temperature was at 4^0C. The LC conditions were set at 5 % B

during 0–5 min, a linear increase from 5 to 100 % B during 5–20 min and maintained at 100% B during 20–25 min with post run time of 5 minutes.

The Mass Spectrometry (MS) parameter for the Agilent 6520 Accurate-Mass Q-TOF mass spectrometer is as follows: The mode was mass spectrometry only, with negative ion polarity. Voltage for Vcap, Fragmentor, Skimmer and OCT 1 RF Vpp was 3500V, 125V, 65V and 750V respectively. Capacity of drying gas was 10L/min. Gas temperature was 300^{o}C and the pressure of nebuliser was 45psig. Mass range (m/z) was between 100 (Min) to 3200 (Max). Reference ions used was between 119.03632 to 966.000725. Acquisition rate (spectra/s) was 1.03 and acquisition time (ms/spectrum) was 973. Transients per spectrum was 9632.

For data analysis, Agilent Mass Hunter Qualitative Analysis B.05.00 was used and method adopted was Metabolomics-SA-2017.m. Raw data was processed with Molecular Feature Extraction (MFE), with below settings: Extraction algorithm: Small molecule (chromatographic); Peak Filters: Use peaks with height >=100 counts; Input data range: 400-500m/z; Compound Filters: Only look for compound with absolute height >=5000 counts and relative height >=2.5%; Ion species: Allow positive ions: H^+, Na^+, K^+, NH_4^+ and negative ions: H^-, Cl^-; Isotope grouping: Peak spacing tolerance 0.0025 m/z plus 7.0ppm, isotope model - common organic molecules; Limit assigned charge states to a maximum of 2.

Detected constituents were matched with METLIN_AM_PCDL-N-130328.cdb database. The parameters are as below: Value to match: Mass; Match tolerance: 5 ppm; Spectrum peak searches: Maximum number of peaks to search when peaks are not specified graphically: 5; Positive Ions H^+, Na^+, NH_4^+ and Negative Ions: H^-, Charge state range: 1-2.

3.5 Finding for Optimal Cell Seeding Concentration

The finding of optimum cell seeding density of each cell line was conducted by using MTT assay. The experiment was carried out by seeding cultivated cell lines into a 96-well plate before the cell viability assessment by MTT assays and kept for incubation in a time span of three days. The number of cells in the each well with reagent was as follows: $2.5x10^3$, $5x10^3$, $10x10^3$, $20x10^3$ and $40x10^3$ and $80x10^3$ cells/mL. After the MTT test, the value of absorbance for cell in each well was collected in a spectrophotometer and the reading was set as 570 nm for absorbance. After that, draw a graph for absorbance against cell density. Eventually, from the graph, the middle point of exponential phase on the curved line was adopted as optimum cell concentration. This optimum value of cell concentration can be utilised for future work of seeding the particular cell line in assessing the cell viability and finding half-maximal inhibitory concentration of particular drug material.

3.6 MTT assay

Before the MTT assay experiment started, cultivation of the particular cell line was carried out. Firstly, seeding the cells by its optimum concentration assessed before and seeded them in wells for 100 μL in well plate. Triplicate sample were prepared for each cell density and triplicate control were prepared. The negative control was the well filling with 100 μL of medium and the positive control was the well filling with 100 μL of cells but would not be added with drug later. Positive and negative control were prepared in triplicate too. When the cells had been incubated for 1 day, add 10 μL fresh drug reagent mixture into the wells. The drug concentration was as follows: 100, 50, 25, 12.5, 6.25 and 3.125 μg/ml. Then 90 μL of medium was added up and the cells again were incubated for another three days. After that, removed the solution and the well was added in 200 μL new regent. Volume of 20 μL MTT was pippetted into the well and again put into the incubator for three hours. Later, centifiged the well plates at 3000 rpm for 5 minutes in a temperature of 5 ℃. Then took away the solution for 180 μL and added in 200 μL of DMSO. Kept the mixture in the dark for 15 minutes after shaking it lightly. Each experiment was performem three times separately. Eventually, the well plate was put in spectrophotometer and absorbance was collected. The half maximal inhibitory concentration was evaluated from the graph plotting cell viability against drug concentration.

3.7 RNA extraction

Direct-zol™ RNA Miniprep Plus tools was adopted for carrying out RNA extraction. First of all, prepare gel from mixing 1g of Agarose1% with 100mL of TAE Buffer. Heat up the mixture for 2 minutes with medium heat intensity and meanwhile, added 3 μL of stain into it and stir well. Finally, put the mixture into a cast for electrophoresis purpose when RNA extraction was completed.

The second step was the sample preparation. 600 μL of TRIZO Reagent was added into the cell pellet in the falcon tube and.

The third step was purification. Equal amount of ethanol (600 μL) was topped up and mixed well and transferredthe mixture into a column in a collecting tube and then centrifuged at a speed of 16,000xg for 30 seconds at 4 ℃. Then, transferred the column into another collecting tube and centrifuged again. Removed the flow out. Added the balance from falcon tube into new collecting tube and removed the flow out. Then, added 400 μL of RNA wash buffer and and centrifuged again. Removed the flow out. Mixed 5 μL DNase with 75 μL μl DNA Digestion Buffer in a 1.5mL centrifuge tube. Added the mixture into each column and incubated for 15 minutes. Later, added 40 of 0 μL RNA PreWash into the column and centrifuged and removed the flow out and repeated the step. Then, mixed 700 μL RNA wash buffer to the columnand centrifuged for 2 minutes. Transferred the column to an RNase free tube. Now,

eluted the RNA by adding 50 µL of DNase/RNase free water directly into the column and centrifuged. Put the RNA into 7 µL centrifuged tube. Eventually, frozen the RNA at ≤-70 ℃.

Spectrophotometer was used to check the purity of RNA by referring the 260 nm/280 nm ratio. For pure and undegraded RNA, the standard 260 nm/280 nm ratio is 1.8~2. For running electrophoresis, used voltage at 90 volts with MA unchanged and running time was 60 minutes. When having added 2 µL of loading Buffer or parafilm. Dripped 4 µ/L of elution into the gel.

Figure 3.3: Direct-zol™ RNA Miniprep Plus kit

3.8 Nanostring sample preparation

Table 3.3 below indicates the activities in each process and duration as well as estimated time

Process	Duration	Estimated time
1. Hybridization	1 hour	Day 1: 3- 4.00 pm
2. Overnight hybridization in thermocycler	At least 16 hours	Day1: 4.00 pm to Day 2: 8.30- 9.00 am
3. Prep Station	2.5 hr/cartridge	Day 2: Cartridge 1: 9.30 am- 12.00 pm
4. Digital Analyzer	2.5 hr/cartridge	Day 2: Cartridge 1: 12.00pm- 2.30pm

Table 3.3: Procedure for preparing sample for Nanostring assays

There were four processes for carring out the assays. The procedure is presented as follows:

1. The set up for hybridization. First of all, making master mix by mixing 70 μL of hybridization buffer to reporter codeset.

2. mixed 5 μL of RNA samples to 8 μL of Master Mix.

3. Added 2 μL of Capture Probe Set to master mix.

4. making 12 tubes filling the mixture. 4 tubes for test of I time point.

5. incubated mixture in thermocycler at 65 ℃ for for time span of 16 hours.

6. purified the mixture with MAX/FLEX in the nCounter Prep Station

7. immobilized target-probe complexes onto nCounter Cartridges for 2.5 hours

8. scanned cartridges in nCounter Digital Analyzer for 2.5 hours.

9. Reporter Code Count file was produced for each sample.

10. The nSolver 4.0 software was used to analysize the result

11. 10 housekeeping genes were used to normalize the result.

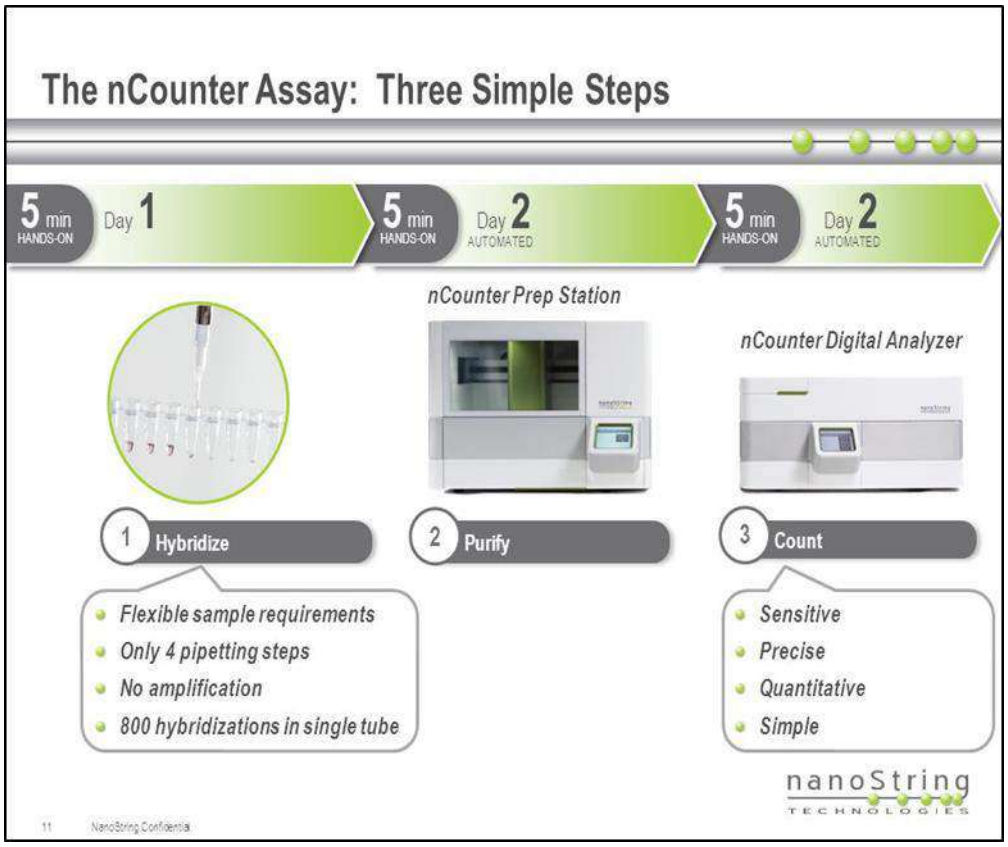

Figure 3.4: Illustration of Nanostring sample preparation procedure

CHAPTER 4

RESULTS

4.1 Metabolite profiling of the individual and combination herbal extracts

As the objectives of this research project include preparing the aqueous-extracted of individual herb such as L1 (Huanglian) (*Coptis chinensis* Franch. *C. deltoidea, or C. teeta* Wall), L2 (Banxia) (*Pinellia ternate (*Thunb.)Breit.), and L3 (Gualuo) (*Trichosanthes kirilowaii* Maxim. *or Trichosanthes rosthornii* Harms) and combination extracts such as L4 (Huanglian and Banxia); L5 (Huanglian and Gualuo); L6 (Banxia and Gualuo); L7 (Huanglian, Banxia and Gualuo). Subsequently the prepared samples were sent to investigate the metabolite profiling by Liquid chromatography– mass spectrometry (LC-MS). The result of LC-MS in each sample revealed that active components was found to consist of primary and secondary metabolites. The percentage of each metabolite in 7 samples namely L1 to L7 are illustrated in single chart and the detail of each compound are listed in the following tables. Each metabolite presented in the chart was inclusive of positive (+ve) and negative (-ve) electrospray ionization (ESI) which were listed in tble of metabolites classification.

4.1.1 L1 (Huanglian)

L1 (Huanglian) consisted of both primary and secondary metabolites. As shown in Figure 4.1, the primary metabolites were made up of amino acid (7 %), Carbohydrate (3 %), Fatty acid (10 %), protein (3 %), vitamin (3 %). Secondary metabolites comprised alkaloid (34 %), glucoside (7 %), phenolic (27 %), phthalide (3 %) and terpene (3 %). The comparative ratio of primary metabolites to secondary metabolites was 26 % to 76 %. Moreover, among the metabolites composition, Alkaloid was found to have highest percentage (34 %) and phenolic was the second in the list (27 %). In L1 (Huanglian), alkaloid composition was made up of purine, hydroxypyrimidines, allylamine, isoquinolines, protoberberine, flavoalkaloid and morpholines. By the way, phenolic composed of coumaric acids and derivatives, carboxylic acids and derivatives, beta hydroxy acids and derivatives, quinic acid, phenylpropanoic acids and phenolic compounds.

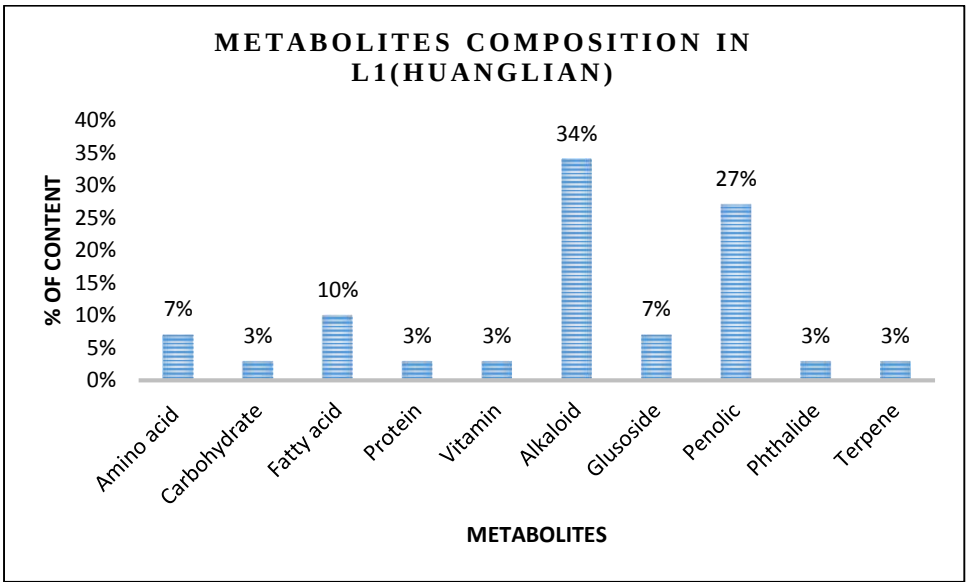

Figure 4.1(i) Chart representing metabolites composition in L1 (Huanglian)

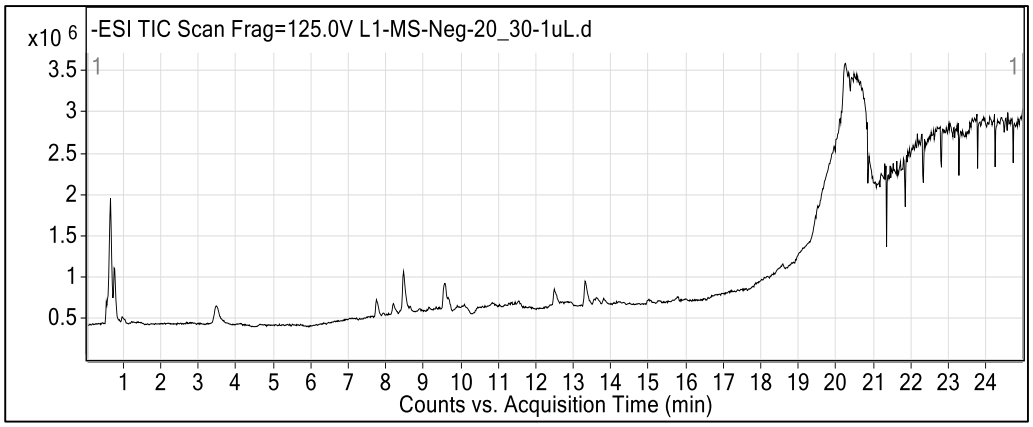

Figure 4.1(ii) Total ion current diagram (-ve) for L1 (Huanglian)

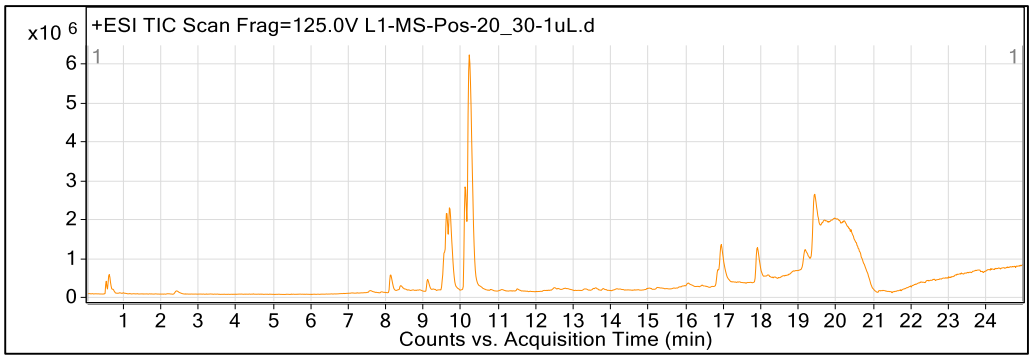

Figure 4.1(iii) Total ion current diagram (+ve) for L1 (Huanglian)

No	Formula	Cmpd Name	Retention Time (RT)	Mass	Cmpd classification	Metabolite
1	C5 H13 O7 P	2-C-Methyl-D-erythritol 4-phosphate	0.634	216.041	Enzyme	Protein
2	C7 H8 N4 O3	3,9-Dimethyluric acid	0.639	196.0593	purine	Alkaloid
3	C8 H10 N4 O4	5-Acetylamino-6-formylamino-3-methyluracil	0.642	226.0699	hydroxypyrimidines	Alkaloid
4	C6 H6 N4 O2	1-Methylxanthine	0.644	166.0483	purine	Alkaloid
5	C7 H8 N4 O2	Theobromine	0.647	180.0645	purine	Alkaloid
6	C12 H22 O11	Nigerose (Sakebiose)	0.667	342.1176	Disaccharide	Carbohydrate
7	C12 H25 N2 O10 P	Fructoselysine 6-phosphate	0.67	388.1229	L-lysine derivative	Amino acid
8	C7 H10 O5	6,7-dihydroxy-4-oxo-2-heptenoic acid	0.752	174.0532	Fatty Acids and Conjugates	Fatty acid
9	C10 H12 O7 S	Dihydroferulic acid 4-sulfate	0.771	276.0296	coumaric acids and derivatives	Phenolic
10	C4 H6 O5	D-(+)-Malic acid	0.772	134.0221	beta hydroxy acids and derivatives.	Phenolic
11	C4 H4 O4	Fumaric acid	0.773	116.0113	dicarboxylic acids and derivatives	Phenolic
12	C6 H8 O7	Citric acid	0.972	192.0271	tricarboxylic acids and derivatives	Phenolic
13	C5 H7 N O3	N-Acryloylglycine	0.995	129.0425	n-acyl-alpha amino acids.	Amino acid
14	C15 H20 O9	3-Methoxy-4-hydroxyphenylglycol glucuronide	3.052	344.1108	phenolic glycosides	phenolic glycosides
15	C15 H20 O10	Domesticoside	3.494	360.106	phenolic glycosides	phenolic glycosides
16	C17 H20 O9	3-O-Feruloylquinic acid	7.763	368.1106	quinic acid	Phenolic
17	C20 H23 N O4	Carboxyterbinafine derivative2	8.211	341.163	allylamine	Alkaloid
18	C17 H20 O9	3-O-Feruloylquinic acid	8.48	368.1109	quinic acid	Phenolic
19	C19 H17 N O4	N-Methoxycarbonylanonaine	8.512	187.1207	isoquinolines	Alkaloid

20	C20 H21 N O4	Papaverine	9.161	323.1158	isoquinolines	Alkaloid
21	C27 H38 O2	25-hydroxy-16,17,23,23,24,24-hexadehydrovitamin D3 / 25-hydroxy-16,17,23,23,24,24-hexadehydrocholecalciferol	20.906	394.2829	25-Hydroxyvitamin D3 (calcifediol)	Vitamin D

Table 4.1 L1 (Huanglian) Metabolite Classification (-ve ESI)

No	Formula	Cmpd Name	Retention Time (RT)	Mass	Cmpd classification	Metabolite
1	C20 H23 N O4	Cularine	8.138	341.1636	protoberberine	Alkaloid
2	C20 H14 O4	8-O-Methyltetrangulol	9.63	318.0907	tetraphenes	Terpene
3	C20 H19 N O4	Isoficine	9.641	337.1325	flavoalkaloid	Alkaloid
4	C21 H21 N O4	RCS-4 N-(5-carboxypentyl) metabolite	10.13	351.1477	lipid	Fatty acid
5	C20 H14 O4	Musanolone F	10.246	318.0899	phenylpropanoic acids	Phenolic
6	C16 H22 O4	Emmotin A	16.952	278.1526	phenolic compounds	Phenolic
7	C12 H12 O3	3-Butylidene-7-hydroxyphthalide	16.959	204.0789	phthalide monomers	Phthalide
8	C20 H34 O8	Acetyl tributyl citrate	17.917	402.2254	tetracarboxylic acids	Phenolic
9	C16 H33 N O	Palmitic amide	19.202	255.2567	fatty amides	Fatty acid
10	C18 H35 N O	Dodemorph	19.471	281.2724	morpholines	Alkaloid

Table 4.2 L1 (Huanglian) Metabolite Classification (+ve ESI)

4.1.2 L2 (Banxia)

L2 (Banxia) consisted of both primary and secondary metabolites. As shown in Figure 4.2, the primary metabolites were made up of amino acid (14 %), Fatty acid (25 %), protein (16 %) and glucose (16 %). Secondary metabolites comprised alkaloid (14%), phenolic (21 %), phthalide (2 %), pteridine (2 %), saponin (2 %) and terpene (2 %). Among secondary metabolites, phenolic (21 %) and alkaloid (14 %) had the first and second highest abundancy. The comparative ratio of primary metabolites to secondary metabolites was 57 % to 43 %. Moreover, among the metabolites composition, fatty acid was found to have highest percentage (25 %) and phenolic was the second in the list (21 %). In L2 (Banxia), phenolic composed of tannin, Erythronic acid, tricarboxylic acid, glucoside, phenol. By the way, alkaloid composition was made up of xanthine alkaloid, carboxamide, terpenoids, phenylpropanoid and morpholines.

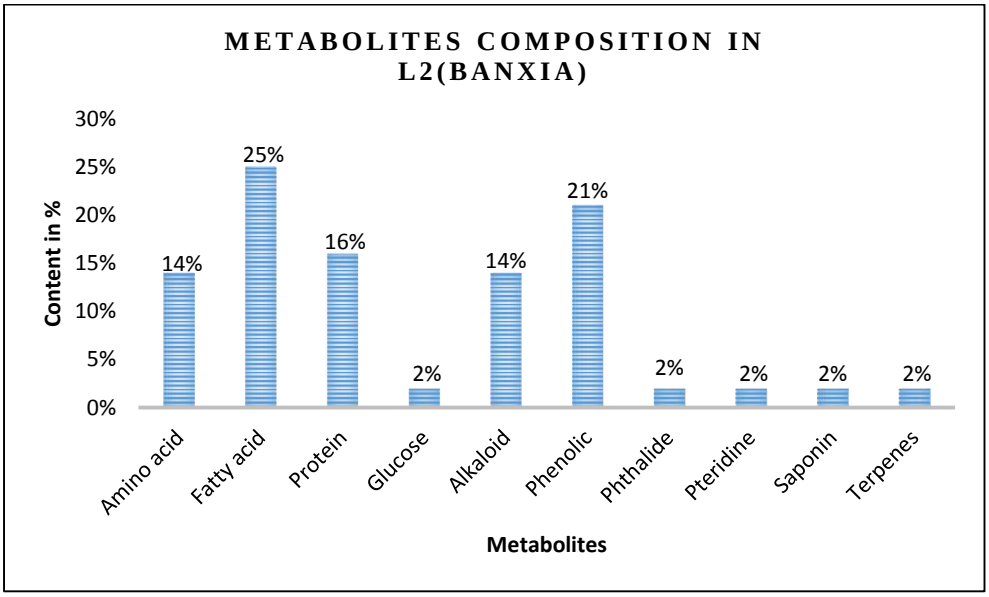

Figure 4.2(i) Chart representing metabolites composition in L2 (Banxia)

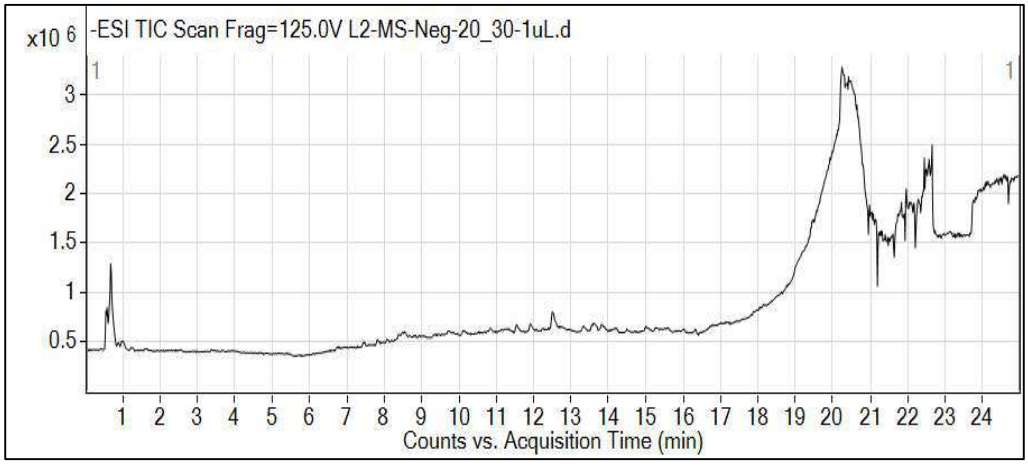

Figure 4.2(ii) Total ion current diagram (-ve) for L2 (Banxia)

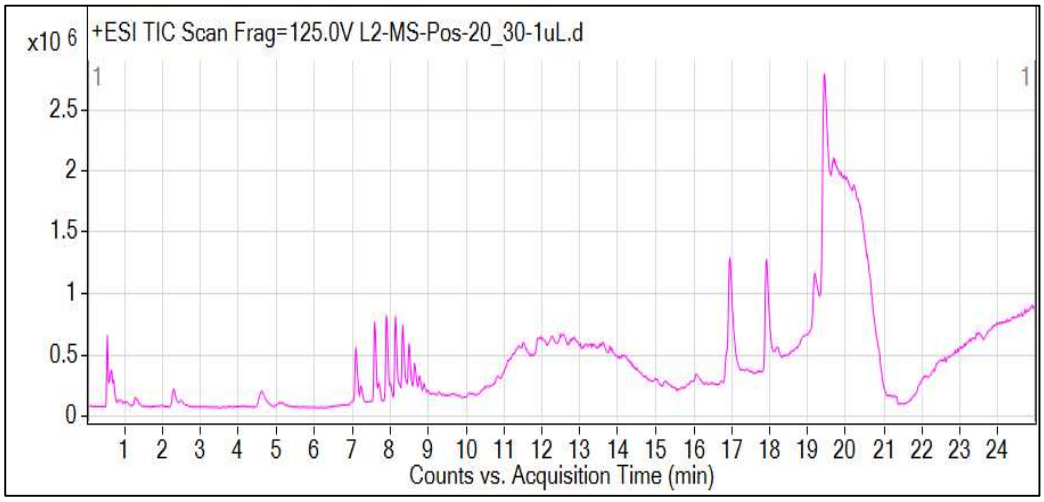

Figure 4.2(iii) Total ion current diagram (+ve) for L2 (Banxia)

No	Formula	Compound name	Retention time (min)	Mass	Compound classification	Classification of Metabolite
1	C5 H9 N O4	L-Glutamate	0.636	147.0532	amino acid	Amino acid
2	C6 H12 O7	D-Mannonate	0.643	196.0584	mannonate dehydratase	Enzyme
3	C5 H10 O6	Apionic acid	0.644	166.0473	Tannin	Phenolic
4	C4 H8 O5	Erythronic acid	0.652	136.0374	D-Erythronolactone	Phenolic
5	C7 H8 N4 O2	Theobromine	0.687	180.0648	xanthine alkaloid	Alkaloid
6	C6 H6 N4 O	1-Methylhypoxanthine	0.694	150.0537	hypoxanthine	Alkaloid
7	C7 H6 N4 O3	6-(Hydroxymethyl)-2,4(1H,3H)-pteridinedione	0.698	194.0441	pteridines	Pteridine
8	C5 H4 N4	Purine	0.742	120.0437	Purine	nucleic acid
9	C5 H10 S2	3,3-Dimethyl-1,2-dithiolane	0.898	134.0228	dithiolane	Protein
10	C6 H8 O7	Citric acid	0.975	192.0272	tricarboxylic acid	Phenolic
11	C5 H7 N O3	N-Acryloylglycine	0.996	129.0426	n-acyl-alpha amino acids.	Amino acid
12	C5 H10 N2 O3	Isoglutamine	1.02	146.0689	glutamic acid	Amino acid
13	C4 H6 O4	Erythrono-1,4-lactone	1.241	118.0269	Carboxylic acid	Phenolic
14	C6 H12 O5	Digitoxic acid	1.608	164.0683	glycoside	Phenolic
15	C8 H16 O6	Ethyl beta-D-glucopyranoside	3.411	208.0943	ethyl glucoside	Phenolic
16	C10 H20 O7	2,3-Butanediol glucoside	6.76	252.1208	acetoin glucoside	Phenolic
17	C15 H24 N4 O5	Pro Gln Pro	7.817	340.1733	dipeptide	Protein
18	C24 H40 O7 S	3-Sulfodeoxycholic acid	8.488	472.2514	sphingolipids	Lipid
19	C9 H17 N O3	KAPA	8.515	187.1205		
20	C27 H48 O9 S	5beta-scymnol sulfate	8.546	548.3037	steroid sulfate oxoanion	Steroid Alkaloid
21	C9 H16 O4	Nonic Acid	9.734	188.1049	dicarboxylic acid.	Lipid
22	C11 H21 N O3	Ethyl 3-(N-butylacetamido)propionate	10.12	215.1519	carboxamide	Alkaloid
23	C42 H62 O16	Licoricesaponin K2	11.914	822.4026	Triterpenoid saponins	Saponin

24	**C13 H18 O3**	**(6S)-dehydrovomifoliol**	**12.507**	**222.1252**	**terpenoids**	**Alkaloid**
25	**C17 H26 O4**	**Gingerol**	**13.332**	**294.1832**	**Phenol**	**Phenolic**
26	**C20 H23 D9 O5**	**Prostaglandin D2-d9**	**13.569**	**361.2826**	**arachidonic acid**	**Fatty acid**
27	**C17 H26 O5**	**methyl 8-[2-(2-formyl-vinyl)-3-hydroxy-5-oxo-cyclopentyl]-octanoate**	**13.65**	**310.178**	**fatty acid methyl ester**	**Lipid**
28	**C20 H23 D9 O5**	**Prostaglandin D2-d9**	**13.826**	**361.2825**	**arachidonic acid**	**Fatty acid**
29	**C17 H26 O4**	**Gingerol**	**14.224**	**294.1823**	**polyphenols**	**Phenolic**
30	**C17 H26 O3**	**6-Paradol**	**15.013**	**278.1875**	**phenols**	**Phenolic**
31	**C14 H26 O4**	**Diisobutyl adipate**	**15.277**	**258.1833**	**fatty acid ester.**	**Lipid**
32	**C15 H22 O2**	**Curcumenol**	**16.021**	**234.1619**	**sesquiterpenoid.**	**Alkaloid**
33	**C14 H21 N O3**	**Furmecyclox**	**17.146**	**251.1517**	**hydroxamic acid**	**Lipid**
34	**C28 H42 N2 O3 S**	**N-(2'-(4-benzenesulfonamide)-ethyl) arachidonoyl amine**	**19.086**	**486.2902**	**Fatty amides**	**Lipid**

Table 4.3 L2 (Banxia) Classification of metabolite (-ve ESI)

No	Formula	Compound name	Retention time (min)	Mass	classification of compound	Classification of Metabolite
1	C11 H10 N2 S	ANTU	0.547	202.0569	naphthalenes.	Terpenes
2	C5 H13 N O	2-Amino-3-methyl-1-butanol	0.609	103.1002	amino alcohol	Amino acid
3	C5 H9 N O2	D-Proline	0.65	115.0635	proteinogenic amino acid	Amino acid
4	C6 H10 O5	Levoglucosan	0.667	162.0535	anhydrous sugar	Glucose
5	C5 H11 N3 O2	Fibrin	0.725	145.0855	protein	protein
6	C6 H13 N O2	L-Leucine	1.069	131.0941	amino acid	Amino acid
7	C11 H18 N4 O2	Pirimicarb	4.624	238.1421	dimethylcarbamic acid	Amino acid
8	C15 H24 N4 O5	Pro Gln Pro	7.708	340.174	dipeptide	protein
9	C18 H33 N O2	(4E,8E,10E-d18:3)sphingosine	15.907	295.2506	Lipid	Lipid
10	C16 H22 O4	Emmotin A	16.957	278.152	phenolic compounds	Phenolic
11	C12 H12 O3	3-Butylidene-7-hydroxyphthalide	16.96	204.0784	Phthalide	Phthlide
12	C21 H30 N4 O4	Val Trp Val	17.918	402.2265	dipeptide	protein
13	C16 H24 O7	Rhododendrin	17.918	328.1529	glycoside and a phenylpropanoid	Alkaloid
14	C23 H34 N4 O4	Leu Leu Trp	17.92	430.2574	tripeptide	Protein
15	C16 H33 N O	Palmitic amide	19.201	255.2568	fatty amide	Lipid
16	C18 H35 N O	Dodemorph	19.467	281.2723	morpholines	Alkaloid
17	C23 H45 N O3	N-stearoyl valine	20.422	383.3396	fatty amide	Lipid
18	C18 H37 N O	Stearamide	20.906	283.2873	fatty acid amide	Lipid

Table 4.4 L2 (Banxia) Classification of metabolite (+ve ESI)

4.1.3 L3 (Gualou)

L3 (Gualou) consisted of both primary and secondary metabolites. As shown in Figure 4.3, the primary metabolites were made up of amino acid (15 %), carbohydrate (3 %), fatty acid (27 %), glucose (3 %) and protein (5 %). Secondary metabolites comprised alkaloid (18 %), benzamide (3 %), phenolic (17 %), phthalide (3 %), phthalate (3 %) and terpene (3 %). Among secondary metabolites, alkaloid (18 %) and phenolic (17 %) had the first and second highest abundancy. The comparative ratio of primary metabolites to secondary metabolites was 53 % to 47 %. Moreover, among the total metabolites composition, fatty acid was found to have highest percentage (27 %) and alkanoid was the second in the list (18 %). In L3 (Gualou), alkaloid composition was made up of indoles, purine, carbohydrazide, pyrrolidine alkaloid. By the way, phenolic composed of dicarboxylic acid, polyphenols and tricarboxylic acid.

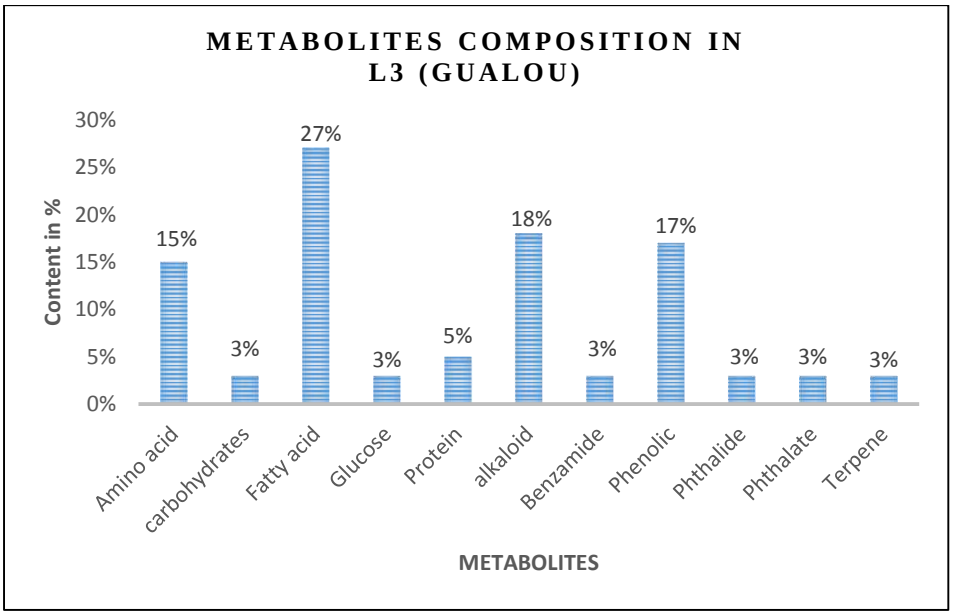

Figure 4.3(i) Chart representing metabolites composition in L3 (Gualou)

Figure 4.3(ii) Total ion current diagram (-ve) for L3 (Gualou)

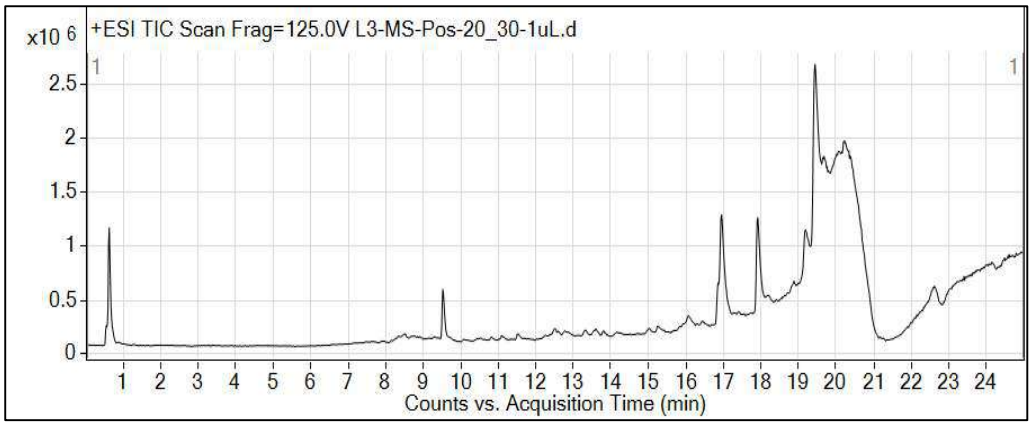

Figure 4.3(iii) Total ion current diagram (+ve) for L3 (Gualou)

Table 4.5 L3 (Gualou) Classification of metabolite (-ve ESI)

No	Formula	Compound Label	Retention time (min)	Mass	compound classification	classification of metabolite
1	C11 H10 N2 O S	Cpd 1: 3-(Isothiocyanatomethyl)-1-methoxy-1H-indole	0.633	218.0521	indoles	Alkaloid
2	C12 H8 O4	Cpd 3: Isobergaptene	0.633	278.0409	furanocoumarin.	Coumarin
3	C7 H10 N4 O2	Cpd 4: Lathyrine	0.635	216.0414	L-alpha-amino acid.	Amino acid
4	C8 H12 N4 O4	Cpd 5: Decitabine	0.639	182.0801	cytosine analogue	unknown
5	C6 H6 N4 O2	Cpd 6: 1-Methylxanthine	0.64	228.0851	Purine alkaloids	Alkaloid
6	C7 H8 N4 O3	Cpd 7: 1,9-Dimethyluric acid	0.641	166.049	xanthines (purine derivatives)	Alkaloid
7	C8 H10 N4 O4	Cpd 8: 5-Acetylamino-6-formylamino-3-methyluracil	0.643	196.0599	hydroxypyrimidines.	Alkaloid
8	C5 H4 N4	Cpd 9: Purine	0.643	226.0702	Purine	Alkaloid
9	C7 H8 N4 O2	Cpd 10: Theobromine	0.645	120.0436	alkaloid	Alkaloid
10	C7 H14 S2	Cpd 11: (-)-1-Methylpropyl 1-propenyl disulfide	0.648	180.0649	organic disulfides	Essential oil
11	C19 H20 N4 O2 S2	Cpd 12: Elesclomol	0.65	162.0539	carbohydrazide	Alkaloid
12	C4 H6 O5	Cpd 14: D-(+)-Malic acid	0.771	134.0219	dicarboxylic acid	Phenolic
13	C6 H8 O7	Cpd 15: Citric acid	0.975	192.027	tricarboxylic acid	Phenolic
14	C9 H17 N O3	Cpd 16: KAPA	8.513	187.1207	unknown	unknown
15	C13 H18 O3	Cpd 22: (6S)-dehydrovomifoliol	12.508	222.1255	sesquiterpenoids.	Terpene
16	C17 H26 O4	Cpd 23: Gingerol	13.33	294.1831	polyphenols	Phenolic
17	C20 H23 D9 O5	Cpd 24: Prostaglandin D2-d9	13.571	361.2829	arachidonic acid	Fatty acid
18	C17 H26 O5	Cpd 25: methyl 8-[2-(2-formyl-vinyl)-3-hydroxy-5-oxo-cyclopentyl]-octanoate	13.65	310.1779	fatty acid methyl ester.	Terpene
19	C20 H23 D9 O5	Cpd 26: Prostaglandin D2-d9	13.825	361.2825	arachidonic acid	Fatty acid
20	C17 H26 O3	Cpd 27: 6-Paradol	15.008	278.1884	phenols	Phenolic
21	C28 H42 N2 O3 S	Cpd 28: N-(2'-(4-benzenesulfonamide)-ethyl) arachidonoyl amine	19.088	486.2901	sulfonamide	Fatty acid

No	Formula	Compound Label	Retention time (min)	Mass	Classification of compond	Classification of Metabolite
1	C6 H14 N4 O2	L-Arginine	0.593	174.1114	amino acid	Amino acid
2	C12 H24 N4 O7	N2-Fructopyranosylarginine	0.615	336.1645	arginine and derivatives.	Amino acid
3	C6 H14 O6	D-Sorbitol	0.62	182.0791	glucitol	Sugar
4	C10 H19 N O7	D-1-[(3-Carboxypropyl)amino]-1-deoxyfructose	0.625	265.1158	amino acids	Amino acid
5	C6 H10 N2 O3	4-Methylene-L-glutamine	0.63	158.0694	amino acid	Amino acid
6	C7 H14 N O3	(-)-Betonicine	0.631	160.0967	pyrrolidine alkaloid	Alkaloid
7	C16 H21 N5 O2	Alizapride	0.631	315.1691	substituted benzamide	Benzamide
8	C6 H10 O6	L-Galactono-1,4-lactone	0.636	178.0471	L-galactonic acid.	Enzyme
9	C6 H12 O6	L-Galactose	0.638	180.0629	monosaccharide	Carbohydrate
10	C6 H10 O5	3-Hydroxy-3-methyl-glutaric acid	0.641	162.0517	dicarboxylic acid	Phenolic
11	C17 H26 O5	methyl 8-[2-(2-formyl-vinyl)-3-hydroxy-5-oxo-cyclopentyl]-octanoate	13.622	310.1793	fatty acid methyl ester	Fatty acid
12	(4E,8E,10E-d18:3)sphingosine	(4E,8E,10E-d18:3)sphingosine	15.909	295.2506	LIPID	Lipid
13	Cpd 16: Emmotin A	Emmotin A	16.953	278.153	phenolic compounds	Phenolic
14	C12 H12 O3	3-Butylidene-7-hydroxyphthalide	16.957	204.0792	Phthalide	Phthlide
15	C16 H24 O7	tetranor-PGDM	17.918	328.152	Prostaglandin D Metabolite-d6	Fatty acid
16	C20 H34 O8	Acetyl tributyl citrate	17.919	402.2258	Phthalate Substitute Plasticizer	Phthalate
17	C23 H34 N4 O4	Leu Leu Trp	17.921	430.2568	dipeptide	Protein
18	C16 H33 N O	Palmitic amide	19.207	255.2563	fatty amides	Fatty acid
19	C18 H35 N O	Oleamide	19.462	281.2729	fatty amide	Fatty acid
20	C23 H45 N O3	N-stearoyl valine	20.425	383.3398	fatty acid amide	Fatty acid
21	C18 H37 N O	Stearamide	20.912	283.2887	fatty acid amide	Fatty acid

Table 4.6 L3 (Gualou) Classification of metabolite (+ve ESI)

4.1.4 L4 (Huanglian+ Banxia)

L4 (Huanglian+ Banxia) consisted of both primary and secondary metabolites. As shown in Figure 4.4, the primary metabolites were made up of amino acid (11 %), carbohydrate (4 %), fatty acid (7 %) and glucose (4 %). Secondary metabolites comprised alkaloid (41 %), phenolic (19 %), saponin (4%) and terpene (3 %). Among secondary metabolites, alkaloid (41 %) and phenolic (19 %) had the first and second highest abundancy. The comparative ratio of primary metabolites to secondary metabolites was 26 % to 68 %. Moreover, among the total metabolites composition, alkanoid was found to have highest percentage (41 %) and phenolic was the second in the list (19 %). In L4 (Huanglian + Banxia), alkaloid composition was made up of formamidopyrimidine, xanthine, quinic acid, terbinafine, opiate alkaloid, cularine, isoquinoline and cannabinoid. By the way, phenolic composed of carboxylic acid, phenolic glycosides, phenylpropanoic acids and tricarboxylic acid.

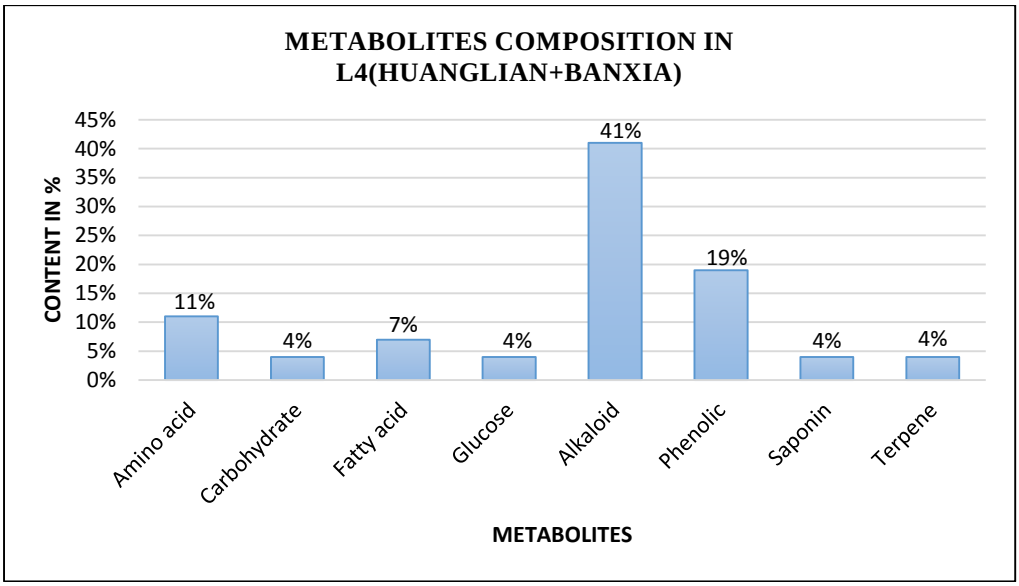

Figure 4.4 (i) Chart for metabolites composition in L4 (Huanglian + Banxia)

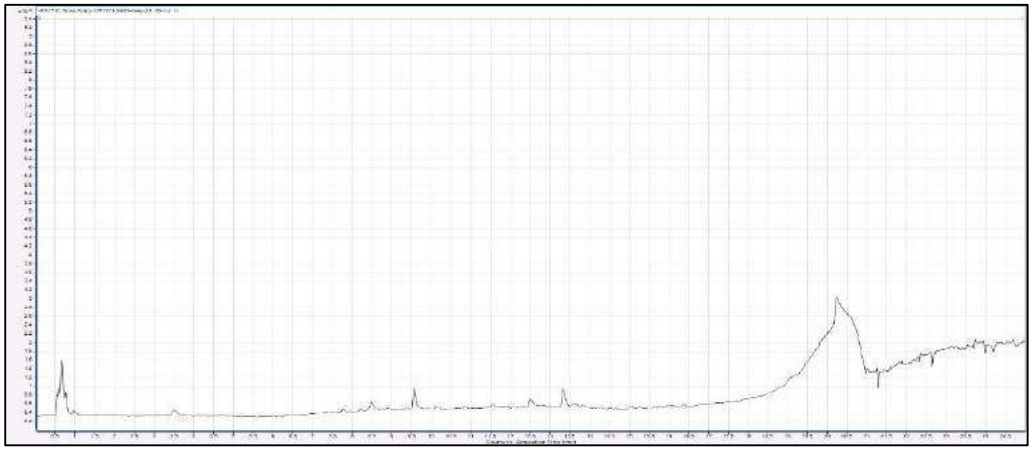

Figure 4.4 (ii) Total ion current diagram (-ve) for L4 (Huanglian + Banxia)

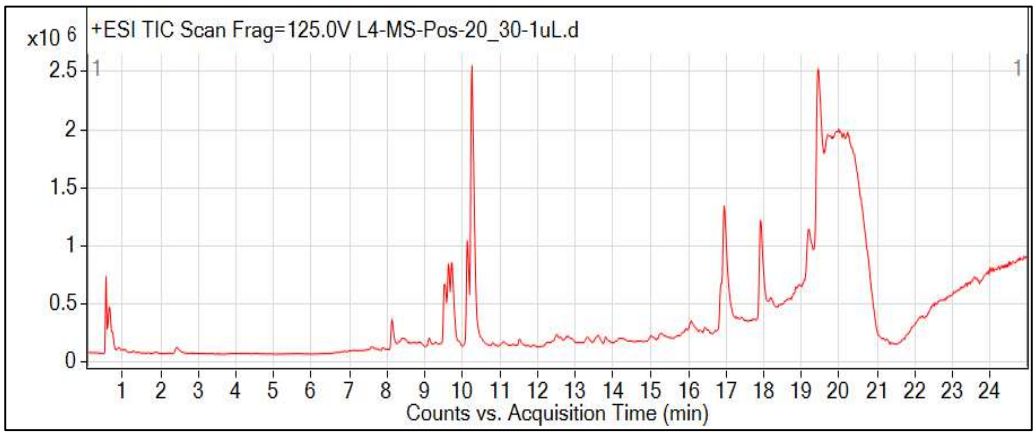

Figure 4.4 (iii) Total ion current diagram (+ve) for L4 (Huanglian + Banxia)

No	Formula	Compound Name	Retention time (min)	Mass	Classification of Compound	Classification of metabolite
1	C5 H13 O7 P	2-C-Methyl-D-erythritol 4-phosphate	0.633	216.0406	Enzyme	Enzyme
2	C8 H10 N4 O4	5-Acetylamino-6-formylamino-3-methyluracil	0.638	226.0697	formamidopyrimidine	Alkaloid
3	C7 H8 N4 O3	1,9-Dimethyluric acid	0.641	196.0598	purine	nucleic acid
4	C6 H6 N4 O2	1-Methylxanthine	0.643	166.0489	xanthine derivatives	Alkaloid
5	C14 H24 O12	Acetyl-maltose	0.666	384.125	Disaccharide	Carbohydrate
6	C12 H25 N2 O10 P	Fructoselysine 6-phosphate	0.667	388.1246	L- lysine derivative	Glucose
7	C18 H29 Br O3	(12Z,15S,18S)-15-hydroxy-18-bromo-12,16,17-octadecatrienoic acid	0.673	372.1297	Fatty acids	Fatty acid
8	C7 H8 N4 O2	Theobromine	0.684	180.065	alkaloid	Alkaloid
9	C6 H6 N4 O	1-Methylhypoxanthine	0.694	150.0539	hypoxanthine	Alkaloid
10	C5 H4 N4	Purine	0.738	120.0437	Purine	Nucleic acid
11	C5 H10 S2	3,3-Dimethyl-1,2-dithiolane	0.772	134.0228	dithiolane	Protein
12	C6 H8 O7	Citric acid	0.975	192.0272	tricarboxylic acid	Phenolic
13	C5 H7 N O3	N-Acryloylglycine	0.997	129.043	n-acyl-alpha amino acids.	Amino acid
14	C4 H6 O4	Erythrono-1,4-lactone	1.243	118.0271	Carboxylic acid	Phenolic
15	C15 H20 O10	3-Methoxy-4-hydroxyphenylglycol glucuronide	3.516	360.1055	phenolic glycosides	Phenolic
16	C17 H20 O9	3-O-Feruloylquinic acid	7.77	368.1105	quinic acid	Alkaloid
17	C20 H23 N O4	Carboxyterbinafine derivative2	8.216	341.1629	Terbinafine	Alkaloid
18	C20 H21 N O4	Papaverine	9.667	339.1469	opiate alkaloid	Alkaloid
19	C42 H62 O16	Licoricesaponin K2	11.918	822.403	Triterpenoid saponins	Saponin
20	C27 H38 O2	25-hydroxy-16,17,23,23,24,24-hexadehydrovitamin D3 / 25-hydroxy-16,17,23,23,24,24-hexadehydrocholecalciferol	20.912	394.2823	opiate alkaloid	Alkaloid

Table 4.7 Metabolite classification (–ve ESI) of L4 (Huanglian+Banxia)

No	Formula	Cmpd Name	Retention time (min)	Mass	Classification of Compound	Classification of metabolite
1	C20 H23 N O4	Cularine	8.139	341.1632	alkaloid	Alkaloid
2	C19 H15 N O4	Cepharadione B	9.125	321.1006	isoquinoline	Alkaloid
3	C20 H14 O4	Musanolone F	9.638	318.0897	phenylnaphthalenes	Terpenes
4	C21 H21 N O4	RCS-4 N-(5-carboxypentyl) metabolite	10.143	351.1477	synthetic cannabinoid	Alkaloid
5	C20 H14 O4	Musanolone F	10.264	318.09	phenylpropanoic acids	Phenolic
6	C16 H24 O7	tetranor-PGDM	17.922	328.1526	Prostaglandin D Metabolite-d6	Fatty acid
7	C20 H34 O8	Acetyl tributyl citrate	17.923	402.2263	tetracarboxylic acids	Phenolic

Table 4.8 Metabolite classification (+ve ESI) of L4 (Huanglian+Banxia)

4.1.5 L5 (Huanglian+ Gualou)

L5 (Huanglian+ Gualou) consisted of both primary and secondary metabolites. As shown in Figure 4.5, the primary metabolites were made up of amino acid (16 %), carbohydrate (3 %), fatty acid (16 %), glucose (3 %), protein (9 %) and vitamin (3 %). Secondary metabolites comprised alkaloid (28 %), phenolic (13 %), terpene (3 %), coblamin (3 %) and benzamide (3%). Among the secondary metabolites, alkaloid (28 %) and phenolic (13 %) had the first and second highest abundancy. The comparative ratio of primary metabolites to secondary metabolites was 50 % to 50 %. Moreover, among the total metabolites composition, alkanoid was found to have highest percentage (28 %) and amino acid and fatty acid were the second in the list (19 %). In L5 (Huanglian + Gualou), alkaloid composition was made up of indoles, deoxycytidine analog, Purine, hydroxypyrimidines, xanthine, cularine, cannabinoid and benzodioxoles. By thway, phenolic comprised of dicarboxylic acids, tricarboxylic acid, beta hydroxy acids and phenylpropanoic acids.

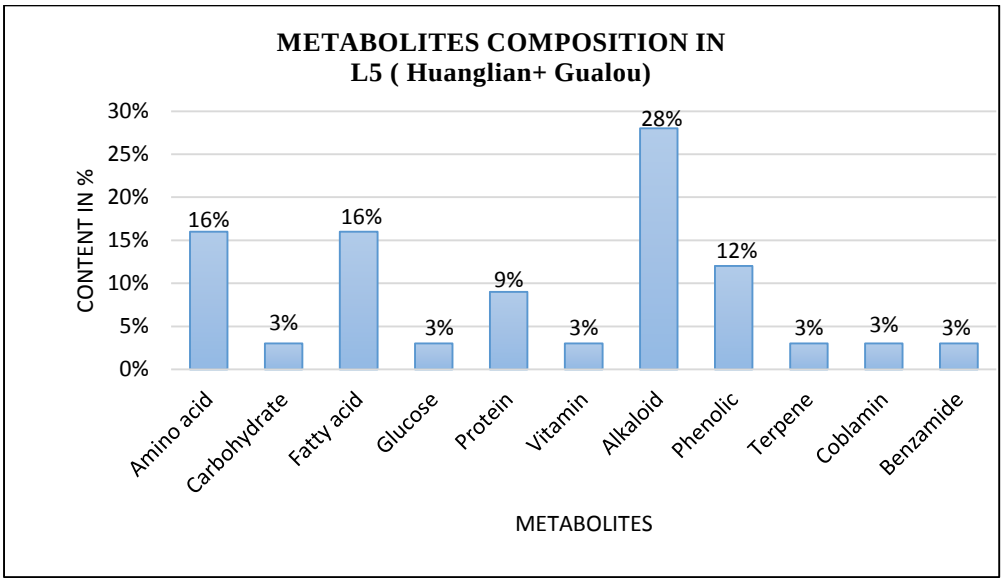

Figure 4.5(i) Chart for metabolites composition in L5 (Huanglian + Gualou)

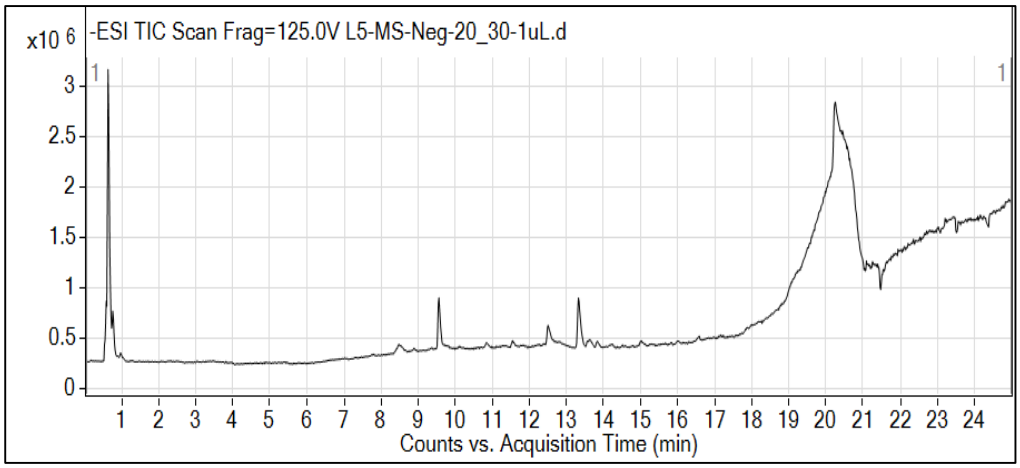

Figure 4.5(ii) Total ion current diagram (-ve) for L5 (Huanglian + Gualou)

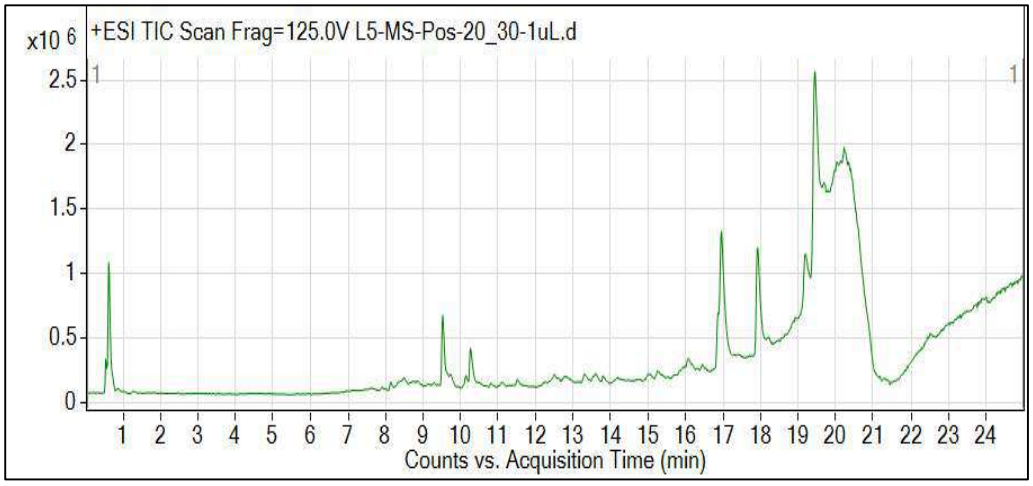

Figure 4.5(iii) Total ion current diagram (+ve) for L5 (Huanglian + Gualou)

No	Formula	Cmpd Name	Retention time (min)	Mass	Classification of Compound	Classification of metabolite
1	C11 H10 N2 O S	3-(Isothiocyanatomethyl)-1-methoxy-1H-indole	0.632	218.0521	indoles	Alkaloid
2	C12 H8 O4	Isobergaptene	0.635	216.0414	furanocoumarin.	Coumarin
3	C7 H10 N4 O2	Lathyrine	0.64	182.0801	L-alpha-amino acid.	Amino acid
4	C8 H12 N4 O4	Decitabine	0.642	228.085	deoxycytidine analog	Alkaloid
5	C6 H6 N4 O2	1-Methylxanthine	0.643	166.0488	Purine alkaloids	Alkaloid
6	C7 H8 N4 O3	1,9-Dimethyluric acid	0.643	196.0599	purine	Nucleic acid
7	C8 H10 N4 O4	5-Acetylamino-6-formylamino-3-methyluracil	0.644	226.0702	hydroxypyrimidines.	Alkaloid
8	C7 H8 N4 O2	Theobromine	0.65	180.0648	xanthine	Alkaloid
9	C7 H14 S2	(-)-1-Methylpropyl 1-propenyl disulfide	0.652	162.0539	organic disulfides	Essential oil
10	C19 H20 N4 O2 S2	Elesclomol	0.654	400.1038	carbohydrazide	Alkaloid
11	C20 H21 Cl N2 O4	Fipexide	0.669	388.121	benzodioxoles.	Alkaloid
12	C4 H4 O4	Fumaric acid	0.773	116.0112	dicarboxylic acids and derivatives	Phenolic
13	C4 H6 O5	D-(+)-Malic acid	0.773	134.0219	beta hydroxy acids and derivatives.	Phenolic
14	C6 H8 O7	Citric acid	0.972	192.0271	tricarboxylic acid	Phenolic
15	C13 H18 O3	(6S)-dehydrovomifoliol	12.511	222.1252	sesquiterpenoids.	Terpene

Table 4.9: classification of metabolite (–ve ESI) in L5 (Huanglian+Gualou)

No	Formula	Cmpd Name	Retention time (min)	Mass	Classification of Compound	Classification of metabolite
1	C6 H14 N4 O2	L-Arginine	0.591	174.1112	amino acid	Amino acid
2	C5 H13 N O	2-Amino-3-methyl-1-butanol	0.61	103.0993	amino alcohol	Amino acid
3	C6 H12 O6	L-Galactose	0.621	180.0638	monosaccharide	Carbohydrate

4	C6 H14 O6	D-Sorbitol	0.627	182.0793	glucitol	Glucose
5	C10 H19 N O7	D-1-[(3-Carboxypropyl)amino]-1-deoxyfructose	0.627	265.1162	amino acids	Amino acid
6	C6 H10 N2 O3	4-Methylene-L-glutamine	0.63	158.0693	amino acid	Amino acid
7	C16 H21 N5 O2	Alizapride	0.632	315.1691	substituted benzamide	Benzamide
8	C6 H10 O5	3-Hydroxy-3-methyl-glutaric acid	0.639	162.0521	hydroxy fatty acids	Fatty acid
9	C6 H10 O6	L-Galactono-1,4-lactone	0.64	178.0475	L-galactonic acid.	Enzyme
10	C20 H23 N O4	Cularine	8.145	341.1639	Cularine	Alkaloid
11	C20 H14 O4	Musanolone F	9.65	318.0899	phenylpropanoic acids	Phenolic
12	C21 H21 N O4	RCS-4 N-(5-carboxypentyl) metabolite	10.152	351.1469	synthetic cannabinoid	Alkaloid
13	C20 H14 O4	Musanolone F	10.278	318.09	phenylpropanoic acids	Phenolic
14	C19 H22 N4	Corrinoid	16.953	306.1845	vitamin B12	cobalamin
15	C16 H24 O7	tetranor-PGDM	17.924	328.1525	Prostaglandin D Metabolite-d6	Fatty acid
16	C23 H34 N4 O4	Leu Leu Trp	17.927	430.2572	tripeptide	Protein
17	C18 H37 N O	Stearamide	20.914	283.2871	fatty acid amide	Fatty acid

Table 4.10 classification of metabolite (+ve ESI) in L5 (Huanglian+Gualou)

4.1.6 L6 (Banxia + Gualou)

L6 (Banxia + Gualou) consisted of both primary and secondary metabolites. As shown in Figure 4.6, the primary metabolites were made up of amino acid (22 %), protein (14 %), fatty acid (14 %) and glucose (5 %). Secondary metabolites comprised alkaloid (22 %), phenolic (18 %), and flavanoid (5 %). Among secondary metabolites, alkaloid (22 %) and phenolic (18 %) had the first and second highest abundancy. The comparative ratio of primary metabolites to secondary metabolites was 55 % to 45 %. Moreover, among the total metabolites composition, alkaloid and amino acid were found to have highest percentage (22 %) and phenolic was the second in the list (18 %). In L6 (Banxia + Gualou), alkaloid composition was made up of indoles, purine hydroxypyrimidines and xanthine. Besides, phenolic consisted of dicarboxylic acids tyrosols and derivatives and tricarboxylic acids

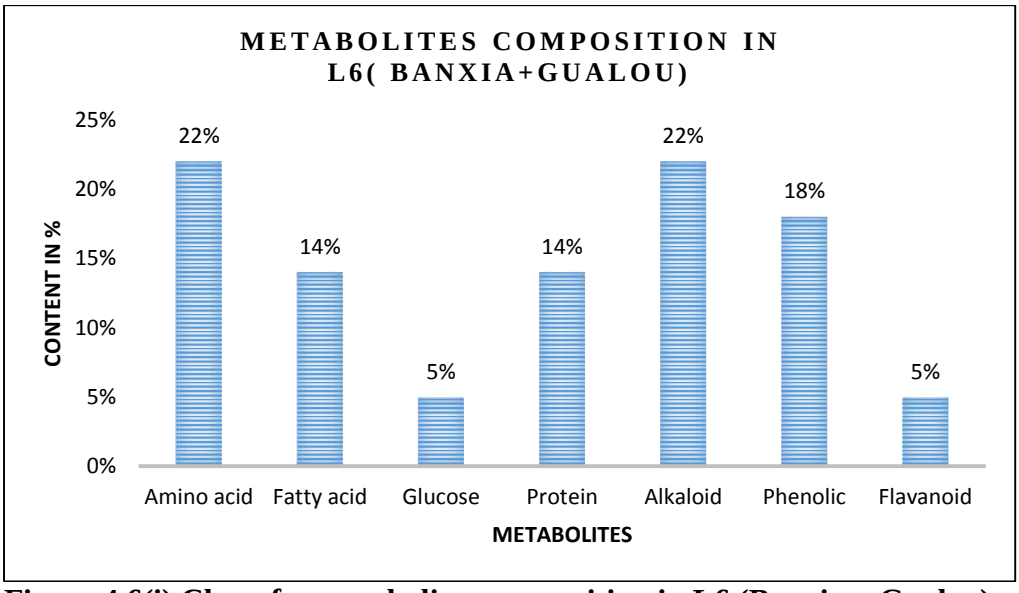

Figure 4.6(i) Chart for metabolites composition in L6 (Banxia + Gualou)

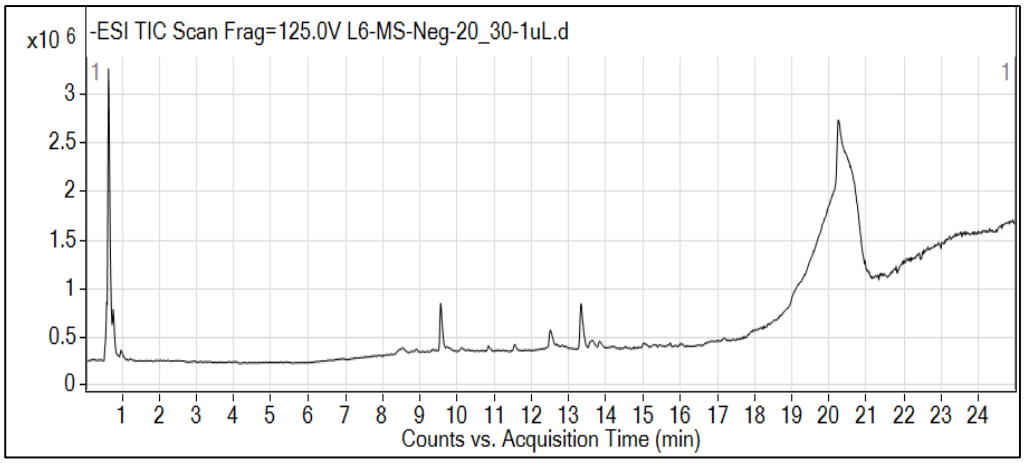

Figure 4.6(ii) Total ion current diagram (-ve) for L6 (Banxia + Gualou)

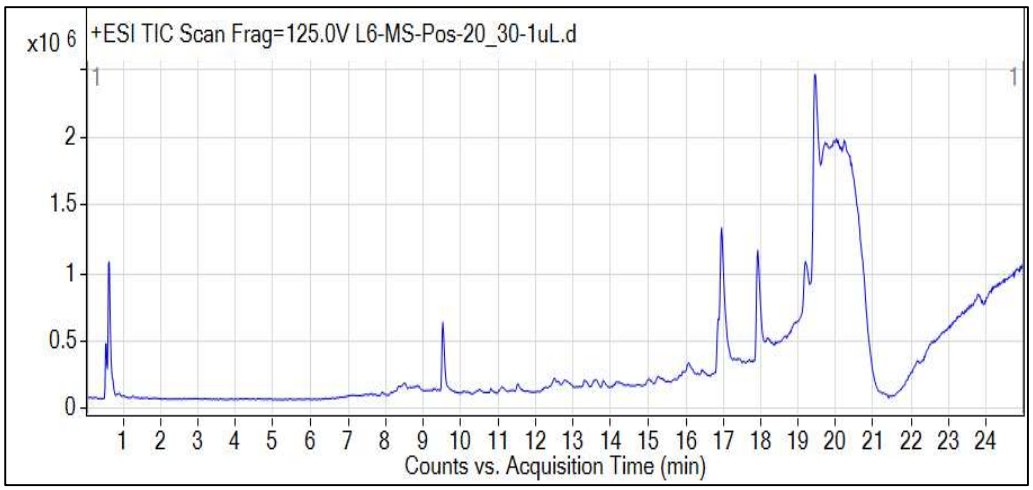

Figure 4.6(iii) Total ion current diagram (+ve) for L6 (Banxia + Gualou)

No	Formula	Cmpd Name	Retention time (min)	Mass	Classification of compound	Classification of Metabolite
1	C11 H10 N2 O S	3-(Isothiocyanatomethyl)-1-methoxy-1H-indole	0.632	218.0514	indoles	Alkaloid
2	C12 H8 O4	Isobergaptene	0.635	216.0417	furanocoumarin.	Coumarin
3	C7 H10 N4 O2	Lathyrine	0.638	182.0803	L-alpha-amino acid.	Amino acid
4	C8 H12 N4 O4	Decitabine	0.639	228.0852	cytosine analogue	unknown
5	C7 H8 N4 O3	1,9-Dimethyluric acid	0.643	196.0602	Purine	Alkaloid
6	C8 H10 N4 O4	5-Acetylamino-6-formylamino-3-methyluracil	0.644	226.0704	hydroxypyrimidines.	Alkaloid
7	C6 H6 N4 O2	1-Methylxanthine	0.645	166.0491	Purine	Alkaloid
8	C7 H8 N4 O2	Theobromine	0.653	180.0651	xanthine	Alkaloid
9	C7 H14 S2	(-)-1-Methylpropyl 1-propenyl disulfide	0.655	162.0547	organic disulfides	Essential oil
10	C4 H4 O4	Fumaric acid	0.771	116.0115	dicarboxylic acids and derivatives	Phenolic
11	C5 H10 S2	3,3-Dimethyl-1,2-dithiolane	0.772	134.0225	dithiolane	Protein
12	C6 H8 O7	Citric acid	0.972	192.0271	tricarboxylic acid	Phenolic

Table 4.11: classification of metabolite (–ve ESI) in L6 (Banxia+ Gualou)

N0	Formula	Cmpd Name	Retention time (min)	Mass	Classification of Cmpd	Classification of Metabolite
1	C6 H14 N4 O2	L-Arginine	0.591	174.1114	amino acid	Amino acid
2	C5 H13 N O	2-Amino-3-methyl-1-butanol	0.611	103.0993	amino alcohol	Amino acid
3	C10 H19 N O7	D-1-[(3-Carboxypropyl)amino]-1-deoxyfructose	0.626	265.1158	amino acids	Amino acid
4	C6 H14 O6	D-Sorbitol	0.626	182.0789	glucitol	Glucose
5	C6 H10 N2 O3	4-Methylene-L-glutamine	0.63	158.0692	amino acid	Amino acid
6	C6 H10 O6	L-Galactono-1,4-lactone	0.638	197.0893	L-galactonic acid.	Enzyme
7	C6 H10 O5	3-Hydroxy-3-methyl-glutaric acid	0.639	178.0472	hydroxy fatty acids	Fatty acid
8	C18 H29 N O4	Betaxolol(hydroxylation)	0.64	162.0519	tyrosols and derivatives.	Phenolic
9	C12 H12 O3	Anofinic acid	16.966	204.0795	2,2-dimethyl-1-benzopyrans	Flavonoid
10	C16 H24 O7	tetranor-PGDM	17.926	402.2257	Prostaglandin D Metabolite-d6	Fatty acid
11	C23 H34 N4 O4	Leu Leu Trp	17.926	328.1521	dipeptide	Protein

Table 4.12: classification of metabolite (+ve ESI) in L6 (Banxia+ Gualou)

4.1.7 L7 (Huanglian + Banxia + Gualou)

L7 (Huanglian + Banxia + Gualou) consisted of both primary and secondary metabolites. As shown in Figure 4.7, the primary metabolites were made up of amino acid (11 %), carbohydrate (4 %), protein (7 %), fatty acid (26 %) and glucose (4 %). Secondary metabolites comprised alkaloid (37 %) and phenolic (11 %). Among secondary metabolites, alkaloid (37 %) and phenolic (11 %) had the first and second highest abundancy. The comparative ratio of primary metabolites to secondary metabolites was 52 % to 48 %. Moreover, among the overall metabolites composition, alkaloid was found to have highest percentage (37%) and fatty acid was the second in the list (26 %). In L7 (Huanglian + Banxia + Gualou), alkaloid composition was made up of indoles, Purine hydroxypyrimidines, xanthine, carbohydrazide, carboxamide, terpenoids and monomethylhydrazine. Besides, phenolic consisted of tricarboxylic acid and polyphenols.

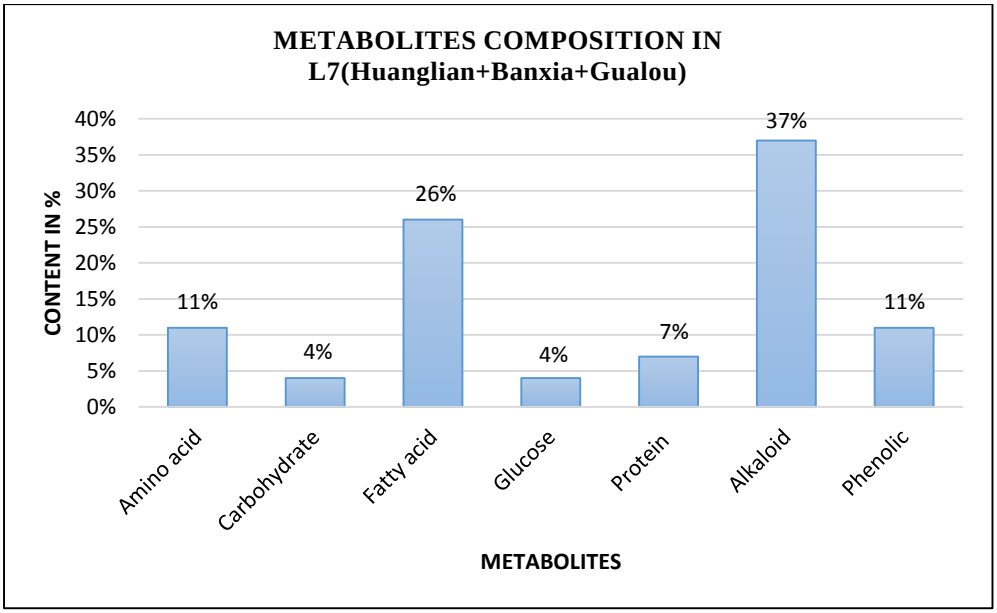

Figure 4.7(i) Chart for metabolites composition in L7 (Huanglian + Banxia+ Gualou)

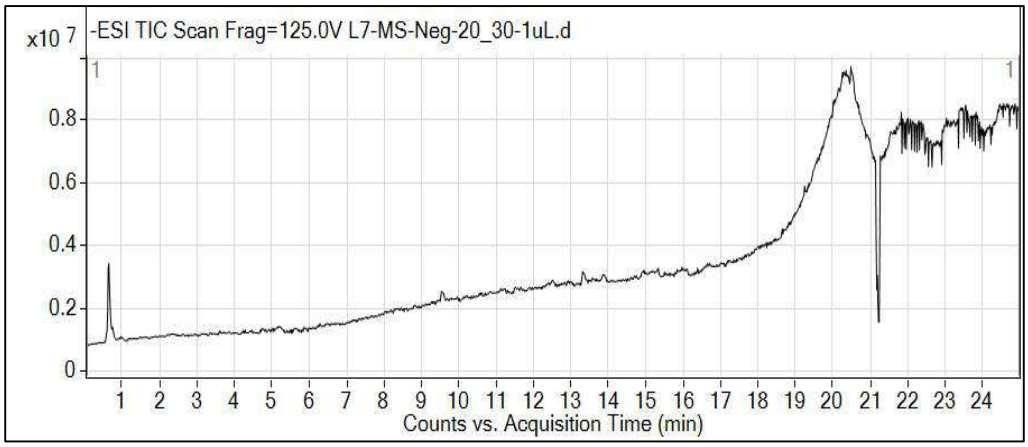

Figure 4.7(ii) Total ion current diagram (-ve) for L7 (Huanglian + Banxia+ Gualou)

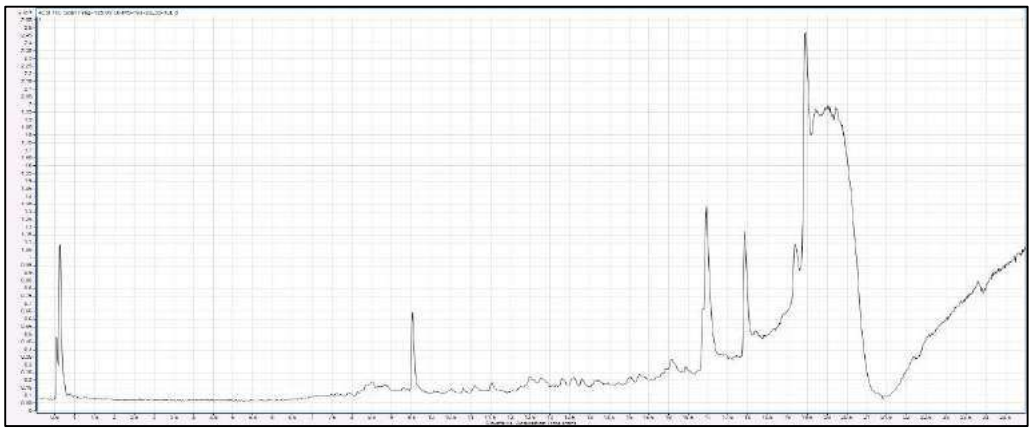

Figure 4.7(iii) Total ion current diagram (+ve) for L7 (Huanglian + Banxia+ Gualou)

Table 4.13 classification of metabolite (-ve ESI) in L7 (Huanglian+Banxia+ Gualou)

No	Formula	Compound C4:C26Label	Retention time (min)	Mass	Classification of Compound	classification of metabolite
1	C14 H14 O5 S	Cpd 2: 2-Butanone, 4-[6-(sulfooxy)-2-naphthalenyl]-	0.618	294.0561	unknown	unknown
2	C11 H10 N2 O S	Cpd 3: 3-(Isothiocyanatomethyl)-1-methoxy-1H-indole	0.63	218.0513	indoles	Alkaloid
3	C12 H8 O4	Cpd 5: Isobergaptene	0.632	216.0414	furanocoumarin.	Coumarin
4	C7 H10 N4 O2	Cpd 6: Lathyrine	0.635	182.0801	L-alpha-amino acid.	Amino acid
5	C8 H12 N4 O4	Cpd 7: Decitabine	0.636	228.0851	deoxycytidine analog	Alkaloid
6	C6 H6 N4 O2	Cpd 8: 1-Methylxanthine	0.638	166.0488	Purine	Alkaloid
7	C8 H10 N4 O4	Cpd 9: 5-Acetylamino-6-formylamino-3-methyluracil	0.64	226.0701	hydroxypyrimidines.	Alkaloid
8	C7 H8 N4 O3	Cpd 10: 1,9-Dimethyluric acid	0.64	196.0601	Purine	Alkaloid
9	C7 H14 S2	Cpd 11: (-)-1-Methylpropyl 1-propenyl disulfide	0.644	162.0538	organic disulfides.	Fatty acid
10	C7 H8 N4 O2	Cpd 12: Theobromine	0.646	180.0648	xanthine.	Alkaloid
11	C19 H20 N4 O2 S2	Cpd 13: Elesclomol	0.655	400.1033	carbohydrazide	Alkaloid
12	C19 H20 N4 O2 S2	Cpd 15: 3,3-Dimethyl-1,2-dithiolane	0.75	134.0225	dithiolane	Protein
13	C5 H10 S2	Cpd 16: Citric acid	0.946	192.027	tricarboxylic acid	Phenolic
14	C6 H8 O7	Cpd 17: KAPA	8.463	187.1206	unknown	unknown
15	C9 H17 N O3	Cpd 20: Nonic Acid	9.718	188.1045	dicarboxylic acid.	Lipid
16	C9 H16 O4	Cpd 21: Ethyl 3-(N-butylacetamido)propionate	10.116	215.1515	carboxamide	Amino acid
17	C11 H21 N O3	Cpd 24: (6S)-dehydrovomifoliol	12.513	222.1253	terpenoids	Alkaloid
18	C13 H18 O3	Cpd 25: Gingerol	13.334	294.1833	polyphenols	Phenolic
19	C20 H23 D9 O5	Cpd 27: Prostaglandin D2-d9	13.577	361.2824	arachidonic acid	Fatty acid
20	C17 H26 O5	Cpd 28: methyl 8-[2-(2-formyl-vinyl)-3-hydroxy-5-oxo-cyclopentyl]-octanoate	13.658	310.1782	fatty acid methyl ester.	Lipid
21	C20 H23 D9 O5	Cpd 29: Prostaglandin D2-d9	13.839	361.2823	arachidonic acid	Fatty acid
22	C17 H26 O3	Cpd 30: 6-Paradol	15.019	278.188	phenols	Phenolic
23	C12 H26 O4 S	Cpd 31: Lauryl hydrogen sulfate	15.892	266.1549	Fatty acid sulfonates	Fatty acid

No	Formula	Cmpd Name	Retention time (min)	Mass	Classification of compound	classification of metabolite
1	C6 H12 O6	L-Galactose	0.769	203.0528	monosaccharide sugar	Carbohydrate
2	C6 H14 O6	D-Sorbitol	0.772	205.0685	sugar alcohol	Glucose
3	C6 H10 O5	3-Hydroxy-3-methyl-glutaric acid	0.783	180.0865	hydroxy fatty acids	Fatty acid
4	C13 H21 N O3	Macrophylline	13.381	240.1596	Indole	Alkaloids
5	C8 H19 N	Octylamine	23.457	130.1589	Amine	Amino acid
6	C17 H37 N O2	Sphinganine	23.469	288.2905	Lipid	Fatty acid
7	C4 H8 N2 O	Gyromitrin	23.47	101.0713	Monomethylhydrazine	Alkaloids

Table 4.14 classification of metabolite (+ve ESI) in L7 (Huanglian+Banxia+ Gualou)

Metabolites derived from the plant serve for may purposes and can be utilised for medical intention. Primary metabolites are fundamently involve in activities such as growth, deveiopment and reproduction. Secondary metabolites basically provide protection to plant itself. Hence they are now derived for curing diseases.Secondary metabolites such as alkaloid and phenolic are most abundantly found in all the seven samples L1 to L7. Alkaloid and phenolic are the main components involved in protection, competition and species interaction.

4.2 Optimal cell density

A total of 2.5x103, 5x103, 10x103, 20x103 and 40x103 and 80x103 cells/mL of cells were seeded in each well accordingly in a 96-well plate. The cells will be incubated for 72 hours. MTT assay facilitated the finding of optimal cell density and hence the evaluation of half maximal inhibitory concentration of drug. Result of cell viability was represented by absorbance value. Conventionally, a graph was plotted with percentage of cell viability in x-axis against drug concentration in y axis. The midde point of exponential phase in the curved lines is the optimum cell concentration. Optimal cell density for each cell line was presented in Table 4.15. Among 8 NPC cell lines tested, TWO4 showed the lowest value for 2.5 x 10^3 (cells per well), whereas CNE1 and CNE2 cell line both showed the highest value at 5.0 x 10^3 (cells per well).

Table 4.15: Optimum cell seeding density of 8 NPC cancer cell lines

No.	Name of NPC cell lines	Optimum cell density (cells per well)
1	TWO1	4.0×10^3
2	C666-1	4.0×10^3
3	CNE 1	5.0×10^3
4	CNE 2	5.0×10^3
5	HONE 1	3.0×10^3
6	HK1	4.0×10^3
7	SUNE 1	5.0×10^3
8	TWO4	2.5×10^3

4.3 Cytotoxicity of 7 samples L1~7

Table 4.16 indicated the values of IC_{50} (μg/mL) for seven samples L1~L7. Huanglian is L1 which showed the most inhibitory effect among all. The IC_{50} value recorded as from 4.48 to 27.30 μg/mL 4.48 μg/mL was the lowest throughout the whole test. It was achieved when treated to HONE-1, Individual Banxia and Gualuo as well as combined Banxia and Gualuo did not gain IC_{50} value. Combined Huanglian and + Banxia treated to CNE-2 achieved 19.00 μg/mL IC_{50} value. Combined Huanglian and Gualuo only gained IC_{50} value of 40.70 μg/mL treated to HONE-1. IC_{50} values of 92.95 and 88.55 μg/mL was achieved by XXXD treated to CNE2 and HONE-1 .

No	NPC cell lines	L1	L2	L3	L4	L5	L6	L7
1	TWO 1	24.46	NA	NA	74.09	NA	NA	NA
2	C6661	27.30	NA	NA	NA	NA	NA	NA
3	CNE1	6.77	NA	NA	NA	NA	NA	NA
4	CNE2	6.32	NA	NA	19.00	NA	NA	92.95
5	HONE1	4.48	NA	NA	38.10	40.70	NA	88.55
6	HK1	11.10	NA	NA	20.12	NA	NA	NA
7	SUNE1	10.72	NA	NA	29.46	NA	NA	NA
8	TWO4	11.77	NA	NA	25.80	NA	NA	NA

Table 4.16: IC_{50} values (µg/mL) showed cytotoxity of L1~7

IC_{50} is explained as half-maximal inhibitory concentration of a particular drug being used to treat experimental cells *in vitro*. Hence, it is commonly regarded as an informative measure of medical drug efficacy on certain cells. It reveals that the quantity of drug needed to inhibit biological cell growth or rather to mean the cytotoxicity effect of particular drug to achieve 50% of cell viability. This information always render a potency of an antagonist drug in pharmacological research. MTT assays are conventionally being used to determine drug cytotoxicity effect on 50% cell viability. Normally, the efficacy of the drug will induce cell apoptosis in dose- dependent manner which implies that the larger the concentration of drug, the lesser will be the cell viability. In other words, the smaller the figure of IC_{50} in µg/mL, the greater is the cytotoxicity of the drug on the particular cells.

Table 4.17-4.23 represent percentage of cell viability at different concentration (µg/mL) of L1 to L7 respectively. Besides, half-maximal

inhibitory concentration (IC_{50}) was presented to reveal the efficacy of cytotoxicity of drugs being used.

In this experimental research, IC_{50} was calculated and achieved in Excel. Firstly, a curve in a graph was plotted with cell viability (as percentage %) in y- axis and concentration of drug used (μg/mL) in x-axis. When a curve has been drawn in excel, choose two points between 50% in y-axis, for example 47.5% and 55% cell viability, and match with concentration of drug at these two particular points. Again plot a new curve in a graph and then click chart elements to choose for trendline. Then choose more option for 'display equation on chart' and click. Subsequently, an equation will be provided such as y= mx + n. Thus, put y value as 50% or 0.5 and x is the value to be calculated for IC_{50}. Moreover, figure for m and n will be provided in the equation. The 50% inhibitory concentration (IC_{50}) is finally obtained. However, if all the values in percentage of cell viability were higher than 50%, half-maximal inhibitory concentration IC_{50} of drug will not be able to be calculated.

Cell lines	Concentration of L1 (µg/mL)							IC_{50} (µg/mL)
	0	3.125	6.25	12.5	25	50	100	
TWO 1	100%	87.71%	74.32%	71.06%	51.26%	25.05%	20.50%	24.46
C6661	100%	60.55%	57.22%	55.03%	53.92%	11.77%	1.64%	27.3
CNE 1	100%	53.60%	52.18%	25.99%	22.08%	24.02%	27.06%	6.77
CNE 2	100%	51.92%	50.21%	28.62%	18.62%	46.23%	46.46%	6.32
HONE 1	100%	54.47%	44.20%	45.61%	31.73%	24.52%	23.74%	4.48
HK1	100%	79.00%	64.36%	45.84%	26.17%	14.97%	12.68%	11.1
SUNE 1	100%	76.05%	58.12%	46.74%	28.52%	18.78%	12.36%	10.72
TWO 4	100%	69.32%	59.95%	48.71%	36.39%	22.17%	18.73%	11.77

Table 4.17: Percentage of cell viability at different concentration (µg/mL) of L1 (Huanglian)

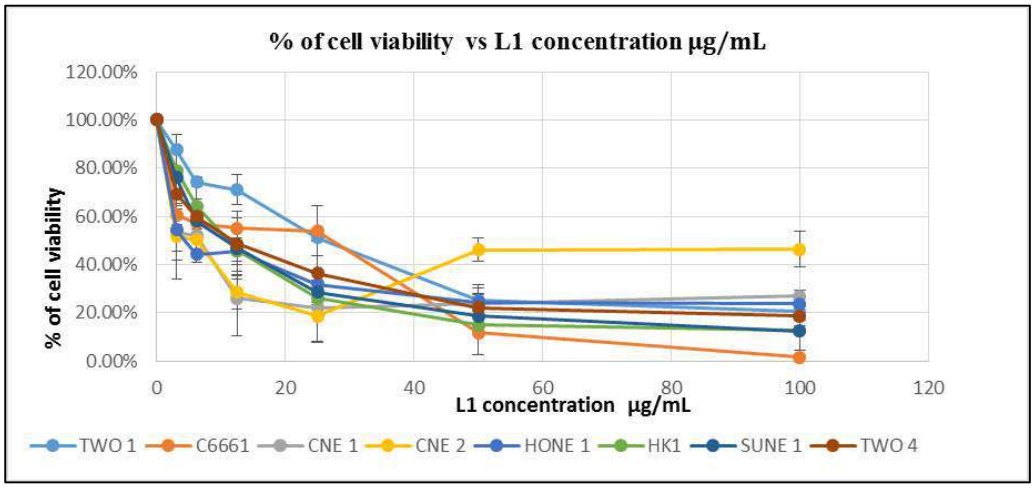

Figure 4.8(i): Graph of cell viability (%) against concentration of L1 (µg/mL)

When L1 (Huanglian) was used to test for its cytotoxic efficacy upon all cell lines such as TWO-1, C666-1, CNE-1, CNE-2, HONE-1, HK-1, SUNE-1, TWO-4, 7 concentration (µg/mL) of L1 were used such as 0, 3.125, 6.25,12.5, 25, 50, 100. The MTT assays result in Fig. 4.17 revealed that HONE-1 treated with L1 gained 4.48 µg/mL in IC_{50} value, the lowest among all 8 cell lines. HONE-1 was most susceptible to L1 in this test. The second and third were CNE-2 and CNE-1 with as 6.32 µg/mL and 6.77 µg/mL respectively. The highest IC_{50} value of 24.24 µg/mL was seen in TWO-1 when treated with L1 which implied

that L1 (Huanglian) had comparatively the least cytotoxicity effect upon this TWO-1in this test.

Cell lines	Concentration of L2 (µg/mL)							IC_{50} (µg/mL)
	0	3.125	6.25	12.5	25	50	100	
TWO 1	100%	93.38%	92.71%	96.63%	96.21%	87.21%	95.84%	Not found
C6661	100%	78.08%	82.02%	80.01%	72.96%	81.26%	82.28%	Not found
CNE 1	100%	104.50%	95.59%	102.45%	101.12%	93.22%	99.42%	Not found
CNE 2	100%	103.11%	92.60%	101.94%	92.88%	91.48%	98.42%	Not found
HONE 1	100%	108.20%	104.06%	104.30%	118.32%	113.77%	113.06%	Not found
HK1	100%	90.55%	82.54%	89.70%	89.12%	77.46%	85.69%	Not found
SUNE 1	100%	80.96%	74.06%	73.86%	76.89%	72.32%	68.98%	Not found
TWO 4	100%	86.53%	89.38%	93.59%	104.38%	84.48%	74.18%	Not found

Table 4.18: Percentage of cell viability at different concentration (µg/mL) of L2 (Banxia)

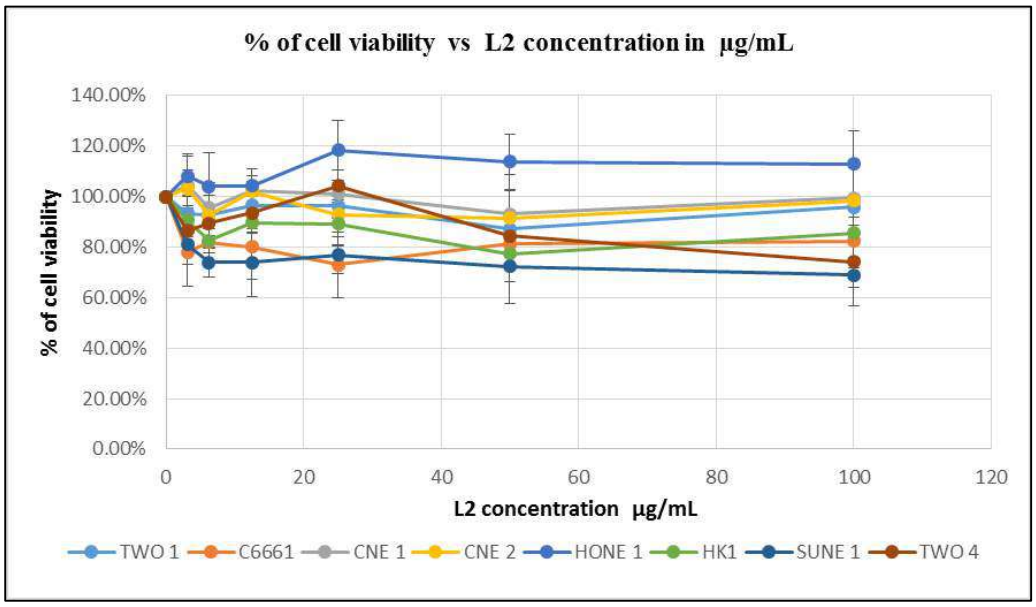

Figure 4.8(ii): Graph of cell viability (%) against concentration of L2 (µg/mL)

When L2 (Banxia) was used to test for its cytotoxicity efficacy upon all cell lines such as TWO-1, C666-1, CNE-1, CNE-2, HONE-1, HK-1, SUNE-1, TWO-4, 7 concentration of L2 were used such as 0, 3.125, 6.25,12.5, 25, 50, 100

μg/mL. The MTT assays result in Fig. 4.18 revealed that no IC_{50} value was found in any concentration when L2 was treated to all 8 cell lines separately. As seen in the table, the cell viability percentage of all cell lines at any L2 concentration (μg/mL) were more than 50%. Hence, IC_{50} could not be found. In this test, it may suggest that L2 (Banxia) comparatively did not exert any cytotoxicity effect upon all NPC cell lines treated.

Cell lines	Concentration of L3 (μg/mL)							IC_{50} (μg/mL)
	0	3.125	6.25	12.5	25	50	100	
TWO 1	100%	96.65%	93.60%	95.83%	92.85%	88.33%	92.90%	Not found
C6661	100%	76.21%	80.52%	75.99%	73.42%	72.60%	71.95%	Not found
CNE 1	100%	94.26%	93.15%	92.96%	87.90%	81.23%	81.13%	Not found
CNE 2	100%	87.85%	78.33%	97.90%	87.30%	94.14%	107.01%	Not found
HONE 1	100%	125.82%	120.64%	122.81%	126.81%	117.64%	111.83%	Not found
HK1	100%	99.96%	96.54%	98.55%	99.80%	94.64%	89.75%	Not found
SUNE 1	100%	85.85%	79.27%	75.14%	77.18%	74.37%	74.99%	Not found
TWO 4	100%	85.38%	82.04%	86.71%	76.97%	77.39%	92.10%	Not found

Table 4.19: Percentage of cell viability at different concentration (μg/mL) of L3 (Gualou)

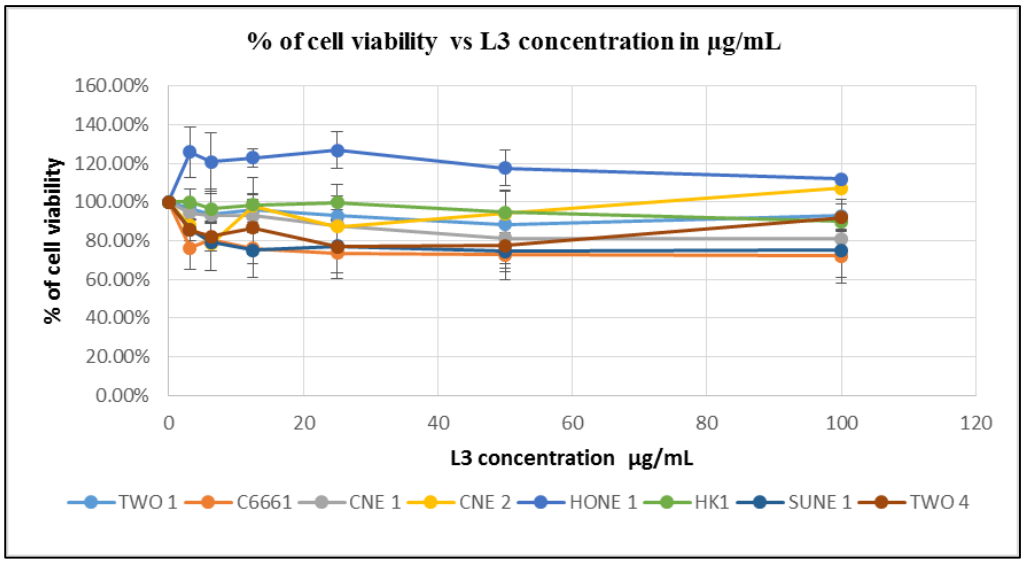

Figure 4.8(iii): Graph of cell viability (%) against concentration of L3 (µg/mL)

When L3 (Gualou) was used to test for its cytotoxicity efficacy upon all cell lines such as TWO-1, C666-1, CNE-1, CNE-2, HONE-1, HK-1, SUNE-1, TWO-4, 7 concentration of L3 were used such as 0, 3.125, 6.25,12.5, 25, 50, 100 µg/mL. The MTT assays result in Fig. 4.19 revealed that no IC_{50} value was found when L2 was treated to all 8 cell lines separately. As seen in the table, the cell viability percentage of all cell lines at any L3 concentration (µg/mL) were more than 50%. Hence, IC_{50} could be not found. In this test, it may suggest that L3 (Gualou) apparently did not exert any cytotoxicity effect upon all NPC cell lines treated.

Cell lines	Concentration of L4 (µg/mL)							IC_{50} (µg/mL)
	0	3.125	6.25	12.5	25	50	100	
TWO 1	100%	98.03%	88.30%	78.21%	72.88%	57.88%	42.05%	74.09
C6661	100%	75.25%	72.83%	73.70%	70.99%	69.37%	60.55%	Not found
CNE 1	100%	88.69%	91.46%	75.44%	80.02%	80.49%	58.50%	Not found
CNE 2	100%	74.31%	44.43%	55.61%	44.57%	39.44%	39.87%	19.00
HONE 1	100%	114.42%	61.14%	52.41%	57.59%	43.66%	39.87%	38.1
HK1	100%	84.13%	70.14%	62.22%	43.00%	38.17%	22.64%	20.12
SUNE 1	100%	81.03%	69.49%	62.36%	52.78%	36.41%	18.82%	29.46
TWO 4	100%	81.55%	71.52%	63.41%	50.35%	42.96%	28.34%	25.8

Table 4.20: Percentage of cell viability at different concentration (µg/mL) of L4 (Huanglian + Banxia)

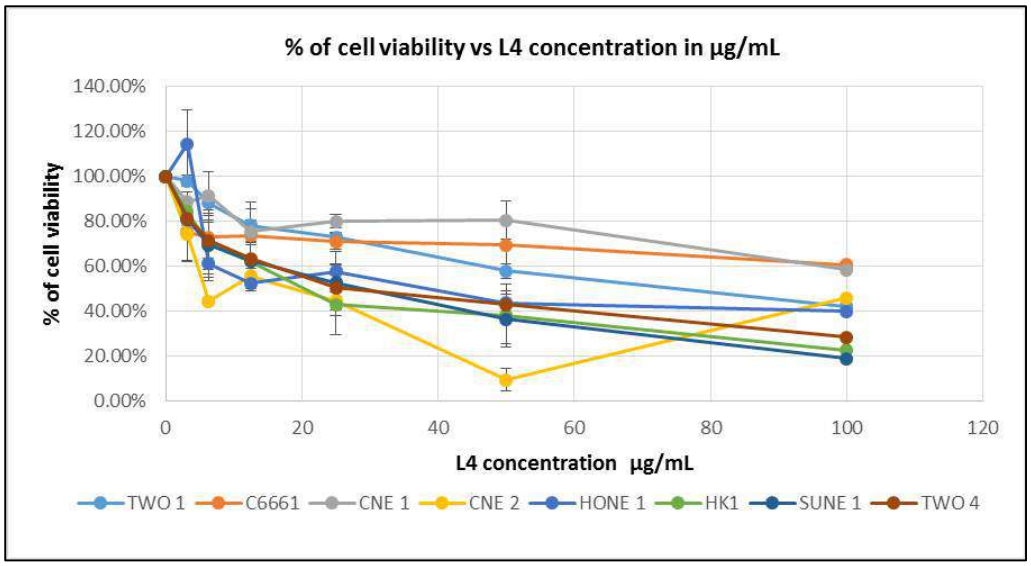

Figure 4.8(iv): Graph of cell viability (%) against concentration of L4 (µg/mL)

When L4 (Huanglian + Banxia) was chosen to test for its cytotoxicity efficacy upon all cell lines such as TWO-1, C666-1, CNE-1, CNE-2, HONE-1, HK-1, SUNE-1, TWO-4, 7 concentrations (µg/mL) of L4 were used such as 0, 3.125, 6.25,12.5, 25, 50, 100. The MTT assays result in Fig. 4.20 revealed that CNE-2 treated with L4 gained 19 µg/mL of IC_{50} value, the lowest among all 8

cell lines. CNE-2 was most susceptible to L4 in this test. The second and third were HK-1 and TWO-4 with as 20.12 µg/mL and 25.80 µg/mL respectively. The highest IC_{50} value of 74.09 µg/mL was seen in TWO-1 when treated with L4. However, no IC_{50} value was found when L4 was treated to CNE-1 and C-6661. This may imply that CNE-1 and C-6661did not expressed their susceptibility to L4. In the nutshell, L4 (Huanglian + Banxia) was most cytotoxicitic towards CNE-2 and on the other hand, it did not exert any cytotoxicity effect upon CNE-1 and C-6661.

Cell lines	Concentration of L5 (µg/mL)							IC_{50} (µg/mL)
	0	3.125	6.25	12.5	25	50	100	
TWO 1	100%	101.17%	97.52%	88.68%	86.79%	78.43%	74.26%	Not found
C6661	100%	74.61%	73.85%	79.32%	72.86%	71.19%	71.53%	Not found
CNE 1	100%	102.92%	82.45%	57.49%	69.36%	71.57%	56.01%	Not found
CNE 2	100%	105.41%	102.75%	94.30%	51.64%	55.94%	53.62%	Not found
HONE 1	100%	114.51%	106.54%	91.97%	63.60%	42.19%	36.06%	40.7
HK1	100%	123.35%	109.21%	123.28%	102.84%	95.60%	84.44%	not found
SUNE 1	100%	93.03%	92.39%	86.49%	78.49%	71.57%	60.74%	not found
TWO 4	100%	90.86%	86.28%	84.84%	75.65%	64.96%	53.78%	not found

Table 4.21: Percentage of cell viability at different concentration (µg/mL) of L5 (Huanglian + Gualou)

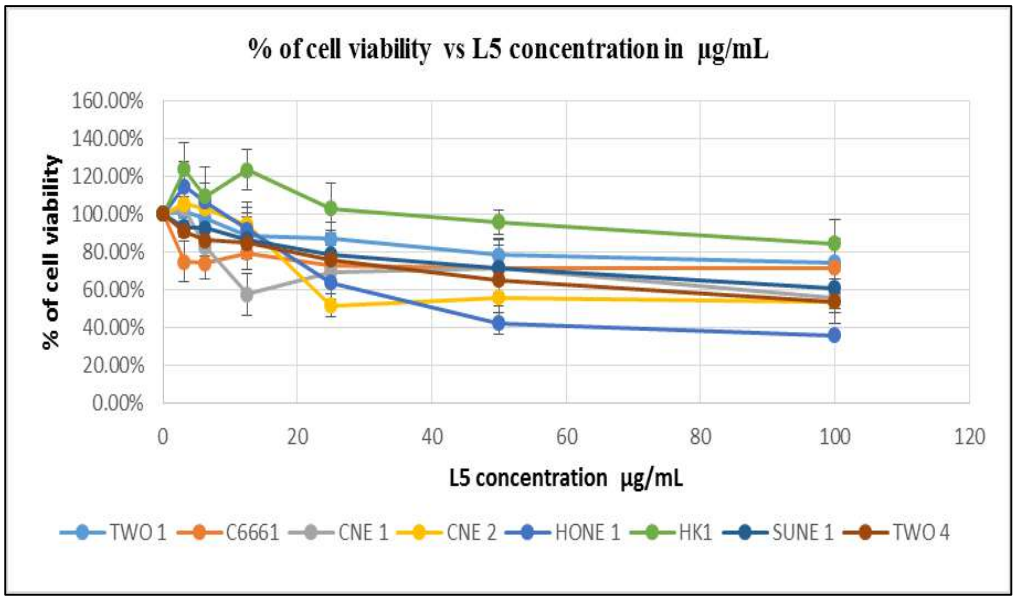

Figure 4.8(v): Graph of cell viability (%) against concentration of L5 (µg/mL)

When L5 (Huanglian + Gualou) was selected to test for its cytotoxicity efficacy upon all cell lines such as TWO-1, C666-1, CNE-1, CNE-2, HONE-1, HK-1, SUNE-1, TWO-4, 7 concentrations of L4 were used such as 0, 3.125, 6.25,12.5, 25, 50, 100 µg/mL. The MTT assays result in Fig. 4.21 revealed that HONE-1 treated with L5 gained 40.70 µg/mL of IC_{50} value, the lowest and the only among all 8 cell lines. HONE-1was most susceptible to L5 in this test. However, no IC_{50} value was found when L5 was treated to other seven cell lines namely TWO-1, C666-1, CNE-1, CNE-2, HK-1, SUNE-1 and TWO-4. This may imply that seven of these cell lines did not expresse their susceptibility to L5. In the nutshell, L5 (Huanglian Gualou) was most cytotoxicitic towards HONE-1 and on the other hand, it did not exert any cytotoxicity effect upon TWO-1, C666-1, CNE-1, CNE-2, HK-1, SUNE-1 and TWO-4.

Cell lines	Concentration of L6 (µg/mL)							IC_{50} (µg/mL)
	0	3.125	6.25	12.5	25	50	100	
TWO 1	100%	95.41%	86.96%	97.25%	90.67%	85.91%	88.24%	Not found
C6661	100%	72.93%	72.73%	77.33%	83.55%	87.29%	87.18%	Not found
CNE 1	100%	80.11%	88.72%	102.24%	88.95%	87.11%	80.44%	Not found
CNE 2	100%	92.71%	104.63%	100.31%	94.39%	95.09%	102.13%	Not found
HONE 1	100%	107.93%	95.27%	102.84%	110.80%	96.24%	102.62%	Not found
HK1	100%	105.43%	96.91%	96.29%	92.01%	80.59%	82.22%	not found
SUNE 1	100%	86.36%	83.37%	86.45%	85.66%	82.52%	82.41%	not found
TWO 4	100%	92.38%	95.02%	85.00%	78.85%	92.31%	75.80%	not found

Table 4.22: Percentage of cell viability at different concentration (µg/mL) of L6 (Banxia + Gualou)

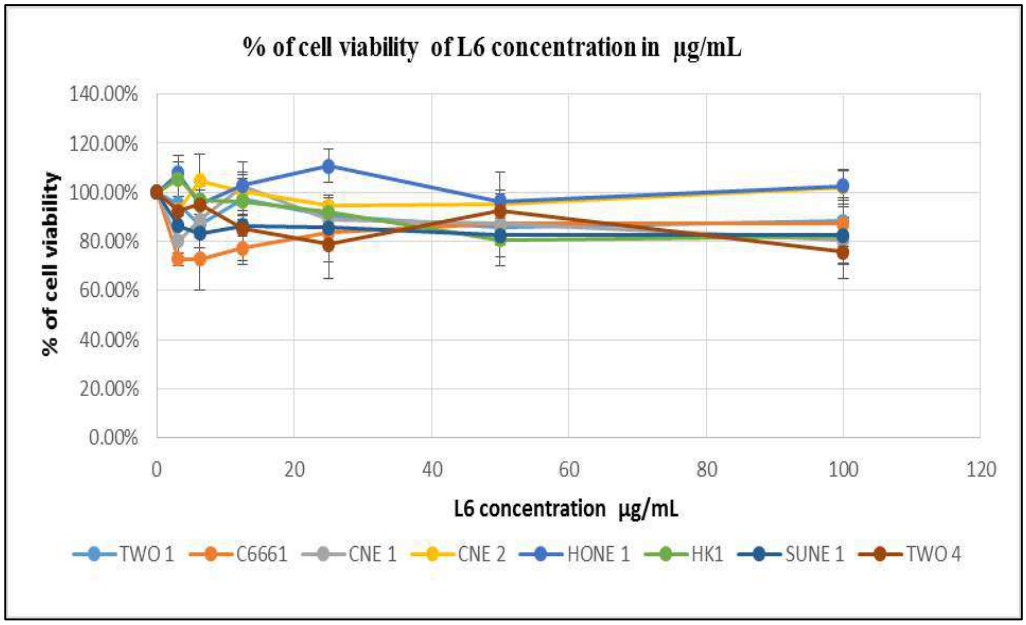

Figure 4.8(vi): Graph of cell viability (%) against concentration of L6 (µg/mL)

When L6 (Banxia + Gualou) was used to test for its cytotoxicity efficacy upon all cell lines namely TWO-1, C666-1, CNE-1, CNE-2, HONE-1, HK-1, SUNE-1, TWO-4, seven concentration of L6 were used such as 0, 3.125,

6.25,12.5, 25, 50, 100 μg/mL. The MTT assays result in Fig. 4.22 revealed that no IC_{50} value was found when L6 was treated to all 8 cell lines separately. As seen in the table, the cell viability percentage of all cell lines at any L6 concentration (μg/mL) were more than 50%. Hence, IC_{50} could be not found. In this test, it may suggest that L6 (Banxia + Gualou) apparently did not exert any cytotoxicity effect upon all NPC cell lines treated.

Cell lines	Concentration of L6 (μg/mL)							IC_{50} (μg/mL)
	0	3.125	6.25	12.5	25	50	100	
TWO 1	100%	97.60%	99.28%	97.37%	95.33%	84.51%	69.85%	Not found
C6661	100%	85.87%	88.81%	85.55%	76.74%	82.89%	82.51%	Not found
CNE 1	100%	75.73%	89.86%	91.42%	81.70%	79.51%	63.02%	Not found
CNE 2	100%	69.91%	88.21%	96.80%	71.86%	55.54%	49.00%	92.95
HONE 1	100%	124.07%	109.82%	114.20%	107.10%	65.43%	45.44%	88.55
HK1	100%	90.25%	84.34%	72.31%	70.01%	69.87%	75.20%	not found
SUNE 1	100%	88.02%	87.31%	89.94%	89.41%	82.02%	64.09%	not found
TWO 4	100%	65.88%	67.08%	73.37%	66.64%	64.43%	65.13%	not found

Table 4.23: Percentage of cell viability at different concentration (μg/mL) of L7 (Huanglian + Banxia + Gualou)

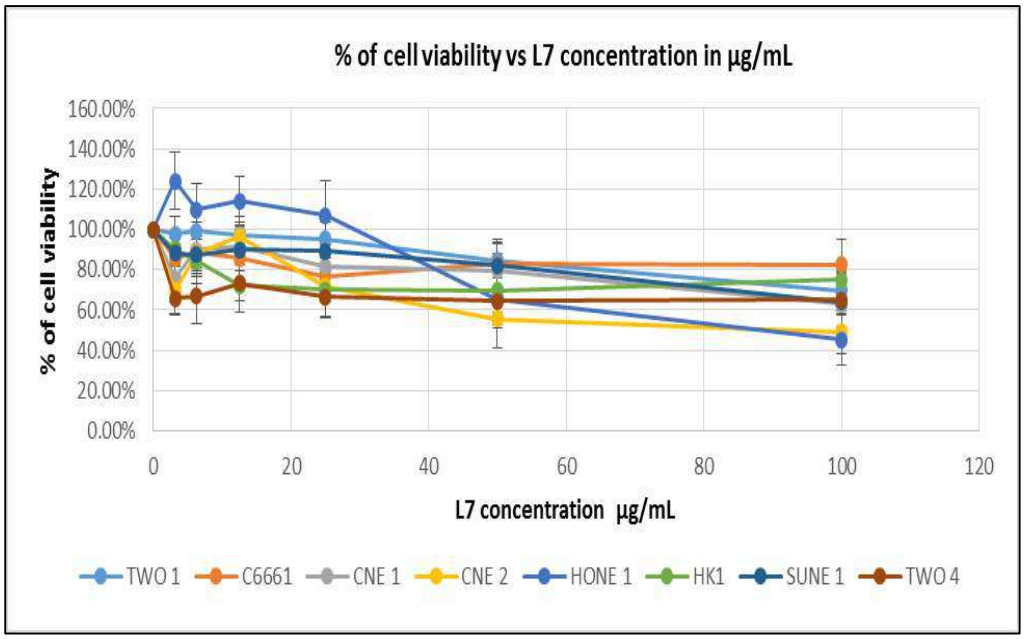

Figure 4.8(vii): Graph of cell viability (%) against concentration of L7 (µg/mL)

When L7 (Huanglian + Banxia + Gualou) was taken to test for its cytotoxicity efficacy upon all cell lines such as TWO-1, C666-1, CNE-1, CNE-2, HONE-1, HK-1, SUNE-1, TWO-4, seven concentrations (µg/mL) of L7 were used such as 0, 3.125, 6.25,12.5, 25, 50, 100. The MTT assays result in Fig. 4.23 revealed that only CNE-2 and HONE-1 treated with L7 gained 92.95 µg/mL and 88.55 µg/mL of IC_{50} value. Hence, HONE-1 was most susceptible to L7 in this test. However, no IC_{50} value was found when L4 was treated to six other cell lines namely TWO-1, C666-1, CNE-1, HK-1, SUNE-1 and TWO-4. This may imply that six of these cell lines did not expressed their susceptibility to L7. In the nutshell, L7 (Huanglian + Banxia + Gualou) was most cytotoxic towards HONE-1 and on the other hand, it did not exert any cytotoxicity effect upon TWO-1, C666-1, CNE-1, HK-1, SUNE-1 and TWO-4.

MTT assays were basically very sensitive and applicable to measure cytotoxicity (loss of viable cells) of experimental drugs. Herbal extracts such as Huanglian, Banxia, Gualou, combined Huanglian and Banxia, combined Huanglian and Gualou, Banxia and Gualou, XXXD were evaluated for their cytotoxic activities against all NPC cell lines such as TWO-1, C666-1, CNE-1, CNE-2, HONE-1, HK-1, SUNE-1, TWO-4. The dose response curve was determined and plotted in the graph of cell viability (y-axis) verse concentration (μg/mL) of each herbal extract (x-axis). The different herbal extract concentrations used and the corresponding cell viability graphs are shown for TWO-1, HONE-1, CNE-1, CNE-2, HK-1, SUNE-1, C666-1, TWO-4 with different colour in Figure 4.8. IC_{50} value for each herbal extract upon particular NPC cell line was hereby determined for the concentration of drug which exhibited 50% cell viability.

In Figure 4.8, results of eight NPC cell lines being treated with L1 (Huanglian) showed that all cell lines were susceptible to cytotoxity of L1. IC_{50} achieved ranged from 4.48 to 24.46 μg/mL where it was lowest when treated to HONE-1. In the test for drug cytotocity of L2 (Banxia), result showed that all curved lines which depicting each NPC cell line lied above 50% of cell viability. IC_{50} could not be found. In this test, it may suggest that L2 (Banxia) comparatively did not exert any cytotoxicity effect upon all NPC cell lines treated. In the test for drug cytotocity of L3 (Gualou), result also showed that all curves which depicting each NPC cell line lied above 50% of cell viability margin in y-axis. IC_{50} could not be found. Again, in this test, it revealed that L3 (Gualou) apparently did not exert any cytotoxicity effect upon all NPC cell lines

treated. In the test for drug cytotocity of L4 (Huanglian + Banxia), result showed that two curved lines depicting C-6661 (orange colour) and CNE-1 (grey) lied above 50% of cell viability margin in y-axis. IC_{50} could not be found for C-6661 and CNE-1 which revealed that L4 could not effectively imposed cytotoxity upon them. However, TWO-1, CNE-2, HONE-1, HK-1, SUNE-1, and TWO-4 were susceptible in L4. IC_{50} determined ranged from 19 to 74.09 μg/mL where CNE-2 gained the lowest IC_{50}. In the test for drug cytotocity of L5 (Huanglian + Gualou), the graph in Figure 4.18 showed that seven curved lines depicting TWO-1, C666-1, CNE-1, CNE-2, HK-1, SUNE-1, TWO-4 lied above 50% of cell viability margin in y-axis except HONE-1 (blue). IC_{50} could only be achieved for HONE-1which was 40.7 μg/mL. In the test for drug cytotocity of L6 (Banxia + Gualou), result showed that all curved lines which depicting each NPC cell line lied above 50% of cell viability margin in y-axis. IC_{50} could not be achieved. In this test, it may suggest that L6 (Banxia + Gualou) apparently could not impose any cytotoxicity effect upon all NPC cell lines treated. In the test for drug cytotocity of L7 (Huanglian + Banxia + Gualou), result showed that six curved lines which depicting TWO-1, C666-1, CNE-1, HK-1, SUNE-1, TWO-4 lied above 50% of cell viability margin in y-axis. IC_{50} could not be achieved for these NPC cell lines apparently implied that L7 could not impose any cytotoxicity effect upon them. However, IC_{50} could be achieved for CNE-2 (orange colour) and HONE-1 (blue) where the value were 92.95 and 88.55 μg/mL respectively.

4.4 RNA Extraction

4.4.1 RNA Extraction for HONE-1 treated with L1 (Huanglian)

4.4.1.1 Nano Photometer results

Results for RNA extraction by 1st elution for HONE-1 treated with L1 at 0hr, 4hr, 8hr and 12hr are shown in Table 4.24 - 4.27. The ratio of A260/280 and A 260/230 generally provides the indication of purity of nucleic acid to be tested. For RNA, recommended range in A 260/280 ratio is around 2.1. Besides, 260/230 ratios within range of 2.0 – 2.2 is considered good. There can be a possibility of RNA contamination if the ratio is higher than this value. The A 260/280 and A 260/230 shown in Table 4.24 – 4.27 were within the acceptable range**.**

Table 4.24:
0 hour - First elution (HONE-1 treated with L1)

Replicate no.	1	2	3
concentration(ng/mL)	19.28	14.12	14.96
A 260/280	1.898	1.918	1.861
A 260/230	2.114	2.292	1.928

Table 4.25:
4 hours - First elution (HONE-1 treated with L1)

Replicate no.	1	2	3
concentration(ng/mL)	22.88	22.36	26.56
A 260/280	1.907	1.827	1.707
A 260/230	2.234	2.175	1.865

Table 4.26: 8 hours - First elution (HONE-1 treated with L1)			
Replicate no.	1	2	3
concentration(ng/mL)	45.52	36.2	33.24
A 260/280	1.773	1.727	1.822
A 260/230	2.236	2.197	2.198

Table 4.27: 12 hours - First elution (HONE-1 treated with L1)			
Replicate no.	1	2	3
concentration(ng/mL)	25.16	18.28	24.24
A 260/280	1.792	1.674	1.772
A 260/230	2.321	2.308	2.27

4.4.1.2 Result of 1% Agarose gel electrophoresis of total RNA

Photograph in Figure 4.9 shows 12 lanes from left to right representing12 replicates which labels 1, 2, 3 collected from 4 different time points of 0, 4, 8 12 hours, respectively. Two bands were present at each lane. The upper and lower band depict 28S RNA and 18S RNA respectively. The third lane for 0 hour replicate and the first lane for 4 hour replicate could possibly be rRNA degradation due to very blur appearance of 28S and 18S bands. Other than these two lanes, the upper and lower bands of overall lanes were visible and without smear. The RNA could be considered intact and without degradation.

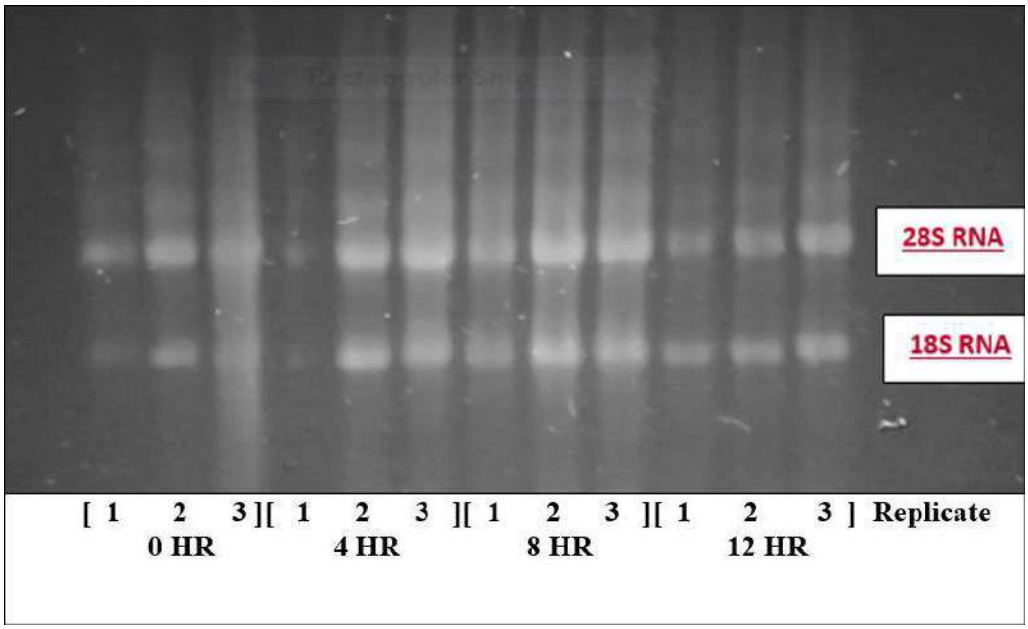

Figure 4.9: 1% Agarose gel electrophoresis of total RNA for HONE-1 treated with L1 at 0/4/8/12hours

4.4.2 RNA Extraction for HONE-1 treated with L7 (XXXD)

4.4.2.1 NanoPhotometer

Results for RNA extraction by 1st elution for HONE-1 treated with L7 (XXXD) at 0hour, 4hours, 8hours and 12hours are shown in Table 4.28 - 4.31. The ratio of A260/280 and A 260/230 generally provides the indication of purity of nucleic acid to be tested. For RNA, recommended range in A 260/280 ratio is around 2.1. Besides, general acceptable 260/230 ratios are in the ratio between 2.0 ~ 2.2. for 260/230 ratios is considered good and pure RNA. There can be a possibility of RNA contamination if the ratio is higher than this value. The A 260/280 and A 260/230 shown in Table 4.28 – 4.31 were within the acceptable range.

Table 4.28 0 hour 1st elution			
Replicate no.	1	2	3
concentration(ng/mL)	12.48	17.6	33.72
A 260/280	1.975	1.811	1.951
A 260/230	2.557	2.126	2.236

Table 4.29 **4hours 1st elution**			
Replicate no.	1	2	3
concentration(ng/mL)	11.6	10.88	26.36
A 260/280	2.566	2.833	2.267
A 260/230	2.302	2.267	2.234

Table 4.30 **8hours 1st elution**			
Replicate no.	1	2	3
concentration(ng/mL)	19.44	44.6	29.88
A 260/280	1.78	1.787	1.787
A 260/230	2.25	2.221	2.257

Table 4.31 **12hours 1st elution**			
Replicate no.	1	2	3
concentration(ng/mL)	29.08	19.84	25.96
A 260/280	1.8	1.81	1.813
A 260/230	2.1	2.255	2.253

4.4.2.2 Result of 1% Agarose gel electrophoresis of total RNA

Photograph in Figure 4.10 shows 12 lanes from left to right representing 12 replicates which labels 1, 2, 3 collected from 4 different time points of 0 hrour, 4 hours, 8 hours and 12 hours, respectively. Two bands were present at each lane. The upper and lower band depict 28S and 18S RNA respectively. The first and second lane for 8 hours replicate could possibly be rRNA degradation due to very blur appearance of 28S and 18S bands. Other than these two lanes, the upper and lower bands of overall lanes were visible. The RNA could be considered intact and without degradation.

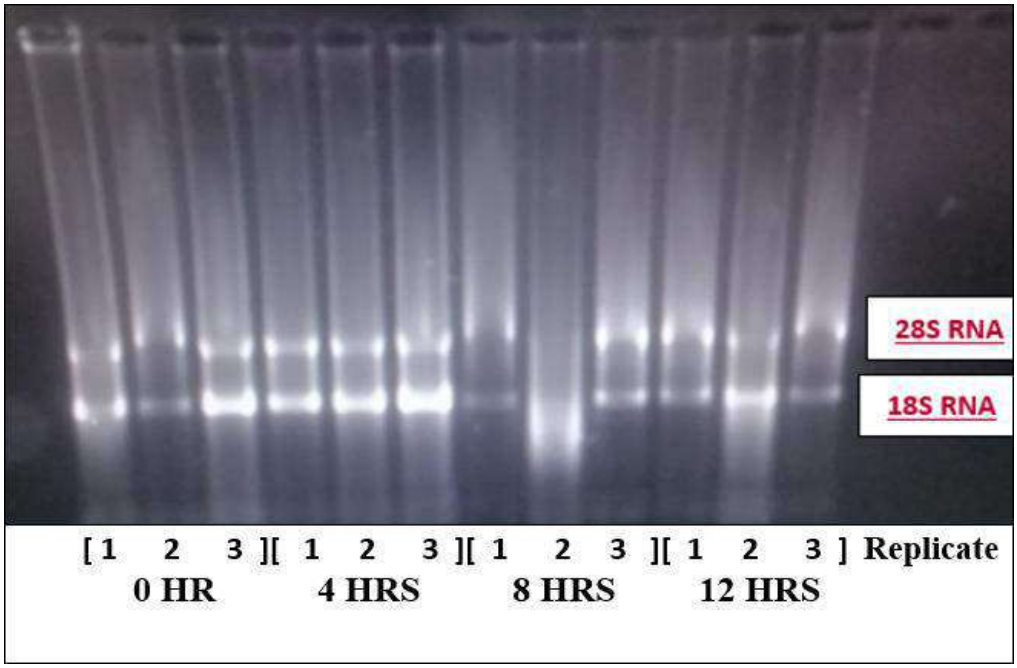

Figure 4.10: 1% Agarose gel electrophoresis of total RNA for L7 treated HONE-1 at 0/4/8/12hours

4.5 Gene expression and pathway analysis

4.5.1 Gene expression and pathway analysis of HONE-1 treated with L1(Huanglian)

The gene expression for a total of 770 genes associated with 13 pathways in Huanglian treated HONE-1 was evaluated by NanoString PanCancer Pathways Panel. The differential expression of each gene at three time points such as 4, 8 and 12 hours were used to differentiate from initial 0 hour. About one million raw counts tallied entire genes in a single sample. When extracted RNA was hydridized by mixing together hydrization buffer to reporter codeset. nSolver 4.0 was adopted to analyse the data produced. Values such as $\log_2$ fold and -log10 and *P* value were exhibited in volcano plot where highly statistically significant genes at the top of the plot above the horizontal lines, and highly differentially expressed genes fall to either side. Horizontal lines indicate various False Discovery Rate (FDR) thresholds or *p-values* thresholds if there is no adjustment to the *p*-values. Genes are coloured if the resulting *p*-value is below the given FDR or *p*-values threshold**.** The 40 most statistically significant genes are labeled in the plot.

4.5.1.1 Gene expression and pathway analysis of HONE-1 treated with L1 (Huanglian) at treatment time 4 hours vs. 0 hour

At this time point, upregulation was seen at 66 genes for positive fold change and downregulation was accounted for 114 genes for negative fold change where ($P < 0.05$ as shown in Figure 4.11a. The top 20 most significant differentiately expressed genes are shown in Volcano plot (Figure 4.11b). Genes involved in some cancer pathways were enriched among the top differentially expressed genes as shown in Table 4.32. The 20 most statistically significantly differentially expressed genes (measured in $\log_2$ fold change) with the selected covariate at treatment time 4 hours vs 0 hour. Regulation of genes at this time point were mainly initiated by signalling pathway such as MAPK, PI3K, RAS, Cell Cycle–Apoptosis, WNT, JAK-STAT, NOTCH, Transcription Misregulation. Gene expression data were mapped onto KEGG pathway graphs by Pathview function of the PanCancer pathway software, providing intuitive views of both up- and down-regulation at the pathway level. Representative graphs for signalling pathway are shown in Figures 4.12 to 4.23.

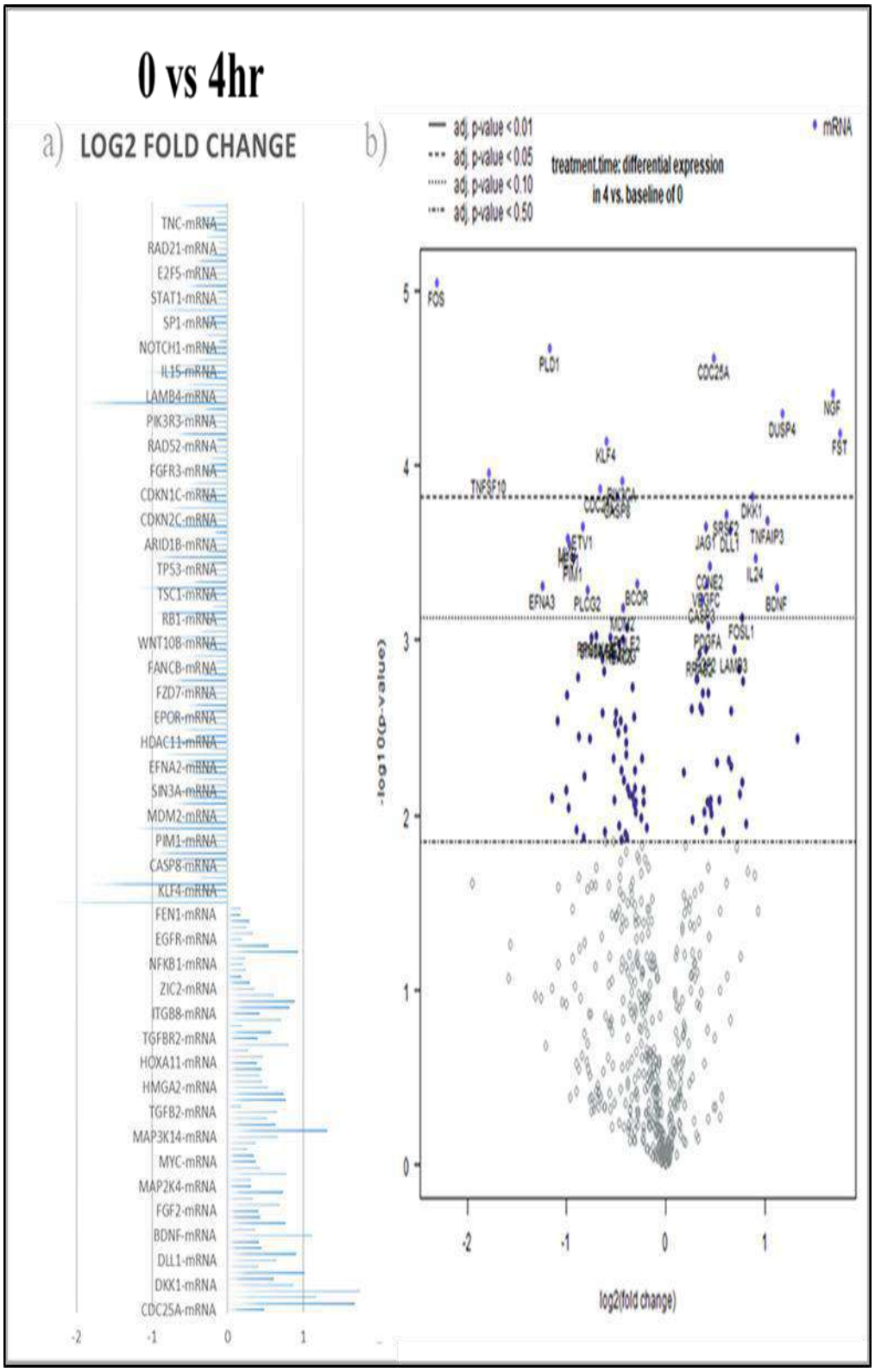

FIG 4.11 a) Log$_2$ fold change difference between 4 hours vs. baseline of 0 hour in HONE 1 cells treated with L1 (Huanglian) with differential expression comparing statistically significant differences (*P* < 0.05) in mRNA expression in the up and down regulated genes separately. A total of 66 up regulated genes show a positive fold change whereas 114 down regulated genes show a negative fold change. b) Volcano plot.

Table 4.32: The top 20 most significant differentially expressed genes (measured in log_2 fold change) with the selected covariate at treatment time 4 hours vs 0 hour with L1 (Huanglian)

Genes	Log_2 fold change	*P*-value	Pathway	Biological Functions
FOS	-2.31	9.01E-06	MAPK	**Fos Proto-Oncogene, AP-1 Transcription Factor Subunit** Modulates cell proliferation, differentiation, and transformation
TNFSF10	-1.78	0.000109	Cell Cycle - Apoptosis	**Tumor Necrosis Factor Ligand Superfamily Member 10** Cytokine, induces apoptosis.
PLD1	-1.17	2.12E-05	Ras	**Phospholipase D1** Enzyme for phosphatidylcholine. involves in signal transduction, membrane trafficking, and the regulation of mitosis
MYB	-0.987	0.000261	PI3K	**MYB Proto-Oncogene, Transcription Factor** Regulates proliferation and differentiation of hematopoietic progenitor cells.
HES1	-0.973	0.000282	Notch	**Hes Family BHLH Transcription Factor 1** An antagonist nuclear transcription factor
ETV1	-0.838	0.000223	Transcriptional Misregulation	**ETS Variant Transcription Factor 1** Regulates biological processes like cell growth, angiogenesis etc
CDC25C	-0.665	0.000136	Cell Cycle - Apoptosis	**Cell Division Cycle 25C** Regulates G2/M progression and DNA damage repair. Activates the cyclin B1/CDK1 complex
KLF4	-0.602	7.18E-05	Driver Gene	**Kruppel Like Factor 4** Controls the G1-to-S transition, mediates DNA damage by mediating the tumuor suppressor gene p53.
CASP8	-0.487	0.000149	Cell Cycle - Apoptosis Driver Gene	**Cysteine-aspartic acid protease (caspase) family** Plays a central role in the execution-phase of cell apoptosis.
PIK3CA	-0.44	0.000121	Cell Cycle - Apoptosis Driver Gene, JAK-STAT, PI3K, Ras	**Phosphoinositide 3-Kinase Alpha** Instruct making of the p110 alpha (p110α) protein, as for PI3K
JAG1	0.401	0.000225	Notch	**Jagged Canonical Notch Ligand 1** Involved in early and late stages of mammalian cardiovascular development.
CDC25A	0.484	2.39E-05	Cell Cycle - Apoptosis	**Cell division cycle 25 A** Dual-specificity protein phosphatase cell cycle regulators for cyclin/CDK complex.
SRSF2	0.61	0.000188	Driver Gene	**Serine And Arginine Rich Splicing Factor 2** Necessary for the splicing of pre-mRNA. Required for formation of the earliest ATP-dependent splicing complex.

DLL1	0.645	0.000233	Notch	**Delta Like Canonical Notch Ligand 1** Mediates cell fate decisions during hematopoiesis. cell-to-cell communication.
DKK1	0.869	0.00015	Wnt	**Dickkopf WNT signaling pathway inhibitor 1** Embryonic, bone development
IL24	0.9	0.000338	JAK-STAT	**Interleukin 24** Induce apoptosis selectively in various cancer cells.
TNFAIP3	1.02	0.000207	Driver Gene	**TNF alpha induced protein 3** Inhibit NF-kappa B activation and TNF-mediated apoptosis.
DUSP4 (MKP)	1.17	5.05E-05	MAPK	**Dual specificity protein phosphatase 4** Cellular proliferation and differentiation
NGF	1.68	3.84E-05	Cell Cycle - Apoptosis MAPK, PI3K, Ras	**Nerve growth factor** Development and survival of nerve cells A marker of tumor progression
FST	1.75	6.49E-05	TGF-beta	**Follistatin** Regulator of pituitary FSH secretion inhibitor to Activin and BPM TGFβ-related growth factors

Continuation of Table 4.32

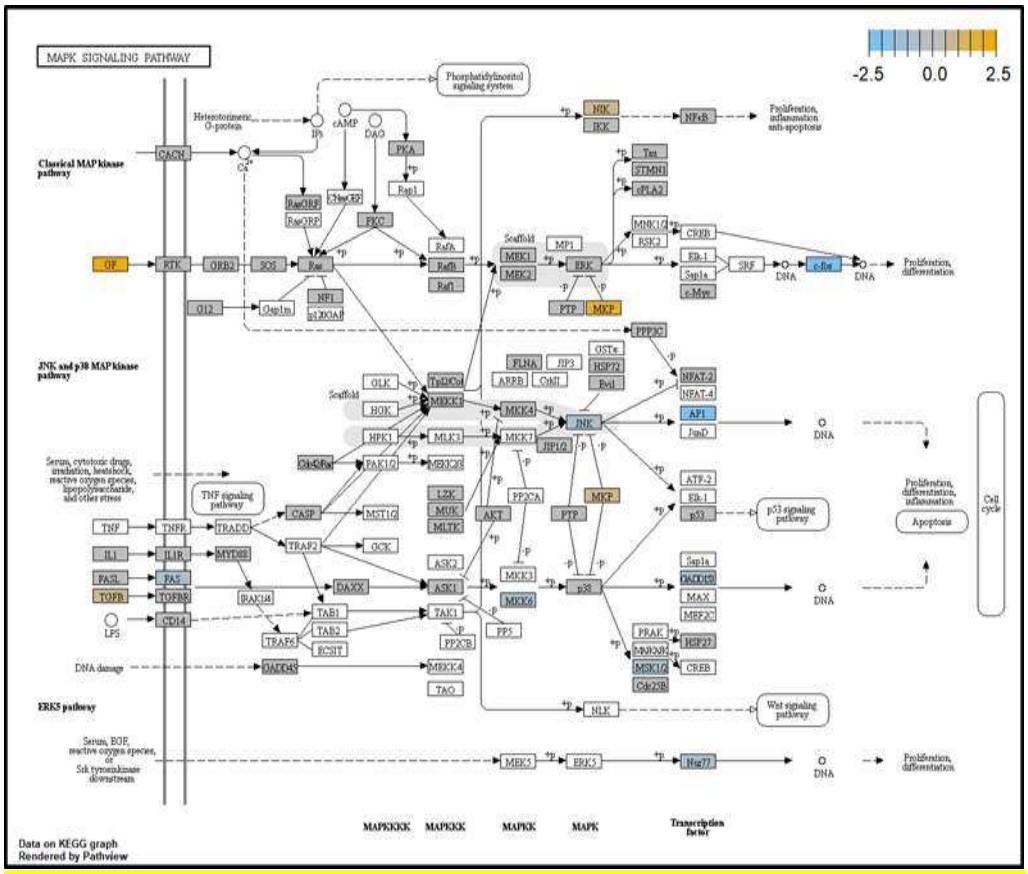

Figure 4.12: MAPK signaling pathway (treatment time: differential expression in 4 hours vs. baseline of 0 hour for HONE-1 treated with L1 (Huanglian)

Upregulated gene: *GF, MKP, TGFβ, MKP, NIK*

Downregulated genes: *eFOS, AP1, FAS, MKK6, JNK*

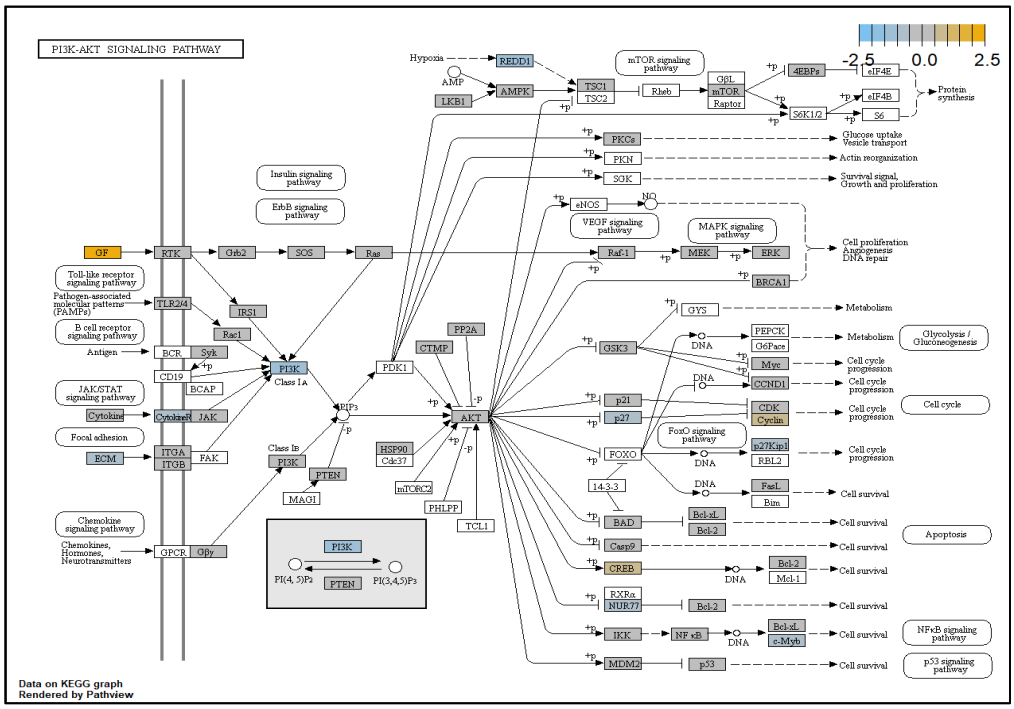

Figure 4.13: PI3K signaling pathway (treatment time: differential expression in 4 hours vs. baseline of 0 hour for HONE-1 treated with L1 (Huanglian)

Upregulated genes: *GF, Cyclin, CREEB*

Downregulated genes: *P13K, p27, ECM, Cytokine F, REDDI*

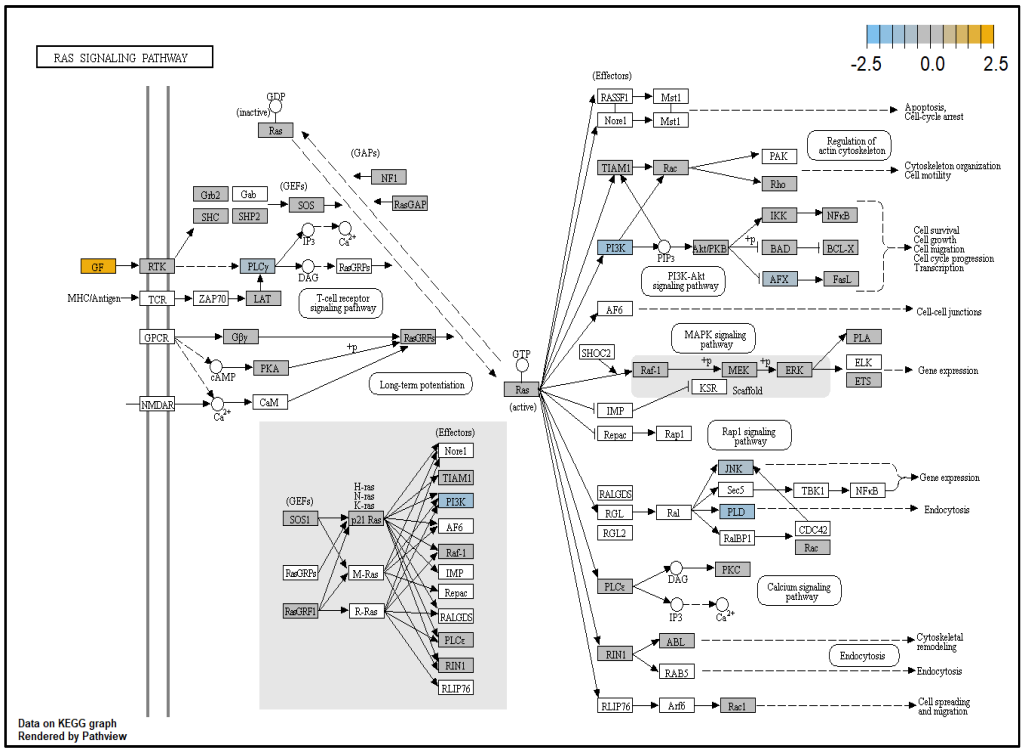

Figure 4.14: RAS signaling pathway (treatment time: differential expression in 4 hours vs. baseline of 0 hour for HONE-1 treated with L1 (Huanglian)
Upregulated genes: *GF*
Downregulated genes: *PLCy, P13K, PLD, AFX*

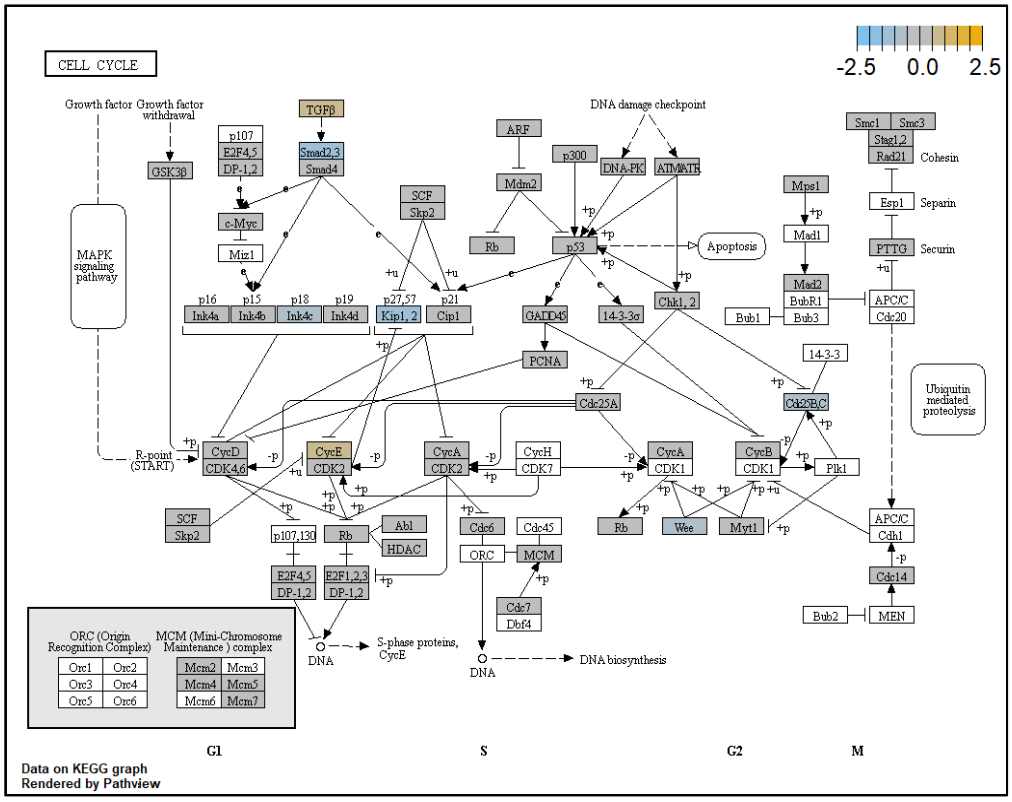

Figure 4.15: Cell-Cycle pathway signaling pathway (treatment time: differential expression in 4 hours vs. baseline of 0 hour for HONE-1 treated with L1 (Huanglian)
Upregulated genes: *CyclinE, TGFβ*
Downregulated genes: *Cd25B,C, Wee, Kip1,2, Smad2,3*

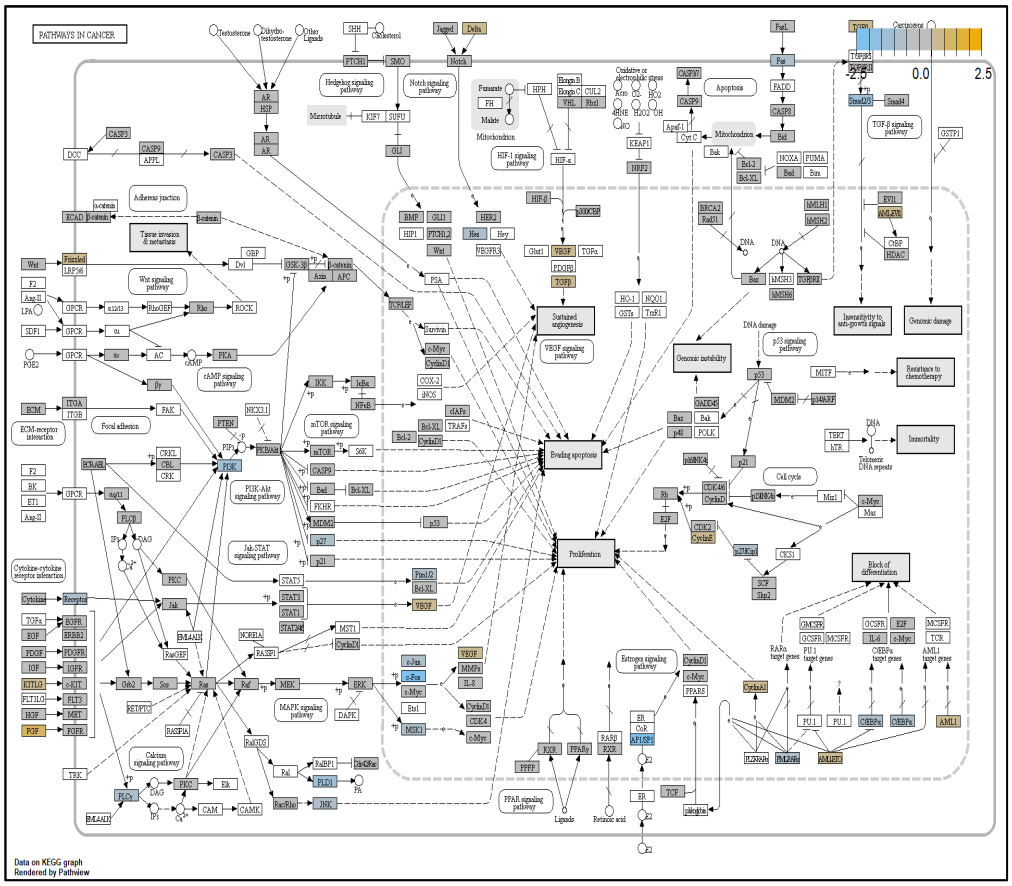

Figure 4.16: Pathway in cancer (treatment time: differential expression in 4 hours vs. baseline of 0 hour for HONE-1 treated with L1 (Huanglian)
Upregulated genes: *Delta*, *VEGF*, *TGFβ, CyclinE, Frizzled*
Downregulated genes: *eFOS*, *P13K*, *HES*

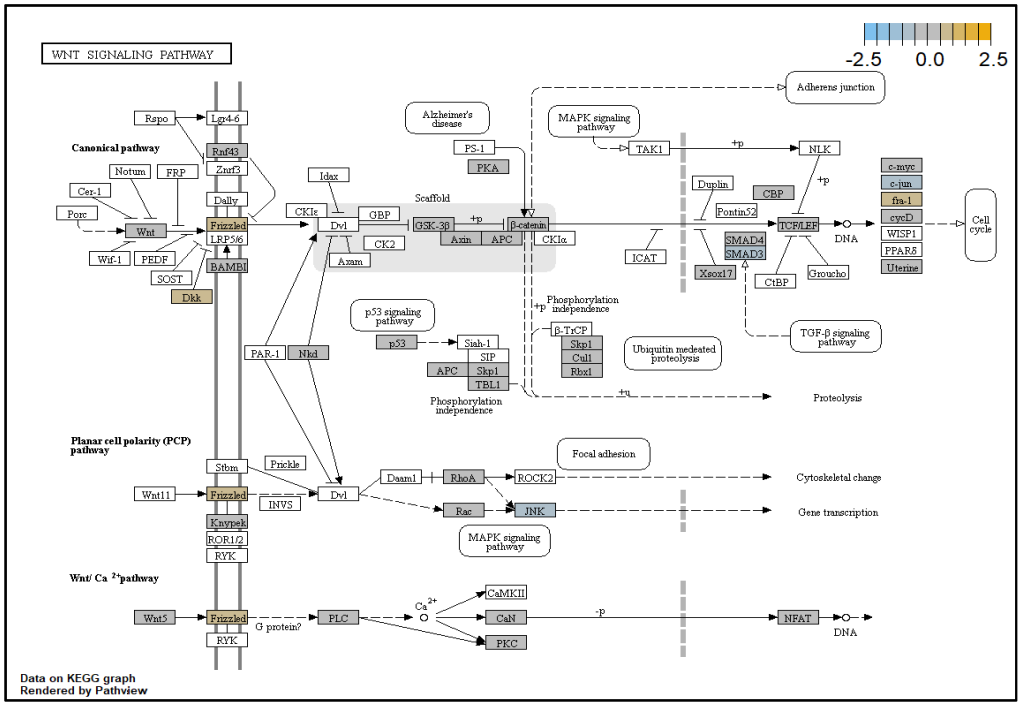

Figure 4.17: WNT Pathway (treatment time: differential expression in 4 hours vs. baseline of 0 hour for HONE-1 treated with L1 (Huanglian)
Upregulated genes: *DKK*, *FRIZZLED*, *fos-1*
Downregulated genes: *SMAD3*, *JNK*, *cjun*

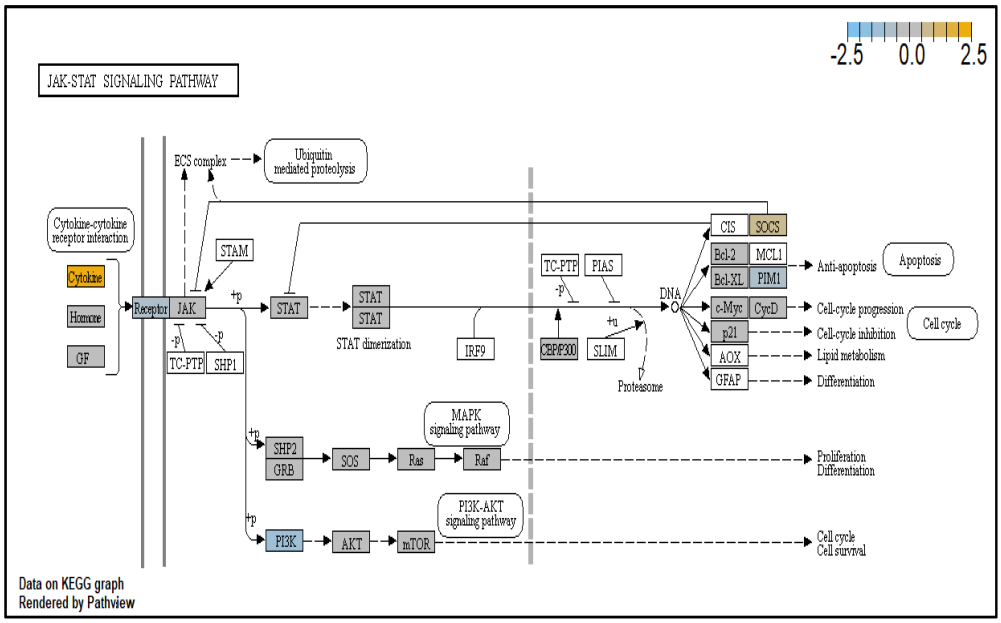

Figure 4.18: JAK-STAT signaling pathway (treatment time: differential expression in 4 hours vs. baseline of 0 hour for HONE-1 treated with L1 (Huanglian)
Upregulated genes: *Cytokine, SOCS*
Downregulated genes: *P13K, PIMI, Receptor*

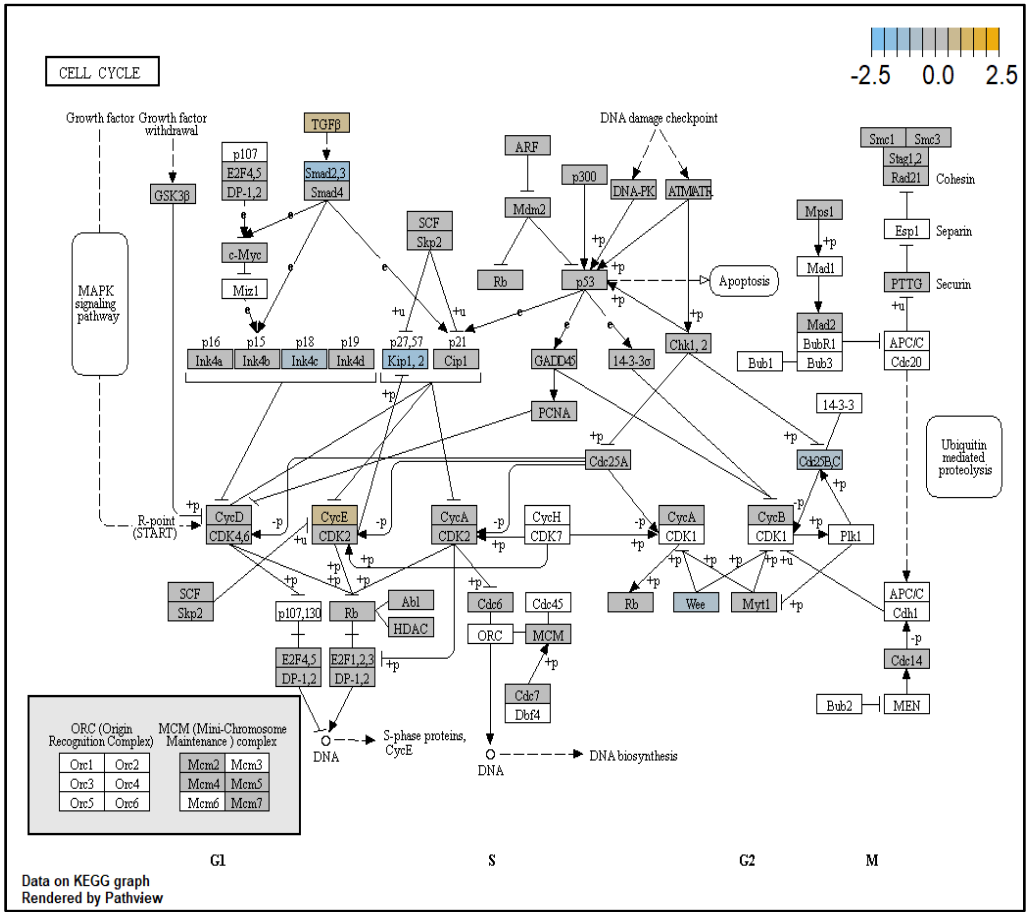

Figure 4.19: Cell-Cycle signaling pathway (treatment time: differential expression in 4 hours vs. baseline of 0 hour for HONE-1 treated with L1 (Huanglian)
Upregulated genes: *CycE, TGFβ*
Downregulated genes: *Smad3, kip1,2, Cd25B,C*

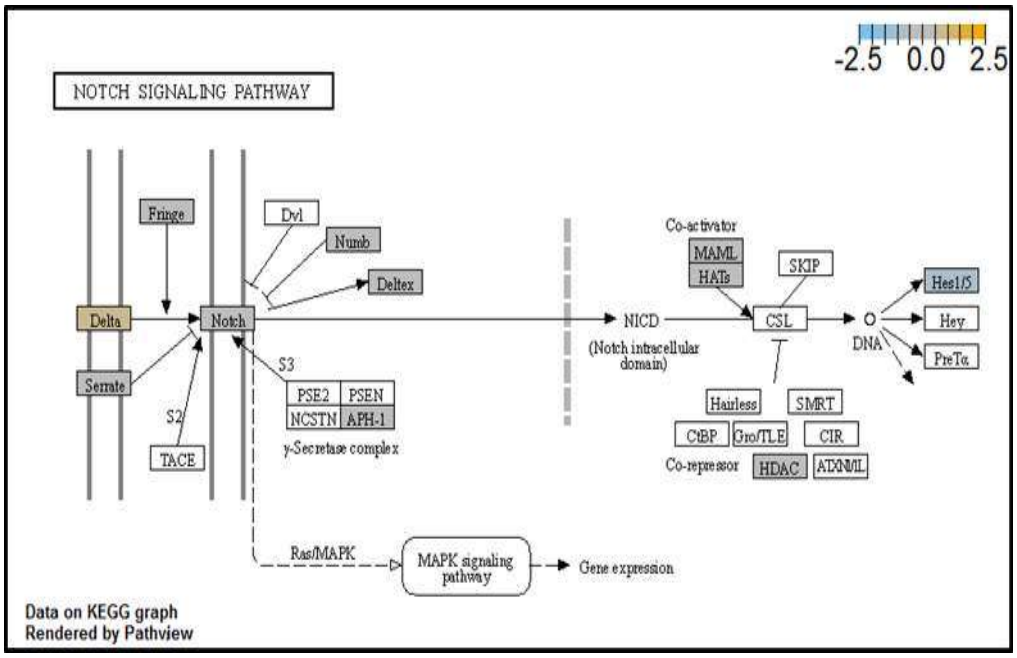

Figure 4.20: NOTCH signaling pathway (treatment time: differential expression in 4 hours vs. baseline of 0 hour for HONE-1 treated with L1 (Huanglian)
Upregulated genes: *Delta*
Downregulated genes: *HES1/5*

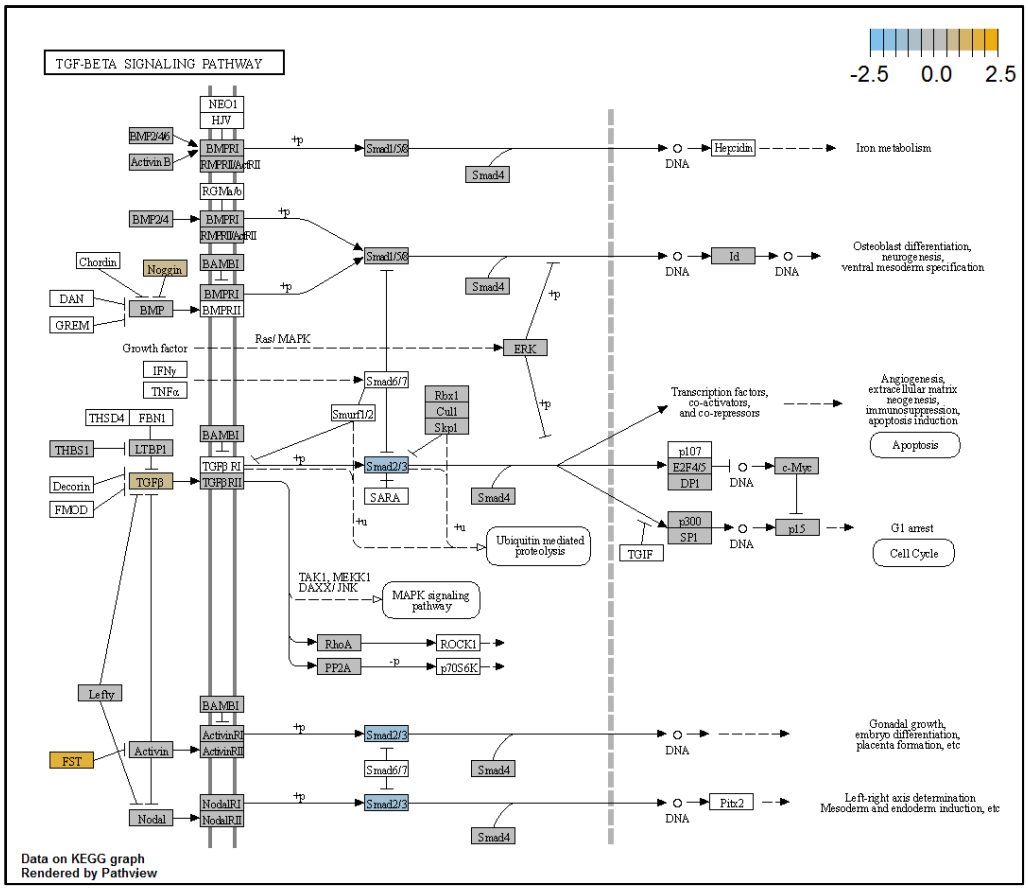

Figure 4.21: TGFβ signaling pathway (treatment time: differential expression in 4 hours vs. baseline of 0 hour for HONE-1 treated with L1 (Huanglian)
Upregulated genes: *Noggin, FST, TGFβ*
Downregulated genes: *Smad2, 3*

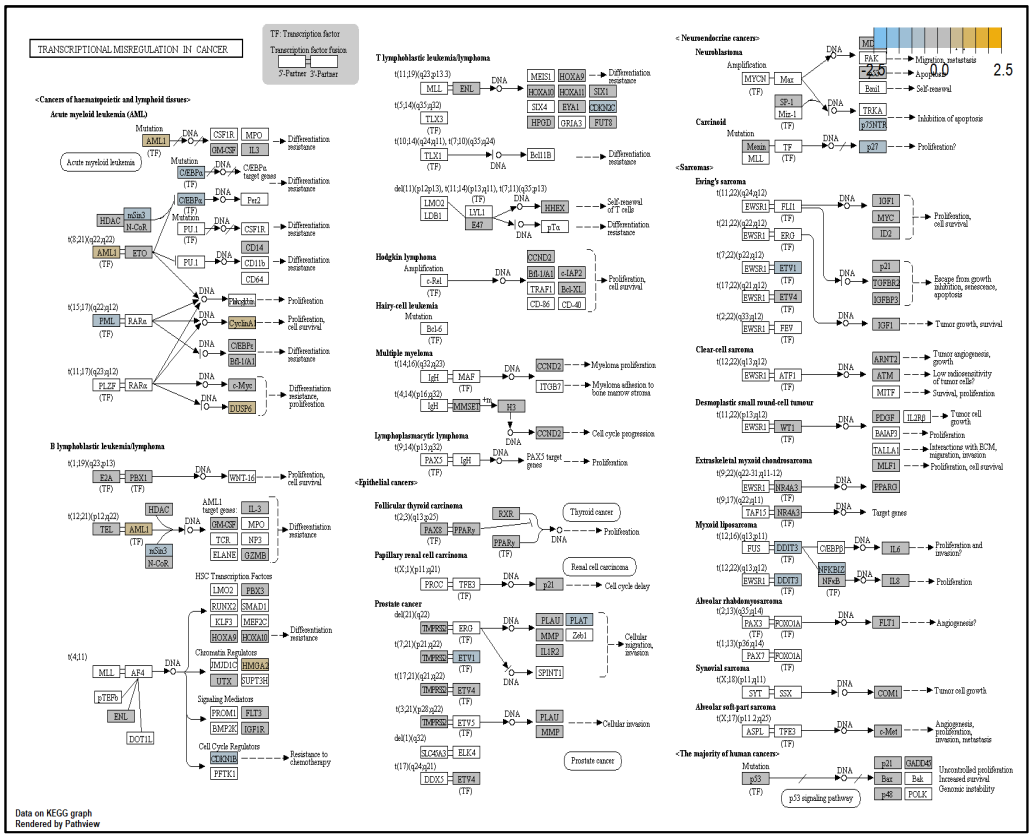

Figure 4.22: Transcription Misregulation signaling pathway (treatment time: differential expression in 4 hours vs. baseline of 0 hour for HONE-1 treated with L1 (Huanglian)
Upregulated genes: *DUSP6*, *CyclinA*, *AML1*
Downregulated genes: *CDKN2C*, *PLAT*, *ETV1*, *DDIT3*

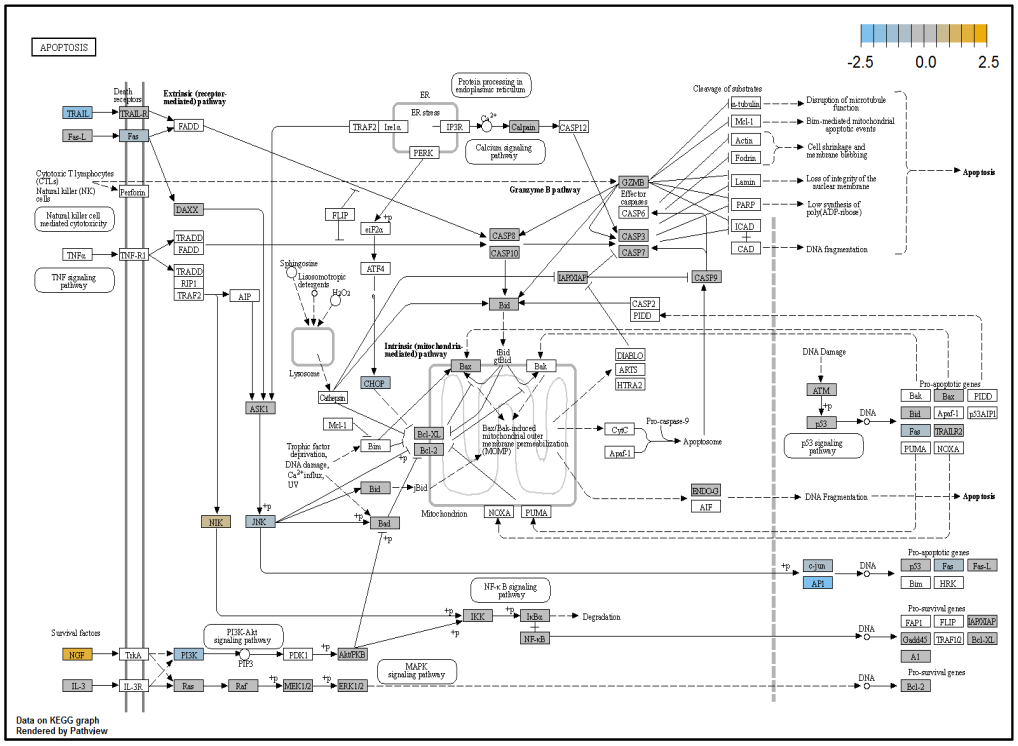

Figure 4.23: Apoptosis signaling pathway (treatment time: differential expression in 4 hours vs. baseline of 0 hour for HONE-1 treated with L1 (Huanglian)
Upregulated genes: *NIK*, *NGF*
Downregulated genes: *TRAIL*, *P13K*, *AP1*, *Fos*

4.5.1.2 Gene expression and pathway analysis of HONE-1 treated with L1 (Huanglian) at treatment time 8 hours vs. 0 hour

Among the 770 genes assayed, 35 up regulated genes showed a positive fold change whereas 114 down regulated genes showed a negative fold change ($P < 0.05$) as shown in Figure 4.24a. The top 20 most significant differentiately expressed genes are shown in Volcana plot (Figure 4.24b). Genes involved in a number of cancer pathways were enriched among the top differentially expressed genes as shown in Table 4.33. Regulation of genes at this time point were mainly initiated by signalling pathway such as MAPK, PI3K, RAS, Cell Cycle–Apoptosis, WNT, JAK-STAT, NOTCH, Transcription Misregulation, TGFβ. Gene expression data were mapped onto KEGG pathway graphs by Pathview function of the PanCancer pathway software (PCPAA), providing intuitive views of both up- and down-regulation at the pathway level. A representative graph for the signalling pathway is shown in Figures 4.25 to 4.34.

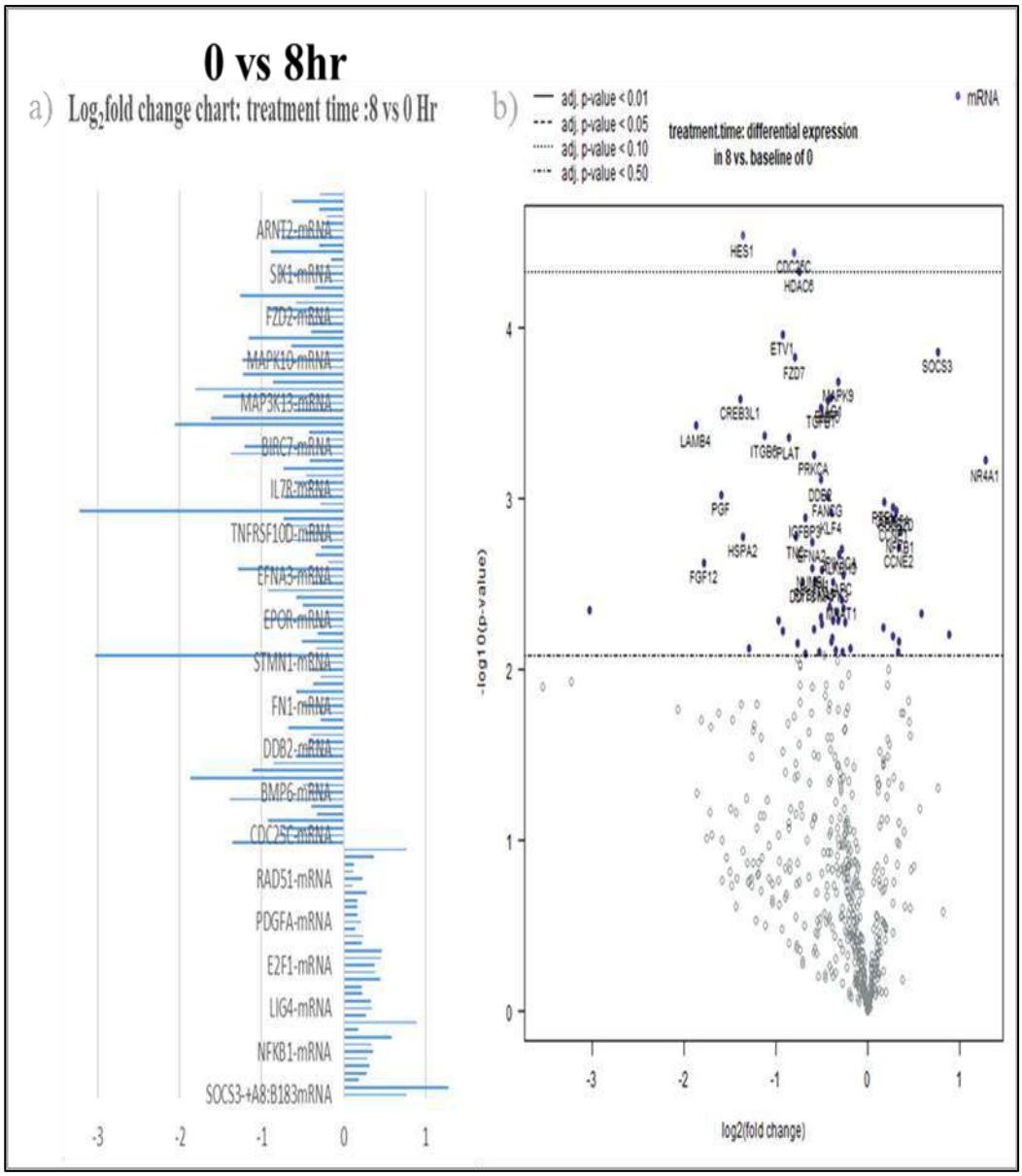

Figure 4.24 a) Log2 fold change difference between 8 hours vs. baseline of 0 hour in HONE1 cells treated with L1 (Huanglian) with differential expression comparing statistically significant differences (*P* < 0.05) in mRNA expression in the up and down regulated genes separately. A total of 35 up regulated genes show a positive fold change whereas 114 down regulated genes show a negative fold change. b) Volcano plot.

Table 4.33: The top 20 most significant differentially expressed genes (measured in log_2 fold change) with the selected covariate at treatment time 8 hours vs 0 hour with L1 (Huanglian)

Gene	Log2 fold change	*P*-value	Gene.sets	Biological Functions
CREB3L1	-1.39	0.000263	PI3K	**CAMP Responsive Element Binding Protein 3 Like 1** • a classical endoplasmic reticulum (ER) stress transducer
HES1	-1.36	2.92E-05	Notch	**Hes Family BHLH Transcription Factor 1** • a antagonist nuclear transcription factor
ITGB6	-1.12	0.000436	PI3K	**Integrin Subunit Beta 6** • adhesion receptors that function in signaling rom the extracellular matrix to the cell.
ETV1	-0.928	0.00011	Transcriptional Misregulation	**ETS Variant Transcription Factor** • regulates biological processes like cell growth, angiogenesis,
PLAT	-0.855	0.000445	Transcriptional Misregulation	**Plasminogen Activator, Tissue Type** • converts the proenzyme plasminogen to enzyme plasmin.
CDC25C	-0.8	3.68E-05	Cell Cycle - Apoptosis	**Cell Division Cycle 25C** • regulates G2/M progression and DNA damage repair. • activates the cyclin B1/CDK1 complex
FZD7	-0.789	0.000152	Wnt	**Frizzled Class Receptor 7** • WNT receptors are coupled to the beta-catenin canonical signaling pathway,
HDAC6	-0.74	4.73E-05	Chromatin Modification	**Histone Deacetylase 6** • regulates transcriptional regulation, cell cycle progression, development.
PRKCA (PKC)	-0.586	0.00056	MAPK, PI3K, Ras, Wnt	**Protein Kinase C Alpha** • involved in diverse cellular signaling pathways.
DDB2	-0.506	0.000787	DNA Damage - Repair	**Damage Specific DNA Binding Protein 2** • DNA repair of ultraviolet light-damaged
TGFB1	-0.505	0.000295	Cell Cycle - Apoptosis, MAPK, TGF-beta	**TGF-beta 1** • Ligands bind with TGF-beta receptors
FANCG	-0.435	0.000979	DNA Damage - Repair	**FA Complementation Group G** • DNA Repair Protein XRCC9
BMP6	-0.429	0.000272	TGF-beta	**Bone Morphogenetic Protein 6** • Ligands bind with TGF-beta receptors
JAG1	-0.393	0.000257	Notch	**Jagged Canonical Notch Ligand 1** • involved in early and late stages of

				mammalian cardiovascular development.
MAPK9	-0.323	0.000209	MAPK, Ras, Wnt	**Mitogen-Activated Protein Kinase 9** • modulate proliferation, differentiation, transcription regulation and development.
PTEN	0.184	0.00106	Driver Gene, PI3K	**Phosphatase And Tensin Homolog** • tumor suppressor by repressing AKT/PKB signaling pathway
CDC25A	0.276	0.00112	Cell Cycle - Apoptosis	**Cell Division Cycle 25A** • dual-specificity protein phosphatase • cell cycle regulators for cyclin/CDK complex
POLR2D	0.312	0.00118	DNA Damage - Repair	**RNA Polymerase II Subunit D** • responsible for synthesizing messenger RNA in eukaryotes
SOCS3	0.765	0.00014	JAK-STAT	**Suppressor of cytokine signaling 3** • cytokine-inducible repressor of cytokine signaling by inhibit the activity of JAK2 kinase.
NR4A1 (Nur77)	1.28	0.000604	MAPK, PI3K	**Nuclear receptor subfamily 4, group A, member 1** • controls bone marrow differentiation • nuclear transcription factor

Continuation of Table 4.33

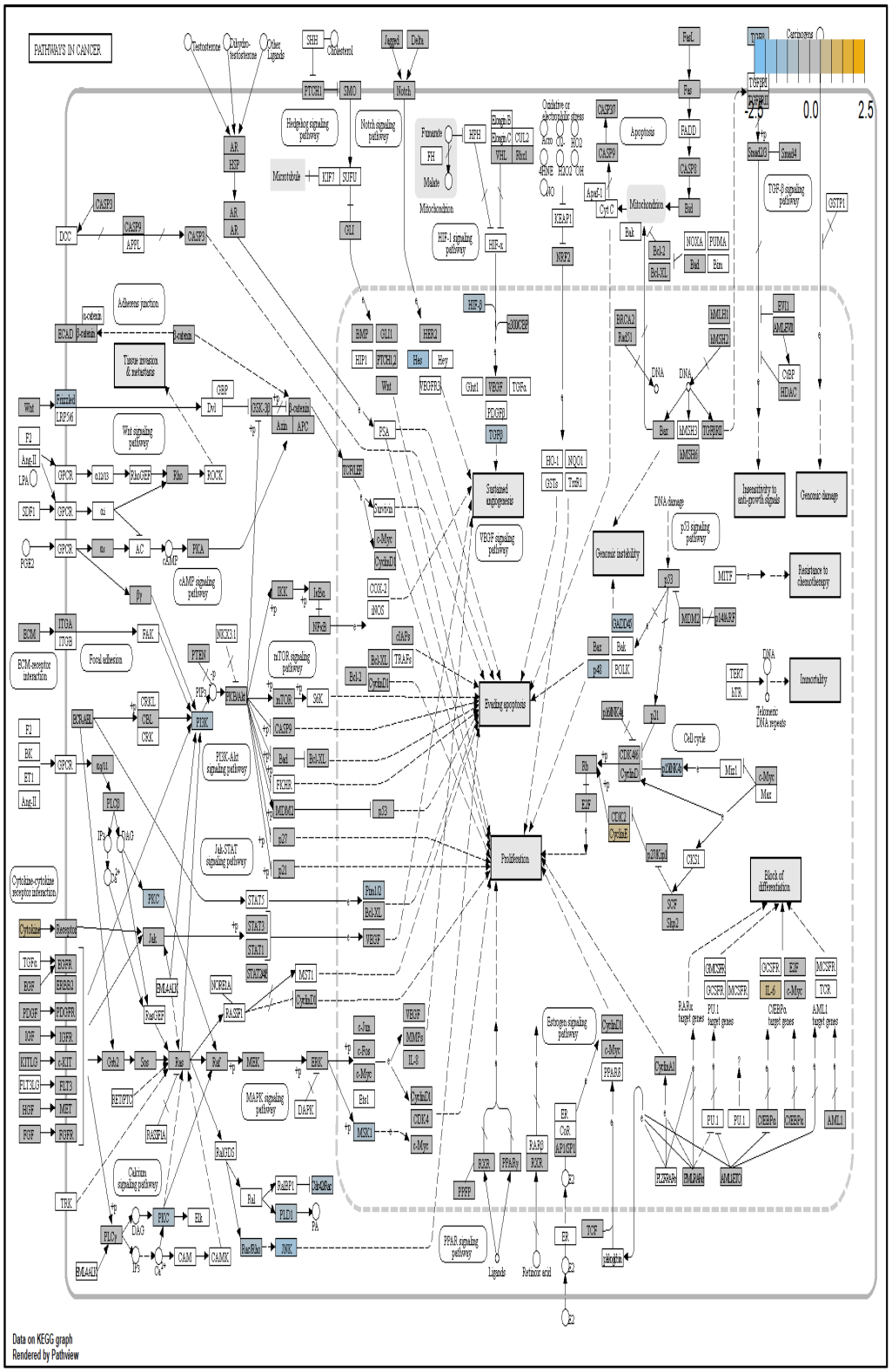

Figure 4.25: Cell Cycle in Cancer signaling pathway (treatment time: differential expression in 8 hours vs. baseline of 0 hour for HONE-1 treated with L1 (Huanglian)
Upregulated genes: *Ctokines, Cyclin, IL6*
Downregulated genes: *Frizzled, HES, P13K, PKC, JNK, TGFβ, MSK1*

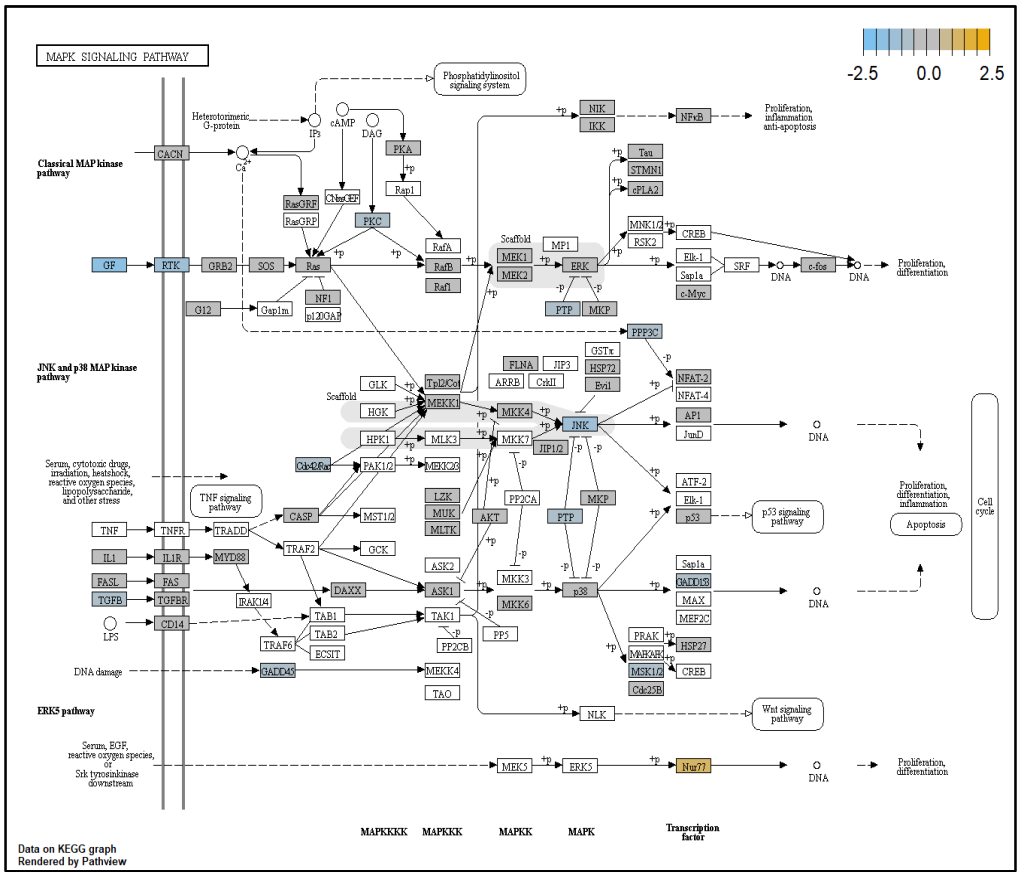

Figure 4.26: MAPK signaling pathway (treatment time: differential expression in 8 hours vs. baseline of 0 hour for HONE-1 treated with L1 (Huanglian)

Upregulated genes: *Nur77*

Downregulated genes: *GF, RTK, JNK, PKC, GADD45, TGFβ, PTP*

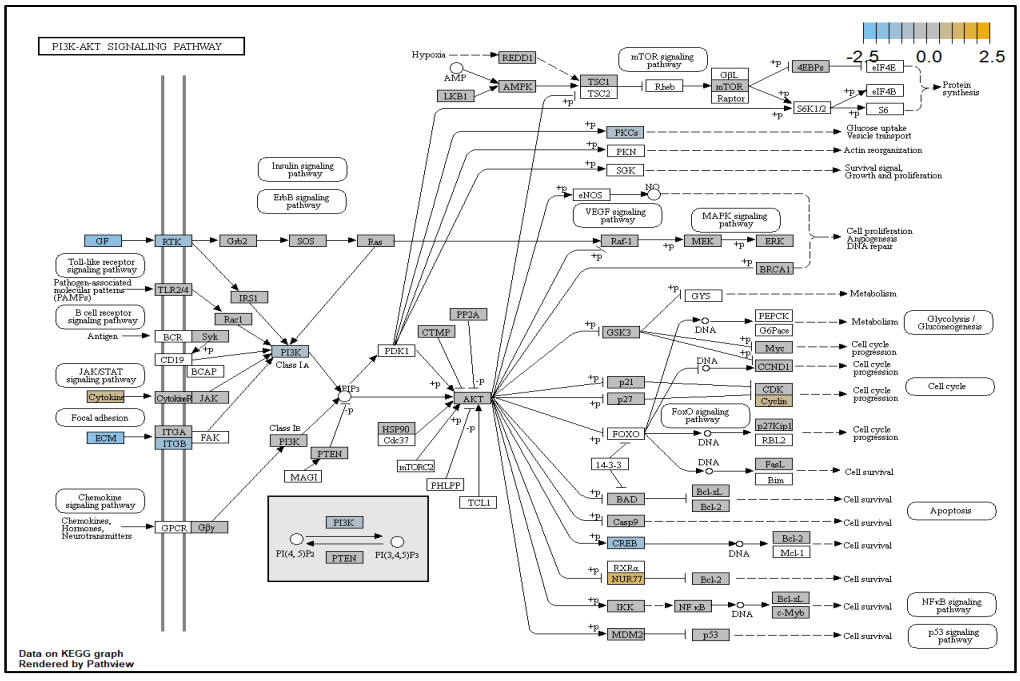

Figure 4.27: PI3K signaling pathway (treatment time: differential expression in 8 hours vs. baseline of 0 hour for HONE-1 treated with L1 (Huanglian)

Upregulated genes: *Cytokine, NUR77, Cyclin*

Downregulated genes: *GF, ECM, ITGB, RTK, CREB, PKC*

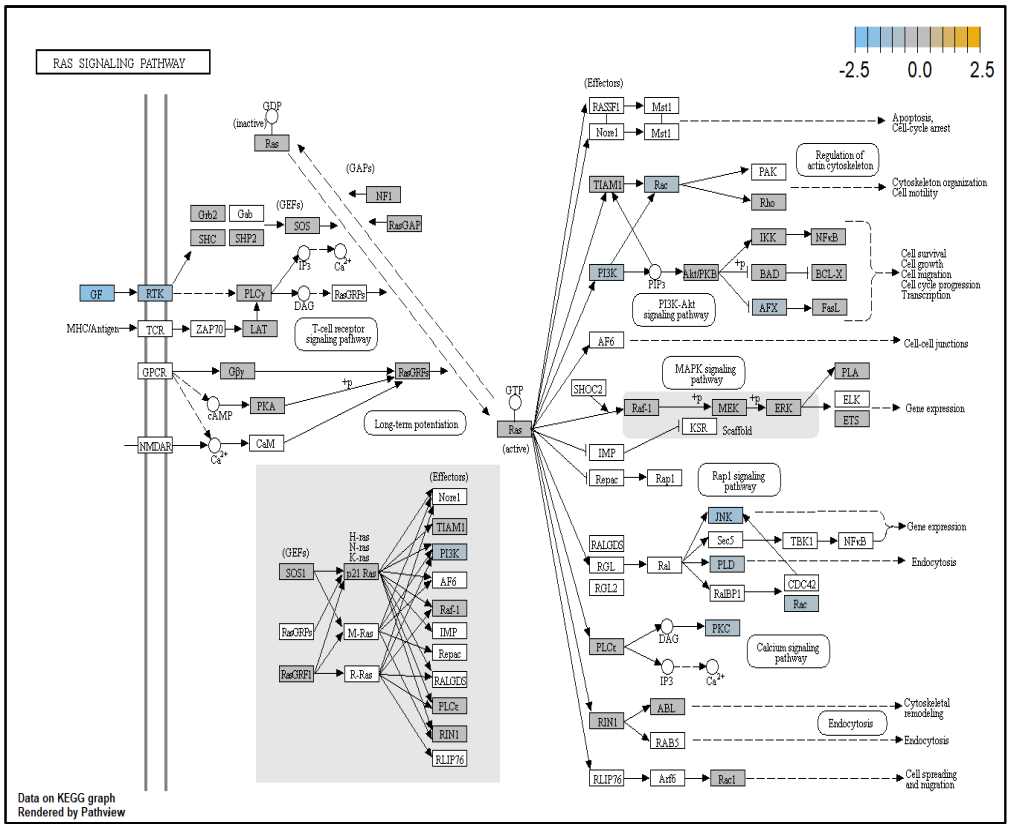

Figure 4.28: RAS signaling pathway (treatment time: differential expression in 8 hours vs. baseline of 0 hour for HONE-1 treated with L1 (Huanglian)
Downregulated genes: *GF*, *RTK*, *JNK*, *PLD*, *PKC*, *P13K*, *RAC*

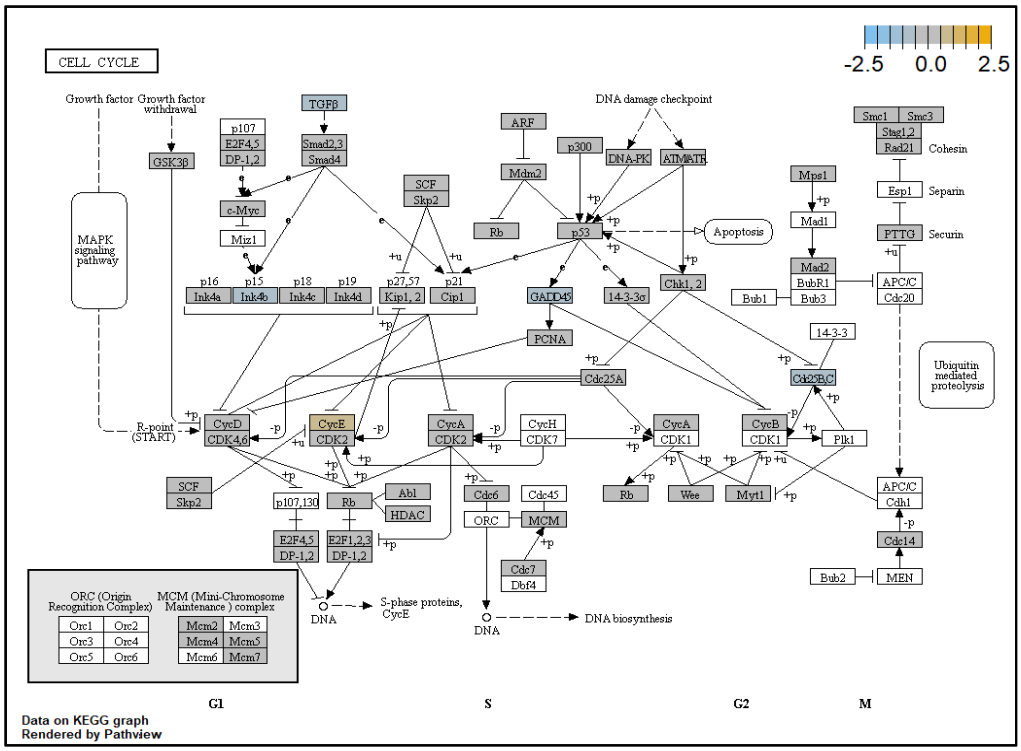

Figure 4.29: Cell Cycle signaling pathway (treatment time: differential expression in 8 hours vs. baseline of 0 hour for HONE-1 treated with L1 (Huanglian)
Upregulated genes: *CyclinE*
Downregulated genes: *TGFβ, GADD45, INK4b, Cdc25*

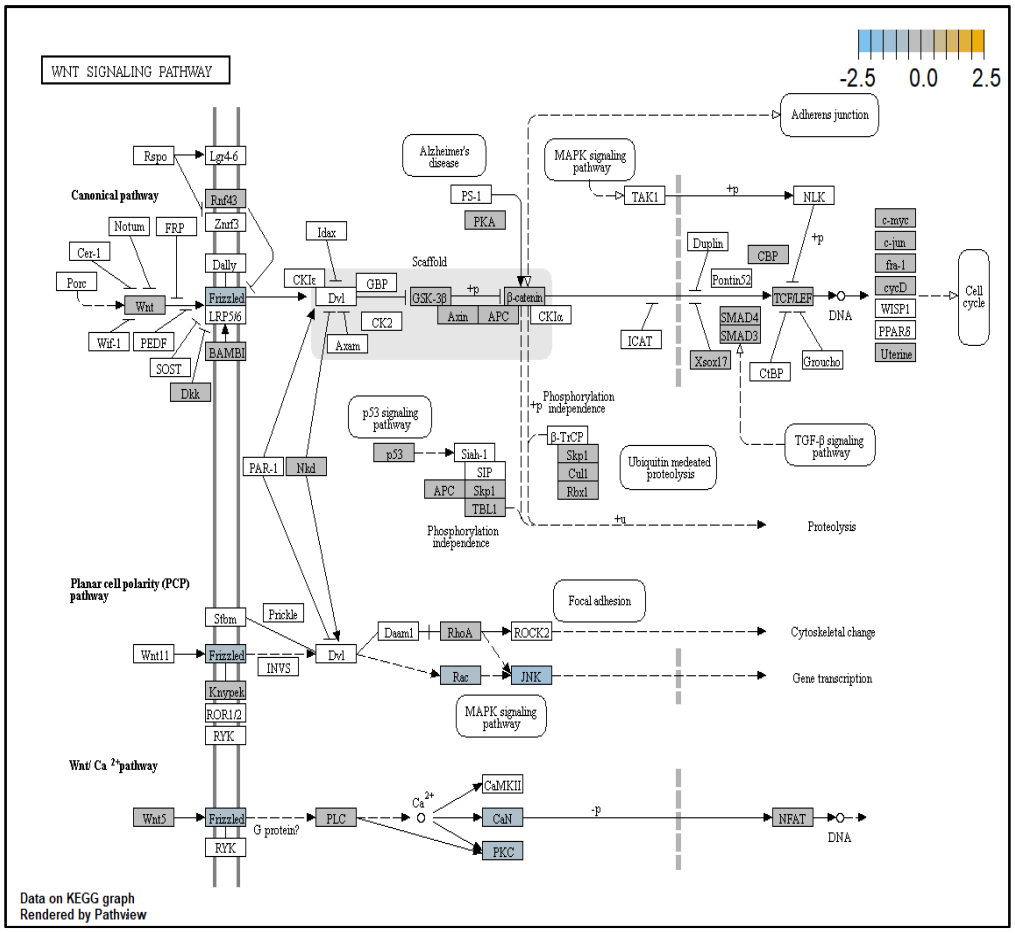

Figure 4.30: WNT signaling pathway (treatment time: differential expression in 8 hours vs. baseline of 0 hour for HONE-1 treated with L1 (Huanglian)
Downregulated genes: *Frizzled, RAC, JNK, PKC, CaN*

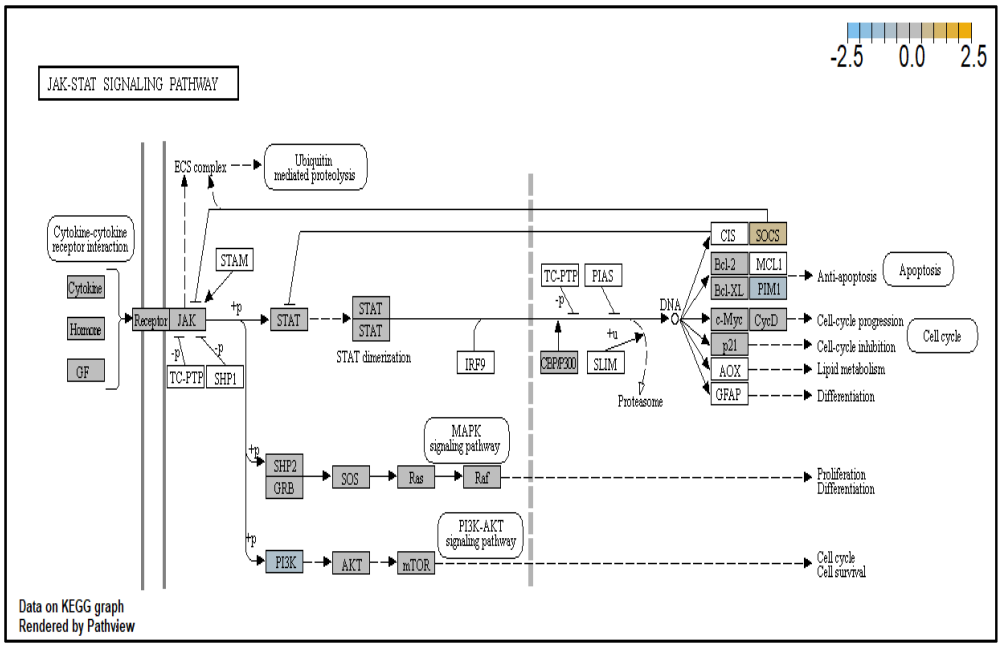

Figure 4.31: JAK-STAT signaling pathway (treatment time: differential expression in 8 hours vs. baseline of 0 hour for HONE-1 treated with L1 (Huanglian)
Upregulated genes: *SOCS*
Downregulated genes: *P13K, PIMI*

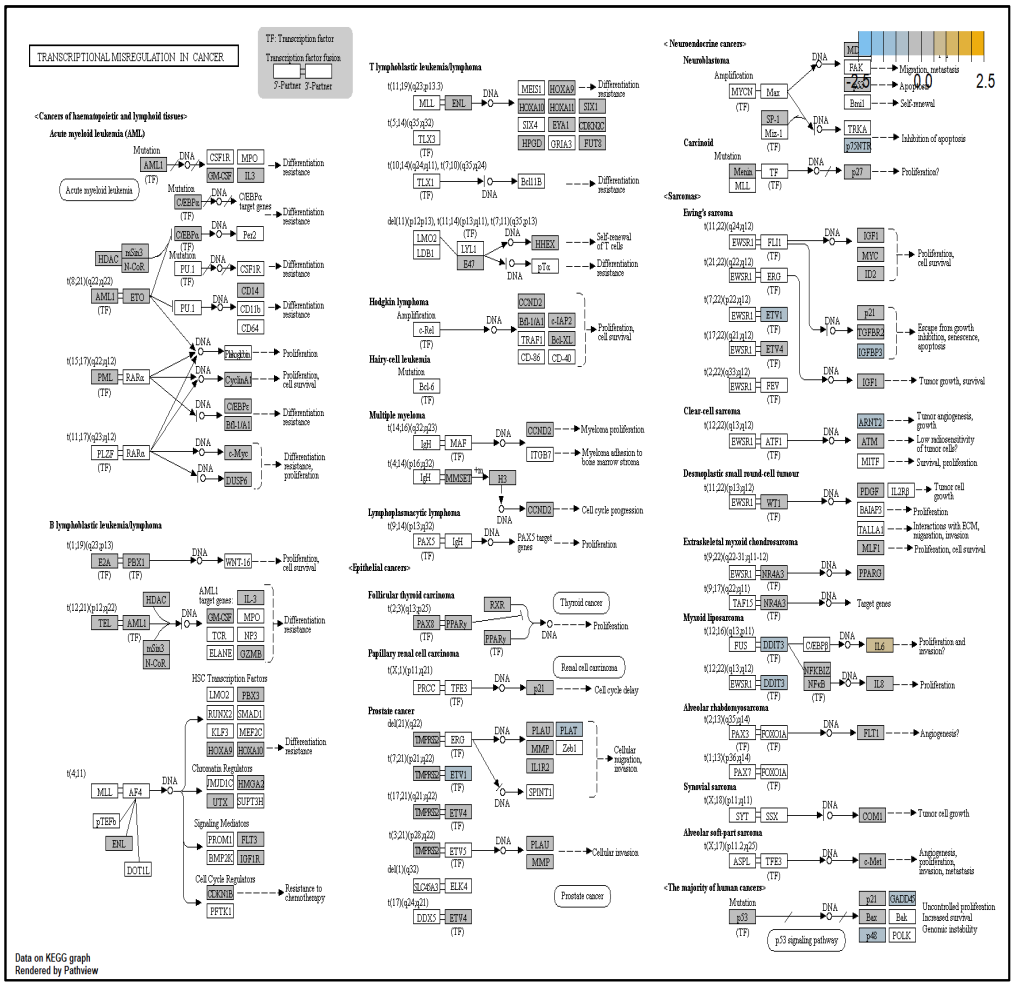

Figure 4.32: Transcription Misregulation signaling pathway (treatment time: differential expression in 8 hours vs. baseline of 0 hour for HONE-1 treated with L1 (Huanglian)
Upregulated genes: *IL6*
Downregulated genes: *IGFBP3, ETV1, DDIT3, p75NTR, GADD45, p48*

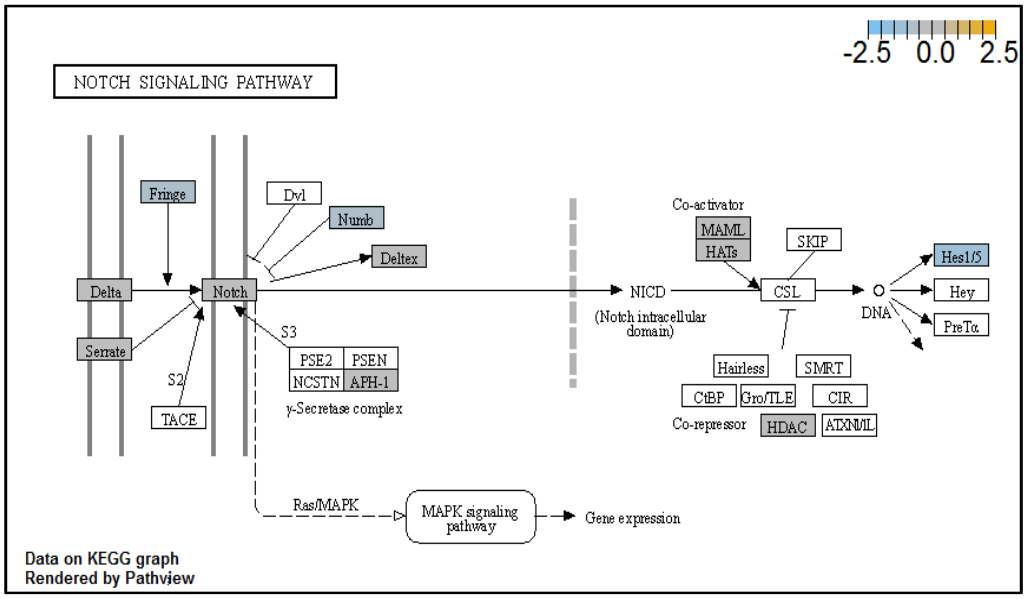

Figure 4.33: NOTCH signaling pathway (treatment time: differential expression in 8 hours vs. baseline of 0 hour for HONE-1 treated with L1 (Huanglian)
Downregulated genes: *Fringe, Numb, Hes1/5*

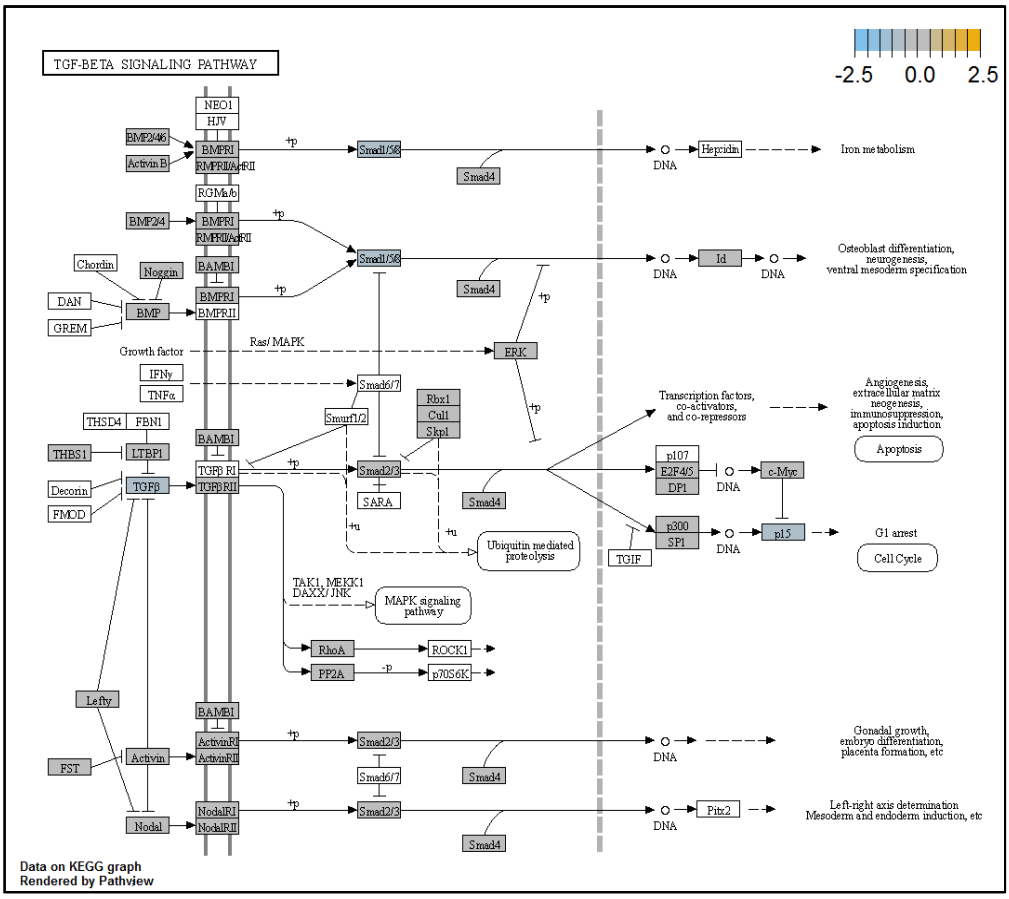

Figure 4.34: TGFβ signaling pathway (treatment time: differential expression in 8 hours vs. baseline of 0 hour for HONE-1 treated with L1 (Huanglian)

Downregulated genes: *TGFβ, p15, Smad*

4.5.1.3 12 hours vs 0 hour gene expression

Among the 770 genes assayed, 77 up regulated genes showed a positive fold change whereas 91 down regulated genes showed a negative fold change ($P < 0.05$) as shown in Figure 4.35a. The top 20 most significant differentiately expressed genes are shown in Volcana plot (Figure 4.35b). Genes involved in a number of cancer pathways were enriched among the top differentially expressed genes as shown in Table 4.34. Regulation of genes at this time point were mainly initiated by signalling pathway such as MAPK, PI3K, RAS, Cell Cycle–Apoptosis, WNT, JAK-STAT, NOTCH, Transcription Misregulation. Gene expression data were mapped onto KEGG pathway graphs by Pathview function of the PanCancer pathway software (PCPAA), providing intuitive views of both up and deregulation at the pathway level. A representative graph for the signalling pathway are shown in Figures 4.36 to 4.45.

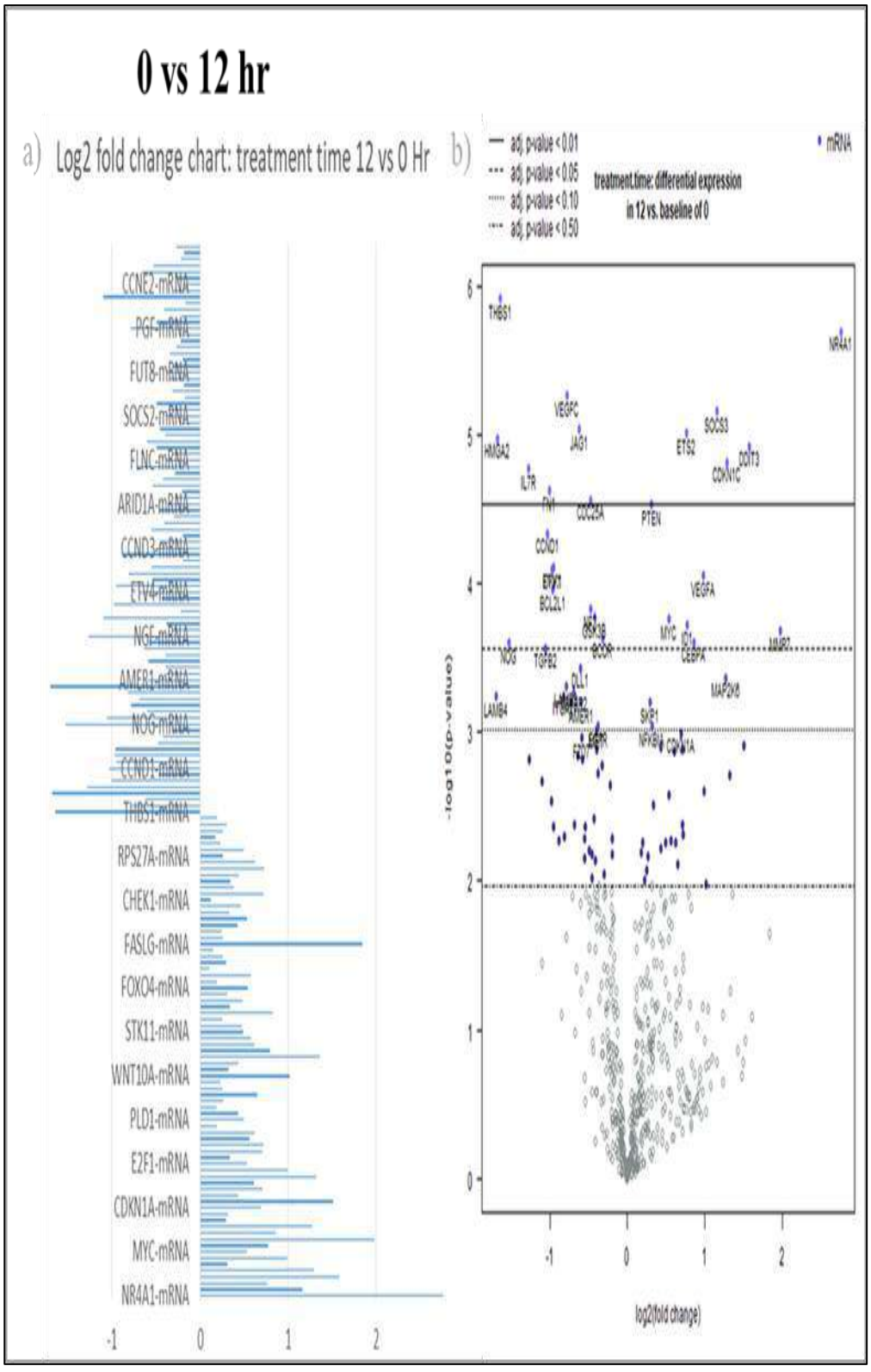

Figure 4.35: a) Log2 fold change difference between 12 hours vs. baseline of 0 hour in HONE 1 cells treated with L1 (Huanglian) with differential expression comparing statistically significant differences (*P* < 0.05) in mRNA expression in the up and down regulated genes separately. A total of 77 up regulated genes show a positive fold change whereas 91 down regulated genes show a negative fold change. b) Volcano plot

Table 4.34: The top 20 most significant differentially expressed genes (measured in log_2 fold change) with the selected covariate at treatment time 12 hours vs 0 hour

Gene	Log_2 fold change	*P*-value	Gene.sets	Biological functions
HMGA2	-1.68	1.06E-05	Transcriptional Misregulation	**High Mobility Group AT-Hook 2** • contains structural DNA-binding domains • transcriptional regulating factor. • cell cycle regulation through CCNA2
THBS1	-1.64	1.22E-06	PI3K, TGF-beta	**Thrombospondin 1** • Adhesive glycoprotein that mediates cell-to-cell and cell-to-matrix interactions.
IL7R	-1.28	1.68E-05	JAK-STAT, PI3K	**Interleukin 7 Receptor** • a receptor for interleukin 7 (IL7)
CCND1	-1.03	4.60E-05	Cell Cycle - Apoptosis, JAK-STAT, PI3K, Wnt	**Cyclin D1** • forms a complex with CDK4 or CDK6, regulates cell cycle G1/S transition.
FN1	-1.01	2.39E-05	PI3K	**Fibronectin 1** • an extracellular matrix (ECM) component • communicate between the intra and extracellular environment
ETV1	-0.972	7.97E-05	Transcriptional Misregulation	**ETS Variant Transcription Factor** • modulate biological processes like cell growth, angiogenesis,
BCL2L	-0.966	0.00011	Cell Cycle-Apoptosis, JAK-STAT, PI3K, Ras, Transcriptional Misregulation	**BCL2 Like 1** • form hetero- or homodimers and act as anti- or pro-apoptotic regulators
DKK1	-0.952	7.88E-05	Wnt	**Dickkopf WNT Signaling Pathway Inhibitor 1** • binds to LRP6 co-receptor, inhibits beta-catenin-dependent Wnt signaling.
VEGFC	-0.778	5.41E-06	PI3K, Ras	**Vascular Endothelial Growth Factor C** • promotes angiogenesis and endothelial cell growth
JAG1	-0.627	9.10E-06	Notch	**Jagged Canonical Notch Ligand 1** • involved in early and late stages of mammalian cardiovascular development.
NF2	-0.476	0.000148	Driver Gene	**Neurofibromin 2** • link cytoskeletal components with proteins in the cell membrane.
CDC25A	-0.475	2.74E-05	Cell Cycle - Apoptosis	**Cell Division Cycle 25A** • regulates G1/S phase progression of cell cycle. • activates the cyclin-dependent kinase CDC2
GSK3B	-0.424	0.000168	Cell Cycle - Apoptosis,	**Glycogen Synthase Kinase 3 Beta** • serine-threonine kinase, negative regulator of glucose homeostasis

			Hedgehog, PI3K, Wnt	
NR4A1	2.76	2.02E-06	MAPK, PI3K	**Nuclear receptor subfamily 4, group A, member 1** • controls bone marrow differentiation • nuclear transcription factor
DDIT3 (CHOP, GADD)	1.58	1.19E-05	MAPK, Transcriptional Misregulation	**DNA Damage Inducible Transcript 3** • transcription factors, implicated in adipogenesis and erythropoiesis, is activated by endoplasmic reticulum stress, and pro- apoptosis.
CDKN1C (KIP2 /p57)	1.29	1.52E-05	Cell Cycle - Apoptosis	**Cyclin Dependent Kinase Inhibitor 1C** • inhibitor of several G1 cyclin/Cdk complexes and a negative regulator of cell proliferation.
SOCS3	1.16	6.91E-06	JAK-STAT	**Suppressor of cytokine signaling 3** • cytokine-inducible repressor of cytokine signaling and inhibit the activity of JAK2 kinase.
VEGFA	0.987	8.92E-05	PI3K, Ras	**Vascular Endothelial Growth Factor A** • induces proliferation and migration of vascular endothelial cells, essential for angiogenesis.
ETS2	0.763	9.85E-06	Ras	**ETS Proto-Oncogene 2, Transcription Factor** • regulates genes involved in development and apoptosis.
PTEN	0.311	2.95E-05	Driver Gene, PI3K	**Phosphatase And Tensin Homolog** • tumor suppressor by repressing AKT/PKB signaling pathway

Continuation of Table 4.34

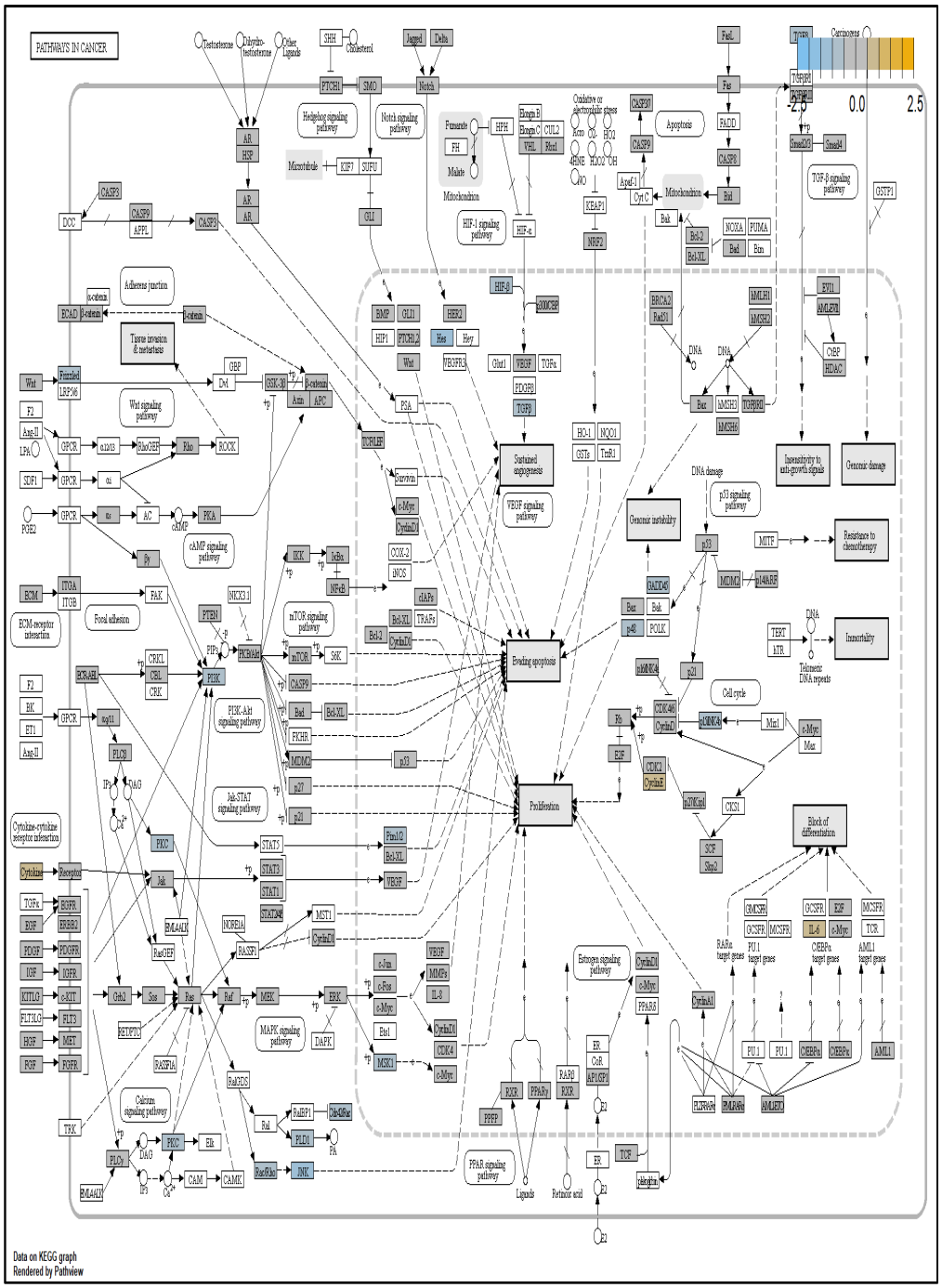

Figure 4.36: Cell Cycle in Cancer signaling pathway (treatment time: differential expression in 12 hours vs. baseline of 0 hour for HONE-1 treated with L1 (Huanglian)
Upregulated genes: *FGFR, p21, cFOS, cMYC. AP1, BMP*
Downregulated genes: *ECM, CycD1, BCL-XL, BCL-2, ITGA, Jagged, Delta, TGFB, Frizzled*

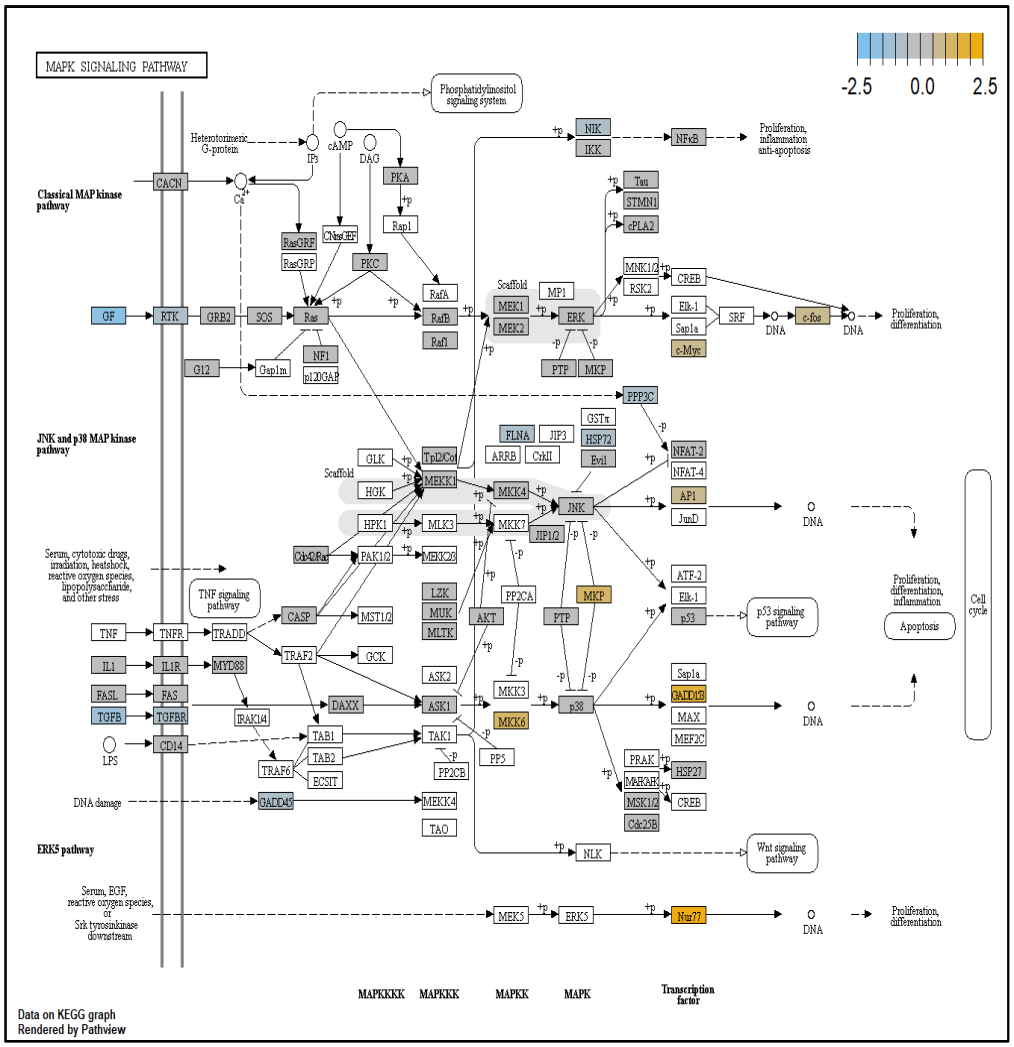

Figure 4.37: MAPK signaling pathway (treatment time: differential expression in 12 hours vs. baseline of 0 hour for HONE-1 treated with L1 (Huanglian)

Upregulated genes: *Nur77, GADD53, MKK6, MKP, AP1, cMYC, cFos*

Downregulated genes: *GF, TGFB, TGFBR, GADD45, PPP3C, FLNA, RTK, HSP72, NIK*

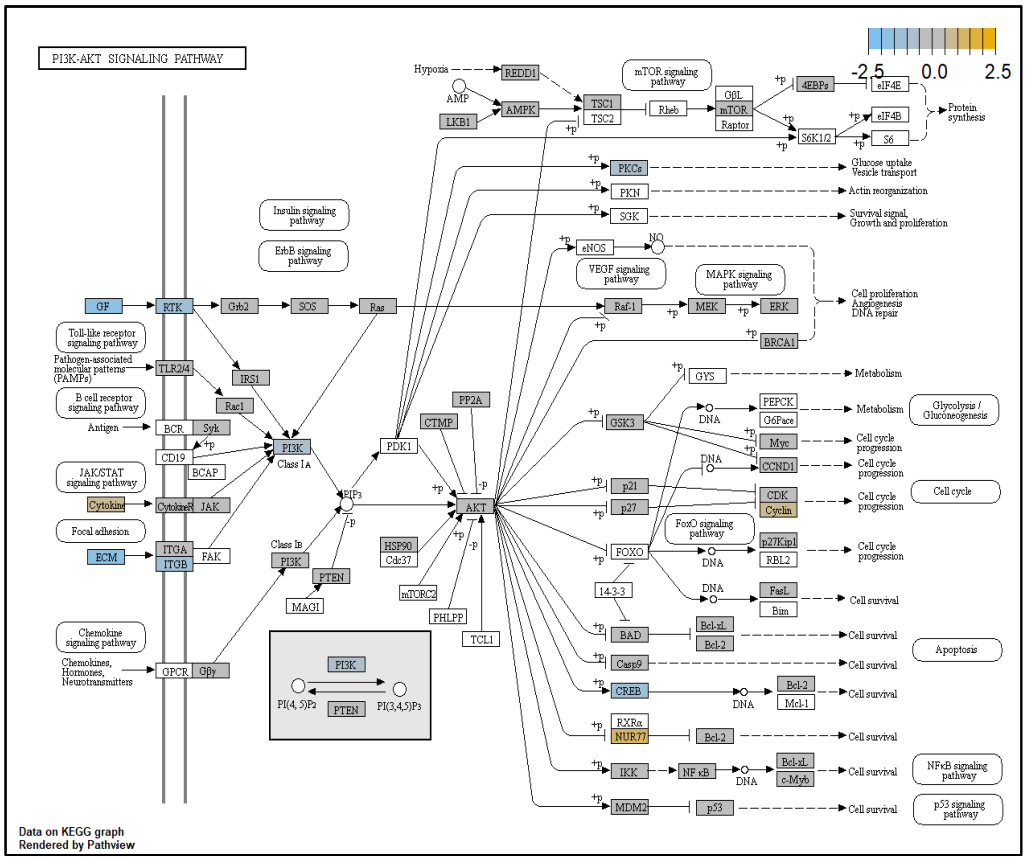

Figure 4.38: PI3K signaling pathway (treatment time: differential expression in 12 hours vs. baseline of 0 hour for HONE-1 treated with L1 (Huanglian)
Upregulated genes: *Cytokine*, *NUR77*, *Cyclin*
Downregulated genes: *GF*, *RTK*, *ECM*, *PI3K*, *PKC*, *CREB*

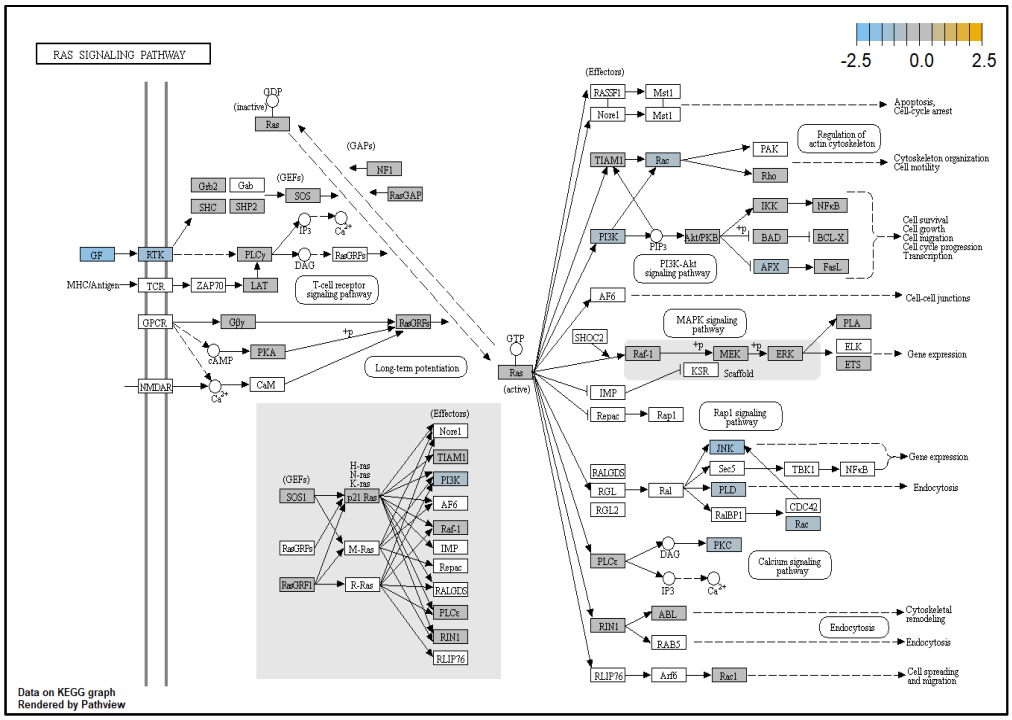

Figure 4.39: RAS signaling pathway (treatment time: differential expression in 12 hours vs. baseline of 0 hour for HONE-1 treated with L1 (Huanglian)
Downregulated genes: *GF*, *RTK*, *P13K*, *RAC*, *AFX*, *JNK*, *PLD*, *PKC*

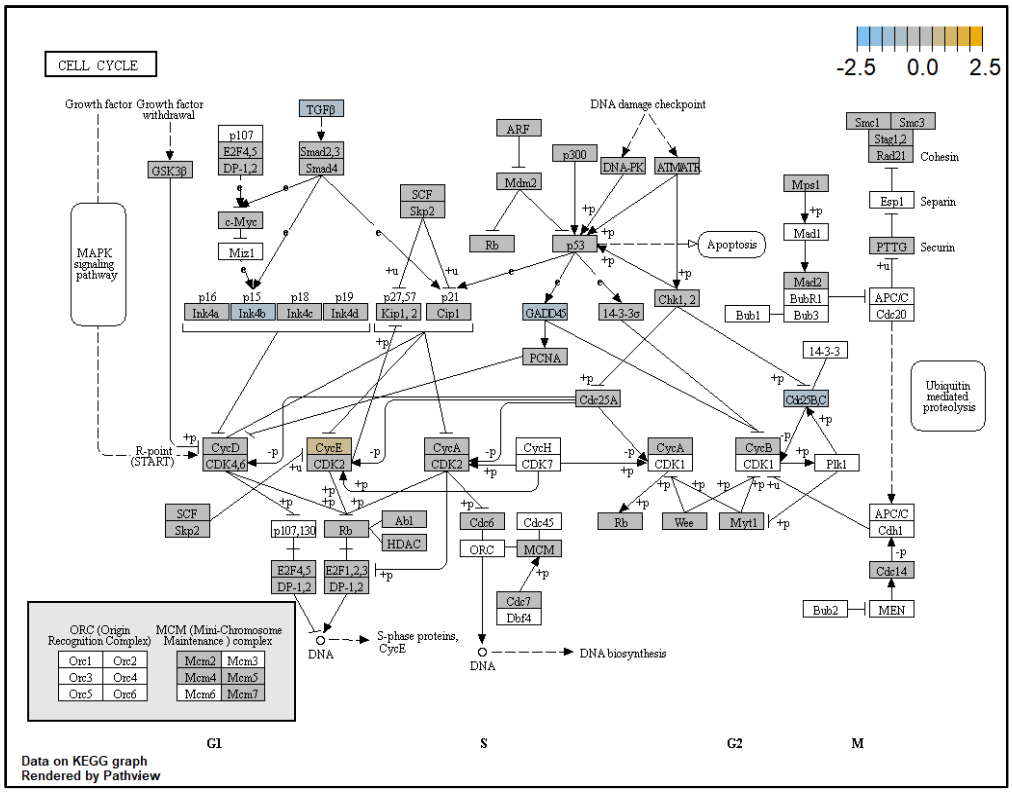

Figure 4.40: Cell Cycle signaling pathway (treatment time: differential expression in 12 hours vs. baseline of 0 hour for HONE-1 treated with L1 (Huanglian)

Upregulated genes: *CycE*

Downregulated genes: *TGFB, Ink4b, GADD45, Cdc25B/C*

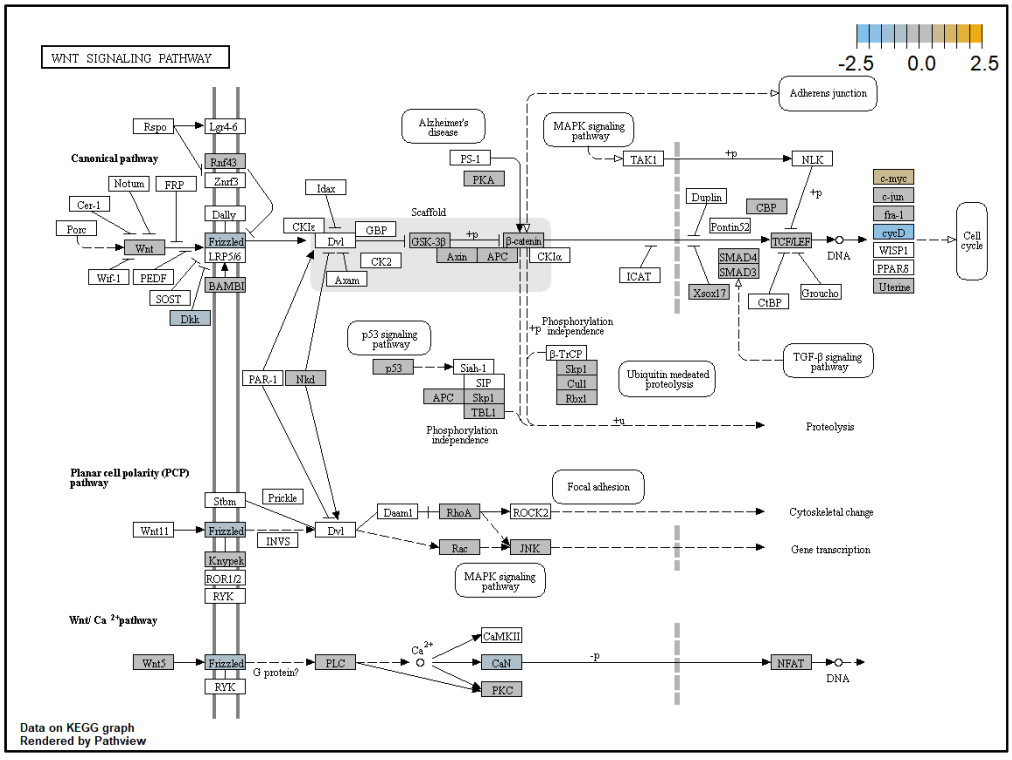

Figure 4.41: WNT signaling pathway (treatment time: differential expression in 12 hours vs. baseline of 0 hour for HONE-1 treated with L1 (Huanglian)

Upregulated genes: *cmyc*

Downregulated genes: *DKK, Frizzled, cycD, CaN*

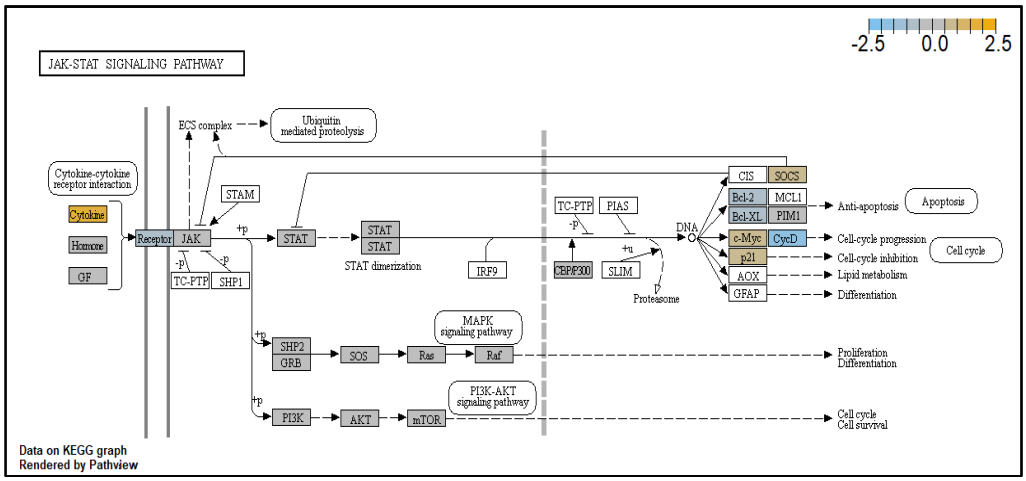

Figure 4.42: JAK-STAT signaling pathway (treatment time: differential expression in 12 hours vs. baseline of 0 hour for HONE-1 treated with L1 (Huanglian)
Upregulated genes: *Cytokine*, *SOCS*, *cMyc*, *p21*
Downregulated genes: *CycD*, *Cytokine Receptor gene*

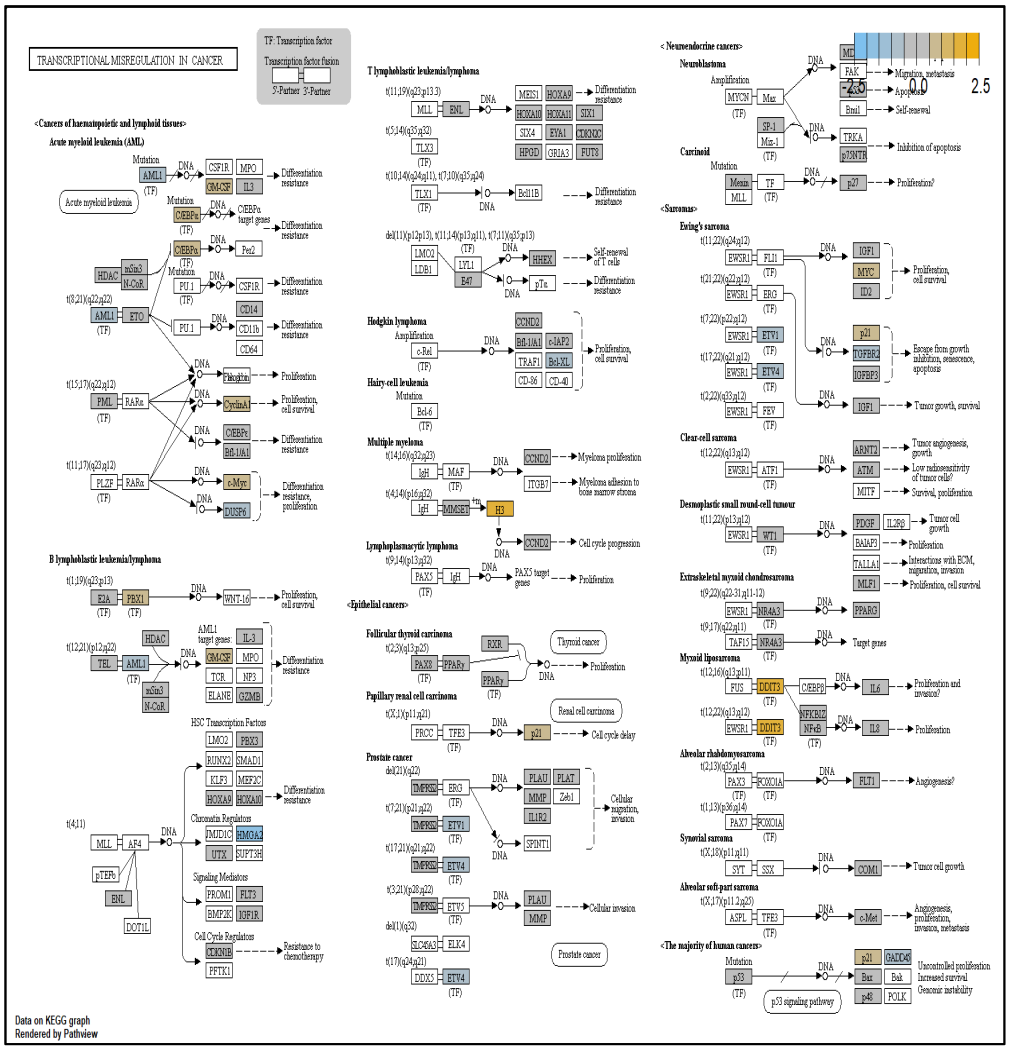

Figure 4.43: Transcription Misregulation signaling pathway (treatment time: differential expression in 12 hours vs. baseline of 0 hour for HONE-1 treated with L1 (Huanglian)
Upregulated genes: *H3, p21, cMyc, CycA, PBX1, GMCSF, DDIT3*
Downregulated genes: *BCL-XL, HMGA2, GADD45, ETV1/4, AML1, DUSP6, TGFBR2*

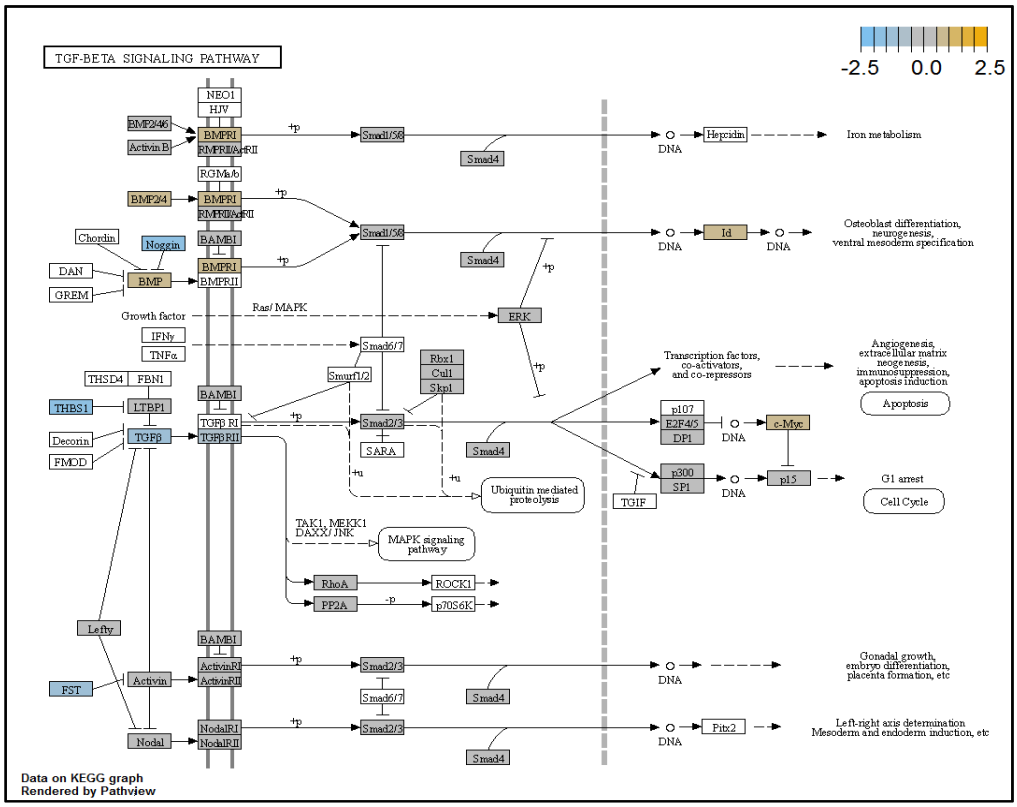

Figure 4.44: TGFβ signaling pathway (treatment time: differential expression in 12 hours vs. baseline of 0 hour for HONE-1 treated with L1 (Huanglian)
Upregulated genes: *BMPR1, BMP, BMP2/4, cMyc, Id*
Downregulated genes: *Noggin, THBS1, TGFB, FST*

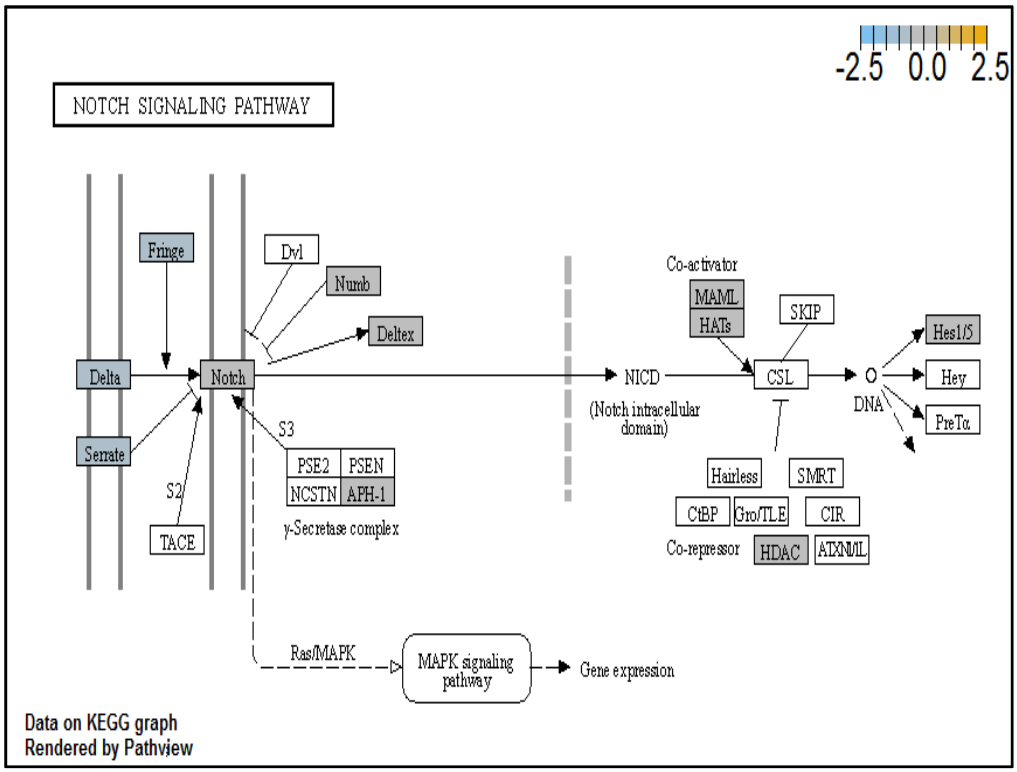

Figure 4.45: NOTCH signaling pathway (treatment time: differential expression in 12 hours vs. baseline of 0 hour for HONE-1 treated with L1 (Huanglian)
Downregulated genes: *Fringe, Delta, Serrate*

4.5.1.4 Venn Diagram

The common differentially expressed genes of HONE1 at three different treatment times such as 4, 8 and 12 hours after exposure to L1, in both upregulated and downregulated gene lists, were identified by using Venny online tool. As shown in Figure 4.5.1.4.1, a total of 212 genes were downregulated and 110 genes were upregulated in HONE1 cells at the three time points. In the case of upregulated genes, a total number of 17 genes (19.3%) were found between 4 and 8 hours treatment time; 3 genes (3.4%) found between 8 and 12 hourrs treatment time and 2 genes (2.3%) found between 4 and 12 hours treatment time whereas none is common in between three treatment times. In the case of downregulated genes, a total number of 45 genes (28.7%) were found between 4 and 8hours treatment time; 7 genes (4.5%) found between 8 and 12 hour treatment time and 1 gene (0.6%) was found between 4 and 12 hours treatment time whereas 1 gene (0.6%) in between three treatment times.

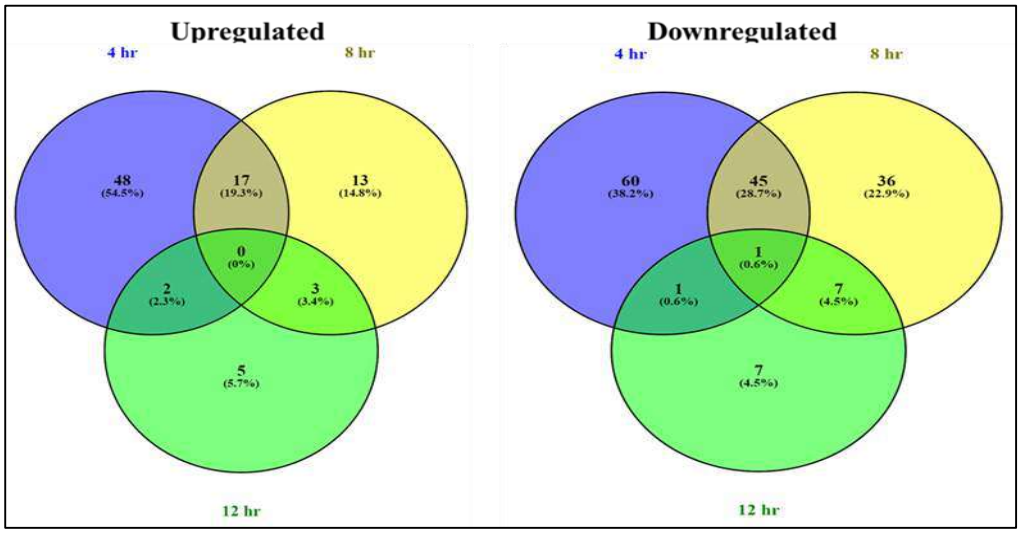

Figure 4.46: **Venn diagram depicting the common genes differentially regulated in HONE1 cells after treatment at different time point. The number of downregulated and upregulated genes in HONE-1 cells after exposure to L1 is indicated in the diagram**

4.5.2 Gene expression and pathway analysis of HONE1 treated with L7 (XXXD)

NanoString PanCancer Pathways Panel gene expression analysis was used to quantify transcript levels of 770 genes representing 13 canonical cancer pathways in HONE1 cells upon treatment with L7 (XXXD). The gene expression was analysed at 4 vs 0, 8 vs 0 and 12 vs 0 hour treatment. Total RNA extracted from HONE1 cells at different time points were hybridized to the codeset with approximately one million raw counts tallied for all genes in each sample. Raw data were processed and normalized using nSolver 4.0 following manufacturer's guidelines (details in Materials and Methods).

4.5.2.1 4 hours vs. 0 hour gene expression

Among the 621 genes assayed, 119 up regulated genes showed a positive fold change whereas 66 down regulated genes showed a negative fold change ($P < 0.05$) as shown in Figure 4.47a. The top 20 most significant differentiately expressed genes were shown in Volcano plot (Figure 4.47b). Table 4.35 shows the top 20 most significant differentially expressed genes (measured in $\log_2$ fold change) with the selected covariate at treatment time 4 hours vs 0 hour. Regulation of genes at this time point were mainly initiated by signalling pathway such as MAPK, PI3K, RAS, Cell Cycle–Apoptosis, WNT, JAK-STAT, NOTCH, Transcription Misregulation, Nucleotide Excision, base Excision. Gene expression data were mapped onto KEGG pathway graphs by Pathview function of the PanCancer pathway software, providing intuitive views

of both up- and down-regulation at the pathway level. Representative graphs for signalling pathway are shown in Figure 4.48 to 4.59.

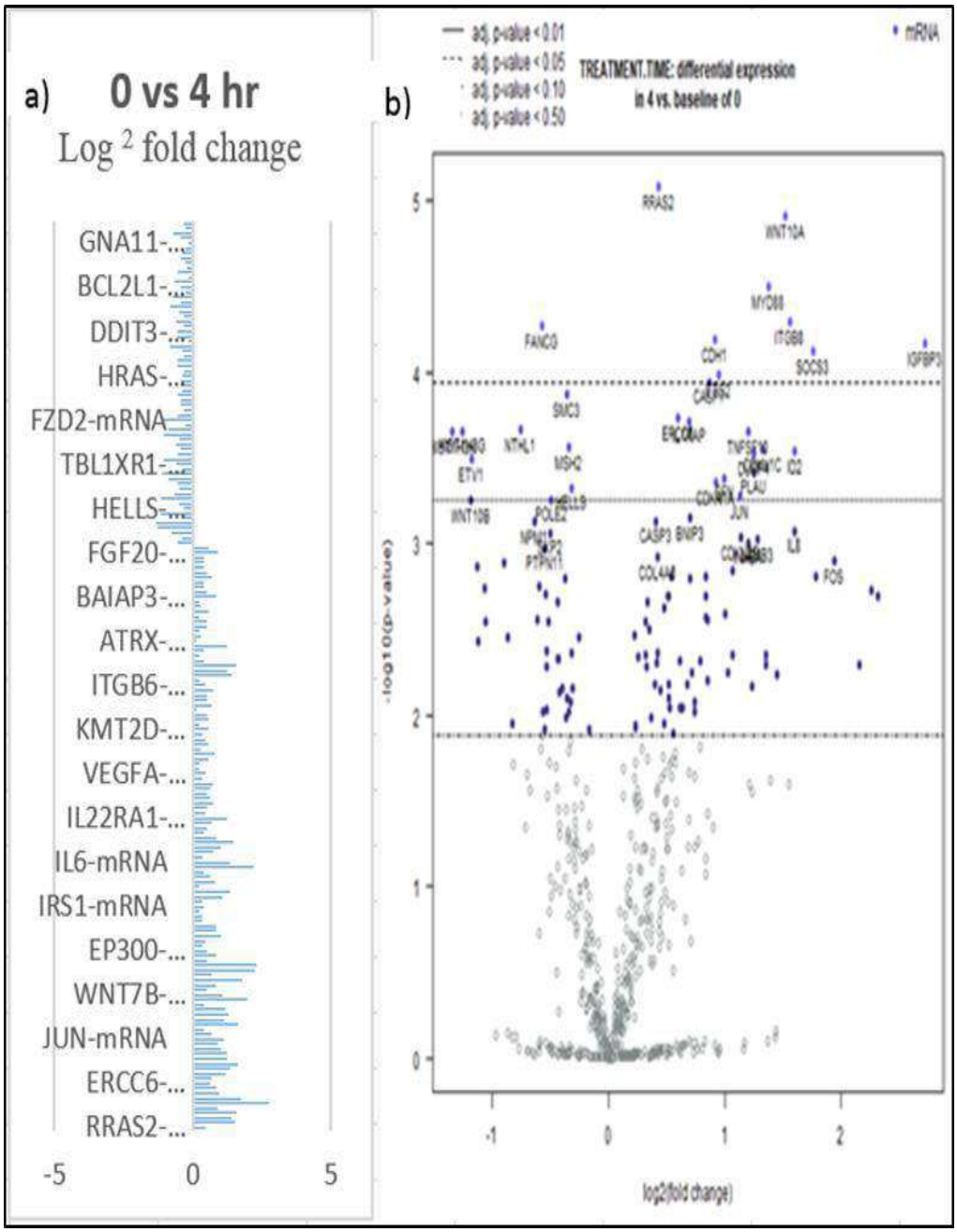

Figure 4.47 a) Log$_2$ fold change difference between 4 hours vs. baseline of 0 hour in HONE- 1 cells treated with L7 (XXXD) with differential expression comparing statistically significant differences (*P* < 0.05) in mRNA expression in the up and down regulated genes separately. A total of 66 up regulated genes show a positive fold change whereas 114 down regulated genes show a negative fold change. b) Volcano plot.

Table 4.35: The 20 most significant differentially expressed genes (measured in log_2 fold change) with the selected covariate at L7 treatment time 4 hours vs 0 hour with L7 (XXXD)

Genes	Log_2 fold change	*P*-value	Gene.sets	Biological Functions
HIST1H3 (H3FK)	-1.35	0.000223	Transcriptional Misregulation	**H3 Clustered Histone 10** • basic nuclear proteins regulate nucleosome structure of the chromosomal fiber in eukaryotes.
HIST1H3 G (H3FH)	-1.26	0.000218	Transcriptional Misregulation	**H3 Clustered Histone 8** • basic nuclear proteins regulate nucleosome structure of the chromosomal fiber in eukaryotes.
NTHL1	-0.754	0.000215	DNA Damage - Repair	**Nth Like DNA Glycosylase 1** • contains oxidized pyrimidine residues and has apurinic/apyrimidinic lyase activity.
FANC	-0.576	5.34E-05	DNA Damage - Repair	**FA Complementation Group A** • DNA repair protein for a postreplication repair or a cell cycle checkpoint function.
SMC3	-0.36	0.000134	Cell Cycle - Apoptosis	**Structural Maintenance of Chromosomes 3** • cohesin complex that holds together sister chromatids during mitosis, enables proper chromosome segregation.
MSH2	-0.345	0.000275	Driver Gene	**MutS Homolog 2** • binds to DNA mismatches thereby initiating DNA repair.
RRAS2 (TC21)	0.429	8.28E-06	MAPK, Ras	**RAS Related 2** • protein associates with the plasma membrane and may function as a signal transducer.
ERCC6	0.596	0.000185	DNA Damage - Repair	**ERCC Excision Repair 6, Chromatin Remodeling Factor** • a DNA-binding protein for transcription-coupled excision repair.
IL1RAP	0.69	0.000192	Cell Cycle - Apoptosis	**Interleukin 1 Receptor Accessory Protein** • initiates signalling events that result in the activation of interleukin 1-responsive genes.
CASP7	0.864	0.000113	Cell Cycle - Apoptosis	**Caspase 7** • activates cascade of caspases responsible for apoptosis.
CDH1	0.915	6.41E-05	Driver Gene	**Cadherin 1** • proteolytically generate the mature glycoprotein.

ETS2	0.947	0.000103	Ras	**ETS Proto-Oncogene 2, Transcription Factor** • regulates genes involved in development and apoptosis.
TNFSF10	1.2	0.000223	Cell Cycle - Apoptosis	**Tumor Necrosis Factor Ligand Superfamily Member 10** • cytokine, induces apoptosis.
CDKN1C	1.33	0.000282	Cell Cycle - Apoptosis	**Cyclin Dependent Kinase Inhibitor 1C** • inhibitor of several G1 cyclin/Cdk complexes • negative regulator of cell proliferation.
MYD88	1.38	3.18E-05	Cell Cycle - Apoptosis, Driver Gene	**MYD88 Innate Immune Signal Transduction Adaptor** • essential signal transducer in the interleukin-1 and Toll-like receptor signaling pathways.
WNT10A	1.52	1.23E-05	Wnt, Hedgehog	**Wnt Family Member 10A** • implicated in oncogenesis including regulation of cell fate and patterning during embryogenesis.
ITGB8	1.56	5.07E-05	PI3K	**Integrin Subunit Beta 8** • adhesion receptors that function in signaling from the extracellular matrix to the cell.
ID2	1.6	0.00029	TGF-beta, Transcriptional Misregulation	**Inhibitor Of DNA Binding 2** • inhibits the functions of basic helix-loop-helix ranscription factors by suppressing their heterodimerization partners through the HLH domains
SOCS3	1.76	7.52E-05	JAK-STAT	**Suppressor of cytokine signaling 3** • cytokine-inducible repressor for cytokine signaling, inhibit the activity of JAK2 kinase.
IGFBP3	2.72	6.75E-05	Transcriptional Misregulation	**Insulin-like growth factor binding protein 3** • changes the interaction of IGFs with their cell surface receptors. • pro- apoptotic effects mediated by its receptor TMEM219/IGFBP-3R.

Continuation of Table 4.35

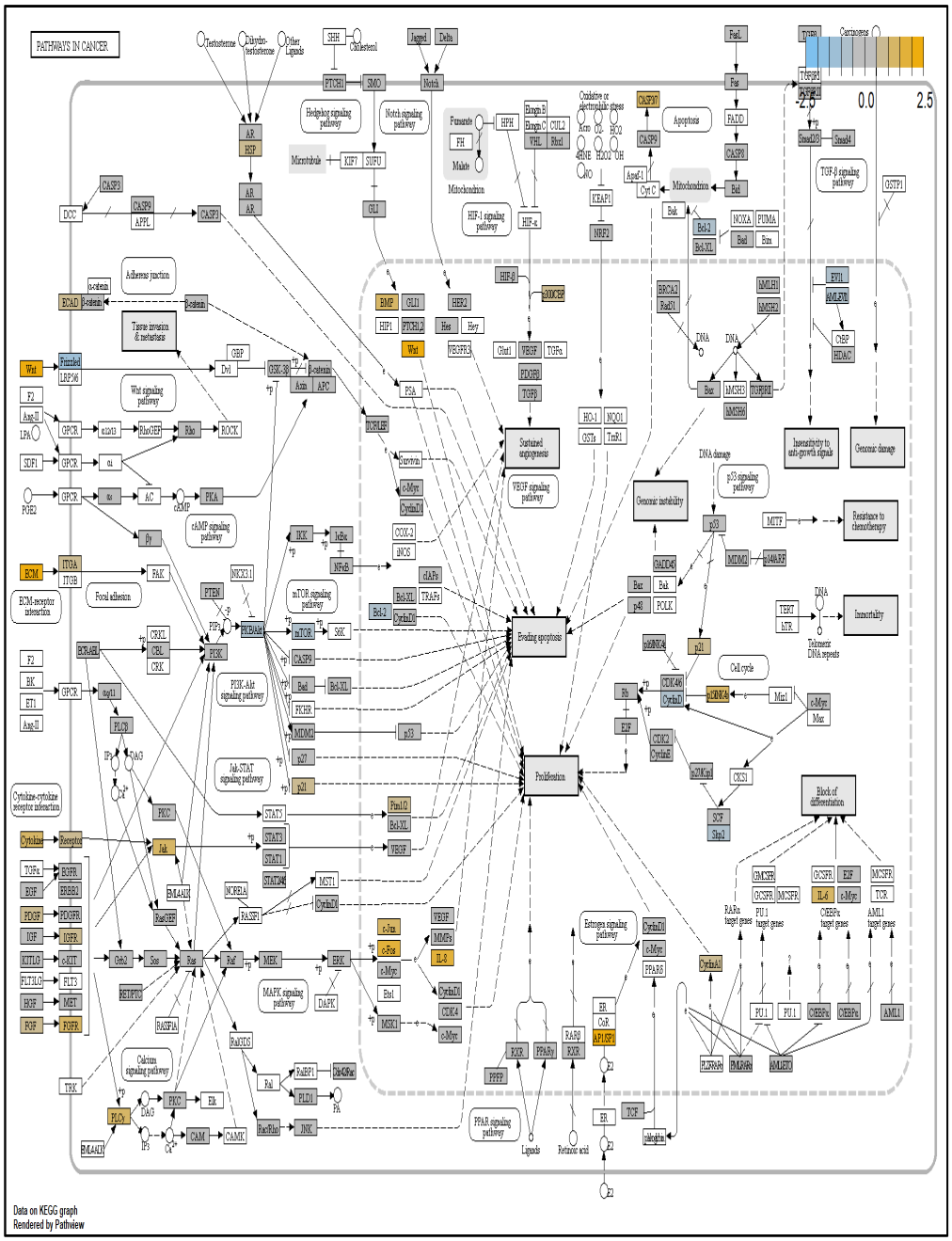

Figure 4.48: Cell Cycle in Cancer pathway (treatment time: differential expression in 4 hour vs. baseline of 0 hour for HONE-1 treated with L7 (XXXD))

Upregulated genes: *WNT, ECM, Cytokine, Receptor, FCF, FCFR, BMP, ITGA, ECAD, JAK, PIM1/2, cFOS, IL8, IL6, p21, AP1, CASP3/7*

Downregulated genes: *Frizzled, PKB/AKT, Bcl-2, cycD, SKP2, mTOR, ETVI*

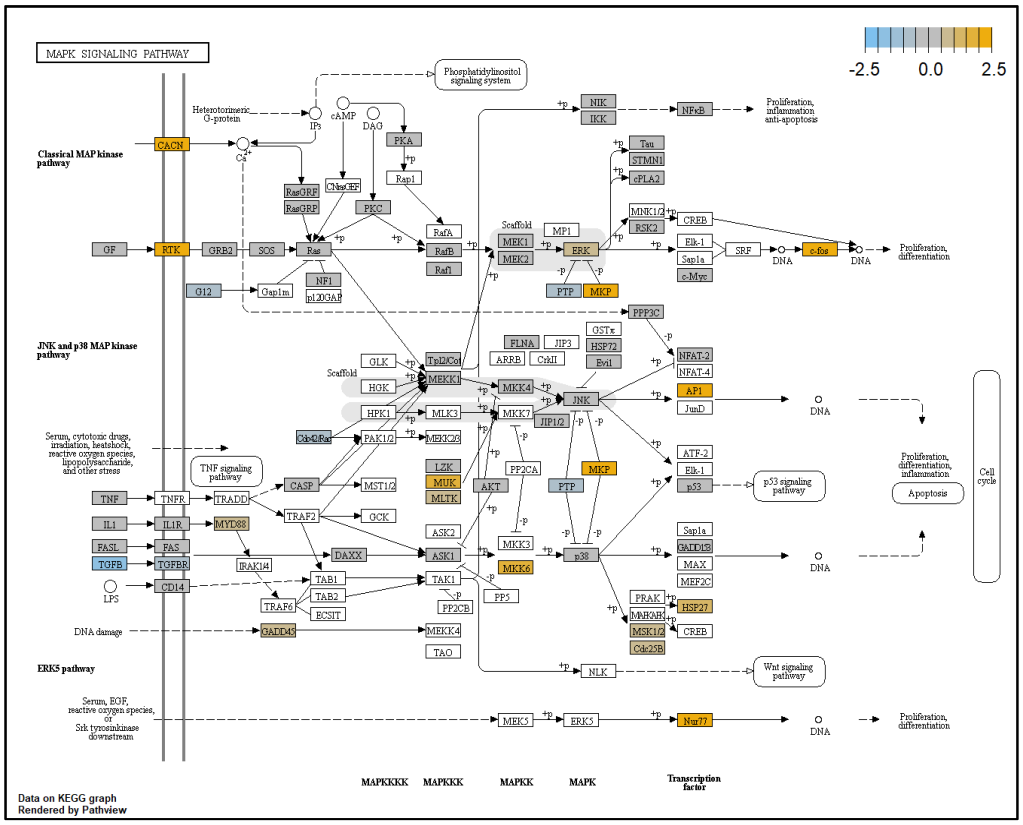

Figure 4.49: MAPK pathway (treatment time: differential expression in 4 hours vs. baseline of 0 hour for HONE-1 treated with L7 (XXXD))

Upregulated genes: *CACN*, *RTK*, *MKP*, *cFos*, *Ap1*, *MSP27*, *Nur77*, *MKK6*, *MUK*, *Cdk25B*

Downregulated genes: *TGFB*, *TGFBR*, *MYD88*, *GADD45*, *G12*, *PTP*

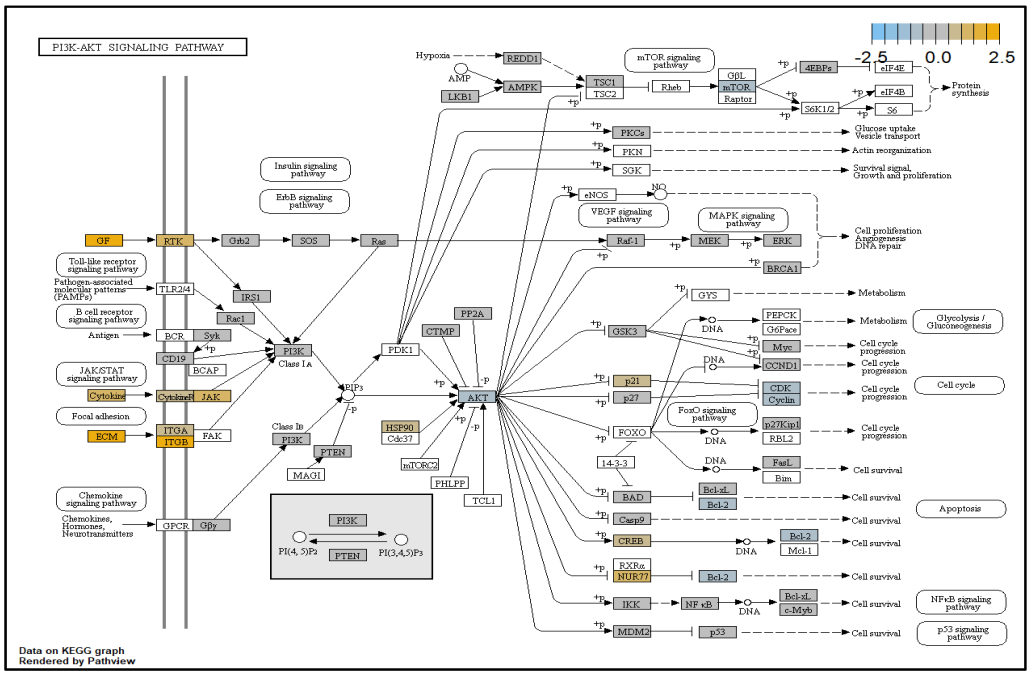

Figure 4.50 PI3K pathway (treatment time: differential expression in 4 hours vs. baseline of 0 hour for HONE-1 treated with L7 (XXXD))

Upregulated genes: *Cytokine*, *CytokineR*, *JAK*, *ECM*, *ITGA/B*, *NUR77*, *p21*, *HSP90*, *GF*, *RTK*

Downregulated genes: *AKT*, *mTOR*, *BCL-2*, *CDK/CYC*

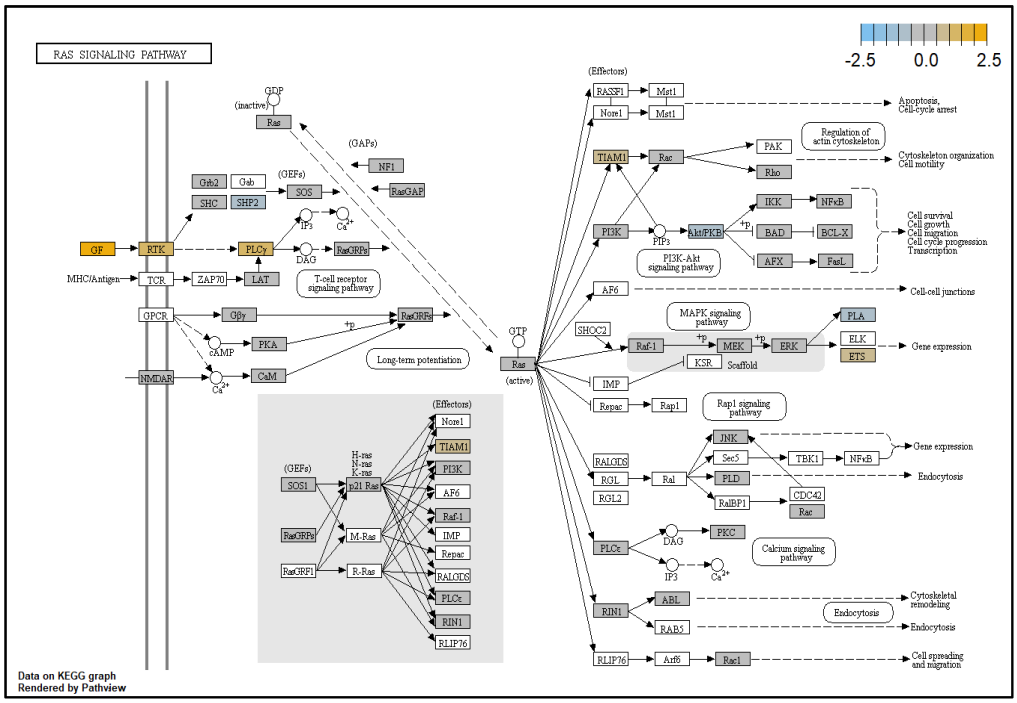

Figure 4.51: RAS pathway (treatment time: differential expression in 4 hours vs. baseline of 0 hour for HONE-1 treated with L7 (XXXD))
Upregulated genes: *GF*, *RTK*, *PLCy*, *ETS*, *TIAM1*
Downregulated genes: *SHP2*, *PKB*, *PLA*

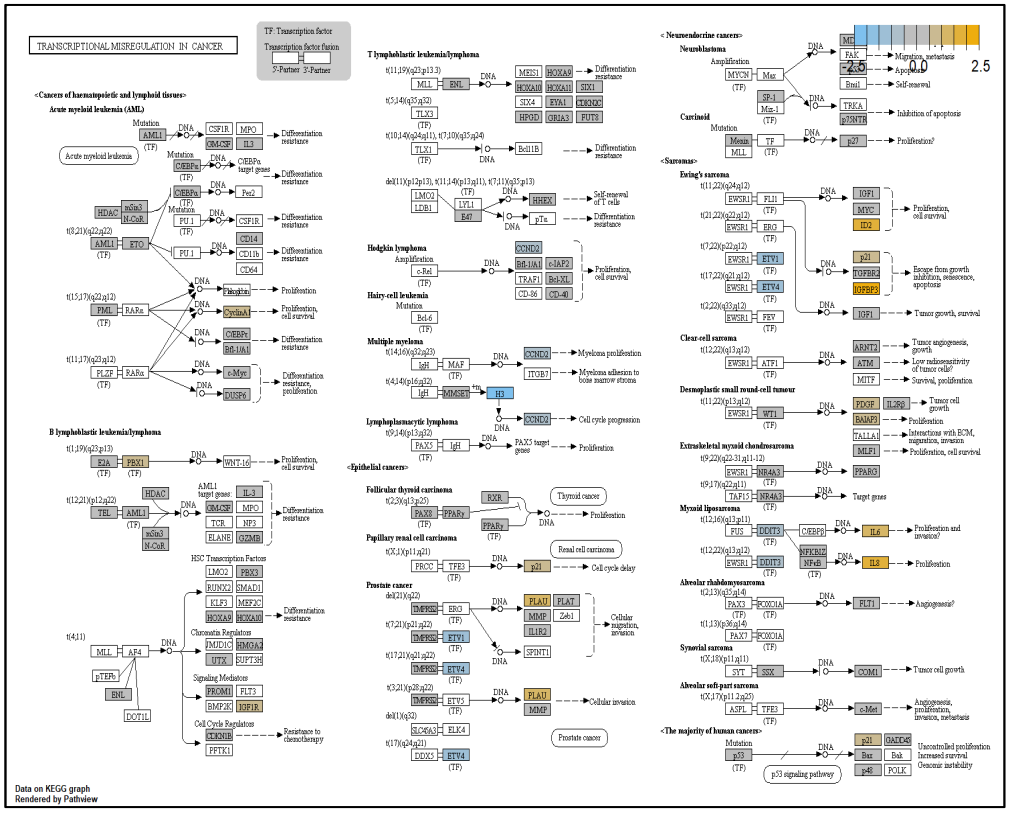

Figure 4.52: Transcription Misregulation pathway (treatment time: differential expression in 4 hours vs. baseline of 0 hour for HONE-1 treated with L7 (XXXD))
Upregulated genes: *CycA*, *PBX1*, *ID2*, *p21*, *IGFBP3*, *PLAU*, *IL8*, *IL6*, *PDGF*, *BALAP3*
Downregulated genes: *H3*, *CCND2*, *ETV1*, *ETV4*, *DDIT3*

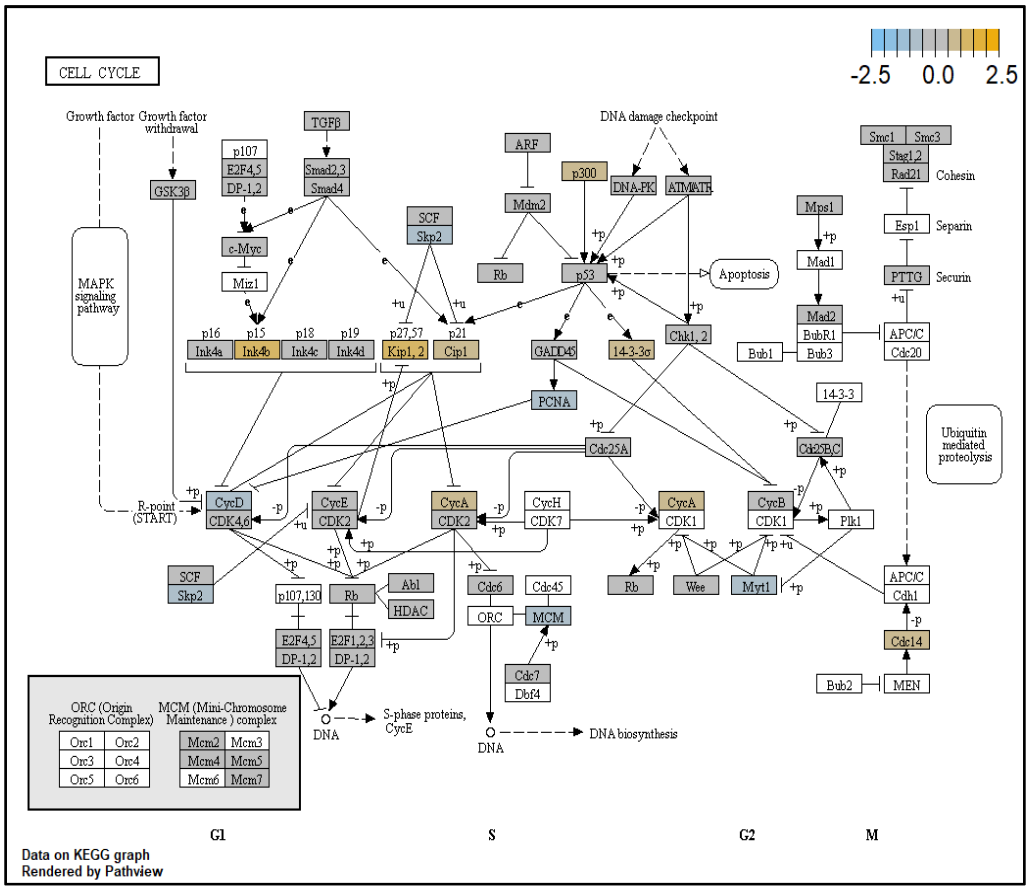

Figure 4.53: Cell Cycle pathway (treatment time: differential expression in 4 hours vs. baseline of 0 hour for HONE-1 treated with L7 (XXXD))
Upregulated genes: *p300, Ink4b, Kip1,2, CycA, Cdc14*
Downregulated genes: *SKP2, CycD, MCM, Myt1, PCNA*

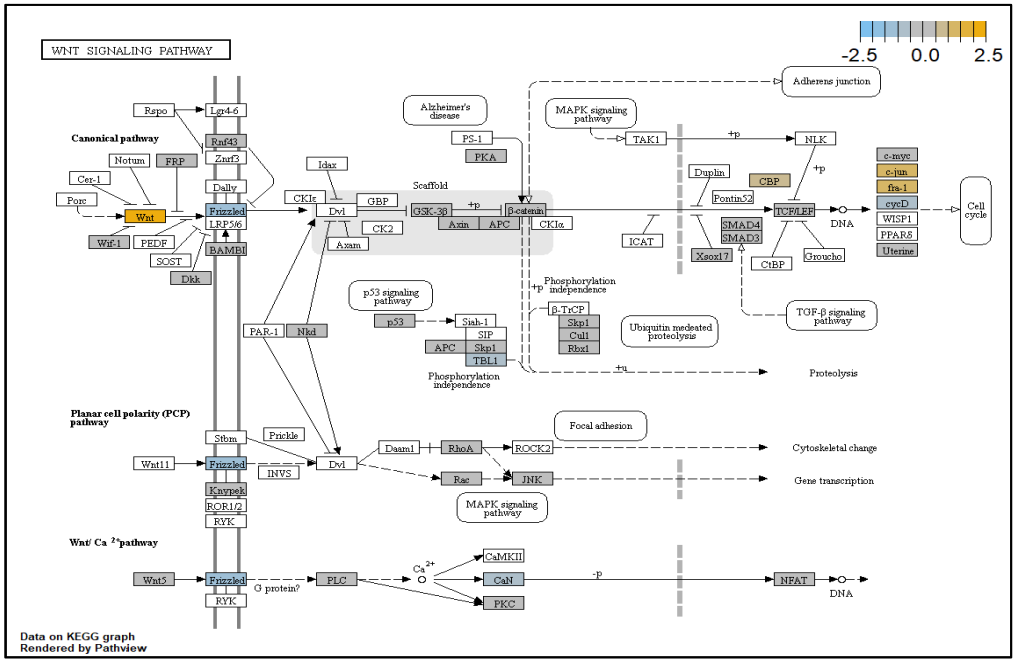

Figure 4.54: WNT pathway (treatment time: differential expression in 4 hours vs. baseline of 0 hour for HONE-1 treated with L7 (XXXD))
Upregulated genes: *WNT, CBP, cjunCBP, fra-1*
Downregulated genes: *Frizzled, TBL1, CaN, CycD*

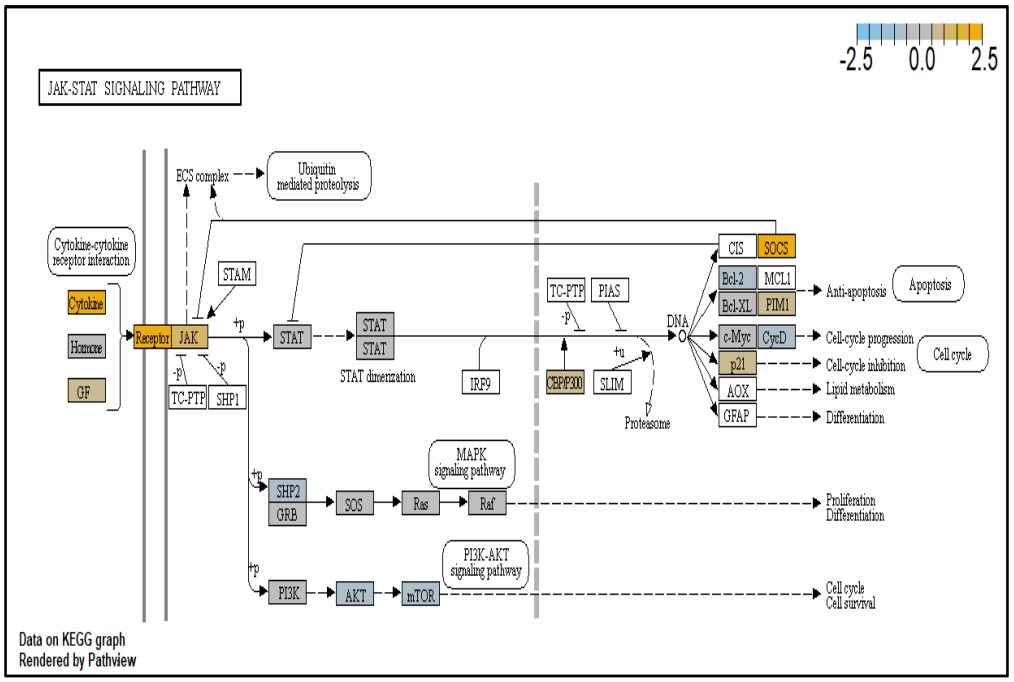

Figure 4.55: JAK-STAT pathway (treatment time: differential expression in 4 hours vs. baseline of 0 hour for HONE-1 treated with L7 (XXXD))
Upregulated genes: *Cytokine, Receptor, CBPP300, p21, SOCS, PIM1, GF*
Downregulated genes: *SHP2, AKT, mTOR, Bcl-2, CycD*

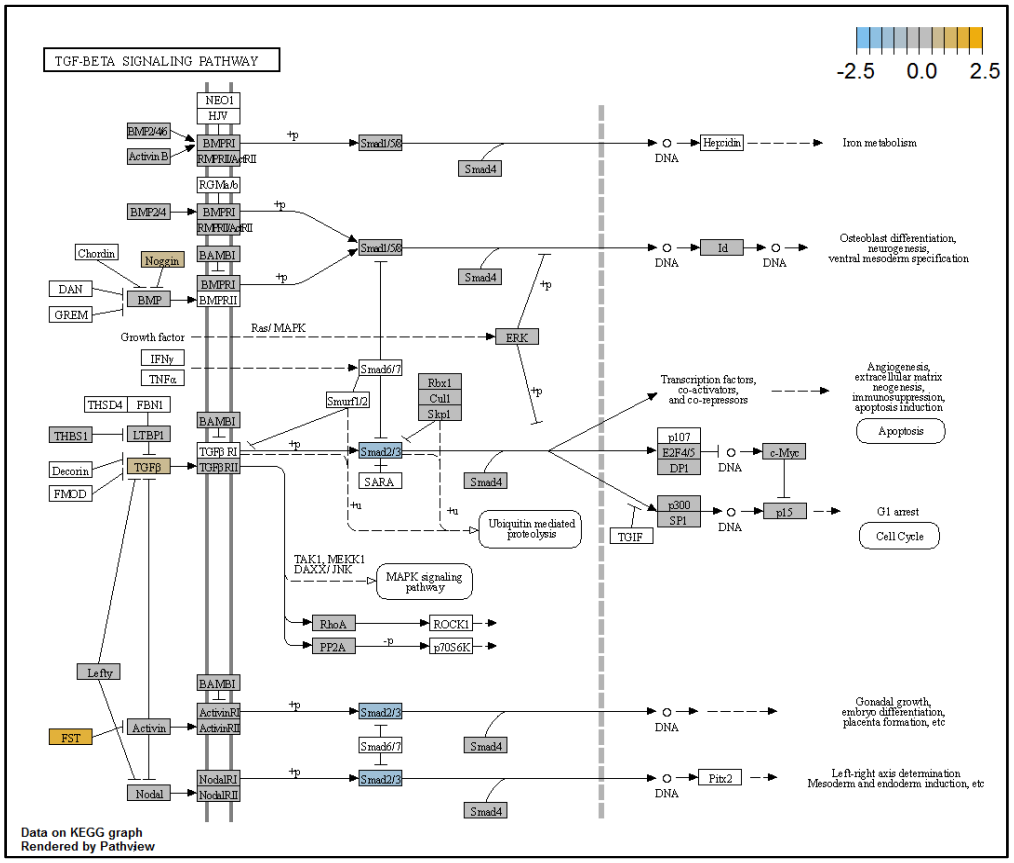

Figure 4.56: TGFβ pathway (treatment time: differential expression in 4 hours vs. baseline of 0 hour for HONE-1 treated with L7 (XXXD))
Upregulated genes: *Noggin, TGFB, FST*
Downregulated genes: *Smad2/3*

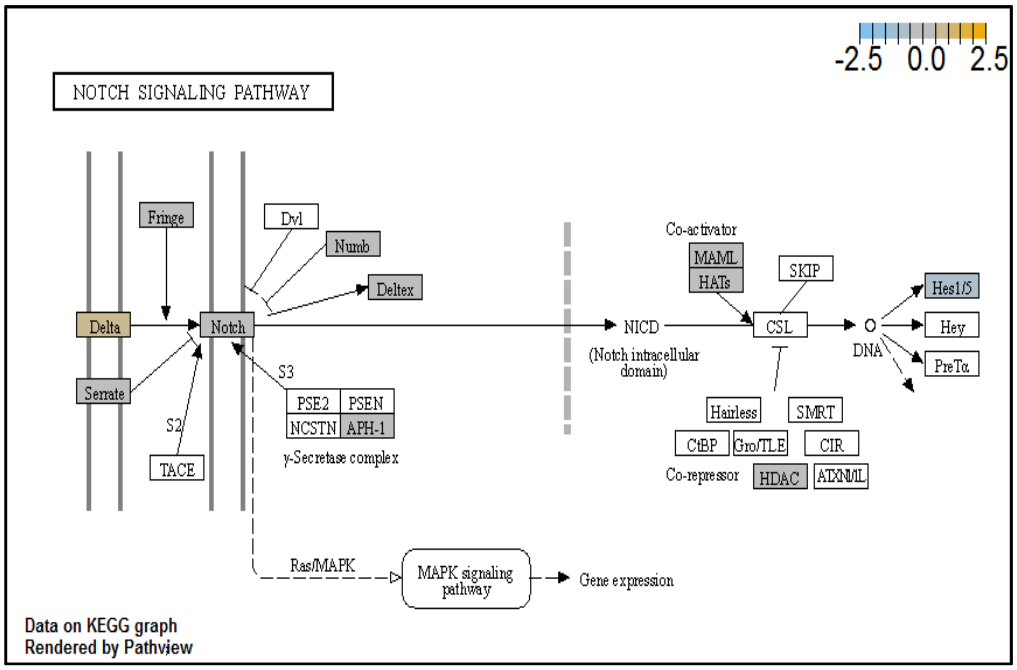

Figure 4.57: NOTCH signaling pathway (treatment time: differential expression in 4 hours vs. baseline of 0 hour for HONE-1 treated with L7 (XXXD))
Upregulated genes: *Delta*
Downregulated genes: *Hes1/5*

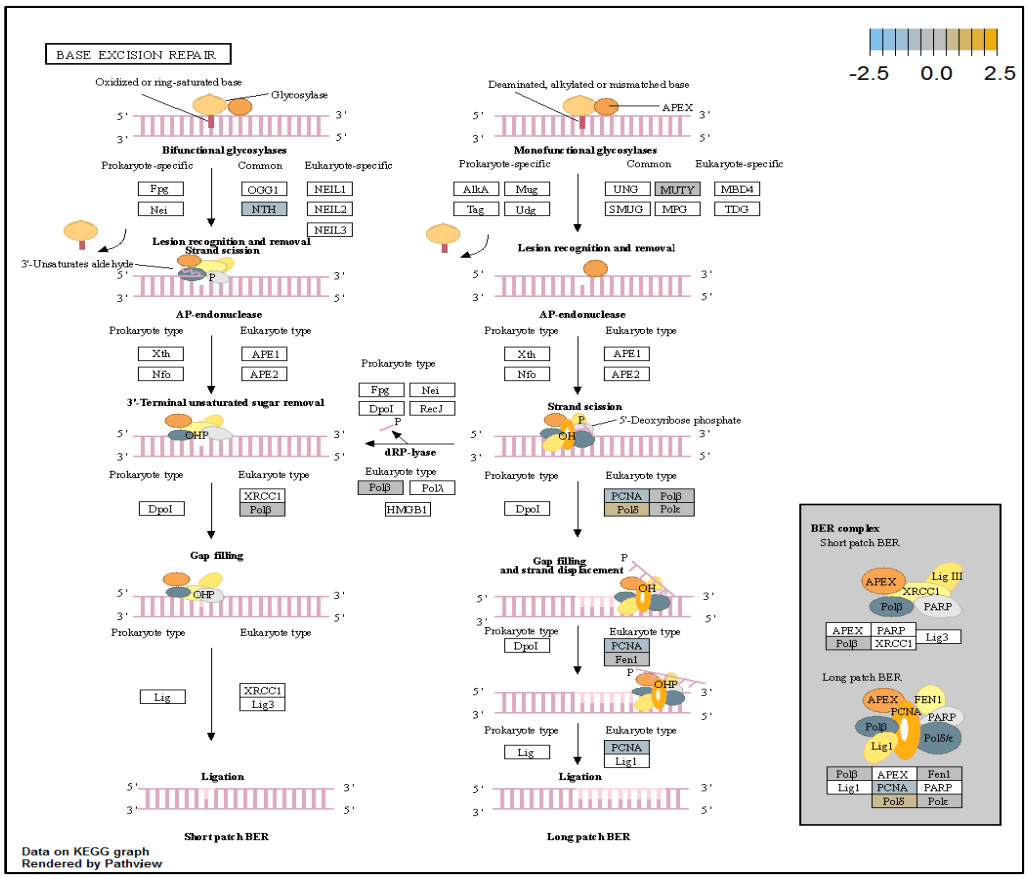

Figure 4.58: Base Excision pathway (treatment time: differential expression in 4 hours vs. baseline of 0 hour for HONE-1 treated with L7 (XXXD))
Upregulated genes: *Pol8*
Downregulated genes: *NTH, PCNA*

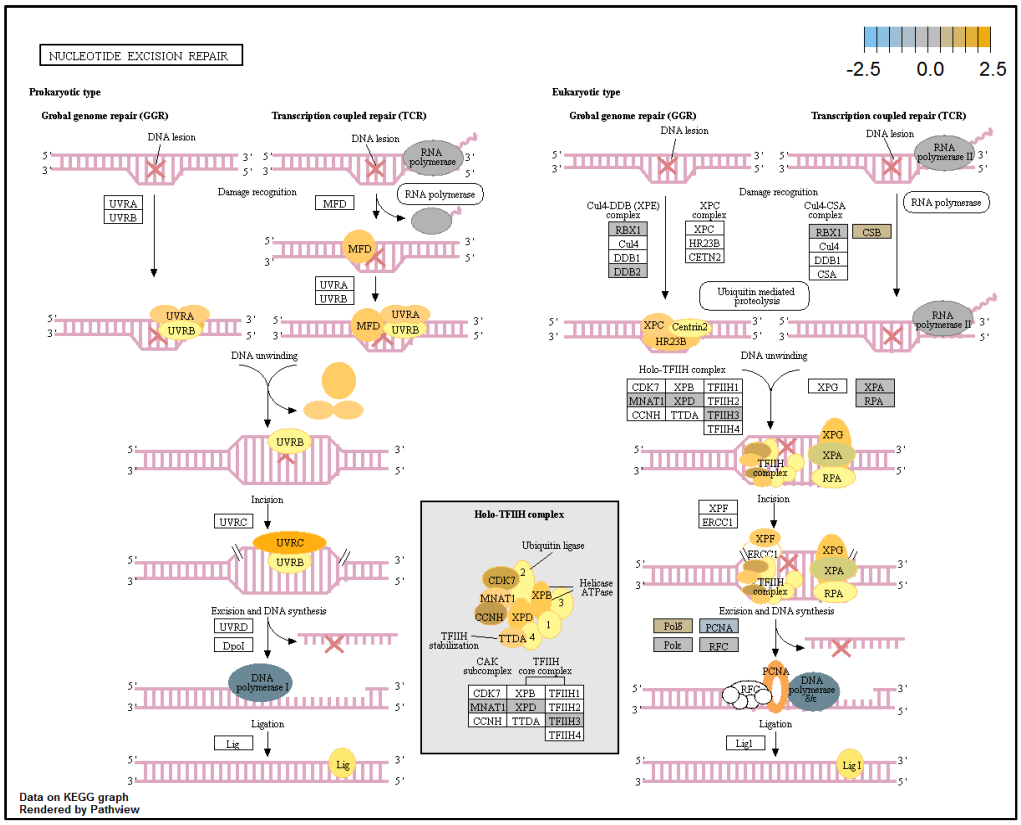

Figure 4.59: Nucleotide Excision pathway (treatment time: differential expression in 4 hours vs. baseline of 0 hour for HONE-1 treated with L7 (XXXD))
Upregulated genes: *GSB, Pol8*
Downregulated genes: *PCNA*

4.5.2.2 8 hours vs 0 hour gene expression

Among the 621 genes assayed, 18 up regulated genes showed a positive fold change whereas 134 down regulated genes showed a negative fold change ($P < 0.05$) as shown in Figure 4.60a. The top 20 most significant differentiately expressed genes are shown in Volcano plot (4.60b). Table 4.5.2.2.1 shows the 20 most significant differentiately expressed genes (measured in $\log_2$ fold change) with the selected covariate at treatment time 8 hours vs 0 hour. Regulation of genes at this time point were mainly initiated by signalling pathway such as MAPK, PI3K, RAS, Cell Cycle–Apoptosis, WNT, JAK-STAT, NOTCH, Transcription Misregulation, TNFκB, cAMP. Gene expression data were mapped onto KEGG pathway graphs by Pathview function of the PanCancer pathway software, providing intuitive views of both up- and down-regulation at the pathway level. Representative graphs for signalling pathway are shown in Figures 4.61 to Figure 4.72.

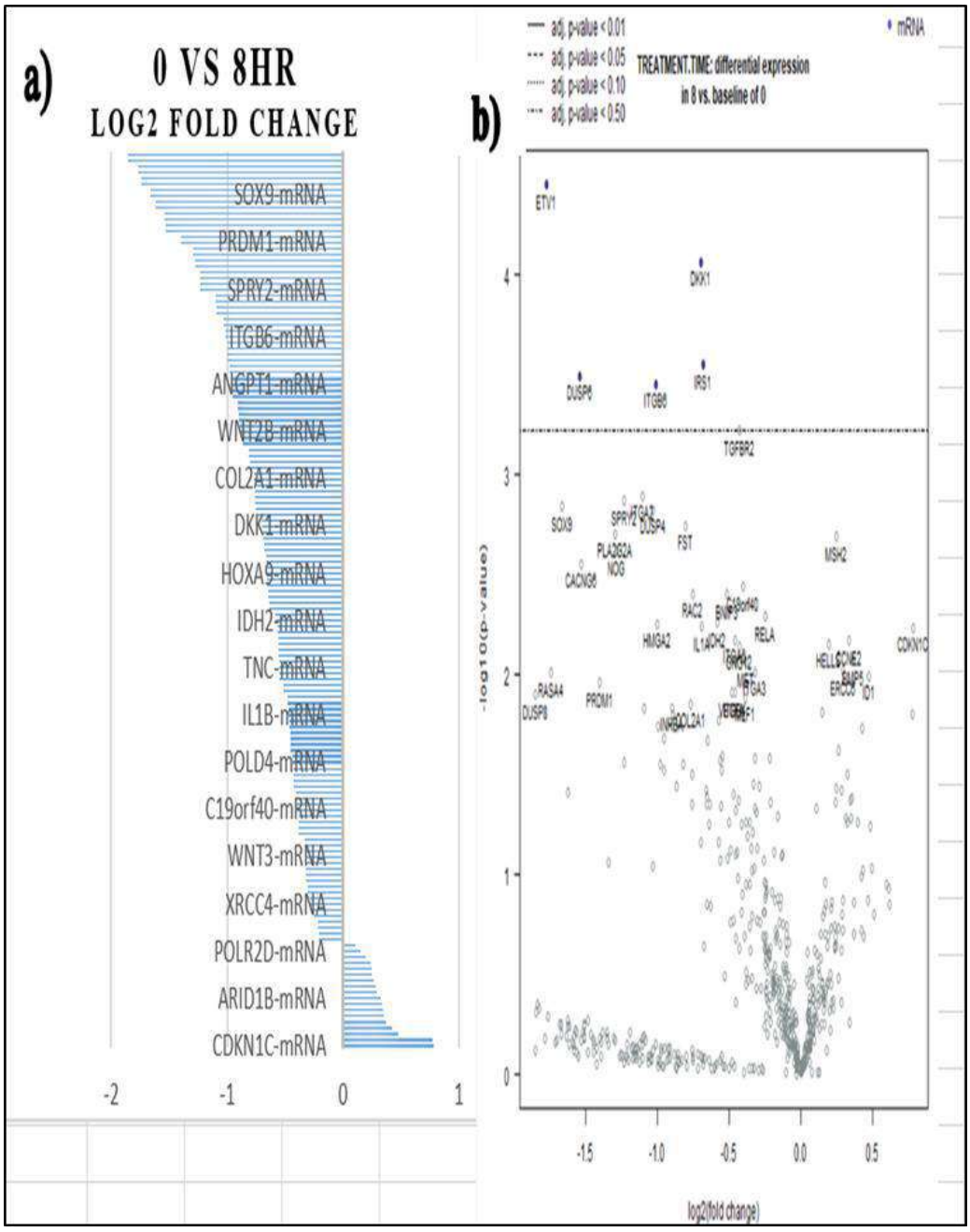

Figure 4.60 a) Log$_2$ fold change difference between 8 hours vs. baseline of 0 hour in HONE 1 cells treated with L7 (XXXD) with differential expression comparing statistically significant differences (*P* < 0.05) in mRNA expression in the up and down regulated genes separately. A total of 18 up regulated genes show a positive fold change whereas 134 down regulated genes show a negative fold change. b) Volcano plot.

Table 4.36: The 20 most significant differentially expressed genes (measured in log_2 fold change) with the selected covariate at L7 treatment time 8 hours vs 0 hour with L7 (XXXD)

Genes	Log_2 fold change	*P*-value	Gene.sets	Biological functions
ETV1	-1.77	3.53E-05	Transcriptional Misregulation	**ETS Variant Transcription Factor** • regulates biological processes like cell growth, angiogenesis,
SOX9	-1.66	0.00144	Driver Gene	**SRY-Box Transcription Factor 9** • regulates transcription of the anti-Muellerian hormone (AMH) gene.
DUSP6 (MKP3)	-1.54	0.00032	MAPK, Transcriptional Misregulation	**Dual Specificity Phosphatase 6** • inactivate their target kinases by dephosphorylating
CACNG6	-1.53	0.00279	MAPK	**Calcium Voltage-Gated Channel Auxiliary Subunit Gamma 6** • membrane protein to stabilize the calcium channel in an inactive state.
PLA2G2A	-1.29	0.00197	Ras	**Phospholipase A2 Group IIA** • involves in the regulation of the phospholipid metabolism in biomembranes.
NOG	-1.28	0.0024	TGF-beta	**Noggin** • secreted polypeptide binds and inactivates TGFβ signaling proteins, such as BMP4
SPRY2	-1.23	0.00135	JAK-STAT	**Sprouty RTK Signaling Antagonist 2** • inhibitory activity on receptor tyrosine kinase signaling proteins
ITGA2	-1.1	0.00128	PI3K	**Integrin Subunit Beta 6** • adhesion receptors that function in signaling from the extracellular matrix to the cell.
DUSP4	-1.03	0.0015	MAPK	**Dual specificity protein phosphatase 4** •Cellular proliferation and differentiation
ITGB6	-1.01	0.00035	PI3K	**Integrin Subunit Beta 8** • adhesion receptors that function in signaling from the extracellular matrix to the cell.
FST	-0.801	0.00181	TGF-beta	**Follistatin** • regulator of pituitary FSH secretion • inhibitor to Activin and BPM TGFβ-related growth factors
RAC2	-0.752	0.00396	MAPK, Ras, Wnt	**Rac Family Small GTPase 2** • sited in plasma membrane, regulates secretion, phagocytosis, and cell polarization.

DKK1	-0.696	8.53E-05	Wnt	**Dickkopf WNT signaling pathway inhibitor 1** • Embryonic, bone development
IRS1	-0.679	0.00028	PI3K	**Insulin Receptor Substrate 1** • phosphorylated by insulin receptor tyrosine kinase.
IDH2	-0.581	0.00551	Driver Gene	**Isocitrate Dehydrogenase (NADP(+)) 2** • Enzyme found in the mitochondria, for intermediary metabolism and energy production
BNIP3	-0.515	0.004	Chromatin Modification	**BCL2 Interacting Protein 3** • mitochondrial protein that contains a BH3 domain and acts as a pro-apoptotic factor.
TGFBR2	-0.425	0.000604	MAPK, TGF-beta, Transcriptional Misregulation	**Transforming Growth Factor Beta Receptor 2** •receptor/ligand complex phosphorylates proteins which enter the nucleus and regulate the transcription of genes related to cell proliferation, cell cycle arrest.
C19orf40	-0.403	0.00365	DNA Damage - Repair	**FA Core Complex Associated Protein 24** • involves in DNA damage response
RELA	-0.248	0.00517	Cell Cycle-Apoptosis MAPK, PI3K, Ras, Transcriptional Misregulation	**RELA proto-oncogene, NF-kB subunit** • Enzyme found in the mitochondria, for intermediary metabolism and energy production
MSH2	0.245	0.00204	Driver Gene	**MutS Homolog 2** • Forms two different heterodimers, binds to DNA mismatches thereby initiating DNA repair.

Continuation of Table 4.36

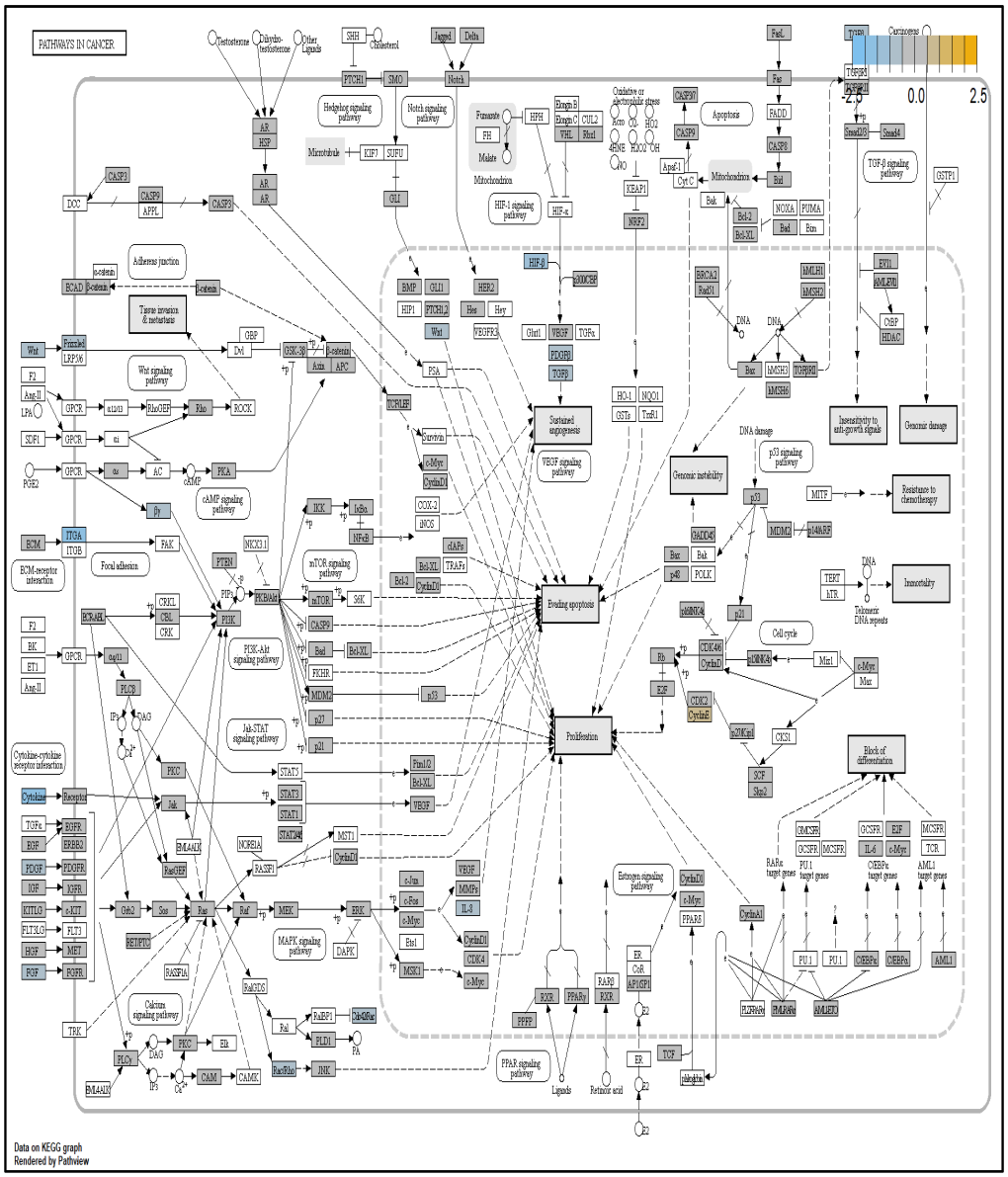

Figure 4.61: Cell Cycle in Cancer pathway (treatment time: differential expression in 8 hours vs. baseline of 0 hour for HONE-1 treated with L7 (XXXD))

Upregulated genes: *CyclinE*

Downregulated genes: *Wnt, Frizzled, ITGA, Cytokine, FGF, PDGF, IL3, TGFβ, HIFβ*

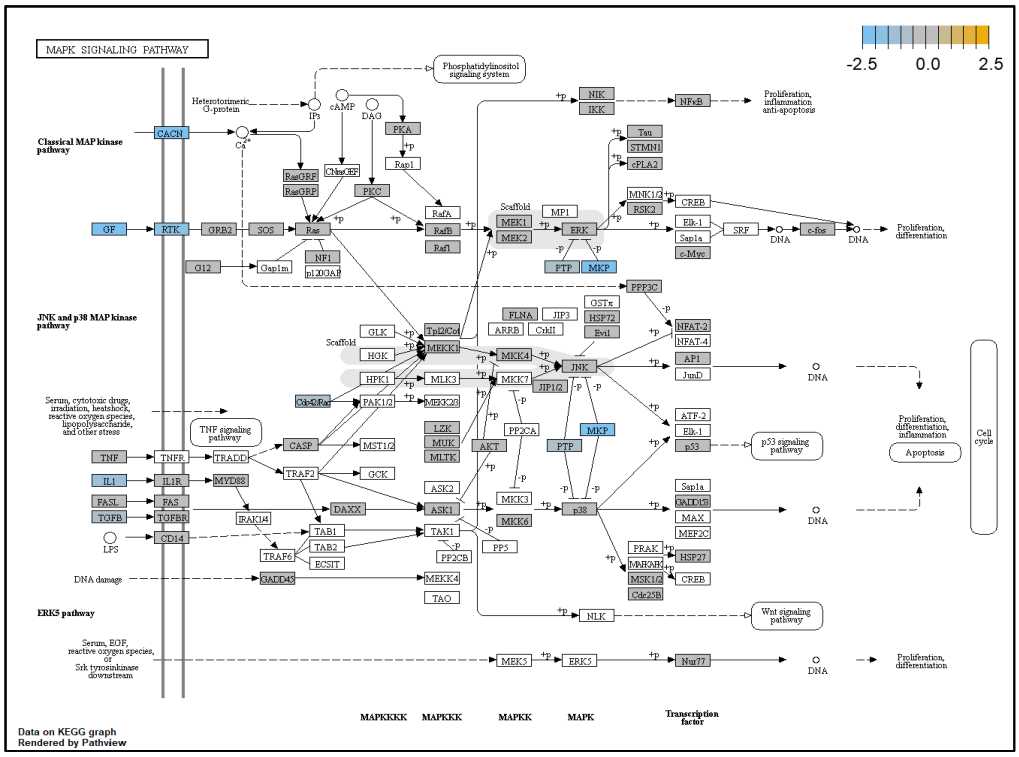

Figure 4.62: MAPK pathway (treatment time: differential expression in 8 hours vs. baseline of 0 hour for HONE-1 treated with L7 (XXXD))
Downregulated genes: *GF, CACN, IL1, MKP, TGFβ*

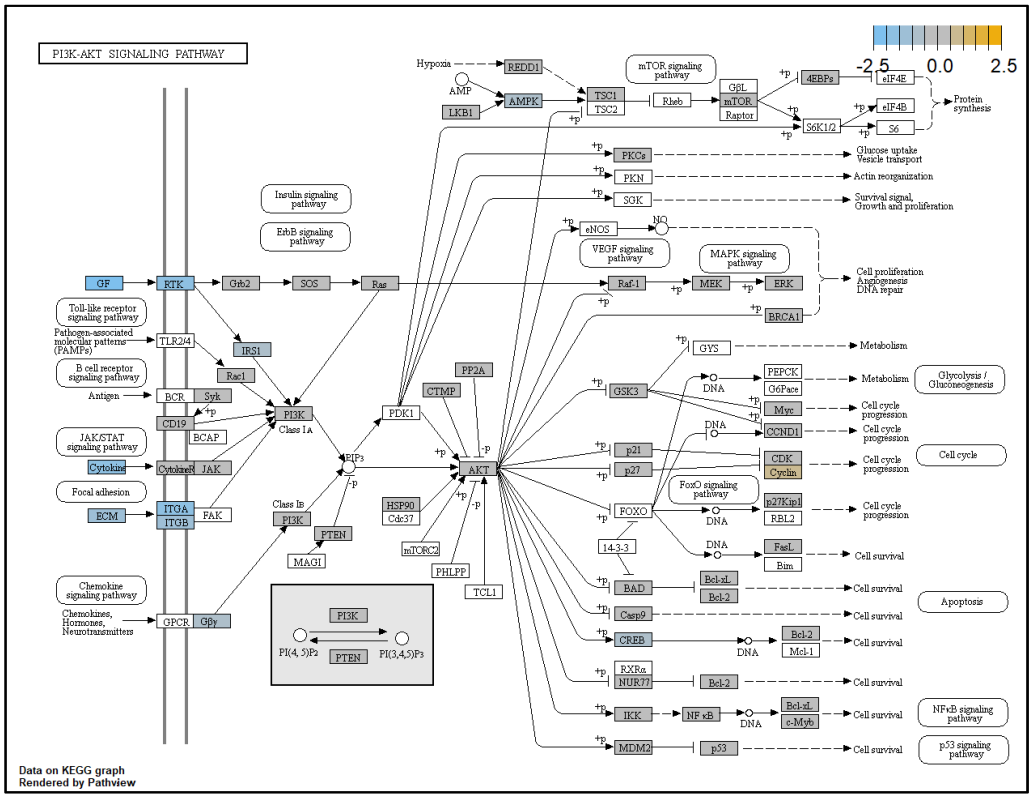

Figure 4.63: PI3K pathway (treatment time: differential expression in 8 hours vs. baseline of 0 hour for HONE-1 treated with L7 (XXXD))
Upregulated genes: *Cyclin*
Downregulated genes: *GF, RTK, CYTOKINE, ECM, ITGA/B, CREB*

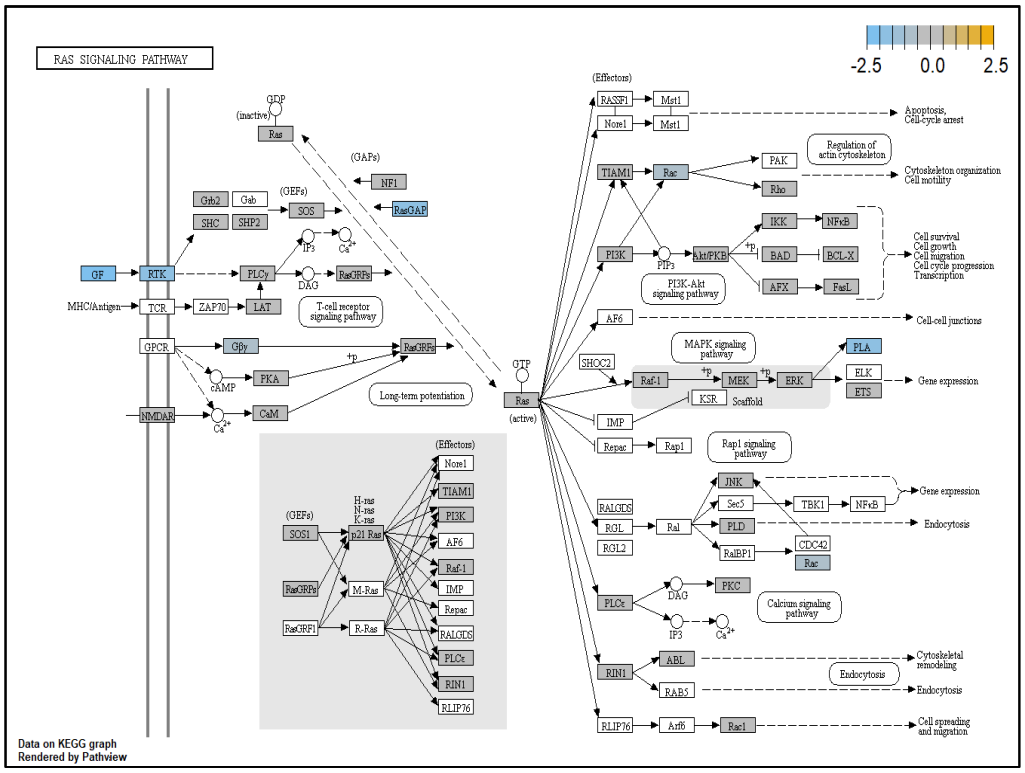

Figure 4.64: RAS pathway (treatment time: differential expression in 8 hours vs. baseline of 0 hour for HONE-1 treated with L7 (XXXD))
Downregulated genes: *GF*, *RTK*, *RasGAP*, *PLA*, *RAC*

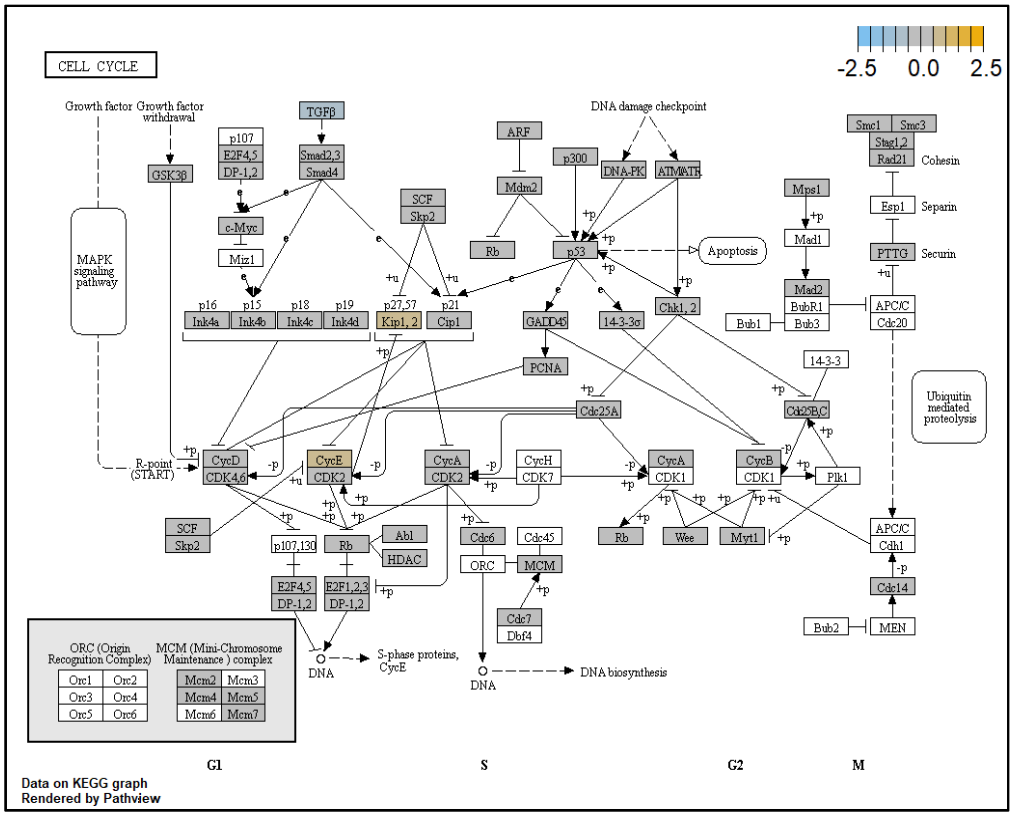

Figure 4.65: Cell Cycle pathway (treatment time: differential expression in 8 hours vs. baseline of 0 hour for HONE-1 treated with L7 (XXXD))
Upregulated genes: *Kip1,2, CycE*
Downregulated genes: *TGFβ*

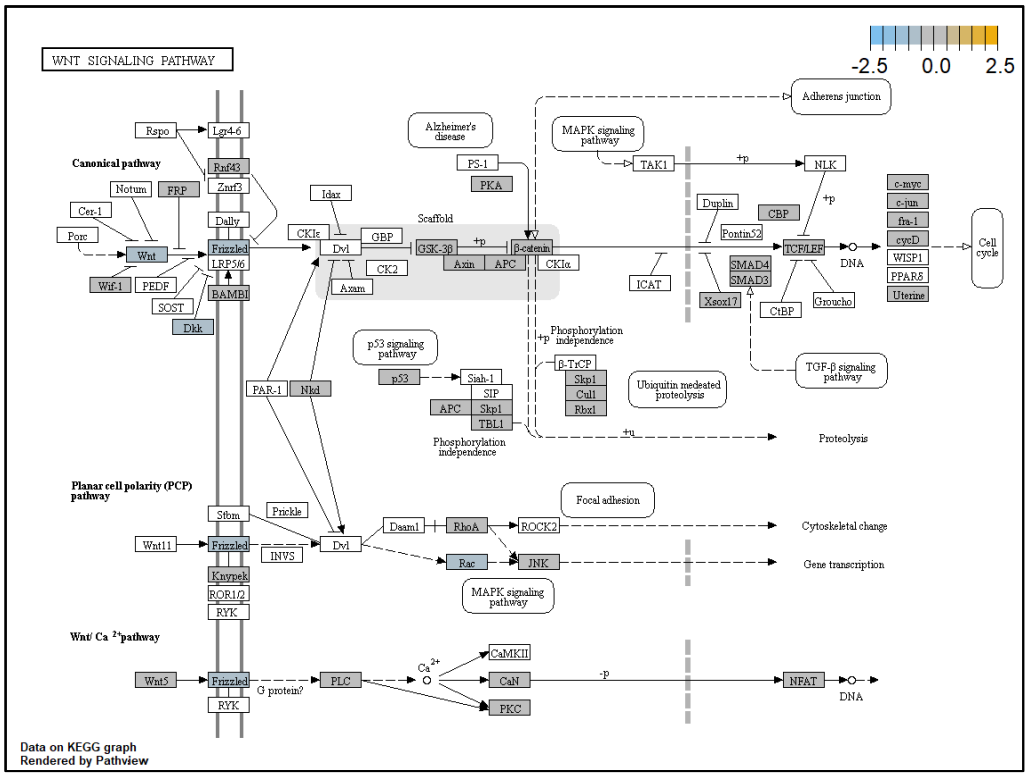

Figure 4.66: WNT pathway (treatment time: differential expression in 8 hours vs. baseline of 0 hour for HONE-1 treated with L7 (XXXD))
Downregulated genes: *WNT, DKK, Frizzled, Rac*

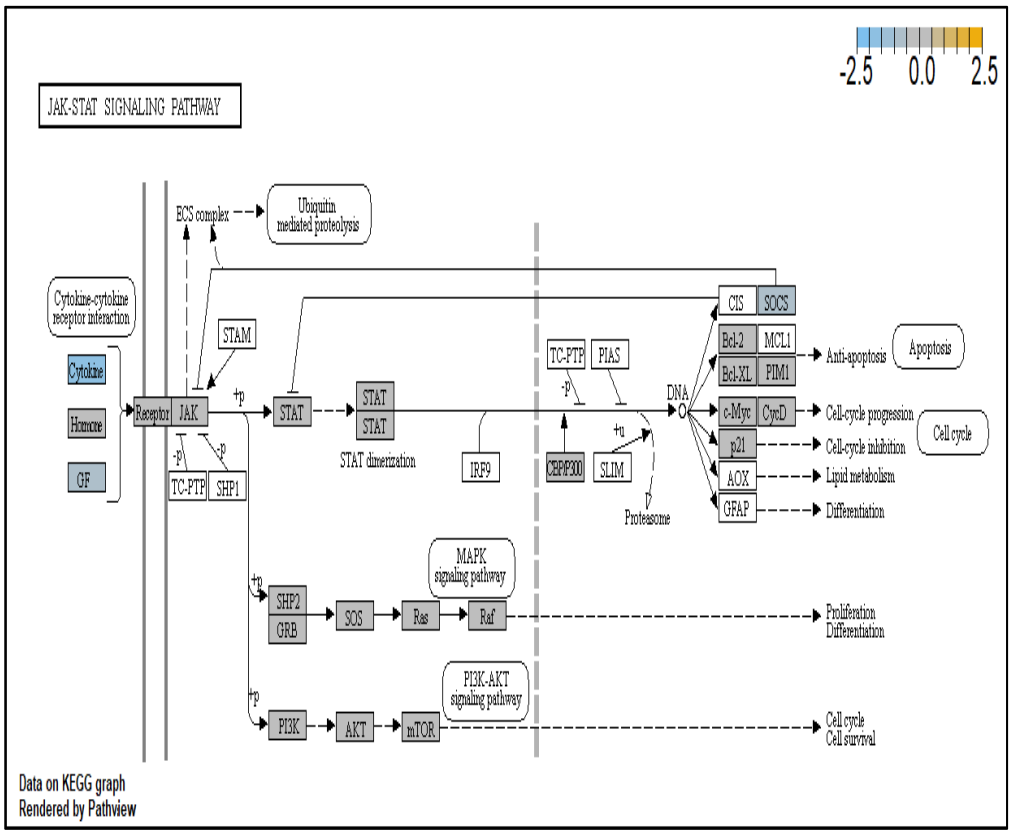

Figure 4.67: JAK-STAT pathway (treatment time: differential expression in 8 hours vs. baseline of 0 hour for HONE-1 treated with L7 (XXXD))
Downregulated genes: *Cytokine, SOCS, GF*

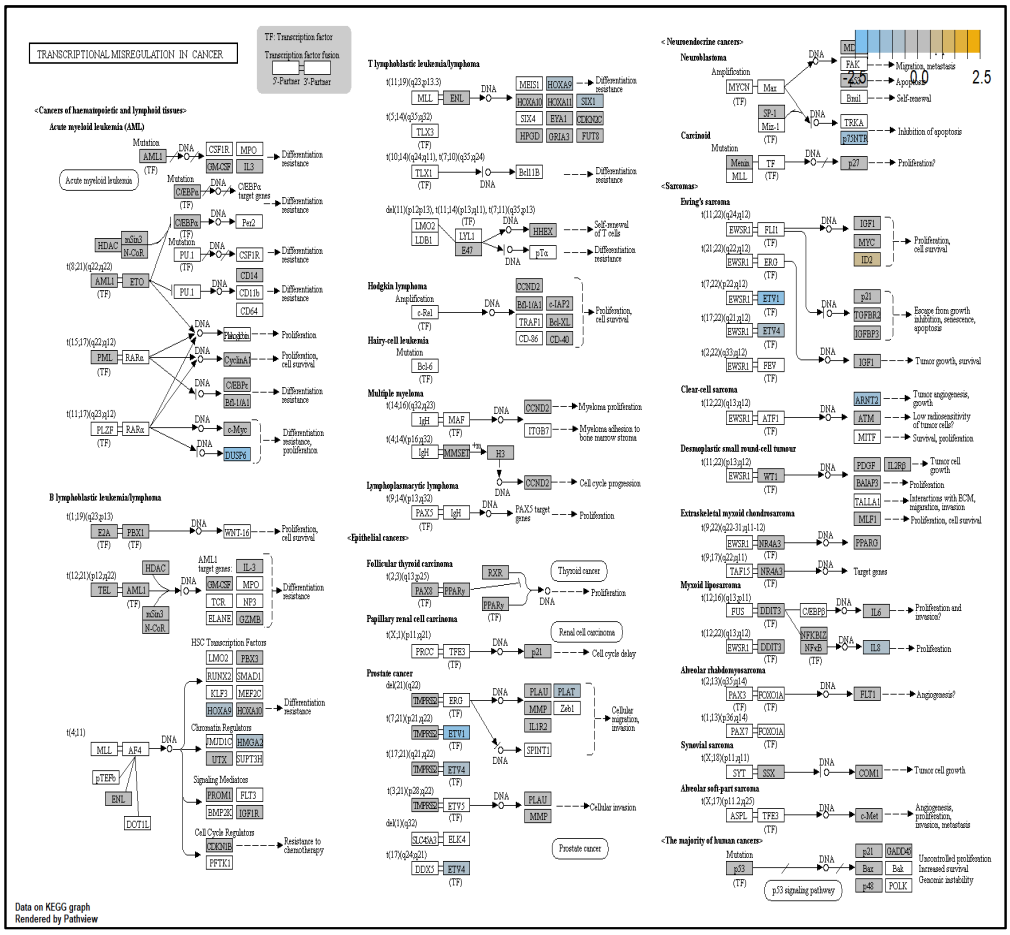

Figure 4.68: Transcription Misregulation pathway (treatment time: differential expression in 8 hours vs. baseline of 0 hour) for HONE-1 treated with L7 (XXXD))

Upregulated genes: *ID2*

Downregulated genes: *DUSP6*, *ETV1*, *ETV4*, *PLAT*, *ARNT2*, *IL8*, *HOXA9*, *HMGA2*

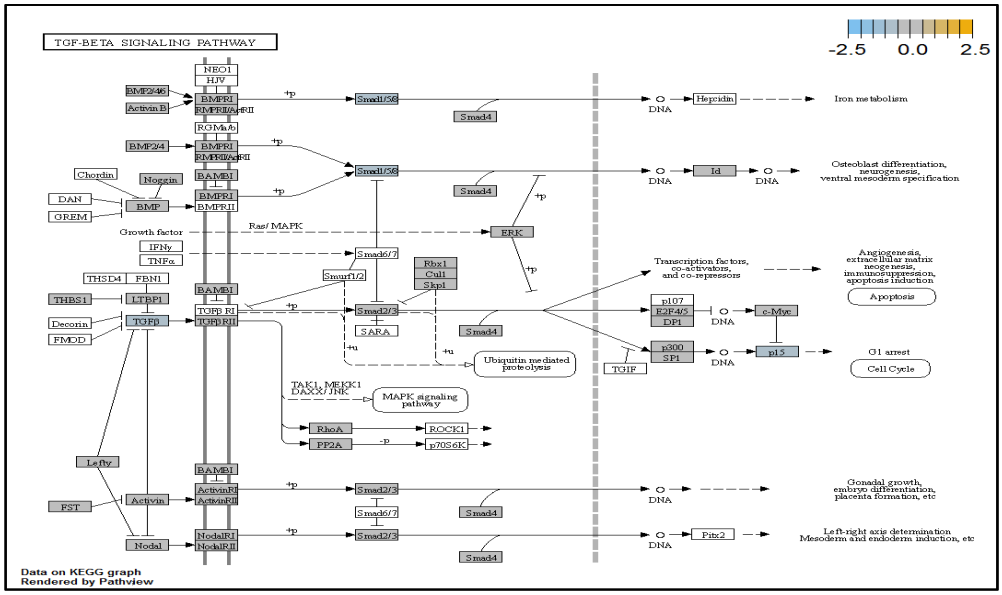

Figure 4.69: TGFβ pathway (treatment time: differential expression in 8 hours vs. baseline of 0 hour for HONE-1 treated with L7 (XXXD))

Downregulated genes: *pl5*, *TGFβ*, *Smad*

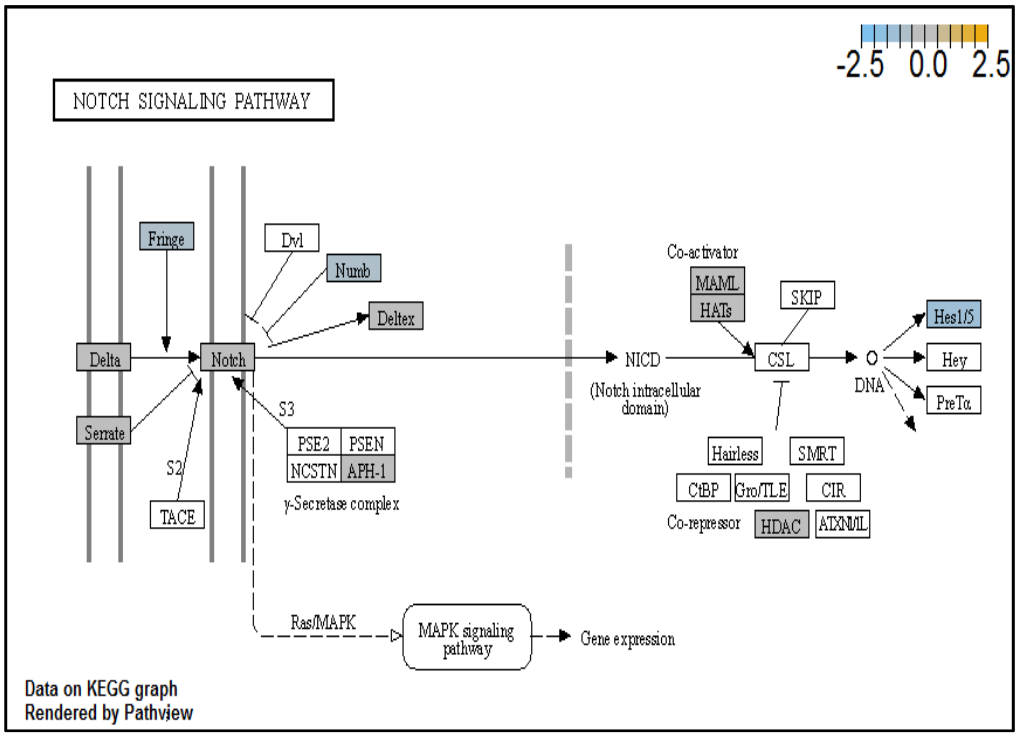

Figure 4.70: NOTCH pathway (treatment time: differential expression in 8 hours vs. baseline of 0 hour for HONE-1 treated with L7 (XXXD))
Downregulated genes: *Fringe, Numb, Hes1/5*

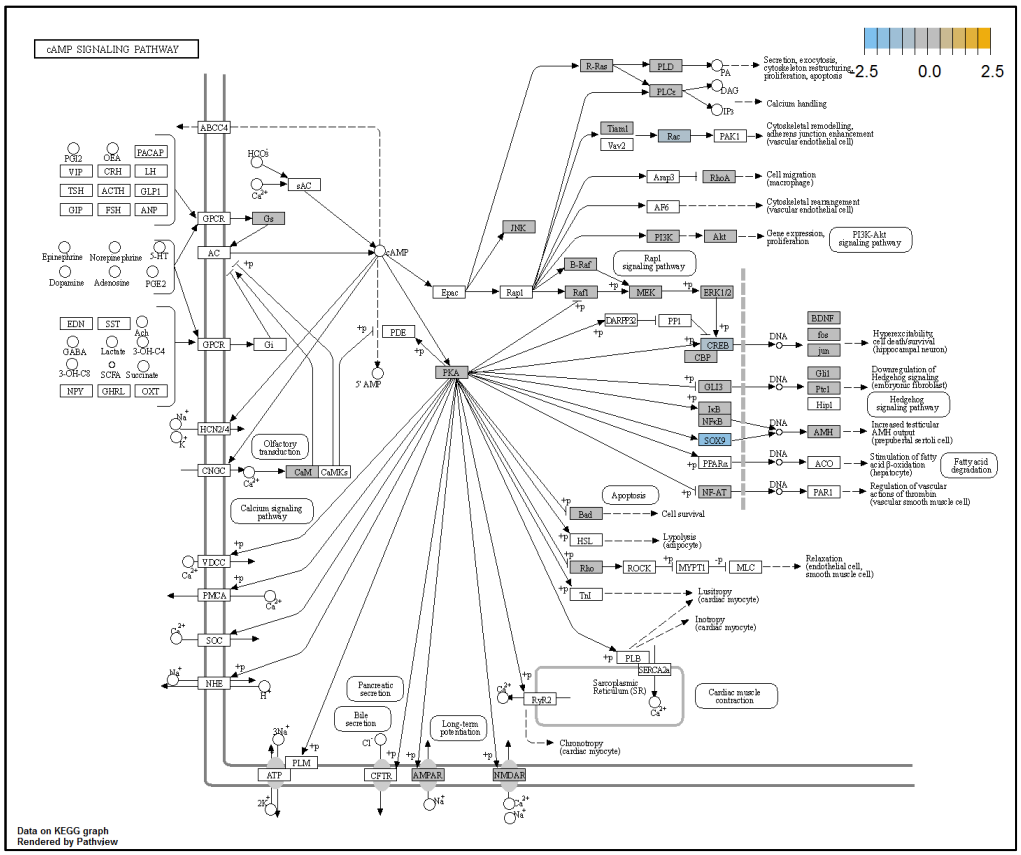

Figure 4.71: cAMP pathway (treatment time: differential expression in 8 hours vs. baseline of 0 hour for HONE-1 treated with L7 (XXXD))
Downregulated genes: *SOX9, CREB, Rac*

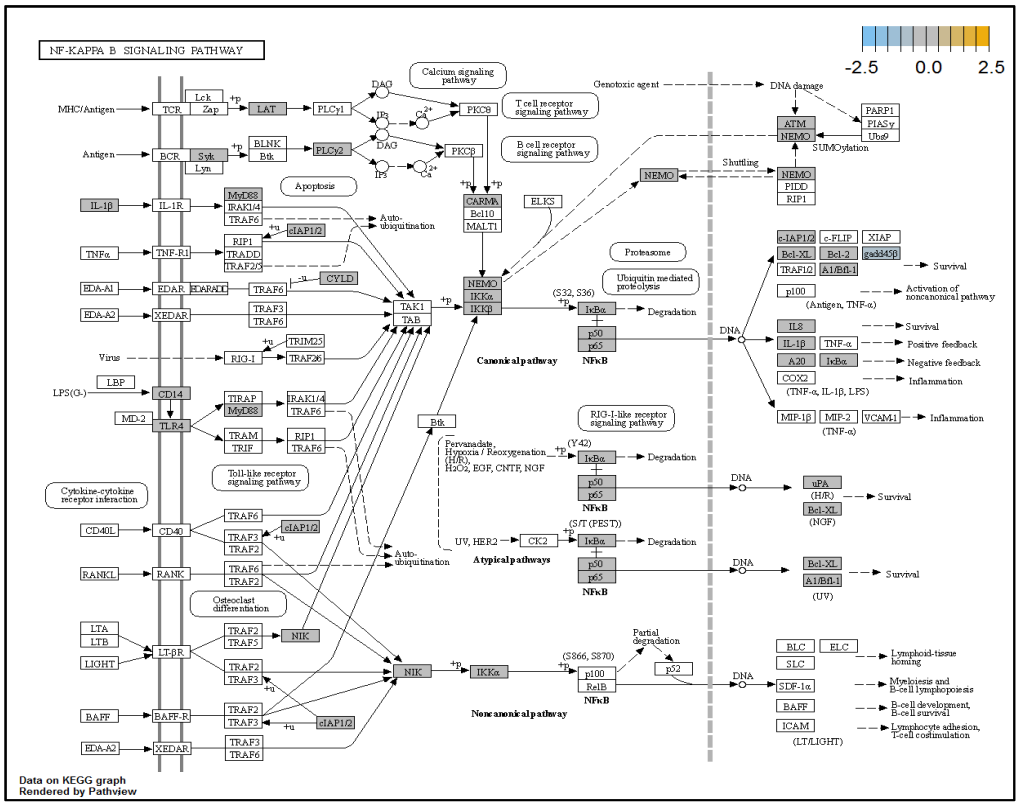

Figure 4.72: TNFκB pathway (treatment time: differential expression in 8 hour vs. baseline of 0 hour for HONE-1 treated with L7 (XXXD))
Downregulated genes: *Gadd45*

4.5.2.3 12 hours vs 0 hour gene expression

Among the 621 genes assayed, 169 up regulated genes shows a positive fold change whereas 64 down regulated genes shows a negative fold change ($P < 0.05$) as shown in Figure 4.73a. The top 10 most significant differentiately expressed genes are shown in Volcano plot (Figure 4.73b). Table 4.37 shows the 20 most significant differentiately expressed genes (measured in $\log_2$ fold change) with the selected covariate at treatment time 12 hours vs 0 hour. Regulation of genes at this time point were mainly initiated by signalling pathway such as MAPK, PI3K, RAS, Cell Cycle –Apoptosis, WNT, JAK-STAT, NOTCH, Transcription Misregulation, TGFβ, FOXO.

Gene expression data were mapped onto KEGG pathway graphs by Pathview function of the PanCancer pathway software, providing intuitive views of both up- and down-regulation at the pathway level. Representative graphs for signalling pathway are shown in Figures 4.74 to 4.83.

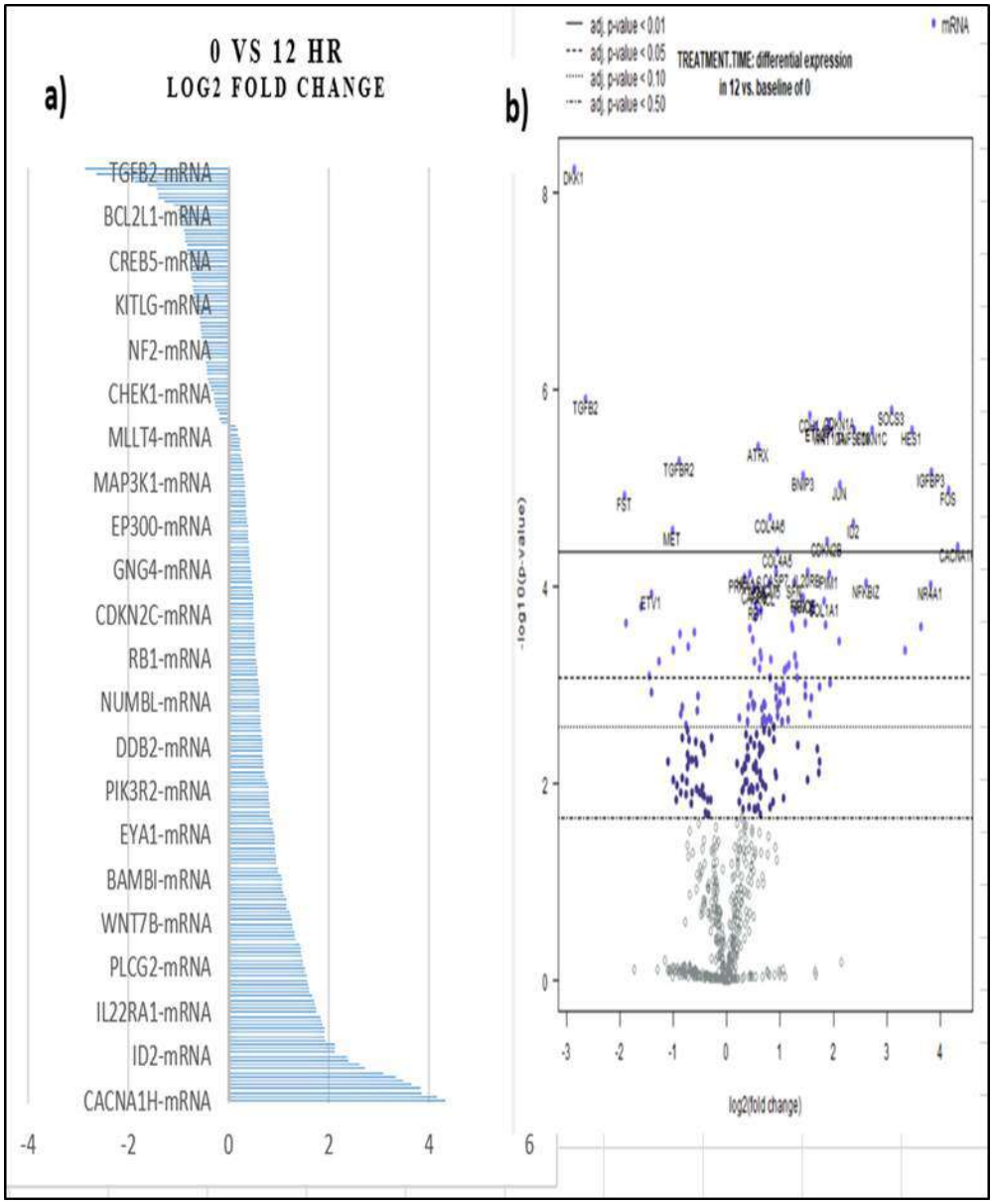

Figure 4.73: a) Log$_2$ fold change difference between 12 hours vs. baseline of 0 hour in HONE 1 cells treated with L7 (XXXD) with differential expression comparing statistically significant differences ($P < 0.05$) in mRNA expression in the up and down regulated genes separately. A total of 169 up regulated genes show a positive fold change whereas 64 down regulated genes show a negative fold change. b) Volcano plot.

Table 4.37: The top 20 most significant differentially expressed genes (measured in Log_2 fold change) with the selected covariate at L7 treatment time 12 hours vs 0 hour with L7 (XXXD)

Genes	Log_2 fold change	*P*-value	Gene.sets	Biological Functions
DKK1	-2.86	5.81E-09	Wnt	**Dickkopf WNT signaling pathway inhibitor 1** • Embryonic, bone development
TGFB2	-2.64	1.26E-06	Cell Cycle-Apoptosis, MAPK, TGF-beta	**Transforming Growth Factor Beta 2** • a secreted ligand of the TGF-beta binds various TGF-beta receptors
FST	-1.91	1.17E-05	TGF-beta	**Follistatin** • regulator of pituitary FSH secretion • inhibitor to Activin and BPM TGFβ-related growth factors
TGFBR2	-0.893	5.21E-06	MAPK, TGF-beta, Transcriptional Misregulation	**Transforming Growth Factor Beta Receptor 2** • receptor/ligand complex phosphorylates proteins which enter the nucleus and regulate the transcription of genes related to cell proliferation, cell cycle arrest
ATRX	0.583	3.8E-06	Driver Gene	**ATRX Chromatin Remodeler** • undergo cell cycle-dependent phosphorylation, involves in the gene regulation at interphase and chromosomal segregation in mitosis
COL4A6	0.812	1.95E-05	PI3K	**Collagen Type IV Alpha 6 Chain** • main structural component of glomerular basement membranes (GBM)
BNIP3	1.43	7.48E-06	Chromatin Modification	**BCL2 Interacting Protein 3** • mitochondrial protein that contains a BH3 domain and acts as a pro-apoptotic factor.
CDH1	1.56	1.86E-06	Driver Gene	**Cadherin 1** • proteolytically generate the mature glycoprotein.
ETS2	1.67	2.4E-06	Ras	**ETS Proto-Oncogene 2, Transcription Factor** • regulates genes involved in development and apoptosis.
ID1	1.91	2.12E-06	TGF-beta	**Inhibitor of DNA Binding 1, HLH Protein** • inhibits the functions of basic helix-loop-helix transcription factors by suppressing their heterodimerization partners through the HLH domains
WNT10A	1.92	2.54E-06	Hedgehog, Wnt	**Wnt Family Member 10A** • implicated in oncogenesis, regulates cell fate and patterning during embryogenesis.

CDKN1A	2.12	1.8E-06	CellCycle-Apoptosis, PI3K, Transcriptional Misregulation	**Cyclin Dependent Kinase Inhibitor 1C** • inhibitor of several G1 cyclin/Cdk complexes, negative regulator of cell proliferation.
JUN	2.12	9.12E-06	MAPK, Wnt	**Jun Proto-Oncogene, AP-1 Transcription Factor Subunit** • interacts directly with specific target DNA sequences to regulate gene expression.
ID2	2.37	2.22E-05	TGF-beta, Transcriptional Misregulation	**Inhibitor Of DNA Binding 2** • inhibits the functions of basic helix-loop-helix transcription factors by suppressing their heterodimerization partners through the HLH domains
TNFSF10	2.38	2.52E-06	Cell Cycle - Apoptosis	**Tumor Necrosis Factor Ligand Superfamily Member 10** • cytokine that belongs to the tumor necrosis factor
CDKN1C (KIP2 /p57)	2.72	2.57E-06	Cell Cycle - Apoptosis	**Cyclin Dependent Kinase Inhibitor 1C** • inhibitor of several G1 cyclin/Cdk complexes and negative regulator of cell proliferation.
SOCS3	3.09	1.61E-06	JAK-STAT	**Suppressor of cytokine signaling 3** • cytokine-inducible repressor of cytokine signaling, inhibit the activity of JAK2 kinase.
HES1	3.47	2.52E-06	Notch	**Hes Family BHLH Transcription Factor 1** • antogonist of transcription factors.
IGFBP3	3.84	6.79E-06	Transcriptional Misregulation	**Insulin-like growth factor binding protein 3** • alter the interaction of IGFs with their cell surface receptors. • pro- apoptotic effects mediated by its receptor TMEM219/IGFBP-3R.
FOS	4.15	1.05E-05	MAPK	**Fos Proto-Oncogene, AP-1 Transcription Factor Subunit** • regulators of cell proliferation differentiation, and transformation

Continuation of Table 4.37

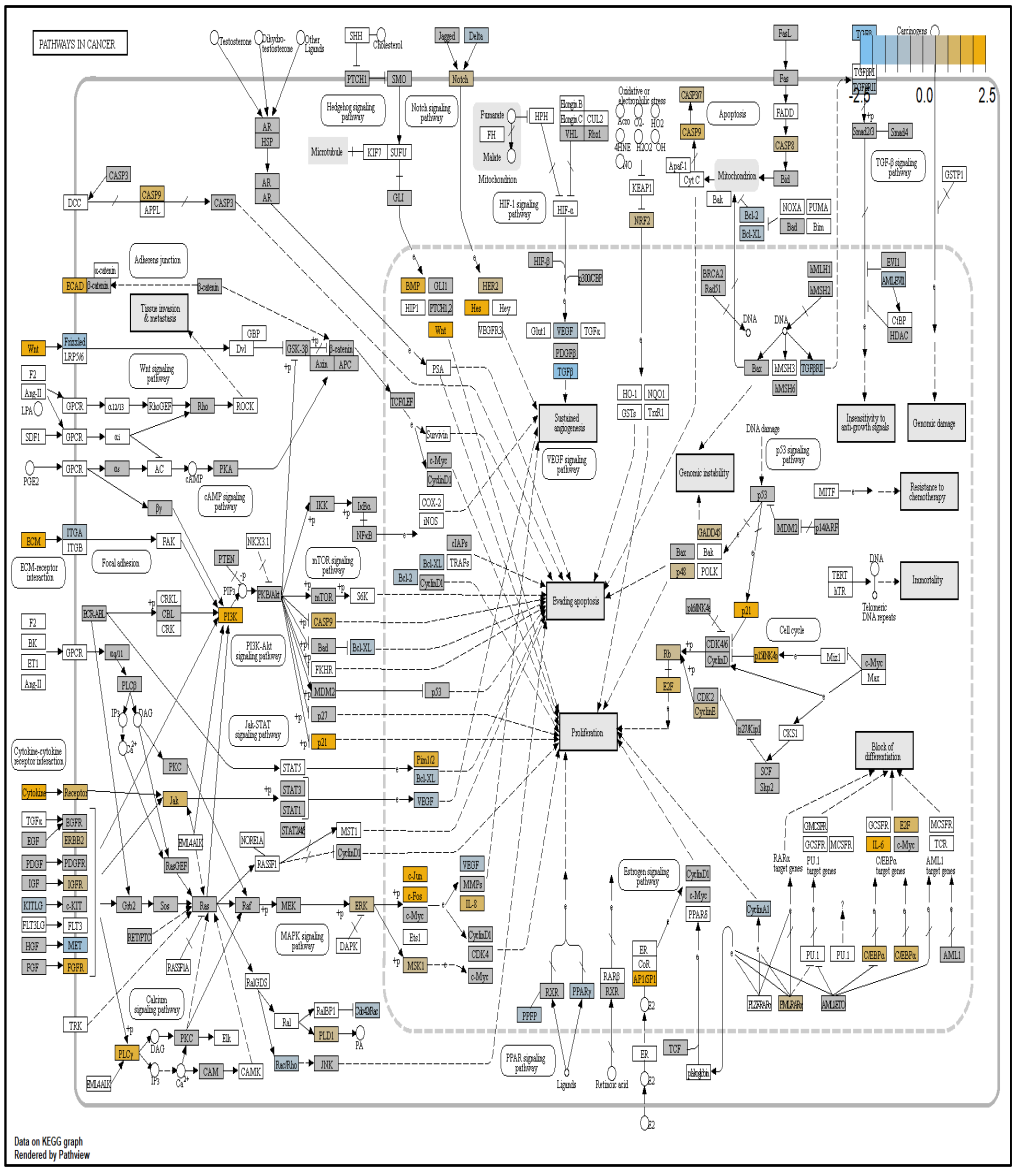

Figure 4.74: Cell Cycle in Cancer pathway (treatment time: differential expression in 12 hours vs. baseline of 0 hour for HONE-1 treated with L7 (XXXD))

Upregulated genes: *CASP9, BCAD, WNT, ECM, Cytokine, Cytokine receptor, FOFR, ERBB2, IGFR, P13K, Jak, p21, PLCy, ERK, PLD1, ejun, eFos, BMP, HES, HERS, Notch, p48, E2F, Cyc E, CASP8, GADD45, IL6, C/EBPα, AP1, NRF2*

Downregulated genes: *Frizzled, ITGA, KITLG, MET, Delta, PPFP, PAARy, BCL-2, BCL-XL, TGFβ*

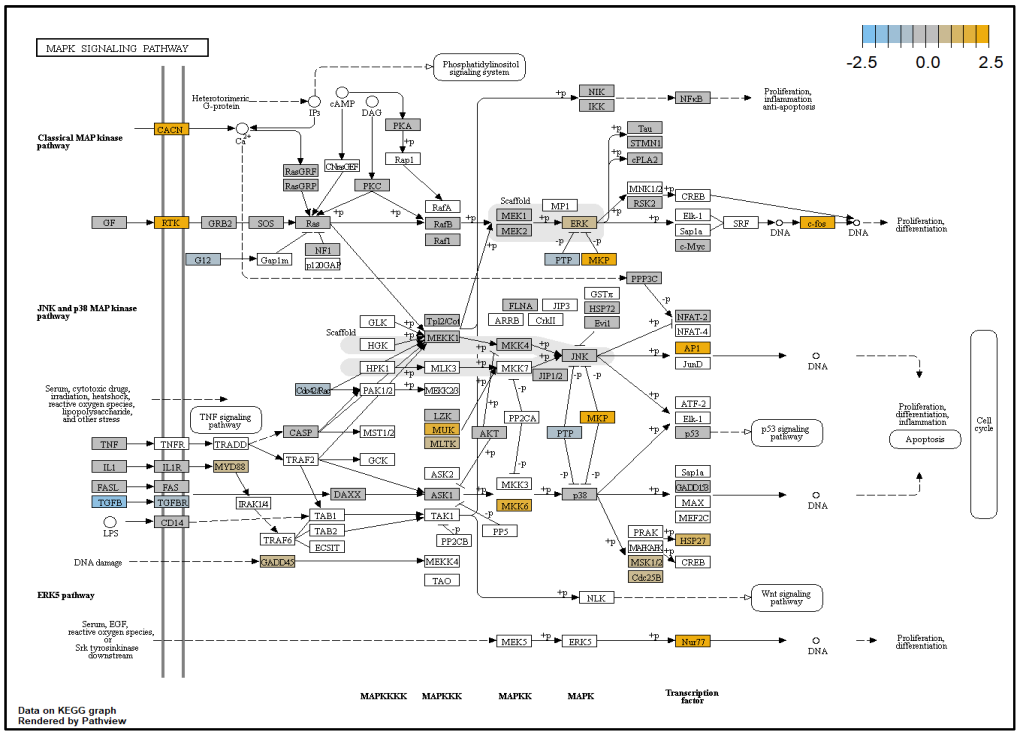

Figure 4.75: MAPK pathway (treatment time: differential expression in 12 hours vs. baseline of 0 hour for HONE-1 treated with L7 (XXXD))

Upregulated genes: *CACN, RTK, MUK, MKK6, GADD45, MAK, MKP, e-Fos, AP1, NUR77, MSK1/2, CDK25B, HSP27*

Downregulated genes: *TGFβ, TGFβR, PTP, G12*

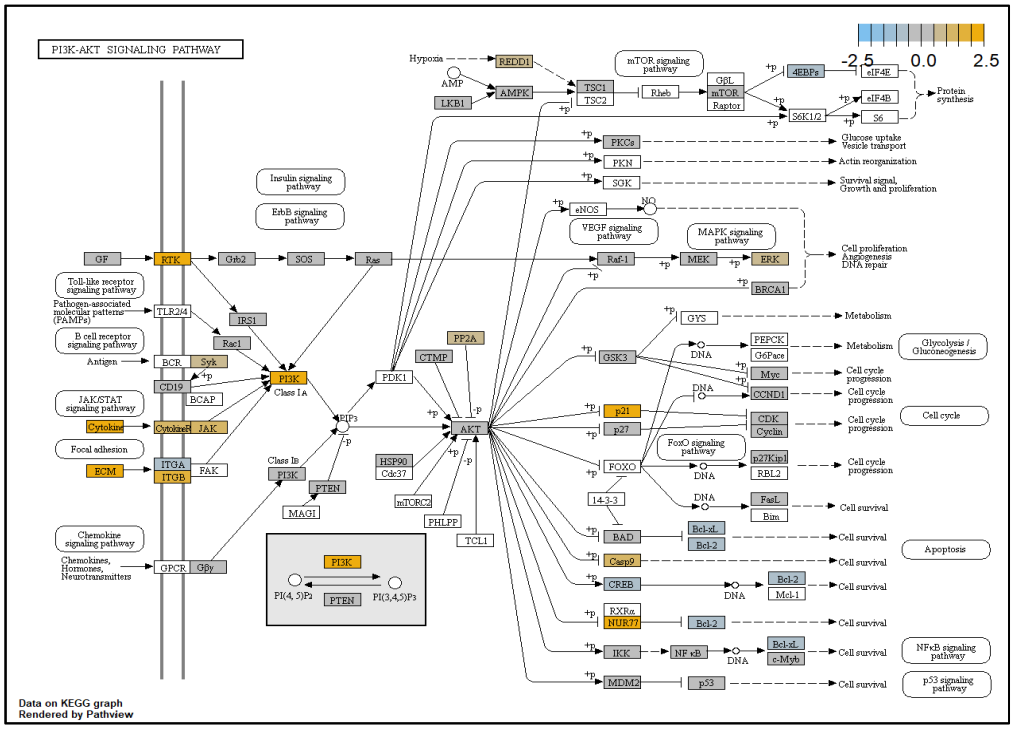

Figure 4.76: PI3K pathway (treatment time: differential expression in 12 hours vs. baseline of 0 hour for HONE-1 treated with L7 (XXXD))

Upregulated genes: *RTK, Cytokine, CytokineR, ECM, ITGB, PI3K, p21, pp2A, ERK, NUR77, CASP9, REDDI*

Downregulated genes: *ITGA, CREB, BCL-2, BCL-XL, 4EBPs*

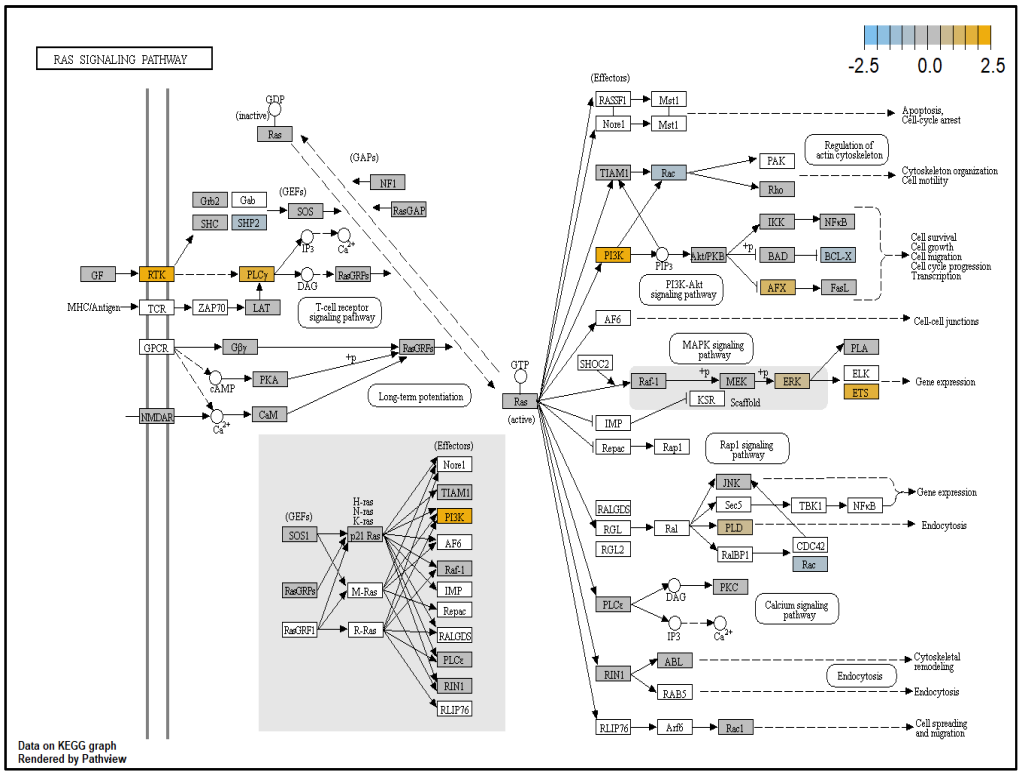

Figure 4.77: RAS pathway (treatment time: differential expression in 12 hours vs. baseline of 0 hour for HONE-1 treated with L7 (XXXD))

Upregulated genes: *RTK, PLCγ, PI3K, ETS, APX, PLD*

Downregulated genes: *SHP2, BCL-X, Rac*

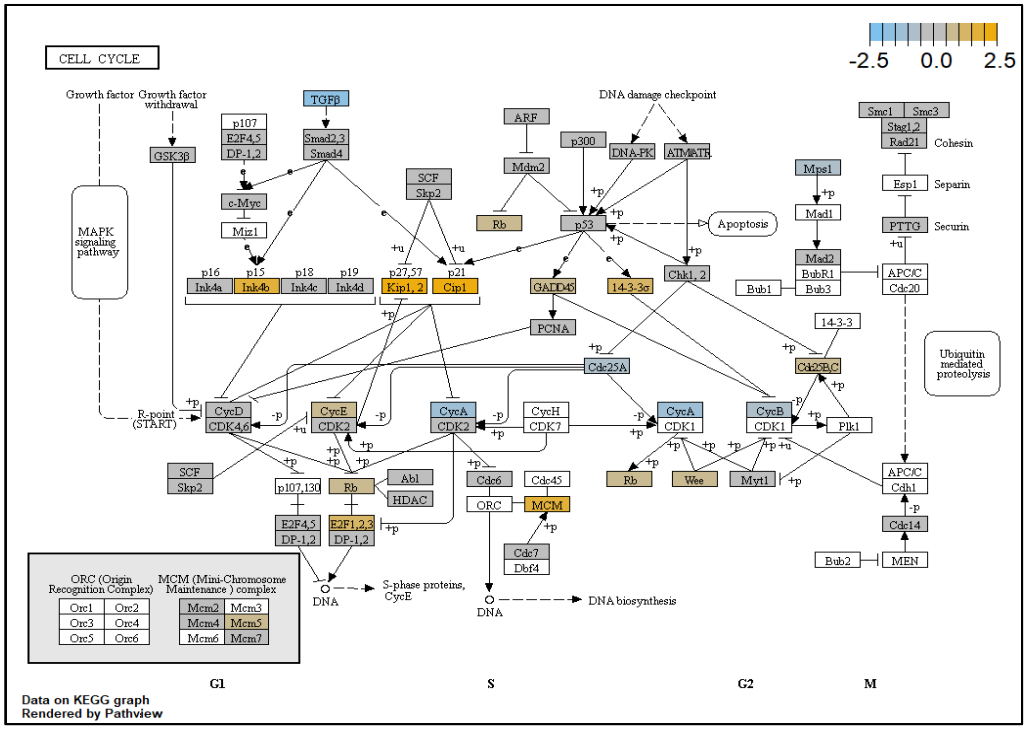

Figure 4.78: Cell Cycle pathway (treatment time: differential expression in 12 hours vs. baseline of 0 hour for HONE-1 treated with L7 (XXXD))

Upregulated genes: *InK4b, Kip1,2, MCM, E2F1,2,3, 14-3-3α, CIP1, Rb, Wee, Cdk25B,C*

Downregulated genes: *CycA, CdK25A, TGF*

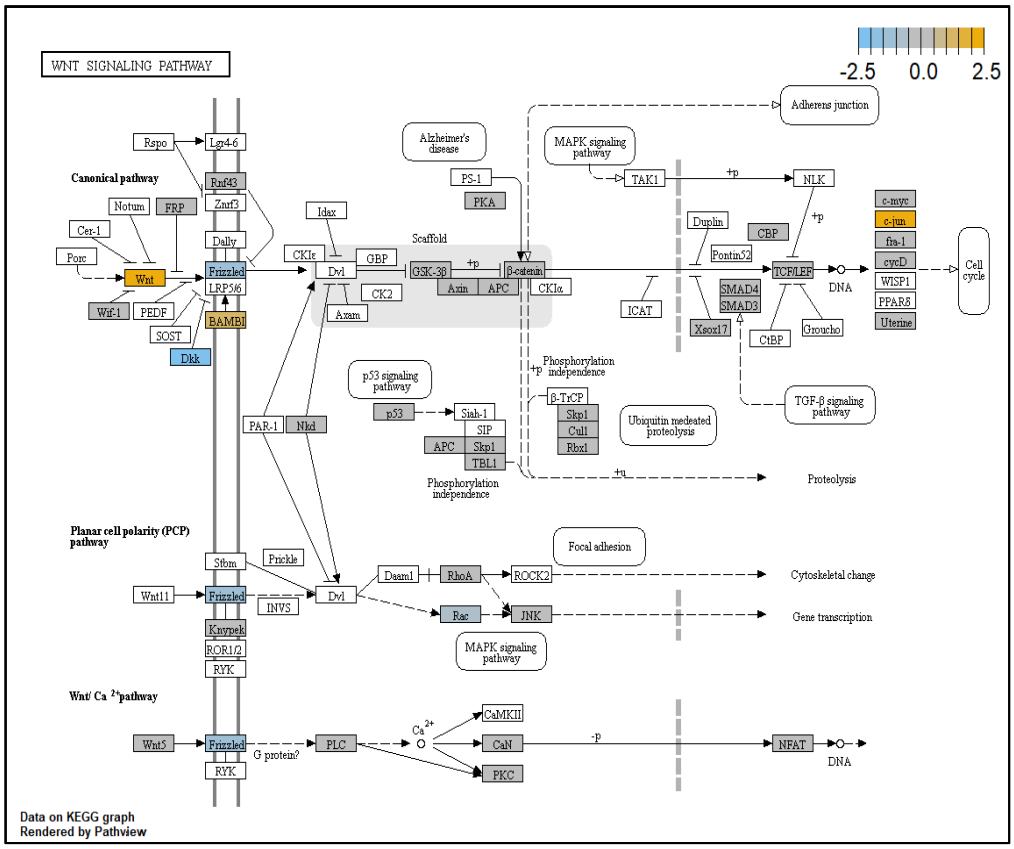

Figure 4.79: WNT pathway (treatment time: differential expression in 12 hours vs. baseline of 0 hour for HONE-1 treated with L7 (XXXD))
Upregulated genes: *BAMB1, Wnt, e-jun*
Downregulated genes: *Frizzled, DKK, Rac*

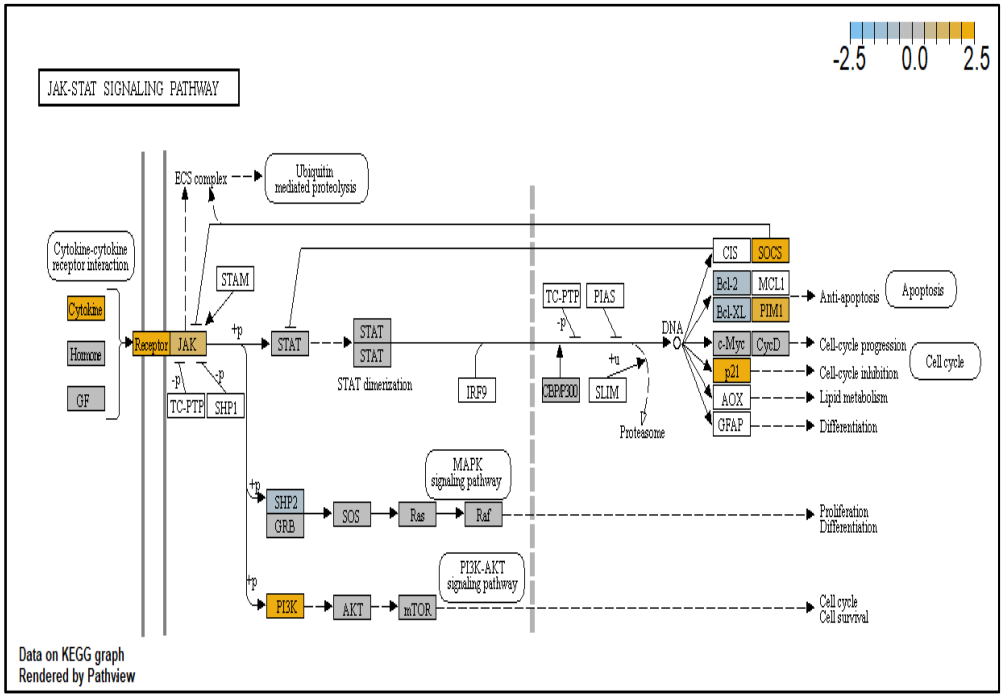

Figure 4.80: JAK-STAT pathway (treatment time: differential expression in 12 hours vs. baseline of 0 hour for HONE-1 treated with L7 (XXXD))
Upregulated genes: *Cytokine, receptor, PI3K, JAK, p21, PIM1*
Downregulated genes: *SHP2, BCL-2, BCL-X*

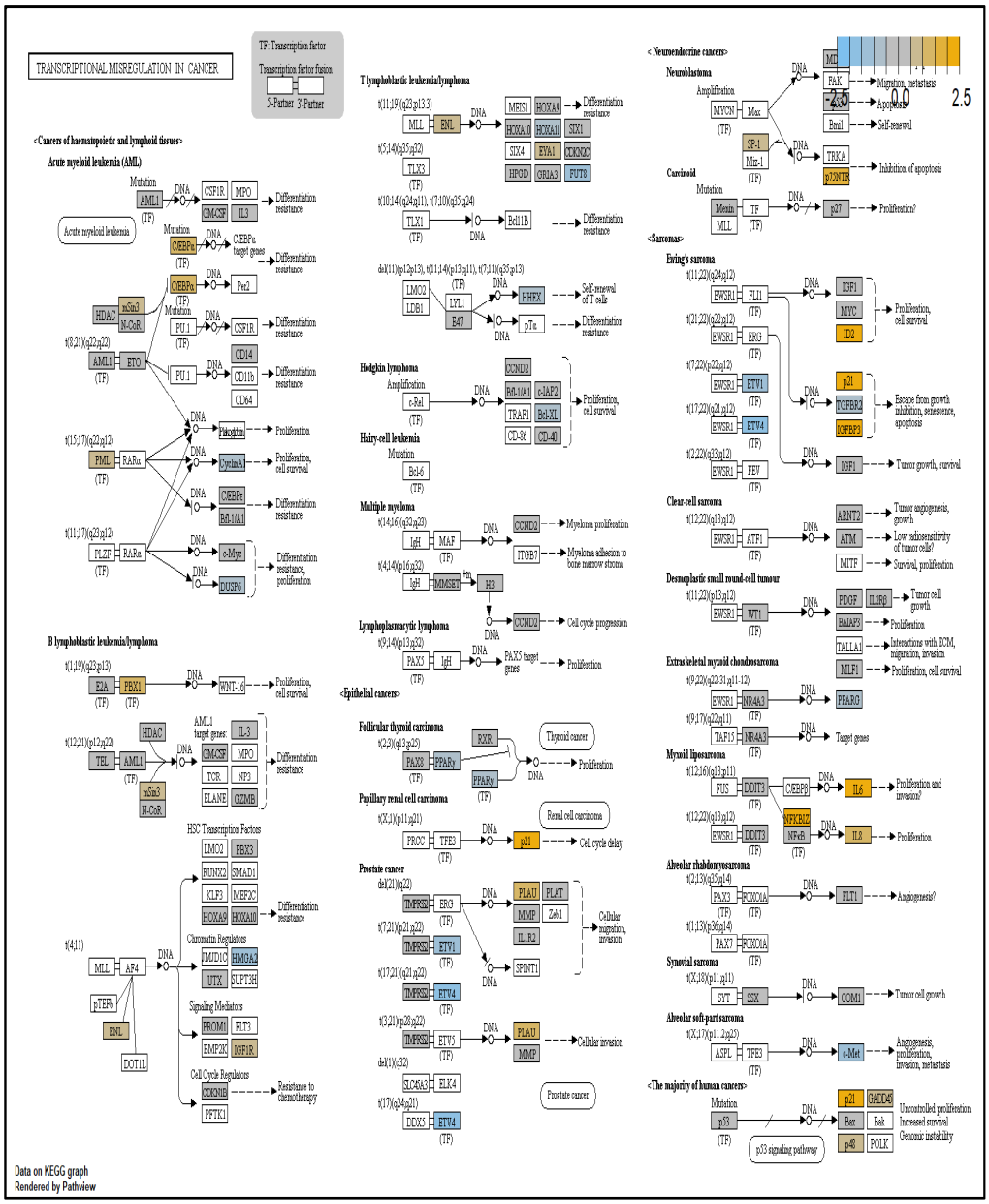

Figure 4.81: Transcription Misregulation pathway (treatment time: differential expression in 12 hours vs. baseline of 0 hour for HONE-1 treated with L7 (XXXD))

Upregulated genes: *C/EBPα, PML, PBX1, ENL, IGFIR, P21, PLAU, IGFBP3, IL6, NFKBIZ, p48*

Downregulated genes: *HMGA2, CycA, ETV1, ETV4, BCL-XL, PPARγ*

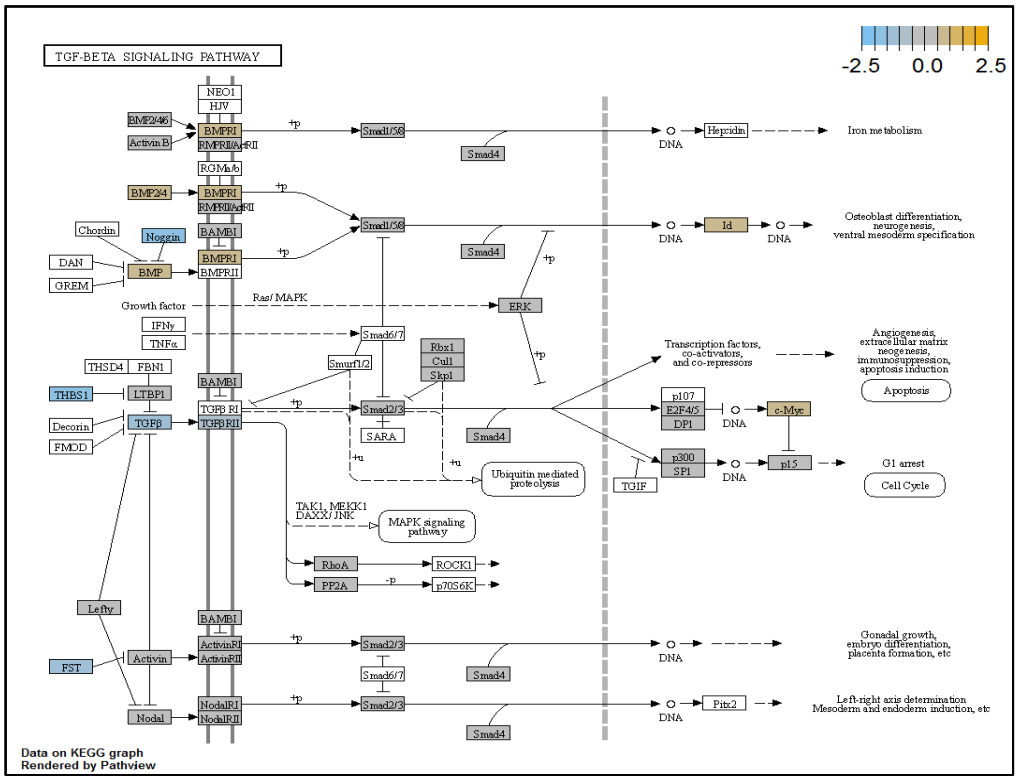

Figure 4.82: TFGβ pathway (treatment time: differential expression in 12 hours vs. baseline of 0 hour for HONE-1 treated with L7 (XXXD))
Upregulated genes: *BMP2/4*, *BMP*, *BMPR*, *Id*, *c-MYC*
Downregulated genes: *THBS1*, *FST*, *TGFβ*, *TGFβR2*

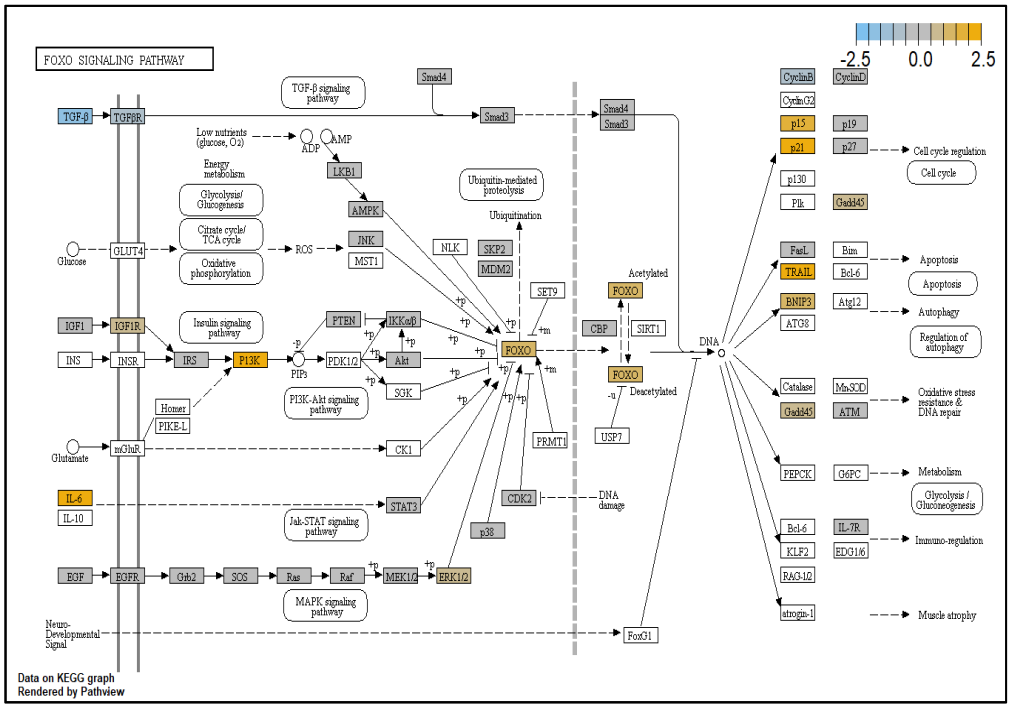

Figure 4.83: FOXO signaling pathway (treatment time: differential expression in 12 hours vs. baseline of 0 hour for HONE-1 treated with L7 (XXXD))
Upregulated genes: *IL6*, *PI3K*, *IGFIR*, *FOXO*, *ERK1/2*, *TRAIL*, *BNIP3*, *GADD45*, *p15*, *p21*
Downregulated genes: *TFDβ*, *TFDβR*, *CycB*

4.5.2.4 Venn Diagram

The common differentially expressed genes of HONE-1 at three different treatment times (4, 8 and 12 hours) after exposure to L7, in both downregulated and upregulated gene lists were identified by using Venny online tool. As shown in Figure 10, a total of 202 genes were up-regulated and 155 genes were down-regulated (Log_2 fold change with $P < 0.05$) in HONE-1 cells at the three time points. In the case of up-regulated genes, no genes was found between 4 and 8 hours treatment time; 7 genes (3.5%) were found between 8 and 12 hours treatment time and 81 genes (40.1%) were found between 4 and 12 hours treatment time whereas 8 genes (4%) were found in between three treatment time. In the case of down-regulated genes, a total number of 4 genes (2.6%) were found between 4 and 8 hours treatment time; 14 genes (9%) were found between 8 and 12 hours treatment time and 16 genes (10.3%) were found between 4 and 12 hours treatment time whereas 4 genes (2.6%) were found in between three treatment times.

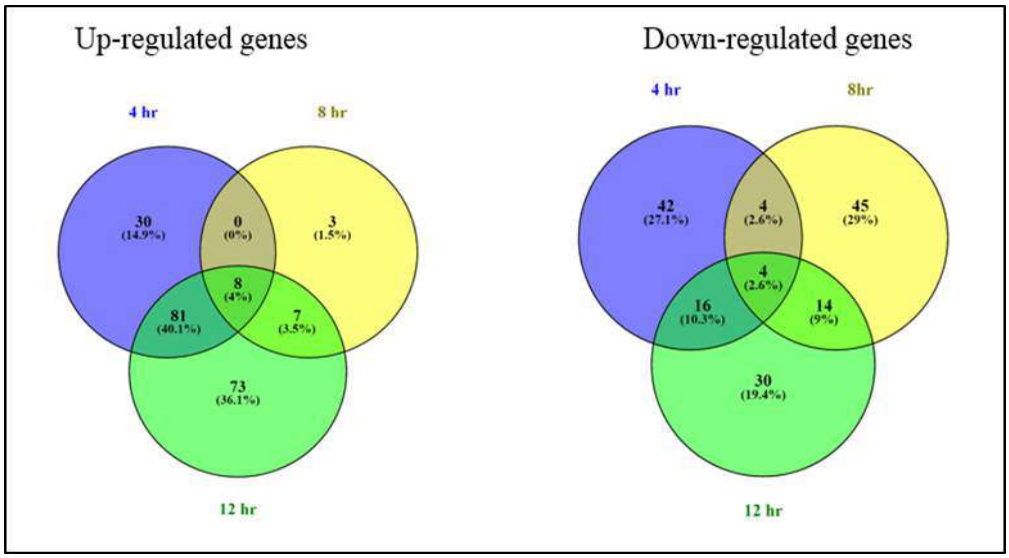

Figure 4.84: Venn diagram depicting the common genes differentially regulated in HONE-1 cells after treatment at different time points. The number of downregulated and upregulated genes in HONE-1 cells after exposure to L7 is indicated in the diagram.

CHAPTER 5

DISCUSSION

This study was designed to unveil alterations in gene expression patterns and pathway mechanisms involved in HONE-1and subsequent comparison at different time points upon treatment with Huanglian and Xiao Xian Xiong Decocion (XXXD).

5.1 Plant Natural products

Nearly 80 % of the world's population depend on traditional medicines and more than 60 % of clinically approved anticancer drugs are derivatives of medicinal plant (Ni et. al., 2014). Plant metabolites exhibit a wide range of biological functions, including anti-cancer, analgesic, anti-inflammation, and anti-microbial activities. Secondary metabolites conduce important functions to the plant, such as protection, competition, and species interactions. These secondary metabolites are widely utilised by humans to make medicines, flavorings, pharmaceuticals, agrochemicals, fragrances, colours, biopesticides, food additives and drugs (Hussain MS et al., 2012).

5.2 Metabolite Profiling of herbal extracts L1~L7

The metabolite profiling obtained by Liquid Chromatography Mass Spectrometry (LC-MS) in this study showed that Huanglian consisted of amino acid (7 %), carbohydrate (3 %), fatty acid (10 %), protein (3 %), vitamin (3 %), alkaloid (34 %), glucoside (7 %), phenolic (27 %), phthalide (3 %) and terpene (3 %). Secondary metabolite such as alkaloid and phenolic composed the largest percentage. Alkaloid in L1 (Huanglian) composed of protoberberine (10 %), isoquinolines (20 %), purine (30 %), pyrimidines (10 %), flavoalkaloid (10 %), morpholines (10 %), allymines (10 %).

Primary metabolites of L2 (Banxia) were made up of amino acid (14 %), Fatty acid (25 %), protein (16 %) and glucose (16 %) where secondary metabolites comprised alkaloid (14%), phenolic (21 %), phthalide (2 %), pteridine (2 %), saponin (2 %) and terpene (2 %). In L2 (Banxia), phenolic composed of tannin, Erythronic acid, tricarboxylic acid, glucoside, phenol. By the way, alkaloid composition was made up of xanthine alkaloid, carboxamide, terpenoids, phenylpropanoid and morpholines.

L3 (Gualou) consisted of primary metabolites which were made up of amino acid (15 %), carbohydrate (3 %), fatty acid (27 %), glucose (3 %) and protein (5 %). Its secondary metabolites comprised alkaloid (18 %), benzamide (3 %), phenolic (17 %), phthalide (3 %), phthalate (3 %) and terpene (3 %). The comparative ratio of primary metabolites to secondary metabolites was 53 % to 47 %. In L3 (Gualou), alkaloid composition was made up of indoles, purine,

carbohydrazide, pyrrolidine alkaloid. By the way, phenolic composed of dicarboxylic acid, polyphenols and tricarboxylic acid.

L4 (Huanglian+ Banxia) consisted primary metabolites which were made up of amino acid (11 %), carbohydrate (4 %), fatty acid (7 %) and glucose (4 %). Secondary metabolites comprised alkaloid (41 %), phenolic (19 %), saponin (4%) and terpene (3 %). The comparative ratio of primary metabolites to secondary metabolites was 26 % to 68 %. In L4 (Huanglian + Banxia), alkaloid composition was made up of formamidopyrimidine, xanthine, quinic acid, terbinafine, opiate alkaloid, cularine, isoquinoline and cannabinoid. By the way, phenolic composed of carboxylic acid, phenolic glycosides, phenylpropanoic acids and tricarboxylic acid.

Primary metabolites L5 (Huanglian+ Gualuo) consisted of of amino acid (16 %), carbohydrate (3 %), fatty acid (16 %), glucose (3 %), protein (9 %) and vitamin (3 %). Secondary metabolites comprised alkaloid (28 %), phenolic (13 %), terpene (3 %), coblamin (3 %) and benzamide (3%). The comparative ratio of primary metabolites to secondary metabolites was 50 % to 50 %. In L5 (Huanglian + Gualou), alkaloid composition was made up of indoles, deoxycytidine analog, Purine, hydroxypyrimidines, xanthine cularine, cannabinoid and benzodioxoles. By the way, phenolic comprised of dicarboxylic acids, tricarboxylic acid, beta hydroxy acids and phenylpropanoic acids.

In L6 (Banxia + Gualou), the comparative ratio of primary metabolites to secondary metabolites was 55 % to 45 %. The primary metabolites were made

up of amino acid (22 %), protein (14 %), fatty acid (14 %) and glucose (5 %). Secondary metabolites comprised alkaloid (22 %), phenolic (18 %), and flavanoid (5 %). In L6 (Banxia + Gualou), alkaloid composition was made up of indoles, Purine hydroxypyrimidines and xanthine. Besides, phenolic consisted of dicarboxylic acids tyrosols and derivatives and tricarboxylic acid.

As for L7 (XXXD), the metabolites composition is as follows: amino acid (11 %), carbohydrate (4 %), fatty acid (26 %), protein (7 %), glucose (4 %), alkaloid (37 %) and phenolic (11 %). Similarly, secondary metabolite such as alkaloid composed the largest percentage. Alkaloid in L7 (XXXD) composed of indoles (20 %), deoxycytidine analog (10 %), purine (30 %), pyrimidines (10 %), carbohydrazide (10 %), terpenoid (10 %) and methylhydrazine (10%).

Alkaloid and phenolic are the main components involved in protection, competition and species interaction. It is widely believed that these compounds have diverse anti-cancer properties, such as anti-proliferation and apoptotic activity (Yang L et al., 2018). Hence, the cytotoxicity effect upon HONE-1 cell lines by Huanglian and XXXD used in this study could be further ascertained by its abundance existence of secondary metabolites such as alkaloid and phenolic.

Methods of extraction of medicinal plants include solvent extraction, distillation method, pressing and sublimation according to the extraction principle. In this experiment, aqueous-extraction of all samples was adopted. The method resembled conventional traditional Chinese medicinal decoction preparation for oral consumption. It was a simple, economical and effective

method for oral consumption and faster absorption in body for curing diseases (Ergil KV et al., 2002).

5.3 Cytotoxicity of Huanglian and XXXD upon HONE-1

This study reports the cytotoxic activity of Xiao Xian Xiong Decoction (XXXD), two combination herbs and individual herb of Huanglian (*Coptidis Rhizome*), Banxia (*Pinellia Rhizome*) and Gualou (*Fructus Trichosanthis*) on human nasopharyngeal carcinoma cancer cell lines. In this study, only one NPC cell line with most susceptible to the herbal extract was selected for further gene expression analysis. After the MTT test, it was observed that all 8 NPC cell lines had expressed their resistance towards different herbal extracts. However, extract Huanglian was observed to have obtained the lowest IC_{50} value upon HONE-1 than 7 other NPC cell lines. In the MTT test, the herbal extract L1 (Huanglian) was the only extract observed of having obtained the IC_{50} value upon all 8 NPC cell lines. Besides, the IC_{50} values of L7 (XXXD Decoction) were only found against HONE-1 (88.55 μg/mL) and CNE 2 (92.95 μg/mL) and it showed the strongest effect towards HONE-1 in terms of cytotoxicity. The IC_{50} (μg/mL) values of L1 (Huanglian) against 8 NPC cell lines are listed as follows: HONE-1 (4.48), CNE-2 (6.32), CNE-1 (6.77), SUNE-1 (10.72), HK-1 (11.10), TWO-4 (11.77), TWO-1 (24.46) and C666-1 (27.30). It is demonstrated that the lowest IC50 value of 4.48 μg/mL is attained for HONE-1. The finding concluded that HONE-1 cell line was most susceptible to herbal extracts L1 (Huanglian), and thus, HONE-1 was chosen for the subsequent experiments.

The result of MTT assays used to test for cytotoxicity eficacy of herbal extract during this research project revealed that L1 (Huanglian) achieved half-maximal inhibitory concentration of 4.48 μg/mL when treated to HONE-1 cells. The MTT result had reckoned Huanglian imposed decreasing cell viability in HONE-1. It is clear that HONE-1 cells exposed to Huanglian lose their capability to proliferate in dose-dependent manner. This finding suggests that Huanglian has the potential to suppress the growth of HONE-1 cells.

The IC_{50} values obtained for L7-treated HONE-1 and CNE-2 were at 88.55 μg/mL and 92.95 μg/mL, respectively. The cytotoxicity effect of Huanglian upon HONE-1 cell line was indicated to be stronger than that of XXXD in terms of IC_{50} values, where the IC_{50} values attained were 4.48 μg/mL and 88.55 μg/mL, respectively.

The 138th clause in Shan Han Lun stated the appropriate syndrome for Xiao Xian Xiong Decoction was the entanglement or stagnation of phlegm and heatiness in chest. According to the clause, this heatiness could be caused by the superficial syndrome (表证) or as a consequence of clinical mistreatment of such syndrome. The excessive heatiness will somehow evolve into fire in the body. Fire will then be able to transform body dampness into phlegm which will gradually accumulate and develop into fatty clump to form clotting in any part of the body. Generally, the aetiology of phlegm formation could be owing to malfunction of Pi (脾). On the other hand, due to the fondness and habitual consumption of large amount of fatty or oily food, subsequently, Qi of Pi (脾气) could be deteriorated to induce the production of excessive dampness in the body

and eventually transform into phlegm with the implication of heatiness. The will cause symptoms such as chest or stomach pain, clump in chest, focal distention in stomach, constipation, coughing with thick and yellowish sputum. Conventionally, XXXD is prescribed to treat diseases such as bronchitis, hepatitis, biliary or epigastria reflux, pyloric infection, vascular or coronary disease, insomnia and etc. where syndrome of entanglement of heatiness and phlegm is diagnosed. The applications of XXXD for cancer diseases are witnessed in recent years and satisfactory results were shown in many international medical journals. However, the literature regarding the application of XXXD in nasopharyngeal carcinoma has not been seen so far. Research done by L.L. Ni et al. (2014) had shown inhibitory effect of XXXD upon lung cancer cell (NSCLC). This research was set from the hypothesis that XXXD could possess anti-cancer effect of on NPC because Chinese Medicine’s Visceral Theory (脏腑学说) stated that nasopharynx belongs to the lung system where nose is the opening of lung system (肺开窍于鼻) and they all participate in the respiratory activities and functions. Clinically, a large number of NPC patients are diagnosed for having entanglement of heatiness and phlegm（痰热互结证） identical to XXXD syndrome such as nasal congestion with thick yellowish mucus associated with sinusitis, mouth tasted bitter, yellowish and greasy coated tongue, slippery and floating or slippery and rapid pause. Hence, this research is aimed at studying the gene expression of a selected NPC cell line when treated with XXXD and one of its most cytotoxic constituent via an in-vitro experiment.

In the combination of three herbs in XXXD, Gualou is often regarded as the primary role where Huanglian and Banxia remained as secondary when clinical function of XXXD is concerned. Gualou does not only eliminate heatiness in

lung or rather the whole respiratory system, it also removes thick and yellowish phlegm as well as soothing the Qi in the chest. This helps to dissolve nodules and abscesses. Besides, Huanglian can clear away heatiness and dampness together. Banxia reinforce the function of eliminating phlegm as well as sinking the Qi to relieve nausea.

The database of experimental research of treatment of XXXD on many tumours such as colorectal cancer, breast cancer, ovarian cancer, prostate cancer, liver cancer, skin tumours, oral cancer, cervical cancer, lung cancer, pancreatic cancer NPC cell lines are available in most library database. However, database regarding in vitro experimental research of NPC treated with XXXD was not readily found except its single constituents such as Huanglian (Tsang, C. M et al., 2013) (Tsang CM et al., 2015) and Gualou (Wang, W et al., 2018). This is a novel *in vitro* experiment of NPC cell lines treated with XXXD.

Although XXXD did consist of Huanglian components, the overall cytotoxicity effect decreased. This may attribute to the composition arrangement of 3 single herbs such as Huanglian, Banxia and Gulou in XXXD which were 12g, 18g and 40g, respectively. The ratio of weight was derived from the specification stated in Shan Han Lun. Huanglian was not the major constituent (君), but the third place (使) in the prescription in the context of Shan Han Lun. Moreover, the functions of this Chinese medicine formula is to clear heat and internal dampness of body literally means to eliminate phlegm and clumps in chest, and more importantly it also helps to promote the body immunity by uplifting the body resistance towards external threat (causes of disease).

Huanglian is bitter and cold in nature. Although it can clear body heat, dries dampness and eliminates inflammation and toxicity, somehow, in practice, it is not suitable to be prescribed and consumed in big quantity or in single especially for cancer patient. The consequence is that the Yang qi (阳气) of patient could be debilitated and thus result in weaker physical condition. This is contrary to TCM principle of treating a disease in which the practitioners always emphasize "Holistic regulation" and the equilibrium of Yin and Yang in the human body.

5.4 Gene expression in HONE-1 when treated with L1 (Huanglian) at 3 different time points.

5.4.1 Time point at 4 hours vs. 0 hour

The top ten downregulated genes noted in HONE-1treated with L1 Huanglian were *FOS, TNFSF10, PLD1, MYB, HES1, ETV1, CDC25C, KLF4, CASP8* and *PIK3CA*. Besides, the down-regulation was initiated by canonical pathway such as Cell Cycle - Apoptosis, MAPK, PI3K, Ras, Notch, JAK-STAT and Driver Gene.

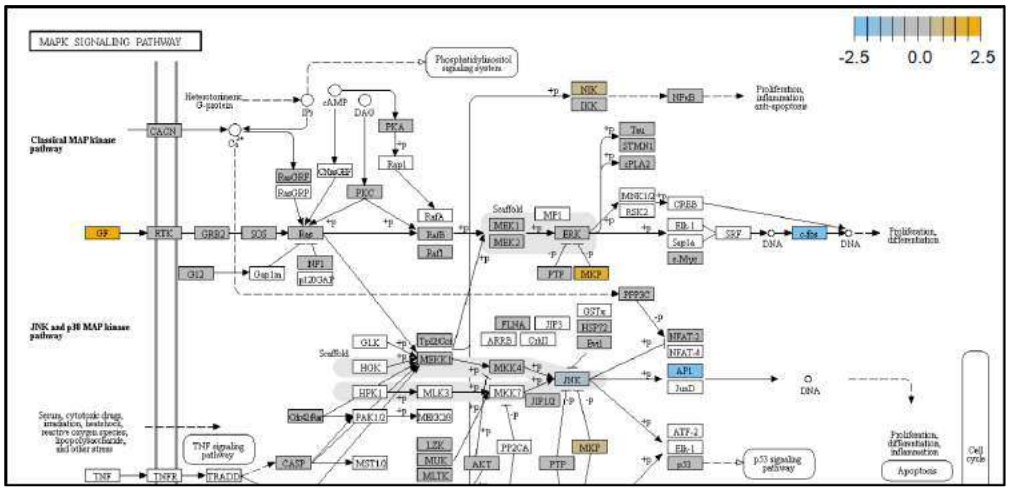

Extract from Figure 4.12 (MAPK pathway)

Among all the downregulated gene, *FOS* as initiated by MAPK pathway (Figure 4.5.1.1.2) scored -2.31 ($P < 0.05$), the least $\log_2$ fold change expression value in the list. *FOS* forms the transcription factor complex *AP-1* by dimerizing with proteins of the JUN family. *AP-1* will subsequently induce downstream genes to proceed with cellular processes such as proliferation, differentiation, and apoptosis (Eferl R and Wagner EF, 2003). As such, the FOS proteins have been implicated as regulators of cell proliferation, differentiation, and transformation. However, the expression of *FOS* can be modulated by inter-reaction with other transcriptional regulators and is affected by upstream kinases. In this experiment, the down-regulation of *FOS* was associated with MAPK pathway where the activation of *ERK* was suppressed by its inhibitor *MKP* (*Duspa*) gene which was highly expressed. Subsequently ERK merely phosphorylated and transduced signal to *C-MYC*, a transcription factor which regulates cell proliferation and apoptosis. C-MYC can regulate apoptosis in cell when induced by cellular stress such as chemotherapeutic drug, hynoxia, glucose insufficiency and DNA damage (Myrtle A et al., 2002). Hence, as shown in the pathview, *C-MYC* induced down-regulation of *FOS*. This led to a cell fate of

differentiation and apoptosis in HONE-1. Meanwhile, in JNK MAPK pathway, *AP-1* was deregulated when expression of *JNK* gene was suppressed by its inhibitor *MPK* with elevated expression. It can be seen in the pathview that the growth factor GF ligand was highly expressed. However, the cytoplasmic signal transducer genes in MAPK pathway did not actively respond. Moreover, elevated expression of *NIK* was detected associating a noncanonical NF-κB signalling pathway. NIK is NF-κB-inducing kinase (also known as Mitogen-Activated Protein Kinase Kinase Kinase 14, MAP3K14). *NIK* was recruited and phosphorylated by MEKK1 (downstream gene of RAS). *NIK* regulates biological activities such as cell growth and survival to immunity and inflammation (Zhang Q et al., 2017). *NIK* is well known for modulating the immune system development and function (Pflug KM, Sitcheran R. 2020). Hence, with the attenuated expression of *FOS* and *AP-1* s well as the upregulation of *NIK* in MAPK pathway, it may postulate that for the first 4 hours of Huanglian interaction, HONE-1 might encounter insustainable cellular stress for cell growth and eventually conduce to reduction of cell proliferation, cell arrest and apoptosis.

TNFSF10 (also known as Trail) protein is a cytokine that belongs to the tumor necrosis factor (TNF) ligand family (Starkey, M. et al., 2014). At this time point, TNFSF10 as a ligand cytokine, was downregulated and bind with D1, D2, D4 and D5 which are called death receptor (Figure 4.23, Apoptosis signaling pathway), The diminished expression of Trail in HONE-1 may due to defense reaction of HONE-1 against the interaction of Huanglian treatment for cell survival at the first 4 hours. TNFSF10 is well known as tumour suppressor and

induces cell apoptosis in cancer (He W et al., 2012). Moreover, TNFSF10 alone or integrated with chemotherapeutics had exhibited favorable anticancer result by mediating apoptosis (Hellwig CT, and Rehm M, 2012). Meanwhile, as observed in the pathview, the upregulated gene *NIK*, having been recruited by MAPK pathway, phosphorylated IKK in which IKK again phosphorylated IκBα targeting it for proteasomal degradation allowing p50-RelA to translocate to the nucleus (Pflug KM, Sitcheran R. 2020). Eventually, it stimulated the transcription of pro-survival genes such as *BCL-XL*, *GADD45*. However, the expression of these transcribed genes were not seen to be in quiscene state.

PLD1 served as phospholipase selective for phosphatidylcholine. Many researchers have noticed that participation of *PLD* can be increasingly significant in cancer tissues and cells, noting that *PLD* gene has critical role in signal transduction, cell proliferation, and anti-apoptotic processes (Cho JH and Han JS, 2017). Bruntz et al. indicated that PLD1 activity and expression are usually increased in various types of cancers (Bruntz et al., 2014a). Since *PLD* is a downstream transcriptional target molecule of Sp1, NFκB, TCF4, ATF-2, NFATc2, and EWS-Fli, all of which contribute to inflammation and carcinogenesis (Brown et al., 2007). Therefore, compounds that suppress or inhibit these transcription factors can regulate *PLD* expression with its reduction in carcinogenesis. In this experiment, PLD1 was downregulated in Ras pathway where upstream RAS was deactivated leading to inhibiting expression of PLD1 and finally conduced to cell apoptosis of HONE-1 (Figure 4.39).

MYB gene encodes nuclear proteins that function as transcriptional transactivators. Expression of *MYB* gene is cell cycle-regulated and inhibition

found to affect cell cycle-progression, cell division and differentiation. In this experiment, *MYB* was downregulated in PI3K pathway where AKT was deactivated and subsequently resorted to NF-κB signaling pathway in which IKK and NF-κB were observed for low level expression causing the transcriptional transactivators *MYB* in downstream became inactive. The consequence was the retardation of cell cycle progress and survival of HONE-1.

HES1 gene belongs to the basic helix-loop-helix family. Its protein is an antagonist transcription factor that plays an important role in cellular differentiation, cell cycle arrest and apoptosis. The Notch signaling pathway plays an important role in cell-cell communication, and regulates embryonic development. In this experiment,

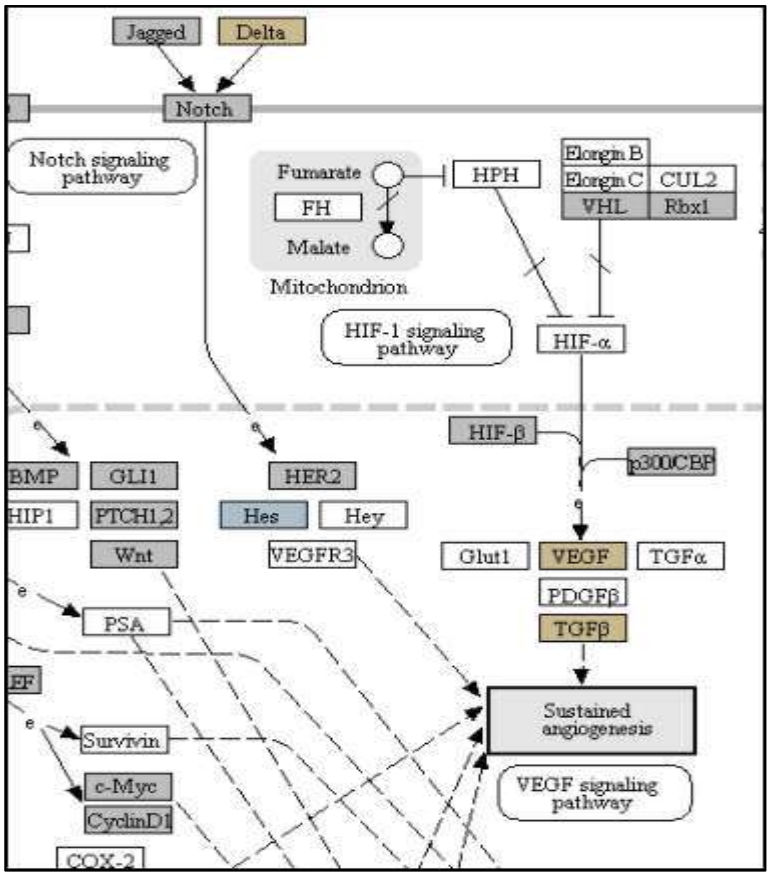

Extract from Figure 4.16 (pathway in Cancer)

NOTCH signalling pathway initiated up-regulation of DLL1 (Delta-Like Protein 1) and JAG1 (Jagged canonical Notch ligand 1) and attenuated expression of transcription factor HES1. The pathway illustrated Notch signaling regulated vascular development. DLL1 and JAG1 ligands were actively bind to Notch receptor and initiated VEGF3 signaling pathway factor for migration and proliferation of endothelial cells. The Notch receptor has extracellular domain Notch LCD and intracellular domain Notch ICD. Meanwhile, Enzyme γ-secretase cleaved the connection of these 2 domains and made NICD independent. Subsequently, NICD transferred to nucleus and stimulated transcription factor HER2, known as human epidermal growth factor receptor 2, in which it would activate angiogenesis in tumour. *HES1*, as a target gene of Notch pathway, is actually an inhibitor to ordinary transcription factor. The down-regulation of *HES-1* would be expected to allow more active transcription of HER2 to DNA. However, this process was seen to fail as the dotted line in the pathview indicated sustained angiogenesis was not accomplished eventually. This may suggest that HONE-1 might encounter huge cellular stress when being treated with Huanglian at 4 hours vs 0 hour time point, hence, angiogenesis development could not be susutainable in precursor period. This may suggest that HONE-1 encountered reduced angiogenesis development from Huanglian treatment at 4 hour vs 0 hour time point although with the expression of critical endothelial Notch ligand DLL1 and JAG1.

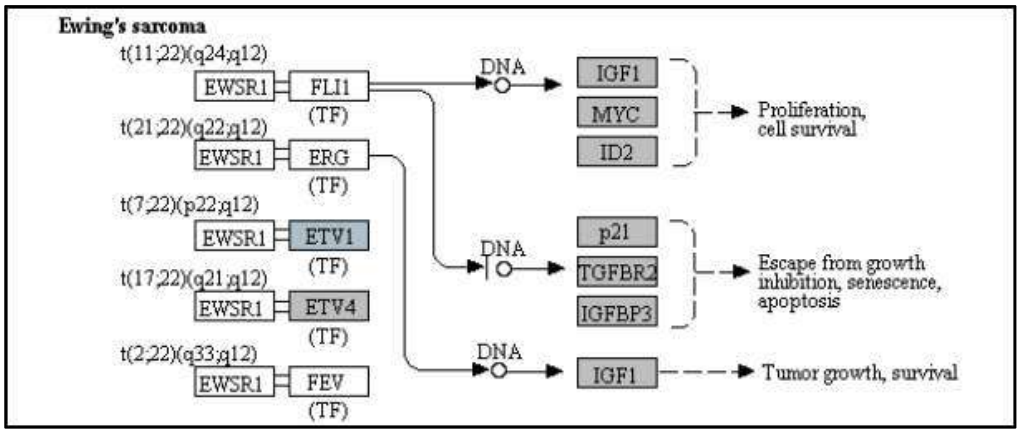

Extract from Figure 4.22 (Transcription Misregulation pathway)

ETV1, known as ETS variant transcription factor 1, encodes proteins regulate many target genes that modulate biological processes like cell growth, angiogenesis, migration, proliferation and differentiation. Segal és L et al., 2019 reported that strong cytoplasmic *ETV1* expression has a negative impact on prostate cancer outcome. In this experiment, *ETV1* was downregulated in Transcriptional Misregulation pathway. As shown in the pathview, conventionally, *EWSR1* binds with *ETV1* to form fusion gene and transformed to induce other genes for cell proliferation and development of Ewing's sarcoma. EWSR1 is a multifunctional protein which regulates transcription and RNA splicing, indicating that it is involved in diverse cellular processes (Junghee Lee et al., 2019). However, EWSR1 is not seen in the pathview which may imply that Huanglian could have suppressed the expression of EWSR1 and as well attenuated expression of ETV1. Nevertheless, low expression of ETV1 could have reduced the cell development in HONE-1.

Cell Division Cycle 25C (*CDC25C*) was downregulated in Cell Cycle pathway (Figure 4.5.1.1.9) in this experiment. This cyclin participates in regulating G2/M progression and in mediating DNA damage repair. It was

indicated in the pathview that conventionally, *CDC25C* was regulated by 14-3-3 protein by means of chelating in the cytoplasm. DNA damage could be envisaged and hence checkpoint protein kinases CHK1 and CHK2 downregulated phosphorylation of *CDC25C*, subsequently, prevented activation of cyclin Cyclin B/CDK1complex in downstream which ultimately arresting the cell cycle in the G2/M phase. Hence, down expression of *CDC25C* can inhibit cell proliferation and arrest of G2/M phase of HONE-1 when treated with Huanglian in the 4 hours time point.

Krüppel-like factor 4 (KLF4) is zinc finger-containing transcription factor that regulates diverse cellular processes such as cell growth, proliferation, and differentiation. It is particularly well known for its role in inducing pluripotent stem cells and regulates the expression of key transcription factors during embryonic development. In this experiment, KLF4 was downregulated by JAk-STAT pathway where ligand LIF (LIF Interleukin 6 Family Cytokine) bind to the receptor LIFR. JAK was phosphorylated and recruited STAT which later formed STAT dimers as transcription factor to enter into nucleus. KLF4 was lowly expressed leading to reduced embryonic development.

CASP8 is best known for its apoptotic functions. CASP8 was mildly downregulated at 4 hours time point. It was observed that the receptor of this extrinsic apoptosis pathway FAS was highly downregualted resorting to empty expression of adapter molecule FADD and had no formation of Death Induced Signal Cascade (DISC). The inactivation of upstream genes resulted downregulation of CASP8.

PIK3CA is a mutated oncogene in human cancers. It controls cell growth and proliferation. Inhibition of PI3K signaling can decrease cell proliferation, and in some circumstances, promote cell death (German S et al., 2013). In this experiment, *PIK3CA* gene was deregulated by *PTEN* gene and did not induce expression in downstream PIP3, PDK1 and PNK as well as SGK respectively which eventually conduce to no survival signal for cell growth and proliferation. This may ascertain HONE-1 underwent apoptosis at the 4 hours time point.

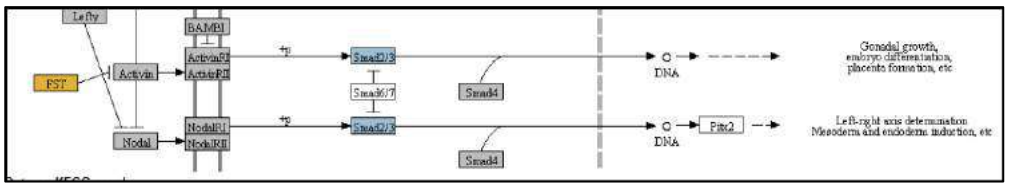

Extract from Figure 4.34 (TGFβ signaling pathway)

FST gene was upregulated in TFG β pathway and gained 1.75 for highest positive $\log_2$ fold change expression value. TFG β pathway is important for embryonic development, cell growth as well as development. FST acted as an antagonist to Activin (Shi L et. al., 2016). At this time point, FST was highly expressed so as to inhibit the expression of ACTIVIN ligand and its receptor. This prevented the active binding of the ligand to receptor. Subsequently, the expression cellular tranducer Smad2/3 was attenuated and subsequently transduction of signal was feeble for the canonical pathway of TGF-β pathway. No transcriptor factor was seen to induce the expression of genes from DNA. This may suggest that the up-regulation of FST gene could inhibit the tumour growth of HONE-1 upon treatment of Huanglian in the first 4 hour.

Besides, up-regulation of *NGF* and *DUSP4* genes were observed in MAPK pathway. *NGF* gene, a nerve growth factor (NGF), known for its

prerequisite for neuronal cell proliferation and survival, being implied clinically as a marker of tumor progression. *DUSP4* gene can negatively regulate members of the mitogen-activated protein (MAP) kinase superfamily (MAPK/ERK, SAPK/JNK, p38), which are associated with cellular proliferation and differentiation. NGF ligand bind with RTK receptor and phosphorylated kinase GRB2 to activate RAS. This further recruited RAF> MEK >ERK mechanism. Elevated expression of DUSP4 (known as MKP in Kegg pathway) was observed having suppressed the expression of ERK. Subsequently, the downstream transcription factors such as ELK1, SAP1a and SRF were not stimulated resulting deregulation of FOS protein in the nucleus. This eventually caused degradation in cell proliferation of HONE-1.

TNFAIP3 is enzyme that contains both ubiquitin ligase and deubiquitinase activities. Involved in immune and inflammatory responses signaled by cytokines, such as TNF-alpha and IL-1 beta, or pathogens via Toll-like receptors (TLRs) through terminating NF-κB activity.

DKK1 was known as an inhibitor to WNT pathway. In this experiment, elevated expression of DKK1 (Dickkopf WNT Signaling Pathway Inhibitor 1) inhibited binding WNT ligand with WNT receptor Frizzled and LRP5/6 trimeric complex and subsequently resulted in Dishevelled (DVL) unexpressed in which upon deactivation mediated down-regulation of downstream cytoplasmic β-catenin followed by low stimulation of TCF/LEF transcription factors for eventual Wnt-responsive gene expression. WNT pathway is generally important in embryonic development and is implicated in cell development. In human cancers, Wnt/β-catenin signaling is highly activated (Paul Polakis, 2021). At this

stage, this may suggest that when HONE-1 was treated with Huanglian, WNT modulated extracellularly negative ligand receptor interactions by highly expressed DKK1 inhibitor and intracellularly modulated to down-regulation of components of the signal transduction machinery downstream.

IL24 (interleukin 24) and *SOCS1* (Suppressor of Cytokine Signaling 1) genes were upregulated in JAK-STAT pathway. JAK-STAT pathway is mainly involved in immunology. It may suggest that *IL24*, as cytokine ligand, was highly expressed when HONE-1 was menaced by Huanglian interaction at this time point. Meanwhile, elevated expression of the intracellular suppressor of cytokine signaling protein *SOCS1* attenuated cytokine signaling by de-regulation at the receptor level. It was illustrated in the JAK-STAT pathway that *SOCS*1 interacted with target kinase JAK by recruiting the E3 ubiquitin ligase complex. The E3 complex polyubiquitinated and degraded JAK by proteasome as well as preventing the kinase JAK from phosphorylating its cytokine receptor. The deregulated JAK kinase could not actively phosphorylate its canonical targets STAT. Subsequently, the un-phosphorylated STAT dimers did not stimulate the downstream transcriptional protein. Hence, the mechanism of action of *SOCS1* had modulated JAK/STAT pathways and its potential therapeutic role in the prevention and treatment of autoimmunity and cancer (Sharma Jatin, Larkin Joseph, 2019).

Summary

Overall, at 4 vs. 0 hour time point upon treatment with Huanglian, HONE-1 could have experienced vigorous cellular stress which subsequently

rendered cell cycle arrest and apoptosis. This can be envisaged particularly from the attenuated expression of FOS, PLD1, MYB initiated by MAPK, PI3Kand RAS pathway which conventionally promote cell growth. Besides, promoter for cell cycle progression such as CDC25C was downregulated in cell cycle pathway. Confronting the cytotoxic interaction of Huanglian, it can be observed that HONE-1 attempted resistance by rebouncing to new growth development. For instance, the upregulation of several growth factor ligand and angiogenesis ligands. However, the intracellular signal transduction to downstream genes was frail which eventually made HONE-1 insustainable for cell proliferation.

5.4.2 Time point at 8 hours vs. 0 hour

When HONE-1 was treated with L1 Huanglian, the most downregulated genes selected from lowest Log_2fold change, P value >0.05, were *CREB3L1*, *HES1*, *ITGB6*, *ETV1*, *PLAT*, *CDC25C*, *FZD7*, *HDAC6*, *PRKCA*, *DDB2*, *TGFB1*, *FANCG*, *BMP6*, *JAG1*, MAPK9 respectively. Besides, the down-regulation was initiated by canonical pathway such as PI3K, Cell Cycle-Apoptosis, MAPK, PI3K, Notch, JAK-STAT, TGF-beta, Chromatin Modification and Transcriptional Misregulation. *CREB3L1* gained the smallest log_2fold change -1.39 in negative differential expression at this time point. Down-regulation of *CREB3L1* was initiated in PI3K Pathway. PI3K-Akt Pathway is an intracellular signal transduction pathway that promotes metabolism, proliferation, cell survival, growth and angiogenesis in response to extracellular signals. CREB is a transcription factor that is known for its role in cell proliferation, differentiation, and survival. It induces downstream *BCL-2* gene to carry out anti-apoptotic activity. However, in this experiment, though CREB3L1 was phosphorylated by

AKT upstream, it was deregulated and subsequently weakened the anti-apoptotic ability of BCL-2 protein and in the other way reduced cell survival rate of HONE-1 when treated with Huanglian. *ITGB6* gene encodes the β6 subunit and was deregulated by PI3K pathway. It was observed ITGB6 receptor formed a dimer with another ITGB receptor of α subunit in extracellular matrix to the cell. This heterodimer will initiate signaling towards PI3K and following genes downstream through PI3K pathway. However, both ligand ECM (extracellular matrix) and ITGB6 receptor were deregulated. This undoubtedly weakened the signal transduction to PI3K and PIP3 protein. Moreover, PIP3 activation was also inhibited by tumour suppressor PTEN which as upregulated at this time point. Subsequently, the signal transduction towards AKT was diminished and resulted a decrease stimulation to transcription factors. The deregulation of ITGB6 and ligand ECM dwindled the chance of tumour growth in HONE-1. As tumor progresses, epithelial tumour cells will transdifferentiate into mesenchyme which regards as EMT. In contrast to epithelia, mesenchymal cells can transfer through the extracellular matrix (ECM) to predispose metastasis (Thiery JP, 2002).

HES1 continued to maintain downregulated in NOTCH pathway from 4 hours vs 0 hour treatment time to 8 hours time point. At this juncture, it was detected that ligands Delta and Jag1 were not as active as previous treatment time. The intracellular domain Notch ICD transduced signal to transcription factor CSL. However, this process was seen to diminish by down-regulation of HES1in down stream. This may suggest that HONE-1 encountered reduced cell development from Huanglian at 8 hours vs 0 hour treatment time.

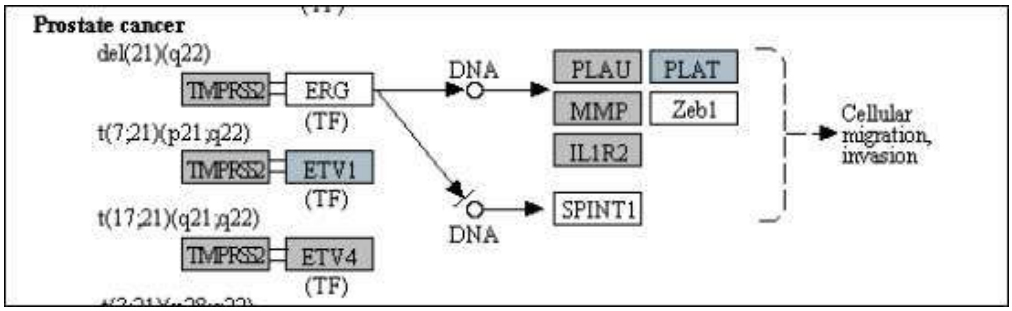

Extract from Figure 4.32 (Transcription Misregulation pathway)

Transcriptional Misregulation pathway initiated deregulation of *ETV1* and *PLAT* gene. As a transcriptional factor, ETV1 is able to modulate biological processes like cell growth, angiogenesis. PLAT is a serine protease that converts the proenzyme plasminogen to fibrinolytic enzyme plasmin and functions in cell migration and tissue remodeling. Increased enzymatic activity causes hyperfibrinolysis for instance excessive bleeding. It was shown in Transcriptional Misregulation pathway, ETV1 conventionally formed gene fusion with TMPRSS2 in epithelial prostate cancer development. Gene fusion can be proto-oncogenic, resembles gene rearrangement and often causes abnormal activation of certain genes. TMPRSS2, is a member of transmembrane protease serines (TMPRSSs), which are a family of proteins with conserved serine protease domains located on the cell membrane. However, as shown in the pathview, the fusion gene of *ETV1* and *TMPRSS2* did not transform to induce any target gene for protein transcription. This may imply that attenuated expression of ETV1 could indicate inhibiting effect of Huaglian treatment. Nevertheless, low expression of ETV1 could have reduced the cell development in HONE-1. Another gene fusion of TMPRSS2 and ERG translocated signal to isoform made up of *PLAU*, *PLAT*, *MMP*, *ILI2* and *ZEB1* genes for cell migration and invasion. However, as observed from the pathview, ERG did not exist in the fusion with TMPRSS2. Hence, it may suggest that Huanglian could have

suppressed the expression of ERG and further induced down-regulation of *PLAT* gene.

The Cell Cycle-apoptosis pathway had initiated the down-regulation of *CDC25C*, *TFGB1* but mildly elevated regulation of *CDC25A*. *CDC25C* continued for being deregulated from 4 hours verse 0 hour treatment time, low expression of *CDC25C* can inhibit cell proliferation and arrest of G2/M phase of HONE-1. TFGB1 triggers chemical signals that regulate cellular activities such as growth and cell proliferation as well as apoptosis. *TFGB1* is also known as tumour suppressor. This ligand was deregulated and subsequently the activation of SMAD2/SMAD3-SMAD4 heterotrimer was weakened. This further conduced to the deregulation of p15Ink4b downstream which is a critical tumour suppressor in the absence of p16Ink4a (Krimpenfort, P et al., 2007). Hence, p16Ink4a is seen in the pathway as an inhibitor to cyclin D-Cdk4/6 downstream. Cyclin D-Cdk4/6 and cyclin E-Cdk2 complexes control the entry into the S phase. *CDC25A* is required for progression from G1 to the S phase of the cell cycle and involved in the DNA damage checkpoints. *CDC25A* is considered an oncogene and is often over-expressed in tumour. In 8 hours verse 0 hours treatment time, its differential expression was only +0.279 which is considered very little elevation of gene expression. This may suggest the expression may be decreased by interaction of Huanglian treatment.

BMP6 is ligand for TGF-beta pathway. It was deregulated and hence it caused down-regulation of its receptor and SMAD 5 transcription factors.

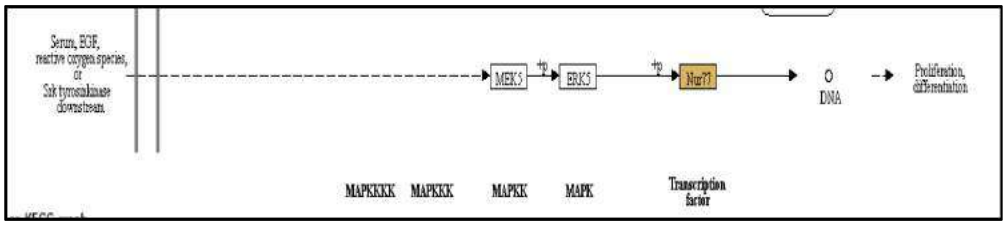

Extract from Figure 4.26 (MAPK pathway)

As refer to the extract from Figure 4.26 shown above, PKC and MAPK9 (JNK) were downregulated by MAPK pathway but NR4A1 (named as NUR77 in pathview) was most highly upregulated at 8 hours vs. 0 hour treatment time. PKC is serine- and threonine-specific protein kinases which regulate cell growth and proliferation by phosphorylating targets such as RAFB and RAS as well as activating signaling cascade involving MAPK1/3 (ERK1/2). The down-regulation deminished phosphorylation of the downstream gene and resulted MAPK1/3 inactive. JNK is also known as c-Jun N-terminal kinases. It phosphorylates transcription factors AP1 which translocate signal for cell proliferation. Hereby, expression of JNK was decreased. Subsequently, the transcriptional activity was dwindled. NR4A1 belongs to steroid-thyroid hormone-retinoid receptor superfamily and acts as a nuclear transcription factor. Although NR4A1 was highly expressed and exhibited oncogenic activity in many solid cancers NR4A1 might act as a tumor suppressor in hematologic malignancies. This is likely that NR4A1 can mediate between cell proliferation and survival verse apoptosis. As a transcription factor, NR4A1 is primarily localized in the nucleus and regulates gene expression to enhance cell proliferation and survival. When NR4A1 is exported from the nucleus to mitochondria, it binds BCL-2 and subsequently induces cell apoptosis (Li, Y et al., 2017). Hence, at this juncture, as initiated by MAPK pathway, NR4A1 could induce apoptosis of HONE-1 when treaed with Huanglian.

Suppressor of Cytokine Signaling 3 (SOCS3) continued to remain upregulated at 8 hours vs. 0 hour treatment time while the cytokine ligand, IL4 was dyregulated. The protein encoded by this gene can bind to JAK2 kinase, and inhibit Janus kinase–signal transducer and activator of transcription (JAK–STAT) pathway to transmit their information into the cell nucleus. It was also illustrated in the JAK-STAT pathway that SOCS1 interacted with target kinase JAK by recruiting the E3 ubiquitin ligase complex. The E3 complex polyubiquitinated and degraded JAK by proteasome as well as preventing the kinase JAK from phosphorylating its cytokine receptor. The deregulated JAK kinase could not actively phosphorylate its canonical targets STAT. Subsequently, the un-phosphorylated STAT dimers did not translocate signal to the nucleus. It was shown in the pathview that anti-apoptosis protein Pim-1 Proto-Oncogene (PIM1) was dyregulated and BCL-2, BCL-XL protein were not expressed.

Summary

At 8 hours vs 0 hour treatment time, HONE-1 continued to endure decresing cell proliferation and survival. This can be witnessed particularly with the downregulation of CREB3L1 which was associated with PI3K pathway and the augmented expression of NR4A1 (NUR 77) associated with MAPK pathway. Moreover, several signalling ligands associated with functions of cell proliferation, development and angiogenesis such as BMP, TGFβ1 and JAG were deregulated, coupled with the deactivation of receptors like ITGB6 and

FZD7. Transcription factors with biological functions in promoting cell proliferation and survival such as HES1 and ETV1 were continued to be lowly expressed from last time point.

5.4.3 Time point at 12 hours vs. 0 hour

At 12 hours vs 0 hour treatment time, *HMGA2* was the most lowly expressed gene initiated in Transcriptional Misregulation pathway. Meanwhile, *ETV1* and *BCL2L1* were downregulated and *DDIT3* was upregulated in this pathway too.

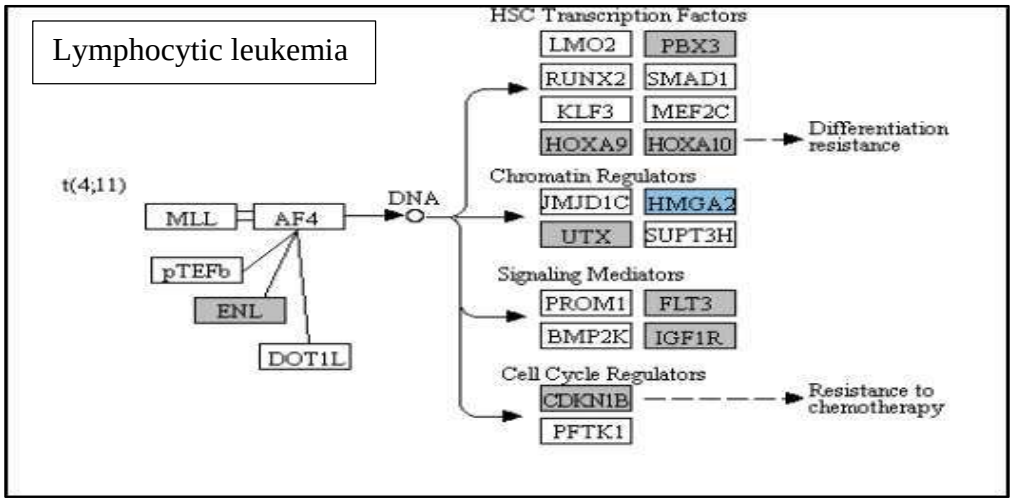

Extract from Figure 4.43 (Transcription Misregulation pathway)

Chromatin-associated protein HMGA2 contains structural DNA-binding domains and may act as a transcriptional regulating factor (Ozturk Nihan et al., 2014). The extracted pathview above shows a conventional pathogenesis of lymphocytic leukemia where mutated MLL and AF4 form a fusion gene and transformed to induce a numbers of transcription factors for tumour growth. HMGA2 binds with other chromatin regulators such as JMJD1C, UTX and

SUT3H. HMGA2 will form a complex transcription factor for the purpose of providing differential resistance. However, MLL and AF4 were not present in the KEGG pathview implying that Huanglian could have suppressed their extression and as well induced downregulation of HMGA2 at this juncture. LET 7 protein is the inhibitor of HMGA2 and acts as a putative tumor suppressor especially in lung cancer (Lee YS and Dutta A. 2007). Kaur H et al. (2015) reported that high expression of HMGA2 could reduce cell apoptosis and augmented tumour development compared to tumours with low HMGA2 expression. This may suggest that the cytotoxicity of Huanglian had been persisting for 12 hours and cell proliferation in HONE-1 was considerably suppressed.

ETV1 had negatively expressed at previous 4 and 8 hours vs 0 treatment time and its differential expression stably maintained at -0.838 and -0.928 $\log_2$ fold change respectively. This gene is a transcription factor which translocate signal to many target genes and modulate the biological activity such as cell growth and development. It binds with *EWSR1* to form fusion in the pathology of Ewing's sarcoma. The *EWSR1-ETV1* fusion gene was believed to be aberrantly expressed so as to misregulate genes for modulating signal transduction and normal cell development. It has long been considered the chromosomal translocation is a hallmark of Ewing Sarcoma and primary cause in its development (Tu J et al., 2017). However, *EWSR1* was not present in the KEGG pathview implying that Huanglian again could have suppressed its expression and imposed downregulation of *ETV1* at this time point. The

diminished expression of ETV1 could be a negative impact for tumour growth in HONE-1.

Instead of Transcriptional Misregulation pathway, down-regulation of *BCL2L1* (BCL-XL) was also initiated in Cell Cycle-Apoptosis, JAK-STAT, PI3K, and Ras pathways. BCL2L1 is known as a strong inhibitor of cell apoptosis by suppressing activation of caspases. It was shown in the Cell Cycle-Apoptosis, PI3K, and Ras pathways that activation of BCL2L1 was suppressed by BAK which is a pro-apoptotic protein. This further ascertained the reduction of cell proliferation in tumour.

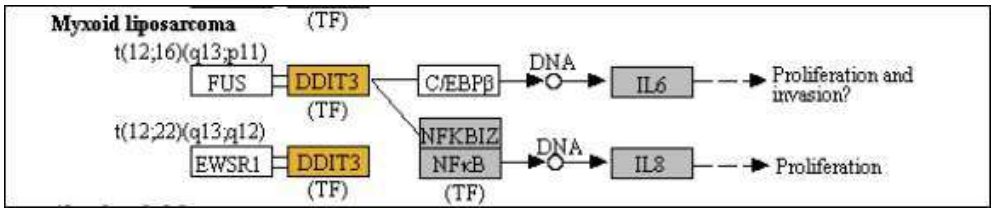

Extract from Figure 4.43 (Transcription Misregulation pathway)

DDIT3 (DNA Damage Inducible Transcript 3, also known as GADD, CHOP) is a transcription factor of CCAAT/enhancer-binding protein (C/EBP) family and a dominant-negative inhibitor by forming heterodimers with C/EBPβ member and preventing their DNA binding activity. The protein is activated by endoplasmic reticulum stress, and promotes apoptosis. In the Transcriptional Misregulation pathway,

Conventionally in the pathogenesis of myxoid liposarcoma, *DDIT*3 forms fusion with *FUS* and *EWSR1* and trnsforms to induce a numbers of transcription factors for tumour growth. However, *EWSR1* and *FUS* were not

present in the KEGG pathview implying that amplification in expression of *ETV1* could be initiated by other protein at this time point.

As iniatiated in MAPK pathway, *DDIT3* was named as *GADD3*. It was upregulated and phosphorylated by P38. *GADD3* (DDIT3) is a pro-apoptosis transcription factor. The augmented expression could ascertain its effect in suppressing cell growth and advocating cell aarrest in HONE-1. Turpin J et al., 2021 had recently reported *CHOP* (GADD, DDIT3) induced cell apoptosis through ER stress to Zika virus.

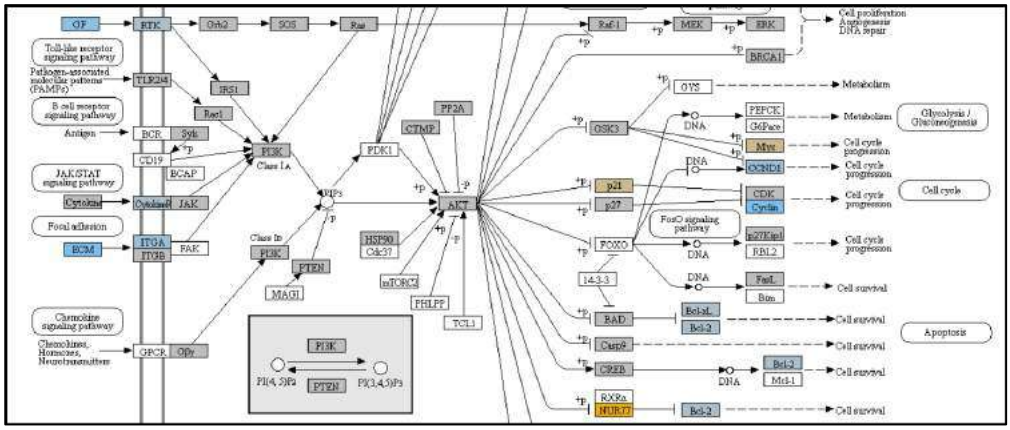

Extract from Figure 4.38 (PI3K pathway)

THBS1, *IL7R*, *CCND*1, *FN1*, *BCL2L*, *VEGEFC* were downregulated in PI3K pathway. THBS1 (thrombospondin1) is an important components of the *ECM*, the extracellular matrix (Daubon, T et al., 2019). THBS1 was first discovered in platelets but now has been shown for having an important role in cancer development (Filleur, S. et al., 2001).

Daubon, T et al., 2019 reported that high expression of *THBS1* in *TGFβ* canonical pathway conduced to the invasive behaviour for glioblastoma

expansion. In this time point, *THBS1* (known as ECM ligand in PI3K pathway) coupled with its receptor, *ITGA*, both were deactivated. Subsequently, no signal was triggered off to induce expression of PI3K protein because its cellular messenger gene namely *FAK* was not stimulated. Hence, the reduction in signaling would dwindle transduction to induce tumour growth in HONE-1.

IL7R is a cytokine receptor in JAK-STAT pathway and was downregulated. The binding of JAK kinase with this receptor triggered signal to non-canonical pathway towards PI3K. However, the effect was diminished considerably.

CCND1 encodes the cyclin D1 protein. *CCND1* is a proto-oncogene that regulates progression through the G1-S phase of the cell cycle. This gene was downregulated and moreover, its activation being inhibited by GSK3 kinase. *GSK3* (Glycogen synthase kinase 3) inhibits *CCND1* by phosphorylation. Attenuation of expression of CCD1 eventually induced cell arrest and apoptosis in HONE-1.

FN1 is involved in synthesis of fibronectin-1 protein such as soluble plasma fibronectin-1 and insoluble cellular fibronectin-1. Cellular fibronectin is assembled into the extracellular matrix, an insoluble network that separates and supports the organs and tissues of an organism. Hence, *FN1* was illustrated as *ECM* ligand in Focal Adhension which bind with *ITGA* receptor in PI3K pathway. Both of the ligand and the receptor were downregulated. As *FN1* is

involved in cell adhesion, growth, migration, and differentiation, its deactivation would weaken the the signling to induce tumour growth in HONE-1.

VEGEF is a member of the PDGF/VEGF growth factor family which induces proliferation and migration of vascular endothelial cells, and is prerequisite for angiogenesis. Both the ligand *VEGEF* and Receptor Tyrosine kinases (RTKs) were negatively expressed in the MAPK and PL3K pathway. Subsequently, triggered weak signal towards downstream RAS and MAPK cascade and eventually modulated to degradation of angiogenesis for tumour development.

Besides, *NR4A1* (*NURR*) was again upregulated at this treatment time and its differential expression was double more than that at 8 hours vs. 0 hour. *NR4A1* was phosphorylated by AKT and inhibited *BCL-2* which is anti-apoptotic. It is shown in the pathview that *BCL-2* was downregulated. Contradictory to its apparent role in cell survival, *NR4A1* also activates several genes involved in cell apoptosis as well as translocating directly into mitochondria to enhance the apoptotic signal (Li et al., 2000; Lin et al., 2004).

DKK1 (Dickkopf 1） was downregulated in the WNT pathway which bind to the LRP6 co-receptor and inhibits beta-catenin-dependent Wnt signaling. Elevated expression of *DKK1* has been observed in numerous human cancers and this protein may promote proliferation, invasion and growth in cancer cell lines (Shi RY et al., 2013). Meanwhile, the receptor *Frizzled* was deregulated and hence mediated down-regulation of downstream cytoplasmic β-catenin

followed by low stimulation of *TCF/LEF* transcription factors for eventual Wnt-responsive gene expression. WNT pathway is generally important in embryonic development and is implicated in cell development and etc.

CDKN1C (Cyclin Dependent Kinase Inhibitor 1C) (also known as p57, KIP2), is a strong inhibitor of several G1 cyclin/Cdk (cyclin E/CDK2, cyclin D/CDK4,6, and cyclin A/CDK2) complexes and a negative regulator of cell proliferation which contributes to cell cycle arrest in G1 phase. Due to its anti-oncogenic function, CDKN1C is normally deregulated in many common human malignancies through several mechanisms, denoting it encompasses anti tumour development functions (Ioannis S et al., 2009). Pateras IS et al., 2009 had reported the correlation of proliferation in non-small cell lung carcinoma with down-regulation of CDKN1C. Moreover, poor prognosis in oral squamous cell carcinoma (Fan GK et al., 2006) and in hepatocellular carcinoma (Ito Y et al., 2001) had been reported with the decreasing expression of CDKN1C. In this experiment, CDKN1C was noted for its up-regulation and its inhibition towards cyclin/Cdk complexes. It may suggest that the cell cycle of HONE-1 in G1 phase could encountered DNA damage and cell arrest under the interaction of Huanglian treatment.

At this juncture, JAG1 remained deregulated by Notch pathway from previous treatment time. Moreover, SOCS3, ETS2, PTEN, CDC25A were upregulated by same pathway from previous treatment time till 12 hours verse 0 hour. The mechanism were similar as explained as for 8 hours verse 0 hour treatment time.

Summary

At 12 hours vs 0 hour treatment time with Huanglian, HONE-1 continued to experience reduction in sustainable cell proliferation and survival. This can be postulated from level of the expression of genes being initiated in PI3K, MAPK and RAS pathways. In a nutshell, genes with biological functions of promoting cell proliferation and growth were downregulated such as *THBS1*, *IL7R*, *CCND1*, *FN1*, *BCL2L* and *VEGEFC*. Generally, PI3K and MAPK pathways are the pathways for cell growth and development. Many tumour phenotypes initiate these pathways to stimulate expression of genes for cyclin synthesis being utilized in cycle cycle for rapid and rampant growth. The cytotoxicity of Huanglian apparently implicated in the cell arrest and boost apoptosis at final time point.

5.5 Gene expression in HONE-1 when treated with L7 (XXXD) at 3 different time points

5.5.1 Time point at 4 hours vs. 0 hour

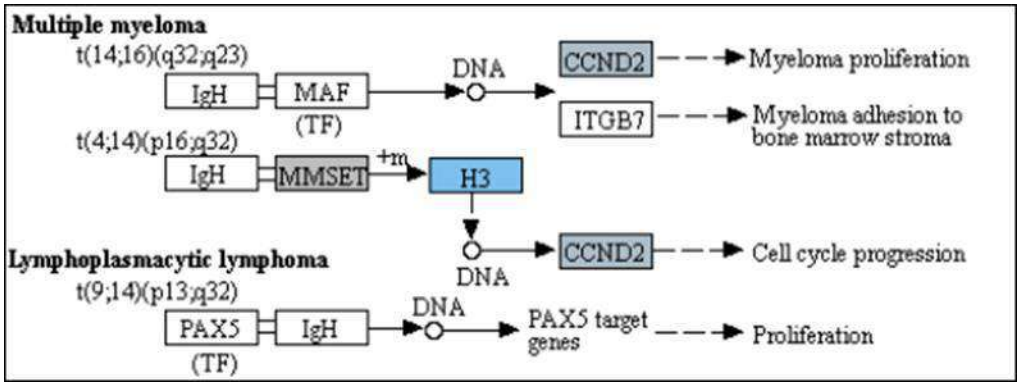

Extract from Figure 4.52 (Transcription Misregulation pathway)

At 4 hours vs 0 hour treatment time, Transcriptional Misregulation pathway initiated the down-regulation of *HIST1H3* and *HIST1F3* as well as up-regulation of *ID2* and *IGFBP3*. *HIST1H3* was the most attenuatingly expressed gene for HONE-1treated with XXXD. *HIST1H3* and *HIST1F3* both encode nuclear protein H3 clustered histone which execute function of organizing of chromatin in eukaryotic cells (Bhasin M et al., 2006). As initiated in Transcriptional Misregulation pathway, it was observed in the molecular pathological pathway of multiple myeloma that H3 was deregulated. In the upstream of H3, *MMSET* gene formed fusion with IgH locus in t (4;14)(p16;q32). MMSET possesses methyltransferase activity for core histone H3 (Marango J, et al., 2008). Enhanced expression of MMSET can be a potential pathogenic factor for multiple myeloma (Marango J, et al, 2007). However it was detected in the pathview that MMSET was in a low expression state but IgH was not

present. Hence, the fusion was not formed. This may imply that XXXD could have suppressed expression of IgH and induced deregulation of H3 and CCND2. CCND2 is responsible for progress of cell cycle. Diminished expression of CCND2 could deter cell proliferation. The elevated expression of CCND2 was particularly associated with tumorigenesis (Santarius T, et al., 2010). Takano Y, et al., 2000 had reported that amplified expression of CCND2 has been implicated in gastric cancer (Takano Y, et al., 2000). Silencing of Cyclin D2 could decrease the development and metastasis of non-small cell lung cancer (He X, et al., 2018). Hence, the attenuated expression of H3 and CCND2 at this time point correlated to negative regulation of cell growth in HONE-1 and might as well contributed to cell cycle arrest and apoptosis o tumour cells.

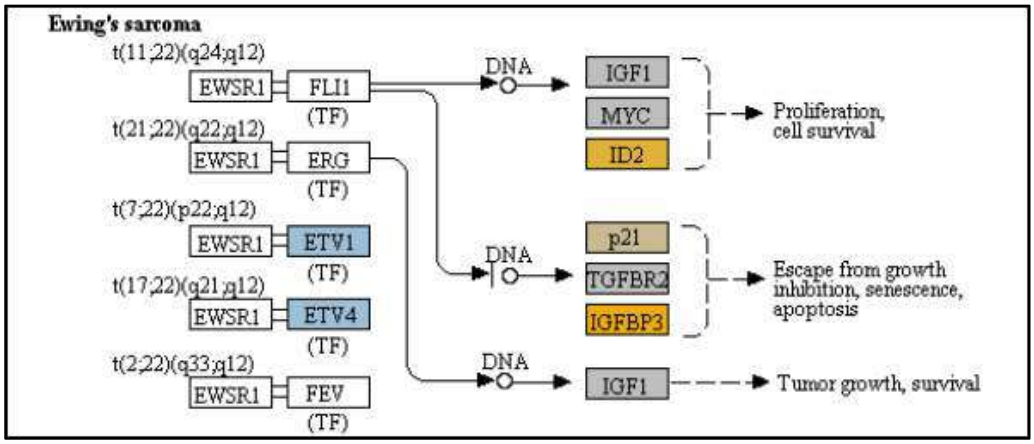

Extract from Figure 4.52 (Transcription Misregulation pathway

The expression of *IGFBP3* was most highly amplified at this 4 hours vs. 0 hour treatment time. It was observed in the pathview of Transcriptional Misregulation pathway, conventionally, Ewing sarcoma gene *EWSR* underwent at (11; 22)(q24;q12) translocation with the FLI1 (Fli-1 Proto-Oncogene, ETS Transcription Factor) to form a fusion gene of Ewing sarcoma. The EWRS-FLI-1 fusion protein is active in transforming the target genes for Ewing's family

tumours development. However, it was shown in the KEGG pathway that EWRS1 and FLI did not exist. This may suggest that XXXD could have suppressed the expression of EWRS1 and FLI and amplified expression of IGFBP-3, p21 and ID2. IGFBP3 can adjust cell development either with IGF1 or independently (Varma Shrivastav Shailly, et al., 2020). Wang YA et al. (2017) reported that elevated expression of IGFBP3 induced apoptosis and increased effect of cisplatin in by deactivating IGF1 signaling. The intracellular signaling via Smad2 would be triggered when IGFBP-3 combined with TGFBR2 receptors and contributed to the activation of type I TGF-β receptors. Subsequently, this pathway was associated to inhibition of proliferation (John F et al., 2004). Meanwhile, P21 was upregualted. Protein p21 has the function of inhibiting cell cycle progression and often being deregulated in some tumours (Shamloo B and Usluer S, 2019). As expression of p21 was amplified at 4hour vs 0 hour time point, it could possibly help to suppress cell proliferation of HONE-1.

Moreover, EWRS-FLI-1 fusion will conventionally induce another set of target genes namely *ID2*, *MYC* and *IGF1* for cell proliferation and survival. It was shown in the extract from Figure 4.52 that EWRS1 and FLI did not exist. However, ID2 was upregulated while *MYC* (MYC Proto-Oncogene, BHLH Transcription Factor) and *IGF1* (Insulin like Growth Factor 1) were both in quiscene state. Upregulation of ID2 could be initiated in TGFβ pathway as illustrated in the Table 4.5.2.1.1. ID2 protein (Inhibitor of DNA Binding 2) is a negative regulators of basic helix-loop-helix transcription factors. It generally represses the cell differentiation and promotes cell proliferation in tumour (Sumida T et al., 2016). Deregulation of ID2 attenuates cell invasiveness of

human salivary gland cancer cells (Sumida T et al., 2016). Low expression levels of ID2 enabled glioblastoma (GBM)-derived cell lines to survive glucose deprivation and hence conduced to greater growth opportunity (Zhang Z et al., 2017). The elevated expression of ID2 in the 4 hours vs 0 hour time point suggests that HONE-1 might struggle for greater cell survival by trigerring signaling in TGFβ pathway.

Nevertheless, activation of MYC proto-oncogene has been an inititaion factor for human cancer occurrence (Gabay M, et al., 2014). IGF1 advocates on cell proliferation and differentiation as well as being a strong suppressor for apoptosis (Fürstenberger G et al., 2002).

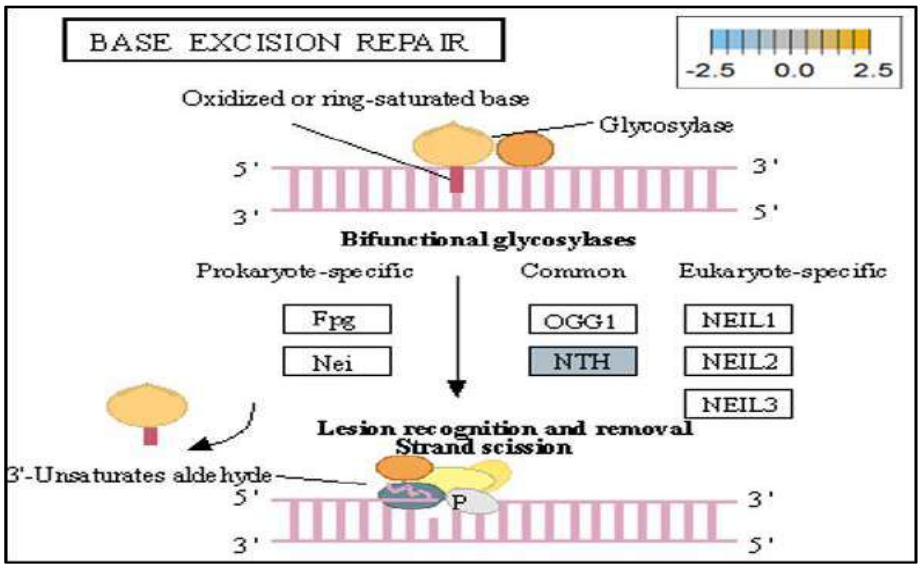

Extract from Figure 4.58: Base Excision pathway

NTHL1 and *FANC* were deregulated in DNA damage- repair while ERCC6 was elevated in expression. The endogenous and exogenous detrimental factors can contribute reactive oxygen species (ROS) which engender DNA damage (Bauer N.C., et al., 2009). The affected cells would initiate base excision

repair (BER) pathway to stabilize genome (Maynard S., et al., 2009). *NTHL1* encodes DNA N-glycosylase activity to catalyze base excision repair. However, augmented expression of NTHL1 protein levels can contribute to DNA damage that cause genomic inbalance and tumorigenesis (Limpose KL, et al., 2018). Increased level of NTHL1 protein and are found in various human cancers such as in lung, breast, prostate, and pancreas. (Albertson DG, 2008). The elevated expression of *NTHL1* gene was noted in non-small cell lung cancer (NSCLC) (Limpose KL, et al., 2018). The deregulation of *NTHL1* in this experiment may ascertain HONE-1 cell growth was under restraint with XXXD treatment.

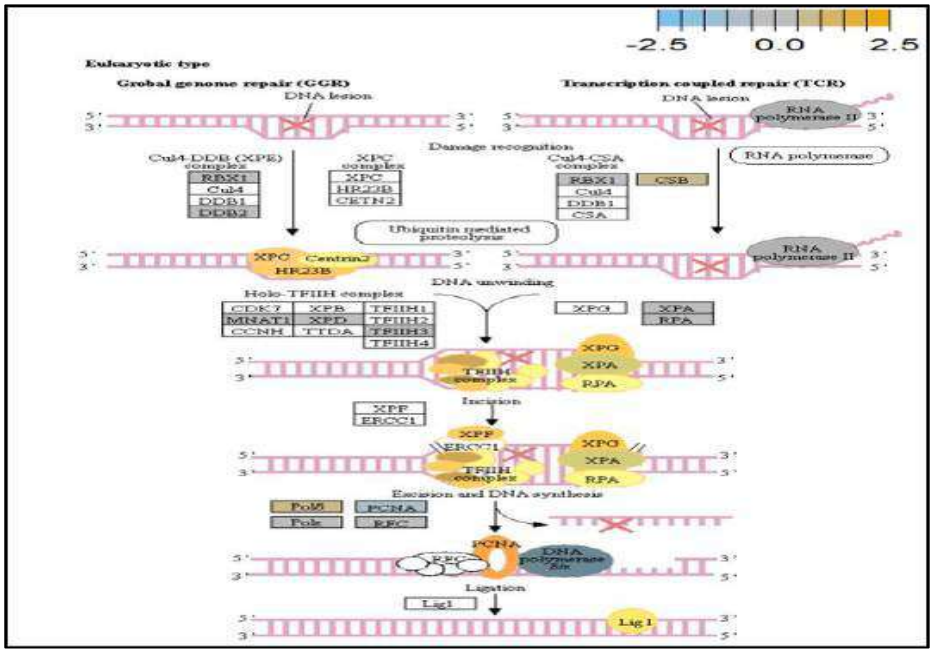

Extract fom Figure 4.5.2.1.13: Nucleotide Excision pathway

ERCC6 (known as CSB) encodes a DNA-binding protein which is essential for transcription-coupled excision repair and is responsible for producing Cockayne syndrome B protein (CSB). CSB repairs damaged DNA so as to remedy with gene transcription. At 4 hours vs 0 hour time point, expression of ERCC6 was elevated.

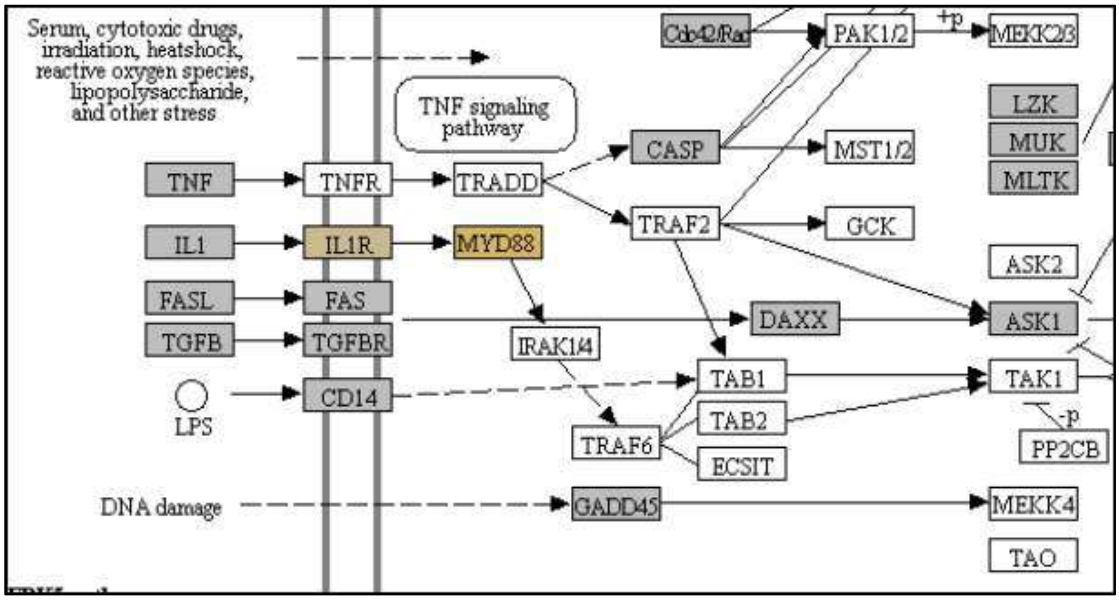

Extract fom Figure 4.5.2.1.3: MAPK signaling pathway

Up-regulation of *MYD88*, *CDKNIC*, *TNFSF10*, *CASP7*, *IL1RAP* were started off by Cell Cycle-Apoptosis pathway except SMC3 was deregulated. Myeloid differentiation factor 88 (MYD88) is an important adaptor protein for signal transducer in the interleukin-1 (IL1) and Toll-like receptor (TLR) signaling pathways. MYD88 triggers signaling molecules that turn on a group of interacting proteins in NF-κB which regulates immunity and pro-inflammation. Conventionally MYD88 will propagate signal to activate downstream IRAKs-TRAF6 and the IKK complex to further trigger NF-κB which controls the production of pro-inflammatory cytokines and type 1 interferon (IFNs) (Saikh KU, 2021). However, it was seen in the pathview that though the expression of MYD88 was amplified together with IL1R receptor (IL1RAP, Interleukin 1 Receptor Accessory Protein), the downstream genes such as IRAKs-TRAF6 did not stimulated. The downstream pathway stopped in MYD88. The up-regulateion of both MYD88 and IL1R receptor in HONE-1 might due to immunity response from interaction of cytotoxicity of XXXD. Lack

of response from downstream genes might cause them to self-destruction or undergo apoptosis.

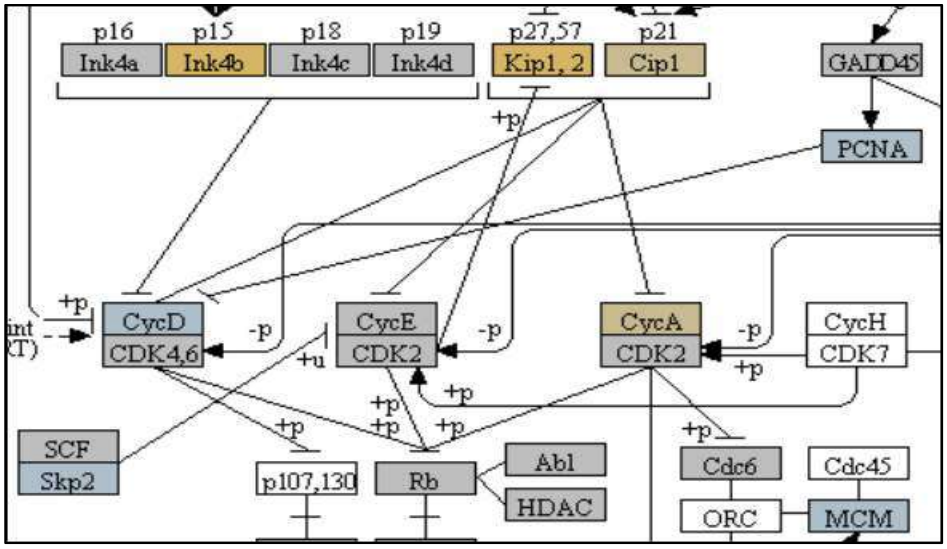

Extract fom Figure 4.53: Cell Cycle signaling pathway

Expression of *CDKNIC* (also known as KIP2 or P57) is seen to have elevated as the down-regulation of its inhibitor Cyclin E/CDK2 complexe which governs the cycle arrest in G1 phase. KIP1, 2 and CIP1 were both upegulated to suppress the amplified expression of Cyclin A/CDK2 and also Cyclin E/CDK2 complexe. CDKNIC is known as tumour suppressor. CDKN1C is normally deregulated in many common human malignancies through several mechanisms (Ioannis S et al., 2009). In this experiment, *CDKN1C* was noted for its up-regulation and its inhibition towards cyclin/Cdk complexes. It may suggest that the cell cycle of HONE-1 in G1 phase could encountered DNA damage and cell arrest under the interaction of XXXD treatment.

TNFSF10 (also known as Trail) protein is a cytokine that belongs to the tumour necrosis factor (TNF) ligand family (Starkey, M. et al., 2014). At 4 hours

vs. 0 hour, TNFSF10 was highly expressed and bind with D1, D2, D4 and D5 which are called death receptor. The augmented expression of Trail in HONE-1 may due to the irritation of XXXD interaction at the first 4 hours. TNFSF10 is well known as tumour suppressor and induces cell apoptosis in cancer (He W et al., 2012). Moreover, TNFSF10 alone or integrated with chemotherapeutics had exhibited favorable anticancer result by mediating apoptosis (Hellwig CT, and Rehm M, 2012).

The up-regulation of CASP7 envisaged the execution of apoptosis of HONE-1 in mitochondrial pathway. Meanwhile, expression of the anti-apoptosis protein BCL-2 was attenuated and CASP 9 stimulated expression of CASP7.

SMC3 (Structural Maintenance of Chromosomes 3) is a component of the multimeric cohesin complex. Its main function is to ensure normal chromosome segregation by gripping sister chromatids during mitosis. At 4 hours vs. 0 hour time point, SMC3 was deactivated with low expression initiated in Cell Cycle pathway. This implied an adverse impact for HONE-1 to proliferate through a normal cell cycle progression.

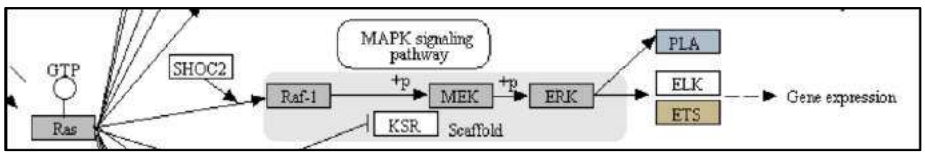

Extract fom Figure 4.51: RAS signaling pathway

ETS2 was mildly upregulated in RAS pathway. It is a transcriptional factor to translocate signal for cell proliferation, apoptosis, and survival in the thymus (Arnaud Zaldumbide et al., 2002). As RAS associated with MAPK

signalling pathway is often initiated for cellular growth and development, the deactivation of MAPK cascade was seen in extract fom Figure 4.51. This may suggest that HONE-1 could encounter cellular stress from intervention of XXXD treatment. The upregulation *ETS2* could mean to transcribe signal for cell apoptosis.

WNT10A is an important ligand governing adult epithelial development as well as region-specific differentiation, and modulate activation downstream β-catenin pathway (Xu, M et al., 2017). WNT10A protein has been implicated in oncogenesis during developmental processes. Etiologic for tooth agenesis (TA) were often been accounted for WNT10A mutations (Zeng Y et al., 2020). At 4 hours vs. 0 hour time point, WNT10A was upregulated but expression of its receptor namely Frizzled was attenuated. Subsequently, no downstream genes was stimulated and thus contributed to deactivation of β-catenin pathway.

PI3K pathway initiated upregulation of ITGB8 receptor and the signaling molecule ECM. Nevertheless, the cellular activator molecule was not seen in the pathview resulting the absence of the signal being triggered towards PI3K and attenuation of cell survival and proliferation of HONE-1. It may suggest that HONE-1 could encounter considerable cellular stress from the treatment of XXXD.

In JAK-STAT pathway, expression of cytokine ligand and the receptor was elevated. Meanwhile, SOCS1 was in higher level of expression than JAK Kinase. SOCS1 inhibited target kinase JAK by recruiting the E3 ubiquitin ligase

complex. The E3 complex polyubiquitinated and degraded JAK by proteasome as well as preventing the kinase JAK from phosphorylating its cytokine receptor. The suppressed JAK kinase could not actively transduct signal to its canonical targets STAT. Consequently, STAT dimers translocated signal to the nucleus and induced the attenuated expression of cell cycle progression promoter Cyclin D and pro-survival BCL-2, BCL-XL and augmented the expression of cell cycle progression inhibitor p21. It could be prostulated that HONE-1 could adopted an autophgy process.

Summary

As for cellular sustainability of HONE-1 at 4 vs. 0 hour time point, it is observed that HONE-1 confronted with huge detrimental impact from the XXXD treatment. This can be witnessed from the level of expression in majority genes being induced to perform primarily on inhibition in cell proliferation and to advocate cell differentiation and apoptosis in HONE-1. Particularly in Cell Cycle pathway, high level expression of CDKN1C, P21, TNFS10 protein conduced to greater cell cycle arrest and apoptosis whereas deregulation of Cyclin D and pro-survival BCL-2, BCL-XL protein eventually decresed the survival rate of HONE-1. Meanwhile, signalling ligand receptors for promoting growth such as WNT10A and Frizzled in WNT pathway as well as ECM and ITGD8 of PI3K pathway, ID2 and MYD88 in MAPK pathway were highly activated , however, the transduction of signal by these genes within cytoplasmic downstream were mostly deregulated. This may suggest that HONE-1 could

endure intensive cellular stress from interaction of XXXD during 4 hours vs. 0 hour period.

5.5.2 Time point at 8 hours vs. 0 hour

At 8 hours vs. 0 hour time point, Transcriptional Misregulation pathway initiated the down-regulation of *ETV1*, *SOX9*, *TGFBR2* and *RELA*. *ETV1* was the most negatively expressed gene at 8 hours vs 0 hour treatment time for HONE-1treated with XXXD.

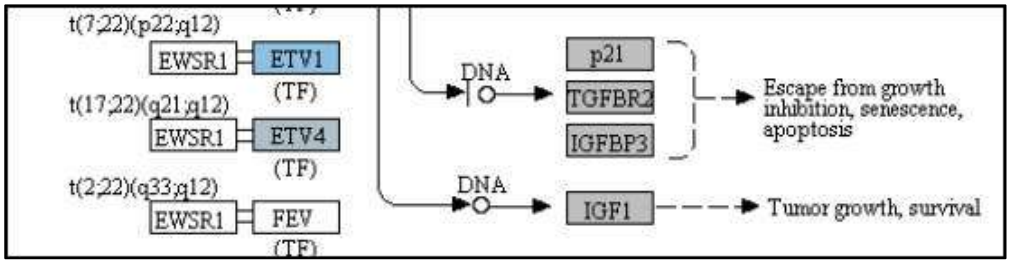

Extract fom Figure 4.68: Transcription Misregulation signaling pathway

ETV1 belongs to the ETS family of transcription factors. Often associated with MAPK, PI3K pathway, ETV1 protein modulates biological processes like cell growth, angiogenesis, The EWSR1-ETV1 fusion proteins are thought to be the "oncogenic drivers" in Ewing sarcoma. Conventionally, Ewing sarcoma gene EWSR underwent a t(7;22)(p22;q12)(so-called breakpoint region) translocation with the ETV1 to form a fusion gene primarily associated with the pathogenesis of Ewing's sarcoma for cell growth and proliferation (Cantile Met al., 2013). EWSR1 was detected absent in EWSR1/ETV1 fusion. Hence, this may imply that XXXD could have suppressed expression of EWSR1 and induced low expression of ETV1 and ETV 4. Conventionally, EWSR1/ETV1

and EWSR1/ETV4 in association with EWSR1/FEV tended to exert its influence for neoplasm localization (Im YH et al., 2000). At 8 hours vs 0 hour treatment time, ETV1 as well as ETV4 were dyregulated. It could be postulated that the pathogenesis for HONE-1 cell growth and proliferation was reasonably degraded due to the deactivation of biological functions of these two proteins.

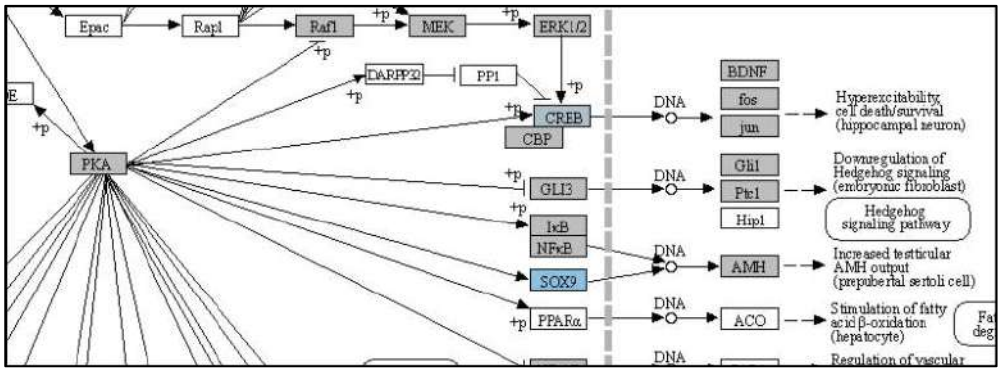

Extract fom Figure 4.71: cAMP pathway

SOX9 is an important transcription factor for both sex and skeletal development. PKA induced attenuated expression of SOX9 in C-AMP pathway. This eventually did not stimulate the expression of AMH. AMH encodes protein that is involved in male sex differentiation. AMH protein secreted from testes cell during male fetuses development.

Both Transcriptional Misregulation and MAPK pathway initiated the down-regulation of DUSP6 (Dual Specificity Phosphatase 6, also known as MKP-3 in MAPK pathway). MKP-3 and MKP-2 (DUSPA 4) deactivates its target kinases ERK, JNK and P38 by dephosphorylation which contributed to reduction of cellular proliferation and differentiation of HONE-1.

CACNG6 (Calcium Voltage-Gated Channel Auxiliary Subunit Gamma 6) is an integral membrane protein to stabilize the calcium channel in an inactive (closed) state. The calcium (Ca^{2+}) concentration inside the cell will influence expression of genes which are important for neuronal development. The inflow of Ca^{2+} into L-type Calcium Channel (LTCs) can effectively activate transcription factors such as CREB and MEF-2. Binding of Ca^{2+}-Calmodulin (CaM) is important to transfer the Ca^{2+} signal to the nucleus and is essential for activating RAS/MAPK pathway and stimulate the genes necessary for neuronal survival and plasticity purposes (Ricardo E et al., 2001). At 8 hours vs 0 hour treatment time, it was shown that expression of CACNG6 was attenuated in MAPK pathway which regraded signalling to nucleus by an L-type Calcium Channel– Calmodulin Complex via RAS and MAPK cascade.

IRS1 (Insulin Receptor Substrate 1) modulates biological processes such as proliferation and survival. IRS1 is an intracellular signalling adaptor protein particularly for insulin hormone ligand. It was envisaged that IRS1 was dyregulated together with the growth factor ligand in MAPK pathway which conferred to deactivation of downstream genes.

Down-regulation of PLA2A2G (Phospholipase A2 Group IIA) and RAC2 (Ras-related C3 botulinum toxin substrate 2) were initiated in RAS pathway. PLA2s are commonly found in nature either as an intracellular or extracellular enzymes (Six DA et al., 2000). Augmented expression of PLA2G2A has been noted to implicate in various types of malignant tumour such as pancreatic cancer and prostate cancer (Kashiwagi M et al., 1999) (Jiang

J et al., 2002). In RAS pathway, ERK kinase deregulate the transcription factor PLA2 and hence, confer the degradation of cell proliferation in HONE-1. RAC2 is a members of Rho family of GTPases protein and localizes to the plasma membrane. It modulates cell growth, cytoskeletal reorganization, and the activation of protein kinases. The attenuated expression of RAC2 might deactivate RAS as well.

ITGA2 and ITGA6 receptors as well as the signaling molecule ECM were downregulated by the PI3K pathway. It was envisaged that the cellular activator FAK did not respond to receptor and triggered no signal towards PI3K downstream.

DKK1 is the suppressor for receptor Frizzled of WNT pathway. At 8 hours vs 0 hour treatment time, WNT pathway initiated the downregulation of DKK1, ligand WNT10A, Frizzled receptor together. Subsequently, the no downstream genes was stimulated and appeared in the pathview conferring to deactivation of β-catenin pathway.

TGFβ pathway initiated attenuation of expression of *NOG*, *FST*, *TGFBR2*, *NOG* and *FST* are the inhibitor to ligand BMP and Activin in TGFβ pathway respectively. As shown in the pathview, expression of *NOG* and *FST* were elevated in 4 hours vs 0 hour timepoint but attenuated at 8 hours vs 0 hour. The attenuated expression might correlate with the frail expression of extracellular signaling molecules during XXXD treatment. Meanwhile, TGFβ R2 receptor was deregulated together with the TGFβ ligand too.

The IDH2 encodes protein for producing enzyme called isocitrate dehydrogenase 2. which is found in mitochondria and control intermediary metabolism and energy production. The decreasing expression of IDH2 may implicated that HONE-1 experienced intracellular stress.

BNIP3 (BCL2 Interacting Protein 3) encodes a mitochondrial protein that acts as a pro-apoptotic factor. Expression of BNIP3BNIP3 was attenuated and expressed with negative log_2fold change -0.515.

C19orf40 (FA Core Complex Associated Protein 24, FAAP24) functions in DNA repair through recruitment of the Fanconi anemia core complex to damaged DNA. The expression was attenuated and expressed with negative log2fold change -0.403. The downregulation of *BNIP3* and *C19orf40* may correlate with the apoptosis resistance of HONE-1 throughout the 8 hours treatment time.

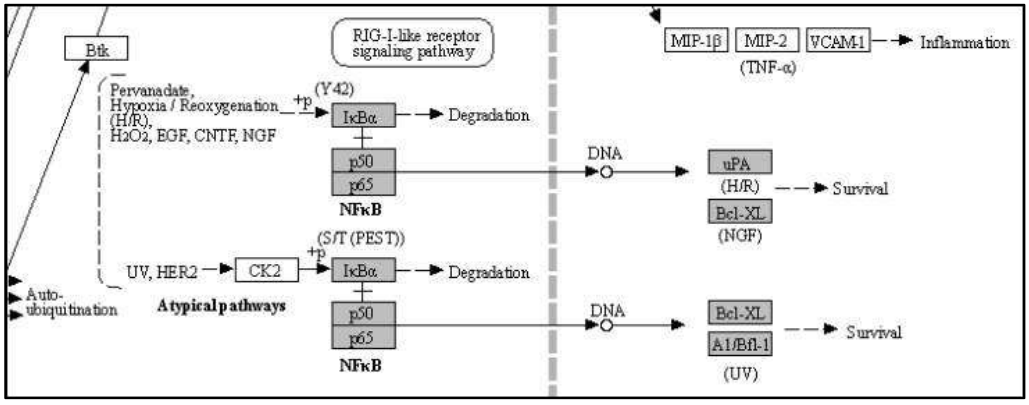

Extract fom Figure 4.72: TNFκB pathway

RELA (also known as p65, NF-kappa-B) is a transcription factor to regulate mainly for cell development and apoptosis, inflammation and immunity. RELA (p65) forms a heterodimeric complex with p50 he dimers bind at kappa-B sites in the DNA of their target genes and the individual dimers have distinct preferences for different kappa-B sites that they can bind with distinguishable affinity and specificity. Different dimer combinations act as transcriptional activators or repressors, respectively. RELA (p65) was downregulated and expressed with negative log_2fold change -0.248. The deactivation of RELA subsequently did not induce activation of uPA and BCL-XL in downstream as shown in extract fom Figure 4.72. uPA (urokinase-type plasminogen activator also known as PLAU) and pro-survival BCL-XL protein was not observed for being regulated. This could further decrease the viability of HONE-1 due to intervention of XXXD. High level expression of uPA often associates with invasive tumour growth and poor prognosis particularly in breast cancer (Banys-Paluchowski M et al., 2019).

MSH2 (MutS Homolog 2) is a tumour suppressor gene and more specifically a caretaker gene that codes for a DNA mismatch repair (MMR) protein, MSH2, which forms a heterodimer with MSH6 to make the human MutSα mismatch repair complex. It also dimerizes with MSH3 to form the MutSβ DNA repair complex. Kagawa M, Kawakami S et al. (2021) recently reported on cases of deficiency of mismatch repair (MMR) protein, MSH2 correlated with prostate cancer in a Japanese. In addition, Malik SS et al., 2021 concluded that MSH2 deficiency may cause breast cancer tumorigenesis and accelerate development and progression. Expression of *MSH2* was elevated at

his time point suggest that XXXD treatment had induced cytotoxicity effect towards HONE-1.

Summary

At 8 hours vs 0 hours treatment time, it can be summarised that XXXD continued to exert its cytotoxicity effect on HONE-1. This again can be witnessed from down-regulation of a number of genes which can instigate cell growth and proliferation, particularly like *ETV1*, *SOX*, *DUSPA6*, *CACNG6*, *IRS1* and *IDH2*. In addition, many growth factor ligands and receptors were upregulated but the intracellular downstream genes either being knockdown or not active, resulting the transduction of growth signal towards transcription factors in vain or frail. Evidence gathered is GF, RTK and IRS1 as well as ECM, ITGA and ITGB which were initinited in PI3K pathway; DKKi and Frizzled which were initiated in WNT pathway. This may suggest that XXXD is imposed considerably suppression for cell proliferation in HONE-1through expression of above mentioned genes associated with their related pathways.

5.5.3 Time point at 12 hours vs. 0 hour

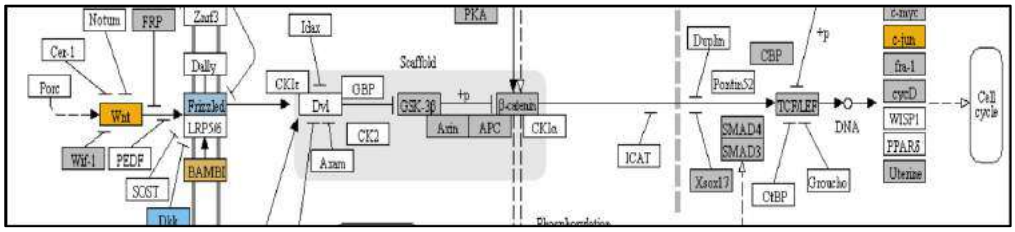

Extract fom Figure 4.5.2.3.7: WNT pathway

At 12 hours vs. 0 hour treatment time, *DKK1* was the most negatively regulated gene initiated in WNT pathway. *DKK1* was downregulated at 8 hours vs. 0 hour time point, but the the down-regulation was larger at 12 hours verse 0 hour treatment time in terms of log_2fold change. DKK1 is the suppressor for receptor Frizzled and LRP5/6 complex of WNT pathway. At 12 hours vs. 0 hour treatment time, WNT pathway initiated the downregulation of DKK1and Frizzled receptor together but there was amplification of expression in *WNT10A* ligand and *BAMPI* gene. BAMPI is membrane-bound inhibitor for LRP5/6 and an important modulator for cell proliferation so as to increase Wnt/β-catenin signaling. In the receptor complex, knock-down of LRP5/6 was detected. Signal to be conveyed for cellular activation became frail. Subsequently there was no recruitment of Dvl proteins to the plasma membrane was observed in the pathview. The phosphorylation of β-catenin was phosphorylated by destruction complex (made up by axin, APC, CK1, and GSK3β) leads to its ubiquitination by β-TrCP targeting it for proteasomal degradation, resulted in the binding of the repressor complex containing TCF/LEF to the target gene and thereby repressing its activity (Patel Sonal et al., 2019). Eventually, *C-JUN* (also known as AP-1) was upregulated in WNT pathway and was also regulated upon phosphorylation mitogen-activated protein kinases (MAPK). C-JUN is a protooncogene which encodes a nuclear protein, cJun. C-JUN monitors the cellular responses to stimuli that control cell development, immunity response apoptosis and the response to toxic agent or stress (Angel and Karin, 1991). Bin Xu et al., 2012 had reported that downregulation of C-JUN expression inhibited apoptosis and cytotoxicity induced by salvicine in both MDR and parental K-562 cells. This may postulate that the up-regulation of C-JUN could have

conferred cell arrest and apoptosis for HONE-1. Wnt/β-catenin signaling plays an essential role during embryonic muscle and adult skeletal muscle development. Wnt signaling activity promotes the expansion and differentiation of tumour cell (Brack, A.S et al., 1996). The Wnt pathway has multiple players that can be effectively targeted to modulate the signaling cascade, thereby inhibiting cancer proliferation. Targeting Wnt signaling to suppress cancer growth by modulating the signaling cascade for instance are anti-Frizzled antibodies, mimetics of Wnt molecules, inhibitors for disheveled, tankyrase and TCF/CBP interactions, axin stabilizers are being applied in different stages of clinical practice (Patel Sonal et al., 2019).

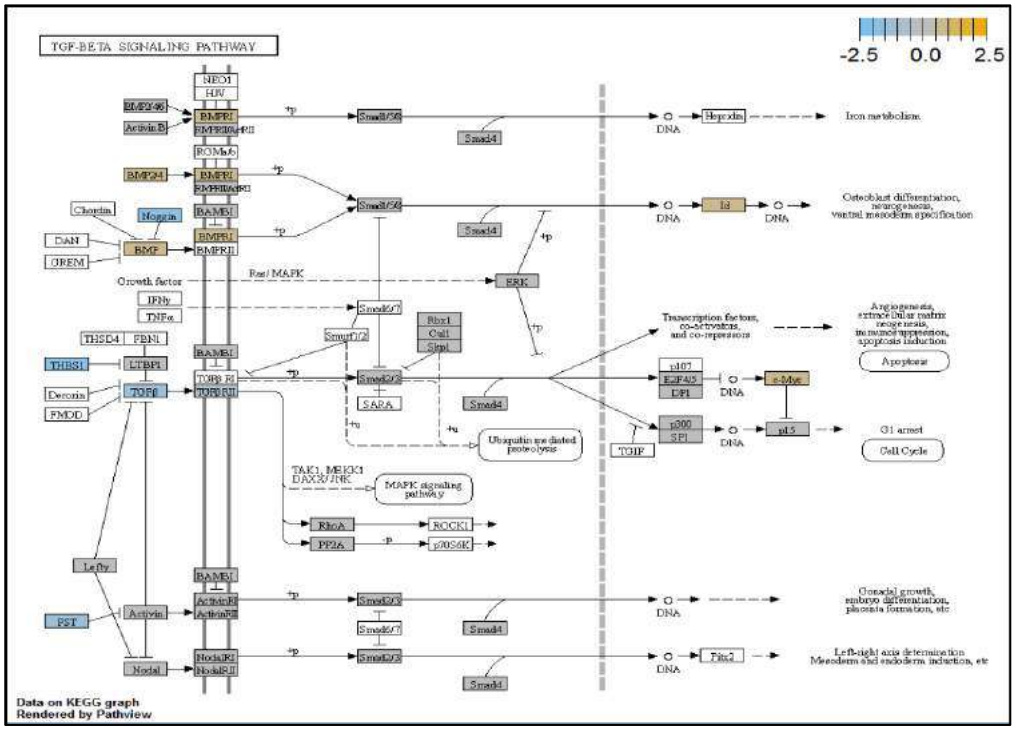

Extract from Figure 4.5.2.3.10: TFGβ pathway

TGFβ pathway initiated down-regulation of *TGFβ2*, *TGFβR2*, *FST* but amplified expression of *ID2*. FST is the inhibitor for TGFβ ligand ACTIVA, ACTIVA bind with the receptor and induced signal to SMAD and further to SMAD4,

which then translocated messages to nucleus through the canonical pathway. *TGFβ2* and *TGFβR2* were deregulated and led deactivation to downstream genes. Inhibitorfor BMP NOGGIN was dyregulated and BMP ligand had elevated expression together with BMP receptor. It phosphorylated SMAD and trigger signal to SMAD4 which eventually translocated message to nucleus and stimulated up-regulation of ID2. ID2 is inhibitor of DNA-binding (ID) protein which is the suppressor for basic helix-loop-helix transcription factors. ID2 conventionally induce cell proliferation and inhibit differentiation (Sumida T et al., 2016). A knock-down of ID2 significantly promoted human salivary gland cancer cells growth by decreasing expression of N-cadherin, vimentin and Snail but stimulatinthe E-cadherin expression (Sumida T et al., 2016). Moreover, ID2 encouraged glioblastoma cells growth during glucose deprivation by inhibiting reactive oxygen species (ROS) production to attenuate mitochondrial damage (Zhang Z et al., 2017). TGF-β signaling has two aspects for tumorigenesis. In the initial stage of tumour progress, TGF-β usually suppress the growth by initiating cell cycle arrest and apoptosis. Nevertheless, after a longer time of cell resistant to apoptosis, TGF-β will in turn become a driver of mutated gene in tumour and subsequently enhance the development and invasiveness (Shuchen Gu et al., 2018). Hence, this may suggest the up-regulation of ID2 at 12 hours vs. 0 hour time-point and HONE-1 might struggle to revive after 12 hours of XXXD treatment.

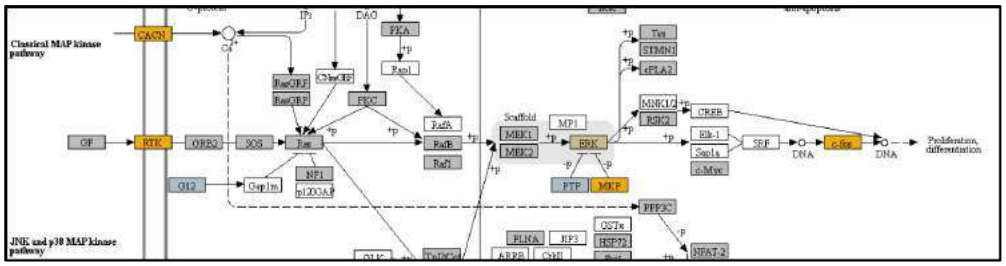

Extract from Figure 4.5.2.3.3: MAPK pathway

MAPK initiated the elevation of expression of *FOS* gene. *FOS* scored 4.15 for the most positive $\log_2$ fold change in differential expression. FOS forms the transcription factor complex AP-1 by dimerizing with C-JUN in which its up-regulation was associated with WNT pathway at the 12 hours vs. 0 hour time-point. Amplification in expression of AP-1 was induced by JNK kinase of MAPK pathway. CACN, the membrane protein which regulate the inflow of Ca^{2+} into L-type Calcium Channel (LTCs) was highly expressed so as to allow active inflow of Ca^{2+} into L-type Calcium Channel (LTCs) through ERK and transcription factors RSK2 to nucleus. RTK (Membrane Plasminogen Receptor) binds plasminogen via a C-terminal lysine exposed on the cell surface and activates plasminogen on the cell surface, was upregulated. Growth signal was triggered to RAS and phosphorylated MAPK cascade. ERK, though dephosphorylated by inhibitor MPK, stimulated transcription factor c-MYC to express *FOS* gene in nucleus. FOS proteins play a role in cell proliferation, and differentiation (Eferl R and Wagner EF, 2003). Elevated expression of FOS and AP-1 in MAPK pathway might implicate HONE-1 rebounded to more active tumour cell development.

Expression CDKNIA (also known as CIP1 or P21) and CDKNIC (also known as KIP2 or P57) as well as TNFSF10 (TRAIL) were augmented in Cell

Cycle pathway. CDKNIA and CDKNIC are inhibitor to Cyclin C, D/CDK4, 6, Cyclin E/CDK2, Cyclin A/CDK2 complexe which governs the cycle arrest in G1-S phase. CDKNIA and CDKNIC are also known as tumour suppressor.

Expression of CDKNIC (also known as KIP2 or P57) was seen to have elevated as the down-regulation of its inhibitor Cyclin E/CDK2 complexe which governs the cycle arrest in G1 phase. KIP1/2 and CIP1 were both upegulated to suppress the amplified expression of Cyclin A/CDK2 and also Cyclin E/CDK2 complexe. CDKNIC is known as tumour suppressor. CDKN1C is normally deregulated in many common human malignancies through several mechanisms, denoting (Ioannis S et al., 2009). In this experiment, CDKN1C was noted for its up-regulation and its inhibition towards cyclin/Cdk complexes. It may suggest that the cell cycle of HONE-1 in G1 phase could encountered DNA damage and cell arrest under the interaction of XXXD treatment. TNFSF10 (also known as Trail) protein is a cytokine that belongs to the tumour necrosis factor (TNF) ligand family (Starkey, M. et al., 2014). In 12 hours vs. 0 hour treatment time, TNFSF10 as a ligand cytokine was highly expressed. TNFSF10 is well known as tumour suppressor and induces cell apoptosis in cancer (He W et al., 2012). Moreover, TNFSF10 alone or integrated with chemotherapeutics had exhibited favorable anticancer result by mediating apoptosis (Hellwig CT, and Rehm M, 2012). The amplified expression of CDKNIA, CDKNIC and TNFSF10 might be prostulated for rebounce of cell proliferation in HONE-1 at 12 hours vs. 0 hour time-point.

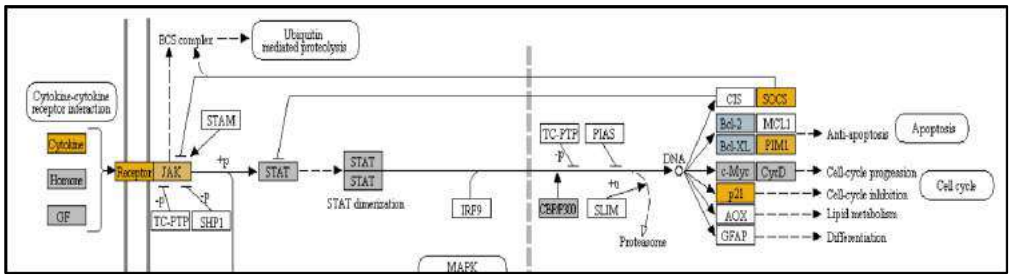

Extract from Figure 4.80: JAK-STAT pathway

In JAK-STAT signaling pathway, *SOCS3* was expressed in $\log_2$ fold change of 3.09. Cytokine ligand and its receptor which bind with JAK in the cellular membrane were upregulated as shown in extract from Figure 4.80 above. SOCS3 is the inhibitor to JAK2 signal activator. Mediated by IL-12, SOCS3 inhibits STAT4 dimerisation to decrease Th1 differentiation and enhance Th2 skewing (Seki Y-I et al., 2003). Some researches showed that SOCS3 exhibits dual roles in T cell regulation (Kinjyo I et al., 2006). STAT3 enhances the production of both anti-inflammatory cytokines (such as TGF-β and IL-10) and also inflammatory cytokines such as IL-17 and IL-6 (Yasukawa H et al., 1999). In the nutshell, SOCS proteins is important in regulating immune responses, especially the outcome of Th cell polarization. Their function is specific for cytokines but not for JAKs/STATs (Seif, F et al., 2017). The effect of the final translocated signal to nucleus stimulated the high level expression of PIMI and p21 and frail expression of *BCL-2* and *BCL-XL* gene. PIMI (Pim-1 Proto-Oncogene, Serine/Threonine Kinase) involves in cell survival and cell proliferation and thus promotes tumorigenesis. However, the up-regulation of p21 might counter or weaken the activation of PIMI. P21 is a strong cyclin-dependent kinase inhibitor (CKI) which suppress the activity of cyclin-CDK2, -CDK1, and -CDK4/6 complexes in regulating cell cycle progression at G1 and S phase. Moreover, with frail expression of anti-apoptotic protein BCL-2 and

BCL-XL, it may postulate that HONE-1 encounter resistance in reviving tumour cell growth after 12 hours of XXXD treatment.

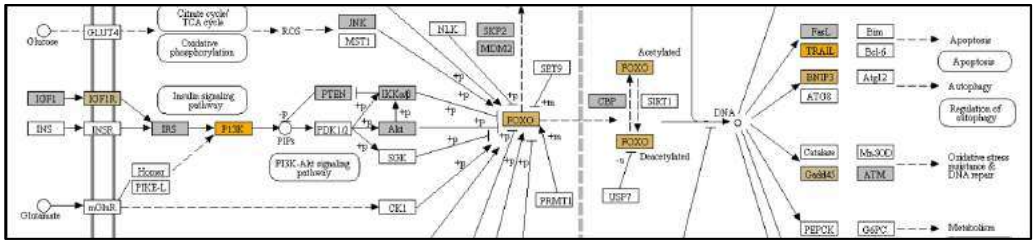

Extract from Figure 4.83: FOXO signaling pathway

Elevated expression of BNIP3 was induced by FOXO transcription factor through PI3K pathway. BNIP3 is a proapoptotic protein which induces both cell death and autophagy through a mitochondrial pathway induce both cell death and autophagy (Boyd JM et al., 1994). In tumour cells, hypoxia tends to regulate BNIP3 and tumour growth was correlated with low expression of BNIP3 (Zhang, J and Ney, P, 2009). Expression of BNIP3 at 12 hours vs 0 hour time point might suggest HONE-1 could possibly be induced to autophagy.

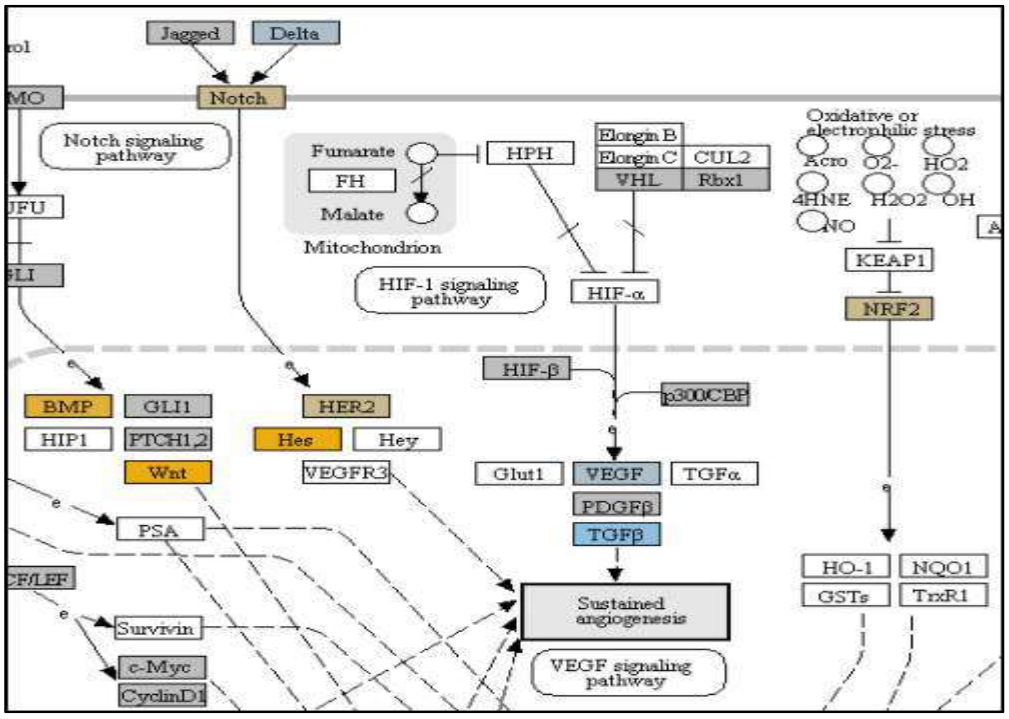

Extract from Figure 4.74: pathway in cancer

Notch signalling pathway initiated the elevation of expression for NOTCH receptor, HER2 transcription factor and HES1 antagonist transcription factor. Notch signaling pathway plays an important role in cell-cell communication, and further regulates embryonic development. However, aberrant Notch pathway was associated in many types of cancer. Notch receptor bind Jagged ligand and the complex was cleaved by Adam/Tace, a cleavage mediator followed by poteolytic cleavage enzyme γ-secretase. After this, intracellular domain (NICD) was released and translocated to nucleus to induce activation of DNA-binding factors CSL and MAML, as well as the basic helix-loop-helix (bHLH) Hes family antagonist transcription factor HES1(Iso T et al., 2003). As shown in the extract from Figure 4.74 above, HER2 was induced by receptor Notch. HER2 (also known as ERBB2). HER2 was implicated in various malignancy of cancer and was reported for correlation with poor prognosis of osteosarcoma (Gorlick R et al., 1999). Suppression of ERBB family signaling by its inhibitor, CI-1033 can deter the tumour growth and induce apoptosis (Hughes DPM et al., 2006). The elevated expression of HER2 at this time point might suggest that HONE-1 fought back for tumour persistence after 12 hours of XXXD treatment.

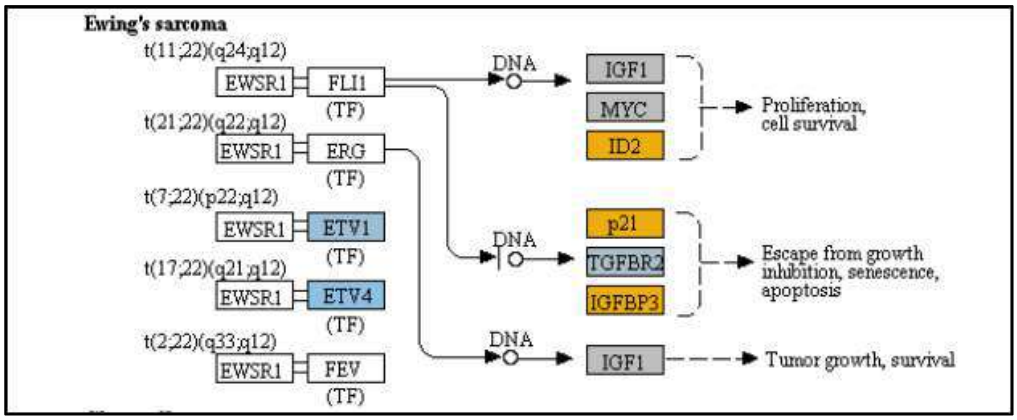

Extract from Figure 4.81: Transcription Misregulation pathway

The expression of IGFBP3 was amplified at 12 hours vs 0 hour treatment time. It was observed in the pathview of Transcriptional Misregulation pathway, as like in 4 hours vs 0 hour treatment time. Conventionally, Ewing sarcoma gene EWSR will undergo at (11; 22)(q24;q12) translocation with the FLI1 (Fli-1 Proto-Oncogene, ETS Transcription Factor) to form a fusion gene of Ewing sarcoma. The EWRS-FLI-1 fusion protein will transform the target genes for Ewing's family tumours development. However, the absence of EWRS and FLI-1 fusion was shown in the pathview. Hence, XXXD could have again suppressed expression of EWRS and FLI-1 and amplified the expression of IGFBP-3, p21, ID2 and TGFBR2. In 12 hours vs 0 time point, IGFBP-3 was highly expressed. IGFBP3 can adjust cell development either with IGF1 or independently (Varma Shrivastav Shailly, et al., 2020). Wang YA et al. (2017) reported that elevated expression of IGFBP3 induced apoptosis and increased effect of cisplatin in by deactivating IGF1 signaling. The intracellular signaling via Smad2 would be triggered when IGFBP-3 combined with TGFBR2 receptors and contributed to the activation of type I TGF-β receptors (John F et al., 2004). Subsequently, this pathway was associated to inhibition of proliferation. It may suggest that the elevated expression of IGFBP-3 and p21 could have suppressed cell proliferaton.

HONE-1 did not observe to escape from growth inhibition, senescence, and apoptosis.

Summary

At 12 hours vs 0 hour time point, it can be summarised that XXXD continued to inflict its fatal reaction on HONE-1 by imposing cell cycle arrest and apoptosis. The augmented expression of *CDKNIA*, *CDKNIC* and *TNFSF10* initiated in Cell Cycle pathway apparently inhibited cell cycle progression in HONE-1. Moreover, enhanced expression in *SOCS3* and *ID2* together with down-regulation of anti-apoptotic genes *BCL-2* and *BCL-XL* initiated in JAK-STAT pathway further exacerbated cell fate of HONE-1. Nevertheless, in view of the MAPK signalling pathway, high level expression of genes like *FOS*, *AP-1*, *ERK* and *CACN* may postulate a vigorous rebounce of cell resistance of HONE-1 against the XXXD treatment. Particularly, *FOS* which gained the highest positive $\log_2$ fold change value of 4.15 for differential expression at 12 hours vs 0 hour. *FOS* is proto-oncogene which plays an important role in regulating the development of cells to form the skeleton as well as in signal transduction, cell proliferation and differentiation (Prucca CG et al., 2020). MAPK/ERK pathway activation is a common feature of NPC and these pathways are stimulated by the EBV-encoded LMP1 and LMP2A genes such as HONE-1 to promote the migration and invasion of NPC cells (Tsao t. al., 2015)(Wang et. al., 2014).

5.6 Specific gene

In view of the gene expression of HONE-1 when treated with L1 (Huanglian) at 3 time points within 12 hours, great majority of genes were induced to inhibit cell proliferation and cause apoptosis in HONE-1. It was detected that expression of ETV1 was attenuated at 3 different time points such as 4 hours vs. 0 hour, 8 hours vs. 0 hour and 12 hours vs. 0 hour, and the $\log_2$ fold change value for differential expression were -0.838 (P<0.05), -0.928 (P<0.05) and -0.972 (P<0.05), respectively. Meanwhile, when treated with L7 (XXXD) at 3 different time points within 12 hours, HONE-1 encountered intracellular stress which consequently render to reduction of cell proliferation and apoptosis although there was a sign of persistent cell resistance and rebounce particularly in 12 hours vs. 0 time point. Likewise, it was observed that expression of *ETV1* again was depreciated at 3 different time points such as 4 hours vs. 0 hour, 8 hours vs. 0 hour and 12 hours vs. 0 hour, and the $\log_2$ fold change value for differential expression were -1.18 (P <0.05), -1.77(P <0.05) and -1.41(P <0.05), respectively. The attenuated expression of *ETV1* was consistent as when HONE-1 was treated with L1 (Huanglian) and L7 (XXXD) in two different tests. Thereupon, these findings suggest that *ETV1* could be targeted as the core gene for therapeutic purpose in treating NPC particularly HONE-1.

ETV1 protein is transcription factors which belongs to the PEA3 subfamily of ETS (Oh S et al., 2012). In these two tests, down-regulation of ETV1 was initiated by Transcription Misregulation pathway. As shown in the pathwiew, chromosomal rearrangements of *ETV1* gene occur in Ewing tumours and prostate tumour. Likewise, it was postulated to be one of the major factor in

the genesis of NPC in this experiment. Elevated expression of oncoproteins *ETV1* is often implicated in melanomas, breast and other types of cancer (Oh S et al., 2012). Keld R et al., 2010 had reported that overexpression of *ETV1* associated with MAPKs instigated invasive tumour growth in OE33 esophageal squamous cancer. Hence, methods such as regulation of its expression, interaction with cofactors or inhibiting its crucial target gene products could consequently be utilised to treat cancer (including NPC) which is dependent on the PEA3 group of *ETS* transcription factors (Oh S et al., 2012).

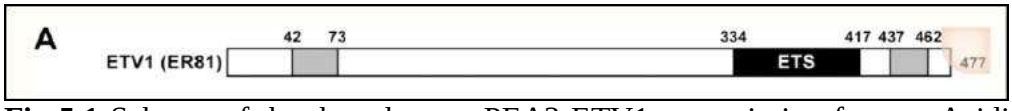

Fig 5.1 Scheme of the three human PEA3 ETV1 transcription factors. Acidic domains are highlighted in grey and the ETS DNA-binding domain in black (Oh S et al., 2012).

ETV1 subfamily PEA3 (polyomavirus enhancer activator 3) is also called E1AF (adenovirus E1A enhancer-binding protein) which means that cellular PEA3/E1AF can be hijacked by viruses for their replication (Xin JH et al., 1992). The Pfam database (http://pfam.sanger.ac.uk/) noted that PEA3 family members do not possess any other protein motif except DNA-binding ETS motif. Hence, *ETV1* has an acidic domain both at the N- and C-terminus (Fig 5.1) (Oh S et al., 2012). Each of which constitutes the core of a transcription activation domain (Janknecht R 1996). The N-terminal activation domain appears to be stronger than the C-terminal and *ETV1* exerts a negative effect on both of its activation domains (Janknecht R 1996).

The intramolecular inhibition of the *ETS* and transactivation can be accounted for two mechanisms such as (i) binding of other proteins may change

the conformation of PEA3 proteins, or (ii) posttranslational modifications. Modulating DNA-binding is via posttranslational modification such as phosphorylation of S334 in *ETV1* inhibits DNA-binding (Baert JL et al., 2002). These serine residues are located at the N-terminal boundary of the ETS domain and targeted by protein kinase A (PKA). PKA may induce *ETV1* transcriptional activity, not only by phosphorylating S334/S367, but can possibly by phosphorylation at sites utilized by MAPKAPKs (Baert JL et al., 2002). Thus, PKA may selectively stimulate target genes that contain high affinity sites for ETV1/ETV5, since the PKA induced reduction in DNA-binding of *ETV1*.

As already being well known that PEA3 factors are implicated in prostate and Ewing tumours melanomas, breast and other cancers as a consequence of chromosomal translocations. Hence, targeting *ETV1* in cancer (NPC) therapy may focus on PEA3 factor activation, target genes and interaction partners (Fig. 5.2 below). Repression of upstream receptor tyrosine kinases, RAS associated with MAPK cascade and target genes such a *MMPs*, *COX-2* and *VEGF* could be useful in in the therapy of PEA3 factor-dependent tumours (Oh S et al., 2012). Multiple ETS target genes are important for cancer progression and function in controlling of cell proliferation (cyclins and cdks), adhesion [cadherins, integrins, cell adhesion molecules (CAMs)], motility/migration (hepatocyte growth factor receptor c-Met, vimentin), cell survival (BCL-2), invasion (uPA & uPAR, PAI, MMPs, TIMPs, heparanase), extravasation (MMPs, integrins), micro-metastasis [osteopontin, parathyroid hormone-related peptide (PTHrP), chemokines/chemokine receptors (RANTES, MIP-3α), CD44], and establishment and maintenance of distant site metastasis and angiogenesis

(integrin β3, VEGF, Flt-1/KDR, Tie2)(Sementchenko VI and Watson DK, 2000). Hence, lowering the expression of *ETV1* undoubtedly will regulate all these related target genes and consequently reduce the invasions and metastasis of tumour,

Activation of *ETV1* depends on binding with its interaction partners such as enzymes p300 or poly (ADP-ribose) polymerase 1 (PARP1)(Brenner JC et al., 2011). Inhibition of such enzymes and binding partners of PEA3 factors could be a prospective treatment for *ETV1*-dependent tumours (Brenner JC et al., 2011). Likewise, in this experiment, the down-regulation of *ETV1* in HONE-1 for both tests may correlate with the interaction of Huanglian or XXXD in deactivating receptor Tyrosine kinase and MAPK cascade or inhibition of the *ETV1* binding enzyme. *ETV1* appears to play a critical role for cancer development, especially in modulating the cellular changes during epithelial–mesenchymal transition and metastasis. Coordination of multiple *ETV1* gene functions also mediates interactions between tumour and stromal cells (Hsu T et al., 2012). From this point of view, there is no ETV1 protein and its target gene was expressed if ETV1 is deregulated. Hence, it is hypothesised that *ETV1* could be considered as the target gene for therapeutic marker of NPC.

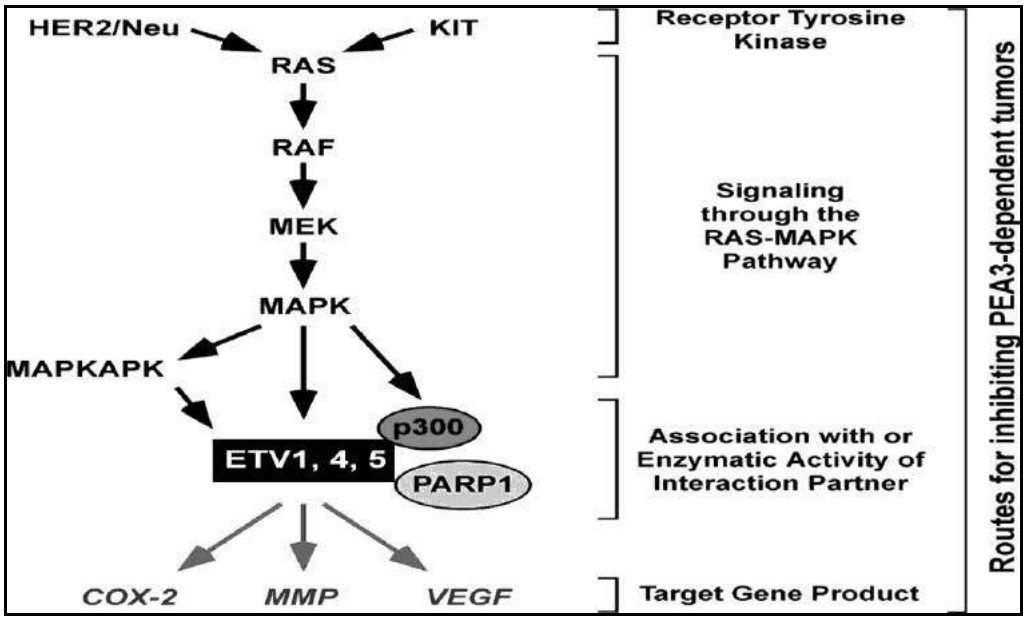

Fig 5. 2 Potential avenues of inhibiting PEA3 factor action

5.7 Significance of Findings

This study justified the potential effect of XXXD and the single constituent of Huanglian in inducing cytotoxicity on HONE-1 cell line. This is a new attempt to study the effect of XXXD and Huanglian extract for the total gene expression on HONE-1 cells. This study demonstrated that both XXXD and Huanglian extracts were able to regulate the expression of the key genes associated with MAPK, PI3K, RAS, WNT, TGFβ, JAK-STAT, Transcription Misregulation and NF-κB signalling pathway in HONE-1 cells. Nevertheless, XXXD or Huanglian induced attenuation or amplification in expression of the related genes, theoretically, impeded the carcinogenesis progression of HONE-1 cells.

In addition, the finding can further ascertain that Chinese Medicinal plants such as XXXD and its constituents particularly Huanglian, could be a useful source for new anti-cancer agents. The positive result attained in this study could provide a new knowledge to be referred by fellow TCM practitioners as well as oncologists for further research as well as treating the relevant cancer diseases in Malaysia and worldwide. Moreover, the finding enhances certainty and confidence in research of Systematic Pharmacology of Chinese Medicine herbs.

5.8 Future Studies

This research involved mainly an *in vitro* experiment of NPC cell lines treated with XXXD and Huanglian. Thus, in vivo study should be carried out to further confirm the findings obtained for the *in vitro* study. The potential effect of XXXD and Huanglian in inducing cytotoxicity on HONE-1 cell line should be further justified animals experiments in the future.

The experimental result can hardly provide sufficient information in molecular mechanism of interaction between proteins and drugs (XXXD or Huanglian) in HONE-1 cells. In this reseach, differential expression which upregulated or downregulated by XXXD or Huanglian in the key genes associated with 13 canoniacl signalling pathways namely MAPK, PI3K, RAS, WNT, TGFβ, JAK-STAT and NF-κB have been studied. However, the detail on cellular mechanism of action caused by the interaction between relevant proteins expressed and the said herbs were not elaborated. In order to understand

thoroughly how XXXD or Huanglian can modulate carcinogenesis in HONE-1, the intriguing cellular response by interaction between ETV1 proteins expressed and herbs treated should be investigated in the future.

In addition, the study in systematic pharmacology for Chinese Medicinal herbs or decoction related to anti-tumour effects should be further pursued. Owing to the complexity of XXXD and its contituents, it is demanding to explain systematically the molecular therapy mechanism of XXXD using conventional methods. Thereupon, systematic or network pharmacology may contribute a fundamental guide to study the multi-targeted mechanism for complicated constituition of any Chinese Medicinal prescription. Hence, through exploration of the complex network of a TCM prescription -therapeutic targets-biological processes-pathways, the therapy mechanism of XXXD for anti-cancer treatment can be elaborated from the perspective of multi-component, multi-target and multi-pathway.

CHAPTER 6

CONCLUSION

Secondary metabolites abundantly found in XXXD and its constituents can justify its anti-cancer effect. Secondary metabolites such as alkaloid, phenolic, phthalide, terpene, glucoside and saponin were determined by Liquid Chromatography Mass Spectrometry (LC-MS). The result shown that L1 (Huanglian) consisted alkaloid (34%), phenolic (27%), glucoside (7%), phthalide (3%) and terpene (3%); L7 (XXXD) consisted alkaloid (37%), phenolic (11%) of total metabolite profiling.

The results obtained for this study indicate that XXXD and Huanglian induced dose-dependent responses associated with cell cycle arrest and apoptosis in HONE-1 by initiating regulation of a large group of genes mainly in MAPK, PI3K, RAS, WNT, TGFβ, JAK-STAT and NF-κB signalling pathway. This reciprocal regulatory mechanism provides clues to further understand the mechanism driving growth inhibition in HONE-1 cells treated with the XXXD and Huanglian.

In addition, the Nanostring assay result provide the fundamental knowledge and suggest that ETV1 could be regarded as the target gene for therapeutic biomaker in treating NPC particularly HONE-1. More functional assay should be conducted to further support this finding.

LIST OF REFERENCES

Akiko, H., I.T. Norio, H. Yoshihiko, U. Shunji, M. Takanobu, T. Ryouichi , M. Koji, H. Shoichi, O. Kiwamu and O. Masaaki; 2005. Molecular dissection of a medicinal herb with anti-tumor activity by oligonucleotide microarray. *Life Sciences*, 77. 991 – 1002.

Albertson DG; 2008. Gene amplification in cancer. *Trends Genet*, 22(8):447-55.

Angel P, Karin M; 1991. *Biochimica Biophysica Acta,* 1072: 129–157.

Arnaud Zaldumbide, Françoise Carlotti, Philippe Pognonec, Kim E. Boulukos; 2002. The Role of the Ets2 transcription factor in the proliferation, maturation, and survival of mouse thymocytes. *The Journal of Immunology,* 169 (9) 4873-4881.

Arun Bahadur Gurung and Atanu Battacharjee; 2015. Significance of RAS signalling in cancer and strategies for its control, *Oncology & Hematology Review*. 11(2):147–52

Aziz A, Ramli RR, Mohamad I, Bhavaraju VK., 2017. Young nasopharyngeal carcinoma: a review of an 8-year experience in the East Coast Malaysia Hospital. *Egypt J Otolaryngol*, 33:490-4

Baharudin Abdullah, Azila Alias, Shahid Hassan; 2009. Challenges in the management of nasopharyngeal carcinoma: A Review. *Malaysian Journal of Medical Sciences*, Vol. 16, No. 4, Pg 50-54

Banys-Paluchowski M, Witzel I, Aktas B, Fasching PA, Hartkopf A, Janni W, Kasimir-Bauer S, Pantel K, Schön G, Rack B, Riethdorf S, Solomayer EF, Fehm T, Müller V; 2019. The prognostic relevance of urokinase-type plasminogen activator (uPA) in the blood of patients with metastatic breast cancer. *Sci Rep*, Feb 19;9(1):2318.

Baert JL, Beaudoin C, Coutte L, de Launoit Y; 2002. ERM transactivation is up-regulated by the repression of DNA binding after the PKA phosphorylation of a consensus site at the edge of the ETS domain. *J. Biol. Chem,* 277:1002–1012.

Bauer N.C., Corbett A.H., Doetsch P.W.; 2015. The current state of eukaryotic DNA base damage and repair. *Nucleic Acids Res*, 43:10083–10101.

Bensky, D.C.S.S.E.G.A., 2004. *Chinese Herbal Medicine Materia Medica*, Seattle: Eastland Press.

Bhasin M, Reinherz EL, Reche PA; 2006. Recognition and classification of histones using support vector machine. *Journal of Computational Biology*, 13 (1): 102–12.

Boundless; 2016. *Altered Gene Expression in Cancer*.

Boyd JM, Malstrom S, Subramanian T, Venkatesh LK, Schaeper U, Elangovan B et al; 1994. Adenovirus E1B 19 kDa and Bcl-2 proteins interact with a common set of cellular proteins. *Cell*, 79: 341–351.

Brack, A.S.; Conboy, I.M.; Conboy, M.J.; Shen, J.; Rando, T.A; 2008. A temporal switch from Notch to Wnt signaling in muscle stem cells is necessary for normal adult myogenesis. *Cell Stem Cell*, 2, 50–59.

Brennan, B., 2006. Nasopharyngeal carcinoma. *Orphanet Journal of Rare Diseases*, 1(1), p.23.

Brenner JC, Ateeq B, Li Y, Yocum AK, Cao Q, Asangani IA, Patel S, Wang X, Liang H, Yu J, Palanisamy N, Siddiqui J, Yan W, Cao X, Mehra R, Sabolch A, Basrur V, Lonigro RJ, Yang J, Tomlins SA, Maher CA, Elenitoba-Johnson KS, Hussain M, Navone NM, Pienta KJ, Varambally S, Feng FY, Chinnaiyan AM; 2011. Mechanistic rationale for inhibition of poly (ADP-ribose) polymerase in ETS gene fusion-positive prostate cancer. *Cancer Cell*, 19:664–678.

Brown HA, Henage LG, Preininger AM, Xiang Y, Exton JH; 2007. Biochemical analysis of phospholipase D. *Methods Enzymol*, 434:49-87.

Bruntz RC, Lindsley CW, Brown HA; 2014. Phospholipase D signaling pathways and phosphatidic acid as therapeutic targets in cancer. *Pharmacol Rev*, 2014 Oct; 66(4):1033-79.

Cantile M, Marra L, Franco R, et al; 2013. Molecular detection and targeting of EWSR1 fusion transcripts in soft tissue tumors. *Med Oncol*, 30(1):412.

Carle, L.N., C.C. Ko and J.T. Castle; 2012. Nasopharyngeal carcinoma. *Head Neck Pathol*, 6(3):364–368.

Chai FN, Ma WY, Zhang J, Xu HS, Li YF, Zhou QD, Li XG, Ye XL; 2018. Coptisine from Rhizoma coptidis exerts an anti-cancer effect on hepatocellular carcinoma by up-regulating miR-122. *Biomed Pharmacother*, 103:1002-1011.

Chakravarthy D, Muñoz AR, Su A, Hwang RF, Keppler BR, Chan DE, Halff G, Ghosh R, Kumar AP; 2018. Palmatine suppresses glutamine-mediated interaction between pancreatic cancer and stellate cells through simultaneous inhibition of survivin and COL1A1. *Cancer Lett*, 2018 Apr 10;419:103-115.

Chan JKC, Bray F, McCarron P, et al., 2005. Nasopharyngeal carcinoma. Who calssification of tumours: *Pathology and genetics of head and neck tumours*, pp:85-97.

Chan JYW, Wei WI; 2012. Recurrent nasopharyngeal carcinoma after salvage nasopharyngectomy. *Arch Otolaryngol Head Neck Surg*, 2012;138(6):572–576.
Chen Lingyun,Yang Guoxiang., 1997. Pharmacological research of PinelliaTernata. *Journal of Yunnan College of Traditional Chinese Medicine*, 20(4), p.12.

Chen Y, Chen S, Li K, Zhang Y, Huang X, Li T, Wu S, Wang Y, Carey L.B, Qian W; 2019. Overdosage of balanced protein complexes reduces proliferation rate in aneuploid cells. *Cell Syst*; 9: 129-142.

Chen WZ, Zhou DL, Luo KS;1989. Long-term observation after radiotherapy fornasopharyngeal carcinoma (NPC). *Int J Radiât Oncol Biol Phys*;16:311-4.

Cheng Her; 2001. Nasopharyngeal cancer and the Southeast Asian patient. *AMERICAN FAMILY PHYSICIAN*, Vol 63,Number 9 / May 1, 2001.

Chi Man Tsang1, Echo Ping Woi Lau , Kaijun Di1, Pak Yan Cheung1, Pok Man Hau1, Yick Pang Ching1, Yong Chuan Wong1, Annie Lai Man Cheung, Thomas S.K. Wan , Yao Tong , S.W.T. and Y.F., 2009. Berberine inhibits Rho GTPases and cell migration atlow doses but induces G2 arrest and apoptosis at high doses in human cancer cells. *Interenational Journal of Molecular Medicine*, 24, pp.131–138.

Chin-CHung Lin, Jai-Sing Yang, Jin-Tang Chen, Shang Fan, Fu-Shun Yu, Jiun-Long Yang, Chi-Cheng Lu, Ming-Ching Kao, An-Cheng Huang, Hsu-Feng Lu and Jing-Gung Chung; 2007. Berberine Induces Apoptosis in Human HSC-3 OralCancer Cells via Simultaneous Activation of the Death Receptor-mediated and Mitochondrial Pathway. *Anticancer Rerearch*, 27: 3371-3378 (2007).

Cho JH, Han JS; 2017. Phospholipase D and Its Essential Role in Cancer. *Mol Cells*, 2017;40(11):805-813.

Collins SL., 1996. Squamous cell carcinoma of the oral cavity and oropharynx. In: Ballenger JJ, Snow JB Jr. *Otorhinolaryngology: head and neck surgery*, 15th ed. Media, Pa.: Williams & Wilkins, 1996:249368.

Constantinou C, Charalambous C, Kanakis D; 2020. Vitamin E and cancer: an update on the emerging role of γ and δ tocotrienols. *Eur J Nutr*, 2020 Apr;59(3):845-857.

Cragg, G.M., D.J. Newman and S.S. Yang; 2016 . Natural product extracts of plant and marine origin having antileukemia potential. *J Nat Prod*, 69, 488-498, 2016.

Cui, Y.-G & Xue, Fan & Lin, Feng & Kong, X.-Y & Liu, W.-Z., 2016. Extraction process of ginger Pinellia and its anti-proliferative and proapoptotic activities on human gastric cancer SGC7901 cells. *Biomedical Research*, 27. 52-55

Daubon, T., Léon, C., Clarke, K. et al; 2019 Deciphering the complex role of thrombospondin-1 in glioblastoma development. *Nat Commun*, 10, 1146 (2019).

Decker DA, Drelichman A, Al-Sarraf M, Crissman J, Reed ML;1983. Chemotherapy for nasopharyngeal carcinoma. A tenyear experience. *Cancer*, 52:602-5.

Ding Rui , Ge Rui Rui , Wang Enyu, Wang Jìng , Zhou Peng , Shao Jīng , Fang Hai Yan , Shi Hui , Wang jing Hui, Huang Jin Ling; 2021. Extract from modified Xiao Xian Xiong Decoction inhibits Epithelial-mesenchymal transition and invasion and migration mediated by TGF-β1 of Human Gastric Cancer MGC-803 cells via Wnt5a/Ca2+/NFAT signaling pathway. *Chinese Journal of Experimental Traditional Medical Formulae,* Vol. 27， No. 4.

Ding Rui, Wang Xiang, Zhou Peng, Wang Enyu, Tang Tongjuan, Li Zhongqiu, Di Mengting, Ge Rui Rui, Huang Jinling; 2020. Research Progress on Antitumor Active Components and Mechanism of Xiao Xianxiongtang. *Chinese Journal of Experimental Traditional Medical Formulae,* Vol. 26， No. 22.

Eferl R, Wagner EF, 2003. AP-1: a double-edged sword in tumorigenesis. *Nat Rev Cancer*, 2003 Nov; 3(11):859-68.

Elmore S; 2007. Apoptosis: a review of programmed cell death. *Toxicol Pathol*, 35(4):495-516.

Ergil KV, Kramer EJ, Ng AT; 2002. Chinese herbal medicines. *West J Med*, 176(4):275-279.

Fan GK, Chen J, Ping F, Geng Y; 2006. Immunohistochemical analysis of P57(kip2), p53 and hsp60 expressions in premalignant and malignant oral tissues. *Oral Oncol*, 42:147–53.

Fulda and Debatin, 2006. Extrinsic versus intrinsic apoptosis pathways in anticancer chemotherapy. *Oncogene,* volume 25, pages4798–4811(2006)

Fürstenberger G, Senn HJ; 2002 . Insulin-like growth factors and cancer. *Lancet Oncol*, May;3(5):298-302.

Gabay M, Li Y, Felsher DW; 2014. MYC activation is a hallmark of cancer initiation and maintenance. *Cold Spring Harb Perspect Med*, 4(6):a014241.

Galletti, B., R. Santoro, V.K. Mannella, F. Caminiti, L. Bonanno, S. De Salvo, G. Cammaroto and F. Galletti; 2016. Olfactory event-related potentials: a new approach for the evaluation of olfaction in nasopharyngeal carcinoma patients treated with chemo-radiotherapy. *J Laryngol Otol*, 130:453–461.

German S, Aslam HM, Saleem S, et al; 2013. Carcinogenesis of PIK3CA. *Hered Cancer Clin Pract*,11(1):5.

Gong C, Hu X, Xu Y, et al., 2020. Berberine inhibits proliferation and migration of colorectal cancer cells by downregulation of GRP78. *Anticancer Drugs*, 2020, 31(2):141-149.

Gorlick R, Huvos AG, Heller G, et al; 1999. Expression of HER2/erbB-2 Correlates With Survival in Osteosarcoma. *J Clin Oncol*,17:2781–8.

Greenwell, M. and P.K. Rahman, 2015. Medicinal Plants: Their Use in Anticancer Treatment. *Int J Pharm Sci Res*, 1;6(10):4103-4112.
Han Ruiwei, He Li, Wang Yi, Liu Chang, Xue Mengmeng, T.M., 2011. The survey of clinical application and pharmacological study of Xiaoxian xiong Decoction. *China Medical Herald,* 8(35).

He W, Wang Q, Xu J, et al; 2012. Attenuation of TNFSF10/TRAIL-induced apoptosis by an autophagic survival pathway involving TRAF2- and RIPK1/RIP1-mediated MAPK8/JNK activation. *Autophagy, 8*(12):1811-1821.

He X, Chen SY, Yang Z, et al; 2018. miR‐4317 suppresses non‐small cell lung cancer (NSCLC) by targeting fibroblast growth factor 9 (FGF9) and cyclin D2 (CCND2). *J Exp Clin Cancer Res*, 37(1):230.

He Z, Liang J, Wang B; 2021 . Inhibin, beta A regulates the transforming growth factor-beta pathway to promote malignant biological behaviour in colorectal cancer. *Cell Biochem Funct.* Mar;39(2):258-266.

Hellwig CT, Rehm M; 2012. TRAIL signaling and synergy mechanisms used in TRAIL-based combination therapies. *Mol Cancer Ther*, Jan; 11(1):3-13.)

Her, C., 2001. Nasopharyngeal cancer and the Southeast Asian patient. *American family physician*, 63(9), pp.1776–82.

Hoppe RT, Williams J, WarnkeR, GoffinetDR, Bagshaw MA; 1978. Carcinoma of the nasopharynx. The significance of histology. *Int J Radiât Oncol Biol Phys,* 4:199-205.

Hou Bao-song et.al., 2018. The clinical research into angina pectoris due to coronary heart disease with syndrome of phlegm-heat accumulation treated with Xiao Xian Xiong Decoction. *Henan Traditional Chinese Medicine,* 2018 February, Vol. 38 No. 2 .

Howie HL, Katzenellenbogen RA, Galloway DA; 2009. Papillomavirus E6 proteins. *Virology*, 384(2):324-334.

Hsieh Ming-Ju, Che-Wei Wange, Jen-Tsun Linf, Yi-Ching Chuanga, Yi-Ting Hsia, Yu-Sheng Loa, Chia-Chieh Lin, Mu-Kuan Chen. Celastrol; 2019. A plant-derived triterpene, induces cisplatin-resistance nasopharyngeal carcinoma cancer cell apoptosis though ERK1/2 and p38 MAPK signaling pathway. *Phytomedicine,* 58-152805

Hsu T, Trojanowska M, Watson DK; 2004. Ets proteins in biological control and cancer. *J Cell Biochem*, 2004; 91(5):896-903.

Huang, J.L; 2007. Experimental study on antitumor effect of Xiao Xian Xiong Decoction. *Chinese Journal of Traditional Medical Science and Technology,* 14(4), pp.239–240.

Hughes DPM, Thomas DG, Giordano TJ, McDonagh KT, Baker LH; 2006. Essential erbB family phosphorylation in osteosarcoma as a target for CI-1033 inhibition. *Pediatric Blood & Cancer,* 46:614–23.

Hussain MS, Fareed S, Ansari S, Rahman MA, Ahmad IZ, Saeed M; 2012. Current approaches toward production of secondary plant metabolites. *J Pharm Bioallied Sci*, 2012 Jan;4(1):10-20.

Huth, H.W, D.M. Santos, H.D. Gravina, J.M. Resende, A.M. Goes, L. de and C. Ropert; 2017. Upregulation of p38 pathway accelerates proliferation and migration of MDA-MB-231 breast cancer cells. *Oncology Reports*, 37, 2497-2505.

Im YH, Kim HT, Lee C, Poulin D, Welford S, Sorensen PH, Denny CT, Kim SJ; 2000. EWS-FLI1, EWS-ERG, and EWS-ETV1 oncoproteins of Ewing tumor family all suppress transcription of transforming growth factor beta type II receptor gene. *Cancer Res*, 60:1536–1540.

Ioannis S. Pateras, Kalliopi Apostolopoulou, Katerina Niforou, Athanassios Kotsinas and Vassilis G. Gorgoulis, 2009. p57KIP2: “Kip”ing the Cell under Control. *Mol Cancer Res,* December 1 2009 (7) (12) 1902-1919.

Iso T, Kedes L, Hamamori Y; 2003. HES and HERP families: Multiple effectors of the notch signaling pathway. *J Cell Physiol*, 2003;194:237–55.

Ito Y, Takeda T, Sakon M, Tsujimoto M, Monden M, Matsuura N; 2001. Expression of p57/Kip2 protein in hepatocellular carcinoma. *Oncology* , 61:221–5.

J.L. Huang ; 2007. Experimental study on antitumor effect of Xiao Xian Xiong Decoction. *Chinese Journal of Traditional Medical Science and Technology,* 14(4), pp.239–240.

Janknecht R; 1996. Analysis of the ERK-stimulated ETS transcription factor ER81. *Mol. Cell. Biol*, 1996;16:1550 –1556.

Jiang J., Neubauer, B. L., Graff, J. R., Chedid, M., Thomas, J. E., Roehm, N. W., Zhang, S., Eckert, G. J., Koch, M. O., Eble, J. N. & Cheng, L; 2002. Expression

of group IIA secretory phospholipase A2 is elevated in prostatic intraepithelial neoplasia and adenocarcinoma*Am. J. Pathol,* 160,667-671.

Kagawa M, Kawakami S, Yamamoto A, Suzuki O, Eguchi H, Okazaki Y, Akagi K, Tamaru JI, Arai T, Yamaguchi T, Ishida H; 2021. Prevalence and clinicopathological/molecular characteristics of mismatch repair protein-deficient tumours among surgically treated patients with prostate cancer in a Japanese hospital-based population. *Jpn J Clin Oncol*, 2021 Apr 1;51(4):639-645.

Kang, J.X. et al., 2005. The extract of huanglian, a medicinal herb, induces cell growth arrest and apoptosis by upregulation of interferon- and TNF- in human breast cancer cells. *Carcinogenesis*, 26(11), pp.1934–1939.

Kashiwagi M, Friess H, Uhl W, et al; 1999. Group II and IV phospholipase A2 are produced in human pancreatic cancer cells and influence prognosis *Gut,* 1999;45:605-612.

Kaur H, Hütt-Cabezas M, Weingart MF, Xu J, Kuwahara Y, Erdreich-Epstein A, Weissman BE, Eberhart CG, Raabe EH; 2015. The chromatin-modifying protein HMGA2 promotes a typical teratoid/rhabdoid cell tumorigenicity. *J. Neuropathol. Exp.Neurol*, 2015, 74, 177–185.

Kim, J.S., H. Tanaka and Y. Shoyama; 2004. Immunoquantitative analysis for berberine and its related compounds using monoclonal antibodies in herbal medicines. *Analyst,* 129, 87 – 91.

Kinjyo I, Inoue H, Hamano S, Fukuyama S, Yoshimura T, Koga K, et al.; 2006. Loss of SOCS3 in T helper cells resulted in reduced immune responses and hyperproduction of interleukin 10 and transforming growth factor–β1. *J Exp Med*, 2006;203:1021–31.

Krimpenfort, P., IJpenberg, A., Song, JY. et al.; 2007. p15Ink4b is a critical tumour suppressor in the absence of p16Ink4a. *Nature,* 448, 943–946 .

Krueger GRF, Wustrow J.; 1981. Current classification of nasopharyngeal carcinoma at Cologne University. In: Grundmann E, Krueger GRF, Ablashi DV, editor. *Nasopharyngeal carcinoma,* Vol. 5. pp. 11–5.

Kuemmerle JF, Murthy KS, Bowers JG; 2004. IGFBP-3 activates TGF-beta receptors and directly inhibits growth in human intestinal smooth muscle cells. *Am J Physiol Gastrointest Liver Physiol*. 2004 Oct;287(4):G795-802.

Lam WKJ, Chan JYK; 2018. Recent advances in the management of nasopharyngeal carcinoma. *Faculty Rev,* 1829.

Lee J, Nguyen PT, Shim HS, Hyeon SJ, Im H, Choi MH, Chung S, Kowall NW, Lee SB, Ryu H; 2019. EWSR1, a multifunctional protein, regulates cellular function and aging via genetic and epigenetic pathways. *Biochim Biophys Acta Mol Basis Dis*, Jul 1; 1865(7):1938-1945.

Lee J, Nguyen PT, Shim HS, Hyeon SJ, Im H, Choi MH, Chung S, Kowall NW, Lee SB, Ryu H; 2019. EWSR1, a multifunctional protein, regulates cellular function and aging via genetic and epigenetic pathways. *Biochim Biophys Acta Mol Basis Dis*, 1865(7):1938-1945.

Lee YS, Dutta A; 2007. The tumor suppressor microRNA let-7 represses the HMGA2 *oncogene Genes Dev*, 21(9):1025-1030.

Lee S.Y., H.M. Jeon, M.K. Ju, C.H. Kim, G. Yoon, S.I. Han, H.G. Park and H. S. Kang; 2012. Wnt/Snail signaling regulates cytochrome C oxidase and glucose metabolism. *Cancer Res*, 72(14):3607-3617.

Li H, Kolluri SK, Gu J, Dawson MI, Cao X, Hobbs PD, Lin B, Chen G, Lu J, Lin F, Xie Z, Fontana JA, Reed JC, Zhang X; 2000. Cytochrome c release and apoptosis induced by mitochondrial targeting of nuclear orphan receptor TR3. *Science*, 289(5482):1159-64.

Li, C.-H. et al., 2014. Berberine hydrochloride impact on physiological processes and modulation of twist levels in nasopharyngeal carcinoma CNE-1 cells. *Asian Pacific journal of cancer prevention*, APJCP, 15(4), pp.1851–1857.

Li F, Mei Y,Wang Y, Chen C, Tu J, Xiao B, et al; 2005. Trichosanthin inhibits antigenspecific T cell expansion through nitric oxide-mediated apoptosis pathway. *Cell Immunol*, 234:23–30.

Li GL, Jiang W, Xia Q, Chen SH, Ge XR, Gui SQ, Xu CJ; 2010. HPV E6 down-regulation and apoptosis induction of human cervical cancer cells by a novel lipid-soluble extract (PE) from Pinellia Pedatisecta Schott *in vitro*. *J Ethnopharmacol*, 2010 Oct 28;132(1):56-64.

Li H, Ko CH, Tsang SY, Leung PC, Fung MC, Fung KP; 2011. The Ethanol Extract of Fructus trichosanthis Promotes Fetal Hemoglobin Production via p38 MAPK Activation and ERK Inactivation in K562 Cells. *Evid Based Complement Alternat Med*, 2011;2011:657056.

Li Ruping, Yang Chengzhi, Di Ling, Hu Weitao; 2017. Effect of XXXD on Liver Caspase-12 expression in rats with Nonalcoholic Fatty Liver Disease. *Journal of Traditional Chinese Medicine*, Vol 58 No.8

Li, X.K., M. Motwani,, W. Tong, W. Bornmann and G.K. Schwartz; 2008. Huanglian, A Chinese herbal extract, inhibits cell growth by suppressing the expression of cyclin B1 and inhibiting CDC2 kinase activity in human cancer cells. *Molecular Pharmacology;* 58, 1287–1293.

Li, Y., Wang, F., Lu, L. et al; 2017. NR4A1 inhibition synergizes with ibrutinib in killing mantle cell lymphoma cells. *Blood Cancer Journal*, 7, 632 (2017).

Limpose KL, Trego KS, Li Z, Leung SW, Sarker AH, Shah JA, Ramalingam SS, Werner EM, Dynan WS, Cooper PK, Corbett AH, Doetsch PW; 2018. Overexpression of the base excision repair NTHL1 glycosylase causes genomic instability and early cellular hallmarks of cancer. *Nucleic Acids Res,* 18;46(9):4515-4532.

Lin B, Kolluri SK, Lin F, Liu W, Han YH, Cao X, Dawson MI, Reed JC, Zhang XK , 2004. Conversion of Bcl-2 from protector to killer by interaction with nuclear orphan receptor Nur77/TR3.*Cel*,116(4):527-40.

Lin Ming-Zhu, Zhao Yan, Cai En-Bo; 2017. Anti-tumor effect of -sitosterol in H22 tumour-bearing mice. *Chinese Journal of Public Health*, 2017, 33(12): 1797-1800.

Liu, C. and Y. Huang., 2016. Chinese Herbal Medicine on Cardiovascular Diseases and the Mechanisms of Action. *Front Pharmacol*, 1;7:469

Liu F, Wang B, Wang Z, Yu S., 2012. Trichosanthin down-regulates Notch signaling and inhibits proliferation of the nasopharyngeal carcinoma cell line CNE2 in vitro. *Fitoterapia*, 83(5):838-42.

Iizuka, N., M. Oka, K. Yamamoto, A. Tangoku, K. Miyamoto, T. Miyamoto, S. Uchimura, Y. Hamamoto, K. Okita., 2003. Identification of common or distinct genes related to antitumor activities of a medicinal herb and its major component by oligonucleotide microarray. *International Journal of Cancer*, 107, 666 – 672, 2003.

Liu J, Wen X, Liu B; 2016. Diosmetin inhibits the metastasis of hepatocellular carcinoma cells by downregulating the expression levels of MMP-2 and MMP-9. *Mol Med Rep*, 2016;13(3):2401-2408.

L.L. Ni, Z. Fang, Y. Fang, and J. Wu; 2014. Xiao XianXiong Decoction inhibits cell growth through G2/M phasecell cycle arrest and migration and invasion

ability of A549 and H1299 cells. *China Journal of Traditional Chinese Medicine and Pharmacy,* 29(5)

Lo KW, To KF, Huang DP; 2004. Focus on nasopharyngeal Carcinoma. *Cancer Cell*, 5:423–8.

Lo, K.-W, Chung, G.T, K.-F., 2012. Deciphering the molecular genetic basis of NPC through molecular, cytogenetic, and epigenetic approaches. *Seminars in Cancer Biology*, 22(2), pp.79–86.

Lv Kun, Sun Qin You, Jiang Bo; 2014. Effect of Xiao Xian Xiong decoction on plaque area and NF-κB expression in aorta of atherosclerotic rats. *Chin Hosp Pharm J*, 34, N0.4.

Mahdavifar, N., M. Ghoncheh, A. Mohammadian-Hafshejani, B. Khosravi and H; 2016. Salehiniya. Epidemiology and Inequality in the Incidence and Mortality of Nasopharynx Cancer in Asia. *Osong Public Health Res Perspect*, 7(6):360-372.

Ma W, Zhu M, Zhang D., 2017. Berberine inhibits the proliferation and migration of breast cancer ZR-75-30 cells by targeting Ephrin-B2. *Phytomedicine*，2017, 25:45-51.

Malik SS, Mubarik S, Aftab A, Khan R, Masood N, Asif M, Bano R., 2021. Correlation of MSH2 exonic deletions and protein downregulation with breast cancer biomarkers and outcome in Pakistani women/patients. *Environ Sci Pollut Res Int,* 28(3):3066-3077.

Marango J, Shimoyama M, Nishio H, et al., 2008. The MMSET protein is a histone methyltransferase with characteristics of a transcriptional corepressor. *Blood*, 111(6):3145-3154.

Maynard S., Schurman S.H., Harboe C., de Souza-Pinto N.C., Bohr V.A., 2009. Base excision repair of oxidative DNA damage and association with cancer and aging. *Carcinogenesis*, 30:2–10.

Misiewicz-Krzeminska I, Sarasquete ME, Vicente-Dueñas C, Krzeminski P, Wiktorska K, Corchete LA, Quwaider D, Rojas EA, Corral R, Martín AA, Escalante F, Bárez A, García JL, Sánchez-García I, García-Sanz R, San Miguel JF, Gutiérrez NC., 2016. Post-transcriptional Modifications Contribute to the Upregulation of Cyclin D2 in Multiple Myeloma. *Clin Cancer Res*, 1;22(1):207-17.

Murthy KN, Jayaprakasha GK, Patil BS., 2015. Cytotoxicity of obacunone and obacunone glucoside in human prostate cancer cells involves Akt-mediated programmed cell death. *Toxicology*, 329:88-97.

Myrtle A. Davis, Elizabeth H. Jeffery; 2002. *Handbook of Toxicologic Pathology* (Second Edition).

Nakagawa T, Zhu H, Morishima N, Li E, Xu J, Yankner BA, Yuan J., 2000. Caspase-12 mediates endoplasmic-reticulum-specific apoptosis and cytotoxicity by amyloid-beta. *Nature*, 403(6765):98-103.

Neel HB 3rd, Pearson GR, Taylor WF Ann., 1994. Antibodies to Epstein-Barr virus in patients with nasopharyngeal carcinoma and in comparison groups. *Otol Rhinol Laryngol.* 1984 Sep-Oct; 93(5 Pt 1):477-82.

Ni Lu-lu1, Fang Zhi-hong, Fang Yuan, Wu Jian-chun, L.Y., 2014. Xiaoxianxiong Decoction inhibits cell growth through G2/M phasecell cycle arrest and migration and invasion ability of A549 and H1299 cells. *China Journal of Traditional Chinese Medicine and Pharmacy*, 29(5).

Ni, L. et al., 2015. Trichosanthes kirilowii fruits inhibit non-small cell lung cancer cell growth through mitotic cell-cycle arrest. *The American journal of Chinese medicine*, 43(2), pp.349–364.

Ni, L.L. Z. Fang, Y. Fang and J. Wu., 2014.Xiaoxianxiong Decoction inhibits cell growth through G2/M phasecell cycle arrest and migration and invasion ability of A549 and H1299 cells. *China Journal of Traditional Chinese Medicine and Pharmacy*. 29(5)

Niehrs C; 2006. Function and biological roles of the Dickkopf family of Wnt modulators. *Oncogene* 25, 7469–7481.

Ng RH, Ngan R, Wei WI, Gullane PJ, Phillips J., 2014. Trans-oral brush biopsies and quantitative PCR for EBV DNA detection and screening of nasopharyngeal carcinoma. *Otolaryngol Head Neck Surg*; 150(4):602-9

Oh S, Shin S, Janknecht R., 2012. ETV1, 4 and 5: an oncogenic subfamily of ETS transcription factors. *Biochim Biophys Acta*; 1826(1):1-12.

Ozturk Nihan, Singh Indrabahadur, Mehta Aditi, Braun Thomas, Barreto Guillermo; 2014. HMGA proteins as modulators of chromatin structure during transcriptional activation. *Frontiers in Cell and Developmental Biology*, 2014 Mar 6;2:5.

Pang, B., Q. Zhou, T.Y. Zhao, L.S. He, J. Guo, H.D. Chen, L.H. Zhao and X.L. Tong., 2015. Innovative Thoughts on Treating Diabetes from the Perspective of Traditional Chinese Medicine. *Evid Based Complement Alternat Med*, 2015(3):905432.

Pang, B., X.T. Yu, Q. Zhou, T.Y. Zhao, H. Wang, C.J. Gu and , X.L. Tong, 2015. Effect of Rhizoma Coptidis (Huang Lian) on treating diabetes mellitus. *Evid Based Complement Alternat Med.* 921416

Patel Sonal, Alam Aftab, Pant Richa, Chattopadhyay Samit; 2019.Wnt signaling and its significance within the tumor microenvironment: Novel therapeutic insights. *Frontiers in Immunology*, volume 10, page 2872, 2019.

Pateras IS, Apostolopoulou K, Koutsami M, et al., 2006. Downregulation of the KIP family members p27 (KIP1) and p57 (KIP2) by SKP2 and the role of methylation in p57(KIP2) inactivation in nonsmall cell lung cancer. *Int J Cancer*, 119:2546–56.

Paul Polakis., 2021. Wnt signaling and cancer. Published *by Cold Spring Harbor Laboratory Press.*

Peng P L, Hsieh Y S, Wang C J, et al.; 2004. Inhibitory effect of berberine on the invasion of human lung cancer cells via decreased productions ofurokinase-plasminogen activator and matrix metalloproteinase-2. *Toxicol Appl Pharmacol,* 214(1), pp.8–15.

Pflug KM, Sitcheran R., 2020. Targeting NF-κB-Inducing Kinase (NIK) in Immunity, Inflammation, and Cancer. *Int J Mol Sci*, 21(22):8470.

Prucca CG, Racca AC, Velazquez FN, Cardozo Gizzi AM, Rodr ́guez Berdini L, Caputto BL; 2020. Impairing activation of phospholipid synthesis by c-Fos interferes with glioblastoma cell proliferation. *Biochem J,* 2020 Dec 11;477(23):4675-4688.

Qiu Feng; 2014. Clinical Study on Simvastatin Combined with Modified Xiao xian xiong Decoction Treatment of Hyperlipidemia. *China Journal of Chinese Medicine,* 2014 (4).

R. Han, L. He, Y. Wang, C. Liu, and M. Xue; 2011.The survey of clinical application and pharmacological study of Xiaoxian Xiong Decoction. *China Medical Herald*, 8(35).

Ramadori, G. & Cameron, S., 2010. Effects of systemic chemotherapy on the liver. *Annals of hepatology*, 9(2), pp.133–43.

Raven, P.H., G.B. Johnson, K.A. Mason, J.B. Losos and S.R. Singer., 2014. Cancer is a failure of cell cycle control. *In Biology*. 10th ed., AP ed., pp. 202-204). New York, NY: McGraw-Hill

Research Group of Traditional Chinese Medicine, D. of & Pharmacy, B.M.C., 1959. The anti-cancer effect of traditional Chinese medicine. *Beijing Medical Journal*, 1, pp.104–107.

Ricardo E. Dolmetsch, Urvi Pajvani, Katherine Fife, James M. Spotts, Michael E. Greenberg; 2001. Signaling to the Nucleus by an L-type Calcium Channel-Calmodulin Complex Through the MAP Kinase Pathway. *Science* (New York, N.Y.), 294. 333-9. 10.1126/science.

Rocha CRR, Silva MM, Quinet A, Cabral-Neto JB, Menck CFM; 2018. DNA repair pathways and cisplatin resistance: an intimate relationship. *Clinics* (Sao Paulo), 73(suppl 1):e478s.

Saikh, K.U; 2021. MyD88 and beyond: a perspective on MyD88-targeted therapeutic approach for modulation of host immunity. *Immunol Res*, 69, 117–128 (2021).

Salehan MR, and Morse HR; 2013. DNA damage repair and tolerance: a role in chemotherapeutic drug resistance. *Br J Biomed Sci*, 70, 31-40.

Santarius T, Shipley J, Brewer D, Stratton MR, Cooper CS., 2010. A census of amplified and overexpressed human cancer genes. *Nat Rev Cancer*, 10(1):59-64. Scheid, V., B. Dan, E. Andrew and B. Randall; 2009. Chinese Herbal Medicine: *Formulas and Strategies*, 2nd ed. Seattle, WA: Eastland Press

Segalés L, Juanpere N, Lorenzo M, Albero-González R, Fumadó L, Cecchini L, Bellmunt J, Lloreta-Trull J, Hernández-Llodrà S., 2019. Strong cytoplasmic ETV1 expression has a negative impact on prostate cancer outcome. *Virchows Arch*, 475(4):457-466.

Seif, F., Khoshmirsafa, M., Aazami, H. et al., 2017.The role of JAK-STAT signaling pathway and its regulators in the fate of T helper cells. *Cell Commun Signal*, 15, 23.

Seki Y-i, Inoue H, Nagata N, Hayashi K, Fukuyama S, Matsumoto K, et al.; 2003. SOCS-3 regulates onset and maintenance of TH2-mediated allergic responses. *Nat Med*, 9:1047–54.

Sementchenko VI, Watson DK., 2000. Ets target genes: past, present and future. *Oncogene*, 19(55):6533-48.

Shamloo B, Usluer S., 2019. p21 in Cancer Research. *Cancers (Basel).* 2019;11(8):1178.

Shanmugaratnam KS, Sobin LH., 1978. Histological typing of upper respiratory tract tumors. Geneva: *World Health Organization*; 1978.

Sharma Jatin, Larkin Joseph; 2019.Therapeutic Implication of SOCS1 Modulation in the Treatment of Autoimmunity and Cancer. Frontiers in Pharmacology Front. *Pharmaco*l., 11 April 2019.

Shaw PC, Lee KM, Wong KB., 2005. Recent advances in trichosanthin, a ribosome-inactivating protein with multiple pharmacological properties.*Toxicon,* 2005;45:683–9.

Shi L, Resaul J, Owen S, Ye L, Jiang WG., 2016. Clinical and Therapeutic Implications of Follistatin in Solid Tumours. *Cancer Genomics Proteomics*, 2016 11-12;13(6):425-435.

Shi RY, Yang XR, Shen QJ, Yang LX, Xu Y, Qiu SJ, Sun YF, Zhang X, Wang Z, Zhu K, Qin WX, Tang ZY, Fan J, Zhou J., 2013. High expression of Dickkopf-related protein 1 is related to lymphatic metastasis 6 and indicates poor prognosis in intrahepatic cholangiocarcinoma patients after surgery. *Cancer*, 119(5):993-1003.

Shuchen Gu, Xin-Hua Feng; 2018. TGF-β signaling in cancer. *Acta Biochimica et Biophysica Sinica*, volume 50, Issue 10, October 2018. Pages 941–949

Six DA, Dennis EA., 2000.The expanding superfamily of phospholipase A(2) enzymes: classification and characterization. *Biochim Biophys Acta*. 2000 Oct 31;1488(1-2):1-19.

Starkey, M., Nguyen, D., Essilfie, A. et al., 2014. Tumor necrosis factor-related apoptosis-inducing ligand translates neonatal respiratory infection into chronic lung disease. *Mucosal Immunol* 7, 478–488 (2014).

Subhuti Dharmananda, 1997. *Oriental Perspectives on Cancer and Its Treatment*.

Sumida T, Ishikawa A, Nakano H, Yamada T, Mori Y, Desprez PY., 2016. Targeting ID2 expression triggers a more differentiated phenotype and reduces aggressiveness in human salivary gland cancer cells. *Genes Cells*. 2016 Aug; 21(8):915-20.

Sun Yi, Gu Jun; 2015. Quercetin inhibits breast cancer cell migration and invasion and its molecules mechanism research. *China Journal of Traditional Chinese Medicine*, 2015, 40(6): 1144-1150.

Swarthout JT, Walling HW., 2000. Lysophosphatidic acid: receptors, signaling and survival. *Cell Mol Life Sci*, 2000 Dec; 57(13-14):1978-85.

Sylvia Yat-Yee Chan, Kwong-Wai Choy, Sai-Wah Tsao, Qian Tao, Tao Tang, Grace Tin-Yun Chungand Kwok-Wai Lo., 2008. Authentication of nasopharyngeal carcinoma tumor lines. *Int. J. Cancer*, 122, 2169–2171 (2008)

Takano Y, Kato Y, van Diest PJ, Masuda M, Mitomi H, Okayasu I., 2000. Cyclin D2 overexpression and lack of p27 correlate positively and cyclin E inversely with a poor prognosis in gastric cancer cases. *Am J Pathol*. 2000;156(2):585-594.

Tao, S., T. Yong, S.T. Man, Y. Hua, Q.F. Xiu, L. Ting, L.C. Chi, G. Hui, X.L. Ya, L.Z. Pei, K.W.T. Anfernee, C. Hui, P.L. Aiand L.Y. Zhi.,2016. Metabolomics reveals the mechanisms for the cardiotoxicity of Pinelliae Rhizoma and the toxicity-reducing effect of processing. *Sci Rep*. 6, 34692, 2016.

Thiery JP., 2002. Epithelial–mesenchymal transitions in tumour progression. *Nat Rev Cancer*, 2002;2:442–454.

Thompson L. D; 2007. Update on nasopharyngeal carcinoma. *Head and neck pathology*, 1(1), 81–86.

Tsang, C. M., Cheung, Y. C., Lui, V. W., Yip, Y. L., Zhang, G., Lin, V. W., Cheung, K. C., Feng, Y., & Tsao, S. W.,2013. Berberine suppresses tumorigenicity and growth of nasopharyngeal carcinoma cells by inhibiting STAT3 activation induced by tumor associated fibroblasts. *BMC cancer*, 13, 619.

Tsang, C.M. et al., 2009. Berberine inhibits Rho GTPases and cell migration at low doses but induces G2 arrest and apoptosis at high doses in human cancer cells. *International journal of molecular medicine*, 24(1), pp.131–138.

Tsang CM, Tsao SW; 2015 The role of Epstein-Barr virus infection in the pathogenesis of nasopharyngeal carcinoma. *Virol Sin*, 2015 Apr;30(2):107-21.

Tu J, Huo Z, Gingold J, Zhao R, Shen J, Lee DF., 2017. The Histogenesis of Ewing Sarcoma. *Cancer Rep Rev.* 2017;1(2):10.15761.

Turpin J, El-Safadi D, Lebeau G, Frumence E, Desprès P, Viranaïcken W, Krejbich-Trotot P; 2021. CHOP Pro-Apoptotic Transcriptional Program in Response to ER Stress Is Hacked by Zika Virus. *Int J Mol Sci*, 22(7):3750.

Varma Shrivastav Shailly, Bhardwaj Apurva, Pathak Kumar Alok, Shrivastav Anuraag; 2020. Insulin-like growth factor binding protein-3 (IGFBP-3):

Unraveling the role in mediating IGF-independent effects within the cell. *Frontiers in Cell and Developmental Biology*, volume 8, pages 286.

Vasef MA, Ferlito A, Weiss LM., 1997. Nasopharyngeal carcinoma, with emphasis on its relationship to Epstein-Barr virus. *Ann Otol Rhinol Laryngol*, 1997;106:348-56.

Wang HY, Chang YL, To KF, et al., 2016. A new prognostic histopathologic classification of nasopharyngeal carcinoma. *Chin J Cancer*, 2016;35:41.

Wang Q, Xu H, Zhao X; 2018. Baicalin Inhibits Human Cervical Cancer Cells by Suppressing Protein Kinase C/Signal Transducer and Activator of Transcription (PKC/STAT3) Signaling Pathway. *Med Sci Monit*, 2018 Apr 3;24:1955-1961.

Wang YA, Sun Y, Palmer J, Solomides C, Huang LC, Shyr Y, Dicker AP, Lu B; 2017. IGFBP3 modulates lung tumorigenesis and cell growth through IGF1 signaling. *Mol Cancer Res*, 2017 Jul;15(7):896-904.

Wang, 2018. Clinical Observation on Xiao Xian Xiong Decoction in treating community acquired pneumonia of phlegm heat obstructing lung syndrome. *Chinese Medicine Modern Distance Education of China*, 16:12.

Wang, N. et al., 2015. Berberine and Coptidis Rhizoma as potential anticancer agents: Recent updates and future perspectives. *Journal of Ethnopharmacology*, 176, pp.35–48.

Wang, W.B., Feng, L.X., Yue, Q.X., Wu, W.Y., Guan, S.H., Jiang, B.H., Yang, M., Liu, X., Guo, D.A., 2012. Paraptosis accompanied by autophagy and apoptosis was induced by celastrol, a natural compound with influence on proteasome, ER stress and Hsp90. *J. Cell. Physiol*, 227, 2196–2206.

Wang W, Tan B, Zhang J, et al., 2018. Human nasopharyngeal carcinoma can be radiosensitized by trichosanthin via inhibition of the PI3K pathway. *Exp Ther Med*, 16(5):4181-4186.

Wang., W, Q. Wen, L. Xu, G. Xie, J. Li, J. Luo, S. Chu, L. Shi, D. Huang, J. Li and S. Fan., 2014. Activation of Akt/mTOR pathway is associated with poor prognosis of nasopharyngeal carcinoma. PLoS One. 9(8), e106098, 2014.

Watkinson JC, Gaze MN, Wilson JA., 2000. Tumours of the Nasopharynx. *Stell & Maran Head & Neck Surgery.* Oxford: Butterworth Heinemann; 2000. p.397–408.

Xiang, Z.X. et al., 2009. The effect of Trichosanthes kirilowii on low immunity mice caused by cyclophosphamimmune. *China Pharmacy*, 20(9), pp.648–650.
Xiankuo, Y., T. Liying, W. Hongwei, Z. Xiao, L. Hanyan, G. Rixin, X. Mengying, Y. Hongjun, F. Jianwei, W. Zhuju and S. Ruiqiang; 2018. Trichosanthis Fructus: botany, traditional uses, phytochemistry and pharmacology. *Journal of Ethnopharmacology*; 224, 177-194, 2018.

Xiao et.al., 2017. Clinical observation of modified Xiaoxianxiong decoction on impaired glucose tolerance of obesity type . *SHANXI J OF TCM* , Vol.33 No.6.

Xiao et.al., 2014. Clinical observation on treatment of primary bile reflux gastritis with liver-stomach heat stagnation with Xiao Xian Xiong Decoction and Sini Powder. *Journal of Yunnan University of Traditional Chinese Medicine,* Vol. 37 No. 6 .

Xin JH, Cowie A, Lachance P, Hassell JA., 1992. Molecular cloning and characterization of PEA3, a new member of the Ets oncogene family that is differentially expressed in mouse embryonic cells. *Genes Dev*, 6:481–496.

Xu, B, Ding, J, Chen, K. X, Miao, Z. H, Huang, H, Liu, H, & Luo, X. M; 2012. Advances in Cancer Chemotherapeutic Drug Research in China. *Recent Advances in Cancer Research and Therapy*, 287–350.

Xu, M, Horrell, J., 2007.WNT10A mutation causes ectodermal dysplasia by impairing progenitor cell proliferation and KLF4-mediated differentiation. *NatCommun*, 8,15397(2017).

Xu Z, Yan Y, Xiao L, Dai S, Zeng S, Qian L, Wang L, Yang X, Xiao Y, Gong Z; 2017. Radiosensitizing effect of diosmetin on radioresistant lung cancer cells via Akt signaling pathway. *PLoS One*, 2017 Apr 17;12(4):e0175977.

Ventola CL.,2017. Cancer Immunotherapy, Part 3: *Challenges and Future Trends*, P T. 42(8):514-521.

Volker Scheid , Dan Bensky , Andrew Ellis , Randall Barolet., 2009. Chinese Herbal Medicine: *Formulas & Strategies* , 2nd Edition 2009 ISBN-13: 978-0939616831.

Yang L, Wen KS, Ruan X, Zhao YX, Wei F, Wang Q., 2018. Response of Plant Secondary Metabolites to Environmental Factors. *Molecules*, 23(4):762.

Yang X, Jiang J, Zhang C, Li Y; 2019. Baicalein restrains proliferation, migration, and invasion of human malignant melanoma cells by down-regulating colon cancer associated transcript-1. *Braz J Med Biol Res*, 54(7):e8934.
Yasukawa H, Misawa H, Sakamoto H, Masuhara M, Sasaki A, Wakioka T, et al. ,1999. The JAK-binding protein JAB inhibits Janus tyrosine kinase activity through binding in the activation loop. *EMBO J*, 18:1309–20.

Young-Hyuck Im, Heung Tae Kim, Cecile Lee, Danielle Poulin, Scott Welford, Poul H. B. Sorensen, Christopher T. Denny and Seong-Jin Kim., 2000.EWS-FLI1, EWS-ERG, and EWS-ETV1 Oncoproteins of Ewing Tumor Family All Suppress Transcription of Transforming Growth Factor β Type II Receptor Gene. *Cancer Res*, (60) (6) 1536-1540.

Yuan., L, H.M. Yi,, H. Yi, J.Q. Qu, J.F. Zhu, L.N. Li, T. Xiao, Z. Zheng, S.S. Lu and Z.Q. Xiao., 2016. Reduced RKIP enhances nasopharyngeal carcinoma radioresistance by increasing ERK and AKT activity. *Oncotarget*. 7(10):11463–11477, 2016.

Zeng Y, Baugh E, Akyalcin S, Letra A.,2021. Functional Effects of WNT10A Rare Variants Associated with Tooth Agenesis. *J Dent Res*, 100(3):302-309.

Zeng., Z.Y., Y.H. Zhou, W.L. Zhang, W. Xiong, S.Q. Fan, X.L. Li, X.M. Luo, M.H. Wu, Y.X. Yang, C. Huang, L. Cao, K. Tang, J. Qian, S.R. Shen and G.Y. Li., 2007. Gene expression profiling of nasopharyngeal carcinoma reveals the abnormally regulated Wnt signaling pathway. *Human Pathology*. 38(1), 120–133, 2007.

Zhang Q, Lenardo MJ, Baltimore D., 2017. 30 Years of NF-κB: A Blossoming of Relevance to Human Pathobiology. *Cell*, 168(1-2):37-57.

Zhang Z, Rahme GJ, Chatterjee PD, Havrda MC, Israel MA., 2017 .ID2 promotes survival of glioblastoma cells during metabolic stress by regulating mitochondrial function. *Cell Death Dis*, 8(2):e2615.

Zhang Z, Rahme GJ, Chatterjee PD, Havrda MC, Israel MA., 2017. ID2 promotes survival of glioblastoma cells during metabolic stress by regulating mitochondrial function. *Cell Death Dis*, 8(2):e2615.

Zhang, C. et al., 2011. Effects of ethanol extract of Rhizome Pinelliae Preparata on intracellular pH value of human gastric adenocarcinoma cells. Zhong xi yi jie he xue bao. *Journal of Chinese integrative medicine*, 9(8), pp.894–900.

Zhang, F. & Zhang, J; 1999. Clinical hereditary characteristics in nasopharyngeal carcinoma through Ye-Liang's family cluster. *Chinese medical journal*, 112(2), pp.185–7.
Zhang, J., Ney, P; 2009. Role of BNIP3 and NIX in cell death, autophagy, and mitophagy. *Cell Death Differ* 16, 939–946

Zhang, Z.J. & Wang, S.H; 2005. *Shang Han Lun:* Beijing: Ren min wei sheng chu ban she, 2005.

Zhao Hao Y, Cui L, Pan Y., 2017. Berberine inhibits the chemotherapy-induced repopulation by suppressing the arachidonic acid metabolic pathway and phosphorylation of FAK in ovarian cancer. Cell Proliferation, 2017; 50: 12393.

Zhao, W., D. Feng, S. Sun, T. Han and S. Sui; 2010. The anti-viral protein of trichosanthin penetrates into human immunodeficiency virus type 1. *Acta Biochimica et Biophysica Sinica*, 42(2):91‐97